Investigating Geochemistry and Habitability at Continental Sites of

Serpentinization: The Cedars, California, USA and the Tablelands, Newfoundland,

CAN

by

© Amanda Rietze, B.Sc. (Hons)

A Thesis submitted to the

School of Graduate Studies

in partial fulfillment of the requirements for the degree of

Master of Science

Department of Earth Sciences

Memorial University of Newfoundland

May 2015

St. John's   Newfoundland

ABSTRACT

This study investigates the geochemistry and habitability of spring fluids associated with active continental serpentinization at The Cedars, California, USA and the Tablelands, Newfoundland, CAN. These ophiolite complexes were host to several springs discharging ultra-basic (>11) and highly reducing (<-400 mV) fluids rich in H_2 gas that were geochemically distinct from the surrounding groundwater.

C_{2+} hydrocarbons at both ophiolite complexes suggest hydrocarbons were thermogenic in origin; however, an abiogenic contribution could not be ruled out. Methane at The Cedars was dominated by a microbial origin with a contribution of non-microbial sources, while methane at the Tablelands was dominated by a non-microbial source (i.e. thermogenic or abiogenic or mixture of the two). Spring fluids lacked electron acceptors and nutrients which adds further complications to the already unusually high pH and limited carbon fixation possibilities in this extreme environment.

ACKNOWLEDGEMENTS

creation of the maps used in this thesis, and Heidi, Lukas and Mark for their assistance in the field.

A special thanks to my family (Mom, Dad, Mark and Courtney) for all their support and love over the past few years. This thesis would not have materialized without your encouragement and support in all shapes and forms especially during the rough periods. Bazey, it was the best of times it was the blusrt of times, but no matter what times they were you saw me through it all. Without your love and friendship I dare say I am not sure where I would be today. You have made my time in Newfoundland an adventure that I will not soon forget.

Table of Contents

List of Tables

List of Figures

List of Symbols, Nomenclature or Abbreviations

‰ – parts per thousand
AC – Austin Creek
BS – Barnes Spring
BSC – Barnes Spring Complex
BTEX – aromatic group consisting of benzene, toluene, ethylbenzene and xylenes
DOC – dissolved organic carbon
EA – elemental analyzer
E_h – reduction potential measurement (a.k.a Redox potential)
EPA – Environmental Protection Agency
FID – flame ionization detector
FSC – Franciscan Subduction Complex
FTT – Fischer-Tropsch Type
f_{UB} – fraction of ultra-basic end member
GA – 1 billion years ago
GC – gas chromatograph
GC-C-IRMS – gas chromatography-combustion-isotope ratio mass spectrometer
GPS – Grotto Pool Spring
HAA – Humber Arm Allochthon
IRMS – isotope ratio mass spectrometer
MA – 1 million years ago
mol – mole, unit of measurement used to express amounts of chemical substance
MSD – mass spectrometer detector
NS – nipple spring
pH – power of hydrogen, measure of hydrogen ion concentration
RSD – relative standard deviation expressed as per cent (%)
TCD – thermal conductivity detector
TDN – total dissolved nitrogen
TIC – total inorganic carbon
TIN – total inorganic nitrogen
TOC – total organic carbon
TON – total organic nitrogen
TU – tritium units
UV – ultraviolet
V-PDB – Vienna-Pee Dee Belemnite, international isotope ratio standard for carbon
V-SMOW – Vienna-Standard Mean Ocean Water, international isotope standard for hydrogen and oxygen
WHB – Winter House Brook
WHC – Winter House Canyon

List of Appendices

Chapter 1: Introduction

1.1 Study Significance

In geologic settings hydrocarbons can be formed by either biogenic or abiogenic processes and possibly result in accumulation mixtures of the two. Biogenic formation of hydrocarbons can be further divided into microbial or thermogenic processes (Schoell, 1988). The precise reaction pathways of abiogenic hydrocarbons in natural settings are still undefined and establishing reliable recognition criteria is the focus of many current research projects. On the other hand, the geochemical indicators (e.g. hydrocarbon composition and carbon isotopic ratios, presence of biomarkers, presence of particular hydrocarbons with specific conformational isomers etc.) of biogenic hydrocarbons have been well established. Hydrocarbon production in natural settings is dominated by thermogenic and microbial sources (Hunt, 1996; Whiticar, 1999). However, there are geologic settings that provide the required conditions for abiogenic hydrocarbon production within the geosphere (Proskurowski, 2010). These settings need to include an inorganic carbon source, high reducing power (often in the form of substantial H_2), elevated pressure and a catalyst. Ultramafic rocks containing olivine and pyroxene can be altered within the subsurface under pressure and elevated temperatures to magnetite, serpentine and other secondary minerals while producing hydrogen gas in the process. Therefore, sites of active continental serpentinization provide the necessary environmental conditions for abiogenic hydrocarbon production in the subsurface; however these conditions are also amenable for microbial hydrocarbon production at

temperatures <100°C. Furthermore if the necessary sedimentary organic matter lies beneath or above the serpentinizing unit in the stratigraphic sequence there is the potential for thermogenic hydrocarbons as well if upward or downward migration is occurring. Therefore, sites of active continental serpentinization provide an environment that may produce microbial, thermogenic and/or abiogenic hydrocarbons. This provides a unique opportunity to study hydrocarbon production pathways and potentially develop more solid geochemical means to distinguish between these three mechanisms of formation.

1.2 Serpentinization Reaction

Modern oceanic crust and the Earth's upper mantle are composed of mafic and ultramafic rocks, including peridotite, which is dominated by the minerals olivine and pyroxene. These minerals are thermodynamically stable at high temperatures present deep within Earths subsurface. At lower temperatures associated with near-surface environments, these minerals become thermodynamically unstable. Tectonic activity can expose mantle material to shallow environments and cause ultramafic minerals to become unstable and reactive in the presence of water, resulting in mineral alteration. Serpentine minerals (e.g. antigorite, lizardite, and chrysolite) are the most common alteration minerals formed through the hydration of ultramafic rocks, which is why the process is referred to as serpentinization (Schulte et al., 2006). Other important secondary minerals formed through this process are brucite and magnetite. The process of serpentinization can be summarized by the following reaction:

$$\text{olivine} + \text{water} \rightarrow \text{serpentine} + \text{magnetite} + \text{hydrogen} \qquad [1.1]$$

$$6[(Mg_{1.5}Fe_{0.5})_2SiO_4] + 7H_2O \rightarrow 3[(Mg_3Si_2O_5(OH)_4] + Fe_3O_4 + H_2$$
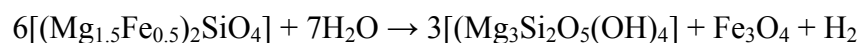
where olivine reacts with the surrounding water to form serpentine, magnetite and hydrogen gas. The oxidation of Fe-bearing minerals (e.g. olivine and pyroxenes) to magnetite and other secondary minerals in ultra-mafic rocks (originating from the Earth's mantle, e.g. peridotite) can be further broken down and represented by 3 general reactions (Schulte et al., 2006). The first reaction is the alteration of forsterite and pyroxene in the presence of water to produce the mineral serpentine (Equation 1.2).

$$\text{forsterite + pyroxene + water} \rightarrow \text{serpentine} \quad\quad [1.2]$$

$$Mg_2SiO_4 + MgSiO_3 + 2H_2O \rightarrow Mg_3Si_2O_5(OH)_4$$

Alternatively, the two end-members of olivine (fayalite and forsterite) can react with water to form minerals serpentine and brucite while producing iron hydroxide as a by-product (Equation 1.3).

$$\text{fayalite + forsterite + water} \rightarrow \text{serpentine + brucite + iron hydroxide} \quad [1.3]$$

$$Fe_2SiO_4 + 5Mg_2SiO_4 + 9H_2O \rightarrow 3Mg_3Si_2O_5(OH)_4 + Mg(OH)_2 + 2Fe(OH)_2$$
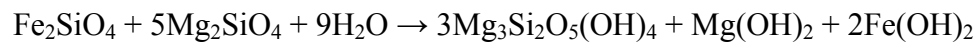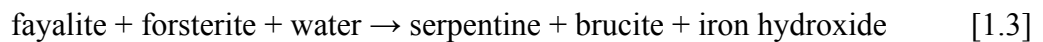
Due to the high solubility of the mineral brucite this reaction contributes OH^- ions to the system resulting in high pH waters. The iron hydroxide formed from the Fe-endmember of olivine in the above reaction can be oxidized to magnetite by the reduction of water to molecular hydrogen (Equation 1.4).

$$\text{iron hydroxide} \rightarrow \text{magnetite + water + hydrogen} \quad\quad [1.4]$$

$$3Fe(OH)_2 \rightarrow Fe_3O_4 + 2H_2O + H_2$$
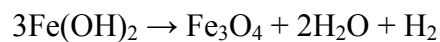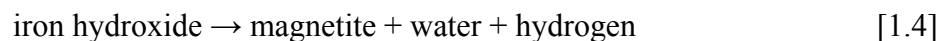
Equation 1.4 produces substantial amounts of hydrogen gas in the fluids associated with the serpentinization reaction.

The reactions involved in the serpentinization process are highly exothermic and in addition to altering ultramafic minerals the process releases substantial amounts of

diatomic hydrogen (H_2) and hydroxide ions (OH^-) creating ultra basic (pH >11-12) and highly reducing (~-650mV) fluids. The geochemically significant waters produced by this hydration reaction are considered extreme for most of life on Earth (Barnes et al., 1967; Sleep et al., 2004). However, the release of H_2 enhances not only the potential for abiogenic hydrocarbon formation, but also facilitates chemolithoautotrophic metabolism by acting as a substrate to generate hydrocarbons (microbial hydrocarbon production) (Kelley et al., 2005; McCollom and Seewald, 2006). Furthermore, these waters can also host and transport thermogenic hydrocarbons if the necessary sedimentary organic matter exists beneath the serpentinizing ultramafic rock. Methane is often associated with serpentinization environments based on its detection at numerous sites of serpentinization, including the Lost City Hydrothermal Field (Kelley et al., 2005; Lang et al., 2010), the Zambales Los Fuegos Eternos ophiolite in the Philippines (Abrajano et al., 1988), and the Tekirova Chimaera ophiolite in Turkey (Hosgormez, 2007). This methane formation requires an available carbon source within the subsurface. In systems of active continental serpentinization, the carbon source could potentially be from the oxidation of organic matter, the thermal breakdown of carbonate or dissolved atmospheric CO_2 from percolated meteoric water.

1.3 Sites of Serpentinization

Serpentinization is a reaction that occurs deep in the subsurface where the hydrothermal circulation of water alters ultramafic minerals found in the lower crust (plutonic rocks) and upper mantle to serpentine minerals. However, this reaction also occurs in near surface environments in both marine and continental systems, where

tectonic processes have uplifted and exposed ultramafic rocks originating from the mantle.

Oceanic tectonic settings, such as spreading ridge networks, fracture zones, non-volcanic passive margins, major transform faults, and subduction zones expose mantle material that can undergo various water-rock interactions, including serpentinization (Fruh-Green et al., 2004; Karson, 1998). Multiple deep-sea hydrothermal fields, including Lost City, Rainbow and Logatchev/Ashadze located along the Mid-Atlantic Ridge are marine systems where exposed mantle outcrops of basalts and peridotites are being serpentinized to create an unique geochemical environment with fluids rich in H_2, CH_4 and higher molecular weight hydrocarbons (Konn et al., 2009; Delacour et al., 2008; Kelley et al., 2005; Sudarikov and Roumiantsev, 2000). Slow spreading ridge environments, such as the Mid Atlantic Ridge, are particularly abundant in ultramafic rocks and support multiple hydrothermal systems and vent fields that are affected by serpentinization. These basalt/peridotite-hosted deep sea hydrothermal systems are just one of many marine environments affected by the process of serpentinization. Others include the Arctic, Antarctica, Mariana forearc, and the Central Indian Ridge network (Schrenk et al., 2013; Edmonds et al., 2003; Dick et al., 2003; Lagabrielle et al., 1998; Fryer et al., 1999). The exposure of fresh and serpentinized mantle-derived ultramafics within the modern oceanic crust is extensive allowing for the *in situ* study of serpentinization and its resulting geochemically significant waters, however, the discovery, accessibility and study of deep sea systems *in situ* is an enormous challenge.

Serpentinization is also occurring in a wide array of different continental systems. Precambrian continental shield rocks found in Canada, Finland, and South Africa have

sealed fracture systems where seawater has been trapped over geologic time scales allowing for extensive water-rock interactions. Among these water-rock interactions is the serpentinization process which occurs in areas where there is a significant proportion of ultramafic rock as seen in the Canadian and Fennoscandian Shields (Sherwood Lollar et al., 2008). These pressurized serpentinizing environments release hydrogen gas and low molecular weight hydrocarbons, potentially generated from abiogenic processes, from fractures and exploration boreholes in gold and base-metal mines (Sherwood Lollar et al., 2006).

Another continental geologic setting that has the potential for serpentinization is ophiolite sequences of the Phanerozoic age. Ophiolite sequences are created through the emplacement of ultramafic rock bodies onto the continental crust through tectonic processes and events including subduction, extension and plume-related events (Dilek and Furnes, 2011; Proskurowski, 2010). As water circulates through the exposed remnants of the seafloor, the process of serpentinization is activated. Ophiolite sequences consisting of exposed peridotites are often associated with geochemically significant fluids that are ultra-basic and highly reducing due to the serpentinization process. Therefore active terrestrial serpentinization springs located in ultramafic rocks at continental ophiolites provide a more accessible opportunity to study *in situ* serpentinization and subsequent hydrocarbon production compared to deep sea hydrothermal vents or deep within the subsurface where similar geochemical conditions are found. The first three well studied ophiolite hosted spring sites associated with serpentinization and hydrocarbon production were: Oman, the Philippines, and Turkey (Abrajano et al., 1988; Fritz et al., 1992; Hosgormez, 2007; Neal and Stanger, 1983). In

the past five years however, many terrestrial peridotite-hosted groundwater springs associated with serpentinization have been identified worldwide and are now actively being studied including the Tablelands at Gros Morne National Park in Newfoundland, Canada and The Cedars located near Cazadero in Northern California, USA.

Ultra-mafic planets in our solar system that contain olivine are also susceptible to the serpentinization reaction in the presence of liquid water. Similar to the modern oceanic crust and mantle material on Earth, the crust and upper mantle of Mars is primarily composed of mafic and ultramafic rocks (Longhi et al., 1992). The discovery of serpentine on the surface of Mars, in various different geologic settings, is cited as evidence of past serpentinization that was active >3-7 Ga in the Naochian time period (Ehlmann et al., 2010). Although there is no evidence of long standing tectonic processes or sustained oceans the process of serpentinization has the potential to play an important role in the circulation of fluids in small planetary bodies in the outer solar system (Vance et al., 2007; Kelley et al., 2005).

While fluid compositions, temperatures and pressures can vary depending on the environmental system (marine vs. continental) and geologic setting, the general geochemical processes and products of serpentinization (H_2 gas, CH_4, serpentine, brucite, and magnetite) remain broadly comparable (Schulte et al., 2006). Within the broader context of serpentinization my research investigates the biogeochemistry and sources of hydrocarbons at these extreme environments to understand sources and fates of carbon in these planetary systems. To achieve these goals, I investigated two continental phanerozoic ophiolite complexes undergoing active serpentinization: The Cedars, California, USA and the Tablelands, Newfoundland, CAN.

1.4 Serpentinization Occurring in Phanerozoic Ophiolite Complexes Found at The Cedars, CA, USA and the Tablelands, NL, CAN

1.4.1 The Cedars, California, United States of America

The Cedars is a partially serpentinized peridotite wedge of the Coast Range ophiolite that was detached, uplifted and incorporated into the Franciscan Subduction Complex (FSC) along the West coast of California, USA, about 170-164 Ma (Figure 1.1) (Coleman, 2000). The Franciscan Subduction Complex is a site of rocks from the Jurassic-Cretaceous period that were tectonically emplaced making up the majority of the Coast Ranges of Western California on the east side of the San Andreas Fault (Oze et al, 2004; Coleman, 2000). The complex of rocks was formed as the ancient oceanic Farallon Plate was subducted beneath the continental North American Plate approximately 200 million years ago. During this subduction event slabs of ultramafic rock and marine sediments of the Farallon Plate were scraped off and accreted to the edge of the North American Plate (Coleman, 2004). Subsequent tectonic activity caused fractures and folding, mixing the deep ocean rocks that included clays and siliceous sediments with basalts and peridotites to form the Franciscan Subduction Complex (Coleman, 2000). As peridotites in this complex came in contact with groundwater at low temperatures the olivine and pyroxenes were altered to form serpentine and other secondary minerals. The mineral alteration associated with serpentinization causes an increase in rock volume and a decrease in overall mass of peridotite wedges (Coleman, 2004; Oze et al., 2004). The volume expansion and the relative low density of the peridotite allowed for its extrusion through more dense material within the complex and its upward diapiric migration towards the surface as it underwent the process of serpentinization (Oze et al., 2004).

Today, The Cedars is a partially serpentinized peridotite wedge exposed at the surface

standing 518 to 670 meters in elevation with deeply cut canyons and talus slopes (Raiche,

2009). The peridotite is approximately 1 km in depth and is cradled by a mélange of

argillaceous marine sediments (Coleman, 2000). The Cedars was the first site where

modern continental serpentinization at shallow depths and lower temperatures was

described (Barnes et al., 1967).

The peridotite located at The Cedars was chosen as the standard (Peridotite Cedars

Cazadero 1 (PCC1)) to which all other peridotites would be compared and thus its

mineralogy and rock geochemistry is well characterized (Flanagan, 1969). The primary

minerals at The Cedars are olivine, orthopyroxene and clinopyroxene which in varying

proportions make the peridotite primarily composed of depleted harzburgite and dunite

(Coleman, 2000). It has been documented that 5-20% of the central ultramafic body of

The Cedars peridotite wedge has been altered to form serpentine minerals along with

100% of its contact with the surrounding rock (Coleman, 2004). Fluids associated with

serpentinization that are ultra-basic (pH>11) and highly reducing (<-500 mV) have been

identified discharging from multiple springs at The Cedars (Barnes et al., 1967; Barnes

and O'Neil, 1969).

1.4.2 Tablelands, Newfoundland, Canada

The Tablelands, also known as the Table Mountain massif, is one of four

Ordovician ophiolites that make up the Bay of Islands Complex (BOIC) which runs along

the west coast of Newfoundland, Canada in the Humber Arm Allochthon (HAA) tectonic

zone (Figure 1.2) (Suhr and Cawood, 1993). The Humber Arm Allochthon is a mixture of

deep sea sediments, mafic crustal material and mantle peridotites from the ancient

seafloor that was assembled and obducted onto the eastern edge of the North American

Craton about 500 MA as the Iapetus Ocean was closing during the Taconian orogeny

(Suhr and Cawood, 1993; Suhr, 1992). The Bay of Islands Complex of the Humber Arm

Allochthon is in its current position due to tectonic reactivation during the Acadian

orogeny which began in the Middle Devonian and climaxed in the early Late Devonian

(Suhr, 1992). The four massifs from north to south that make up the Bay of Islands

Complex are Table Mountain, North Arm Mountain, Blow-Me-Down Mountain and

Lewis Hills (Suhr, 1992). All massifs are associated with mantle and crustal rocks and

some contain a near complete sequence of the ophiolite. At the Tablelands, only

ultramafic rocks and ultramafic to gabbroic lower crustal material is preserved, which is

the lower portion of the ophiolite sequence. Although all massifs within the ophiolitic

complex contain exposed mantle peridotites along the eastern side, the Tablelands massif

has the thickest mantle section of the Bay of Islands Complex preserved (Suhr, 1992).

Enclosing the mantle peridotite at the Tablelands is a mélange of argillaceous marine

sediments and siliciclastic marine sandstones.

The mantle peridotite located at the Tablelands is classified as harzburgite and

lherzolite, which have varying proportions of the ultramafic minerals olivine,

orthopyroxene and clinopyroxene (Suhr, 1992). Groundwater supplied by the last

glaciation (ending ~12,000 years ago) circulated through the unaltered peridotite rock,

and activated the serpentinization process which created springs of highly reducing

(~ -600mV) and ultra-basic (pH >11) waters rich in hydrogen gas, methane and other low

molecular weight hydrocarbons (C_2-C_6) (Szponar, 2012). These geochemically significant

fluids have been identified discharging from multiple active springs in pools of water surrounded by travertine deposits at the Tablelands. While the extent of serpentinization of the peridotite is unknown, evidence of the reaction can be seen on the face of loose peridotite rocks where serpentine minerals have been formed. The volume expansion and fracturing nature of the serpentinization process has resulted in large talus slopes along the sides of the Tablelands massif.

Both The Cedars and the Tablelands have springs of highly reducing and ultra-basic waters that are rich in hydrogen gas and hydrocarbons. These hydrocarbons may have been formed through abiogenic and/or biogenic processes. The harsh conditions created by the serpentinization process are amenable for abiogenic hydrocarbon synthesis, as they provide the necessary requirements for some hydrothermal abiotic reactions. This environment also facilitates chemolithoautotrophic metabolism, creating the potential for microbially derived hydrocarbons to exist. Furthermore, both of these geologic settings facilitate the mobilization of hydrocarbons from the sedimentary organic matter that is buried underneath the serpentinizing peridotite, making it possible for the formation of hydrocarbons from thermogenic processes. The unique natural settings and accessibility of these sites provide an ideal research site for extensive geochemical work on active continental serpentinization and subsequent hydrocarbon production.

1.5 Hydrocarbon Sources

Hydrocarbon compounds are made up of different proportions of the elements carbon and hydrogen. In geologic settings there are three broad mechanisms of hydrocarbon formation: "microbial", "thermogenic" and "abiogenic" (Schoell, 1988).

Microbial hydrocarbons are formed either through biosynthesis or microbial metabolic processes such as methanogenesis (Hinrichs et al., 2006; Whiticar, 1999). Thermogenic hydrocarbon production results from the transformation of sedimentary organic matter through temperature controlled chemical reactions, such as the "cracking" of kerogen (Hunt, 1996). Both of these hydrocarbon production pathways are referred to as "biogenic" as both types involve biological material. Lastly, abiogenic refers to the synthesis of hydrocarbons from inorganic starting materials through chemical reactions under geologic conditions that are independent of biological activity. One example is the Fischer-Tropsch Type (FTT) reaction (Foustoukos and Seyfried, 2004; McCollom and Seewald, 2006; Proskurowski et al., 2008).

1.6 Hydrocarbon Production at Continental Ophiolite Hosted Springs Associated with Serpentinization

Serpentinization reactions alone do not form hydrocarbons, however, the products of serpentinization and the geologic setting (elevated temperatures) in which these reactions can take place increase the potential for the synthesis of hydrocarbons. The highly reducing conditions of the groundwater associated with serpentinization create conditions that are suitable for abiogenic and/or microbial hydrocarbon production. Additionally, the placement and fractured nature of the peridotite bodies, where both volume expansion is occurring and heat is being produced, where the serpentinization springs are discharging allow for thermogenic hydrocarbon formation and mobilization. Therefore sites of serpentinization are locations where hydrocarbons could potentially be

formed by microbial (up to temperatures of approximately 100°C), thermogenic, and/or abiogenic processes.

Abiogenic hydrocarbons are formed by the reduction of inorganic carbon to form methane and longer-chained hydrocarbons through a variety of reactions independent of microbial processes. With catalytically active metals present within the system reactions such as Fischer-Tropsch Type synthesis, iron carbonate decomposition or other vapour-water-rock interactions can form abiogenic hydrocarbon gases (Foustoukos and Seyfried, 2004; McCollom, 2003; McCollom and Seewald, 2001). The simplest reaction for abiogenic hydrocarbon formation is the reduction of inorganic carbon (primarily CO_2) by H_2 to form methane (Equations 1.5 & 1.6).

$$CO_2 + 4H_2 \rightarrow CH_4 + 2H_2O \qquad\qquad [1.5]$$

$$CO + 3H_2 \rightarrow CH_4 + H_2O \qquad\qquad [1.6]$$
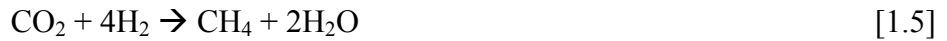
Higher molecular weight hydrocarbons can be further synthesized from methane in crustal environments through abiotic methane polymerization reactions (McCollom, 2013; Sherwood Lollar et al., 2008) (Equation 1.7).

$$nCH_4 \rightarrow C_nH_{n+2} + (n-1)H_2 \qquad\qquad [1.7]$$

Abiotic experiments, conducted by Morrill et al. (submitted), have also demonstrated higher molecular weight (propane, n-butane and n-pentane) synthesis using methylene monomers in a series of catalytic reactions following the general Fischer-Tropsch Type polymerization reaction (Equation 1.8).

$$(C_xH_{2x+1}) + (CH_2) \rightarrow (C_{x+1}H_{2x+3}) \qquad\qquad [1.8]$$

In natural settings, these reactions are largely dependent on the reducing power of the fluid which ultimately depends on the concentration of H_2 produced through water-

rock interactions (Proskurowski, 2010). The reduced ferrous iron (Fe II), found in olivine and pyroxenes, in serpentinization reactions provides an ideal reductant to convert H_2O to H_2, creating the ultra-reducing environment necessary for these reactions. In addition to reducing conditions these reactions also require elevated temperatures and catalysts such as iron or magnesium. It has recently been discovered that Fischer-Tropsch Type reactions can proceed under aqueous hydrothermal conditions, with dissolved CO_2 as a carbon source to form hydrocarbons (Foustoukos and Seyfried, 2004; McCollom and Seewald, 2006), which makes this reaction most applicable to sites of serpentinization. However, the production of hydrocarbons can be one or a combination of several possible abiotic reaction mechanisms.

The harsh and highly reducing conditions in fluids associated with serpentinization can support multiple metabolic strategies that include the cycling of hydrogen, methane, sulfur, and fermentative processes at lower temperatures (<121°C) (Schrenk et al., 2013). Microbial cycling of sulfur is more likely in marine systems where sulfate is abundant. In fresh water systems at continental settings, such as The Cedars and the Tablelands, sulfate concentrations are generally low (Barnes et al., 1978; Marques et al., 2008; Cipolli et al., 2004) making sulfate a more difficult metabolic strategy to sustain. The abundant H_2 and CH_4 in groundwater fluids inevitably create an energy rich environment for autotrophic and heterotrophic microorganisms to carry out metabolic processes using H_2 as an electron donor or CH_4 as a carbon and/or energy source (Brazelton et al., 2012; Schulte et al., 2006). Conversely, this anaerobic environment can also support the production of CH_4 and H_2 through metabolic processes associated with fermentation and methanogenesis (Brazelton et al., 2012; Kelley et al., 2005; Schulte et

al., 2006). The two most common methanogenic processes observed in nature are CO_2 reduction (Equation 1.9), and fermentation of acetate (Equation 1.10) (Wiese and Kvenvolden, 1993; Hunt, 1996; Schoell, 1988).

$$4H_2 + CO_2 + 8e^- \rightarrow CH_4 + 2H_2O \qquad [1.9]$$

$$CH_3COOH \rightarrow CH_4 + CO_2 \qquad [1.10]$$
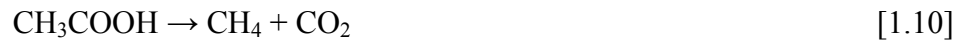
Microorganisms may be able to form methane at sites of serpentinization using the H_2 produced as an electron donor to reduce carbon dioxide (CO_2) to generate methane and water. Organic compounds, such as acetate can also be used as a substrate for microbial metabolism to generate methane, ethane, propane (Hinrichs et al., 2006; Taylor et al., 2000; Whiticar, 1999) and possibly higher molecular weight hydrocarbons. Other organic compounds, including formate, methanol, and monomethylamine, can also be used as the organic substrate for methanogenic processes (Wiese and Kvenvolden, 1993). Organic acids acetate and formate have been detected at the Lost City Hydrothermal Field, so there is the potential for these organic acids to also exist in terrestrial serpentinizing systems (Lang et al., 2010).

Although serpentinization systems have copious amounts of energy and electron donors available the high pH and limitations of bicarbonate, electron acceptors and nutrients create a harsh environment in which only extremophiles can survive. The generation of adenosine triphosphate (ATP) is governed by a proton motive force across the cytoplasmic membrane, but in high pH conditions, like in spring fluids at The Cedars and the Tablelands, the maintenance of this gradient becomes difficult (Schrenk et al., 2013). Ionic gradients involving K^+ or Na^+ have been used as a substitution mechanism to generate adenosine triphosphate by alkaliphiles in alkaline soda lakes (Krulwich, 1995);

however the ionic strength of spring fluids discharging from continental serpentinizing ophiolites is low as seen in Oman (Barnes et al., 1978), Portugal (Marques et al., 2008), and Italy (Cipolli et al., 2004). High pH conditions can also compromise the stability of ribonucleic acid (RNA) which is essential for gene maintenance (Schrenk et al., 2013).

In addition to being ultra-basic, fluids associated with serpentinization in continental settings typically exhibit a low bicarbonate (HCO_3^-) concentration, which is problematic for autotrophic microorganisms. The addition of inorganic carbon from the mixing of shallow fluids containing dissolved atmospheric CO_2 will precipitate as solid carbonate with the abundant Ca^{2+} that exists in spring fluids making it unavailable for microbial usage. Moreover, what limited inorganic carbon that does exist is predominantly in the divalent form carbonate (CO_3^{2-}) and its transformation into more reduced forms of hydrocarbons would involve currently unknown biological fixation pathways. In serpentinizing systems the amount of organic carbon is generally greater and more accessible than inorganic carbon suggesting heterotrophic metabolic pathways will dominate in subsurface fluids associated with serpentinization. Although subsurface fluids associated with serpentinization are generally rich in electron donors, with H_2 and CH_4 gas being the most obvious and abundant, the availability of electron acceptors is usually limited, especially in continental settings (Barnes et al., 1978; Fritz et al., 1992; Cipolli et al., 2004). Nutrients are also limited in continental serpentinite springs like seen in the Cabeço de Vide ophiolite in Portugal (Marques et al., 2008), which can make assimilation for the production of biomass difficult.

Despite all these limitations sites of serpentinization provide copious amounts of energy and reducing power supporting both *Bacteria* and *Archaea*. Cell densities of

serpentinization fluids are typically low ($\leq 10^5$ cells/ml), as seen at the Jordan Maqarin M6 site where the reported cell abundances for spring fluids was 2.4×10^4 cells/ml (Pederson et al., 2004). In habitats, where serpentinization fluids mix with an alternative water source associated with surface processes a greater biomass is reported (Schrenk et al., 2013). Chemical disequilibria that are created through the mixing of different ground waters increases the chance of survival within the subsurface and provides the best conditions for microbial growth (Schrenk et al., 2013). Furthermore, some microorganisms can utilize minerals in the surrounding ultra-mafic rocks and carbonates to extract and exploit their inorganic carbon content and provide themselves with available electron acceptors (Schrenk et al., 2013). The following more in depth look at the aqueous geochemistry of these distinct fluids can provide insight into how these microbes may be contributing to hydrocarbon production and how they are surviving in such extreme environments.

The geologic setting at The Cedars and the Tablelands (i.e. ophiolites) in which present-day continental serpentinization occurs also allows for thermogenic hydrocarbon production; namely catagenesis. During the obduction of mantle (ultramafic) rock, carbonaceous rock units containing marine or terrestrial sedimentary organic matter can be trapped underneath and buried within the Earth's crust. These rocks may contain large amounts of organic matter, which when buried and subjected to high temperatures (>70°C) crack to form hydrocarbons through a variety of maturity reactions (Hunt, 1996). Thermogenic gases produced through the thermal degradation of sedimentary organic matter can be classified as wet or dry depending on its hydrocarbon gas composition. Wet thermogenic gas generated in the oil window contains significant concentrations of higher

molecular weight hydrocarbons (C_2-C_4) and condensate (C_{5+}) hydrocarbons in addition to methane and is often associated with earlier stages of maturity. Dry thermogenic gas generated after the oil window is almost entirely composed of methane and associated with thermally late or over-mature systems (Hunt, 1996). The volume expansion associated with the hydration of ultramafic rocks in the overlying bedrock (serpentinization process) results in extensive fracturing systems, which allow for the upward migration of these thermogenic gases and possible discharge at serpentinization springs (Barnes et al., 1967; Schulte et al., 2006).

1.7 Distinguishing Between Hydrocarbon Sources

At sites of continental serpentinization, all three mechanisms (abiogenic, microbial, and thermogenic) of hydrocarbon formation are possible, and more than one mechanism may be contributing simultaneously. The geochemical signatures of abiogenic gaseous hydrocarbons formed in nature are still under development and there is currently no single reliable measurement or analysis that can distinguish between all these different sources. Consequently, multiple lines of geochemical evidence must be used and all production mechanisms must be considered when sourcing hydrocarbons at The Cedars and the Tablelands.

Most studies focus on methane when trying to source hydrocarbon gases. A geochemical technique that is commonly used to differentiate between methane gas sources is stable isotope ratios of carbon ($^{13}C/^{12}C$) and hydrogen (D/H). Fractionation between the heavy and light isotopes of carbon and hydrogen are different for biological and physical processes (Hunt, 1996), which can give an indication of the hydrocarbon

source. On a CD diagram (δ^2H_{CH4} versus $\delta^{13}C_{CH4}$) for example, as seen in Figure 1.3, stable isotope values can distinguish between different metabolic pathways of microbial methane (CO_2 reduction and fermentation processes) and thermogenic gases. Additional studies and the identification of putative abiogenic hydrocarbons have blurred the boundaries of these traditional fields resulting in the overlap of microbial, thermogenic and abiogenic methane. Due to fields being non-exclusive a CD diagram can not be used alone to distinguish between methane sources.

A plot of $\alpha C_{DIC\text{-}CH4}$ vs $\alpha H_{H2O\text{-}CH4}$ also uses stable isotopic values to distinguish between different sources of methane. The microbial fields used in this plot are based on work by Whiticar et al. (1986) and Valentine et al. (2004) and putative abiogenic hydrocarbons from the Precambrian shield have subsequently been added (Sherwood Lollar et al., 2008). Stable isotope values alone are not always enough to unequivocally demonstrate abiogenic or biogenic hydrocarbon production, as large fractionation ranges can cause different sources to overlap. There may also be a mixing of hydrocarbons formed by different mechanisms, which can alter the isotope data measured.

Another line of evidence that is frequently used is the proportion of methane in relation to other hydrocarbons of a longer chain length (C_{2+}) on a volume percentage basis which is described as a modified Bernard parameter or wetness parameter: C_{CH4}/C_{2+} (Hunt, 1996). The combination of the $\delta^{13}C$ of methane with the modified Bernard parameter (C_{CH4}/C_{2+} vs. $\delta^{13}C_{CH4}$) is used to discriminate between microbial and thermogenic hydrocarbons (Hunt, 1996) as seen in Figure 1.4. Methane produced through microbial processes have a more negative $\delta^{13}C$ value and a higher CH_4/C_{2+} ratio (>10000)

compared to the less negative $\delta^{13}C$ value and lower CH_4/C_{2+} ratio (<100) of methane produced by thermogenic processes. An abiogenic field is not plotted on the modified Bernard plot because the range of abiotic $\delta^{13}C_{CH4}$ is still under investigation and the $\delta^{13}C_{CH4}$ of laboratory studies is not comparable to field studies. However, multiple experimental studies have shown that abiogenic methane has a CH_4/C_{2+} ratio of 30 or less (Fu et al., 2007; Taran et al., 2007; McCollom and Seewald, 2006; Lancet and Anders, 1970). A modified Bernard plot can not be used as a sole diagnostic tool in sourcing methane as microbial methane in some environments have been found to plot outside the traditional microbial field (Tazaz et al., 2013), highlighting the importance of supporting evidence so that data is not misinterpreted.

Isotopic trends of $\delta^{13}C$ and δ^2H with the increasing chain length of linear alkanes (C_1-C_5) are also used to determine the origin of hydrocarbon gases (Proskurowski, 2010). Thermogenic C_1-C_6 alkanes exhibit a general trend of isotopic enrichment of $\delta^{13}C$ with increasing molecular mass due to ^{12}C-^{12}C bonds breaking faster than ^{13}C-^{12}C bonds leaving residual alkanes enriched in ^{13}C (Des Marais et al., 1981; Sherwood Lollar et al., 2006). Abiogenic C_2-C_5 alkanes on the other hand have been suggested to have an isotopic depletion relative to the methane precursor due to ^{12}C-^{12}C bonds forming faster compared to bonds formed with the heavier ^{13}C (Proskurowski et al., 2008; Sherwood Lollar et al., 2008; Sherwood Lollar et al., 2002). These general trends are not definitive as some abiotic experimental studies have shown $\delta^{13}C$ enrichment from methane to ethane and subsequent alkanes through Fischer-Tropsch Type synthesis (Morrill et al., submitted; Taran et al., 2010; Fu et al., 2007).

A Schulz-Flory distribution (log mole fraction versus carbon number) of alkanes C_1-C_5 that yields a correlation coefficient of 0.99 or greater has been proposed to indicate a quasi-pure abiogenic gas (Etiope and Sherwood Lollar, 2013). The positive correlation of the distribution is based on the chain growth probability in the step-wise polymerization of hydrocarbon homologues associated with abiotic reactions (Schulz, 1999). While such a distribution is typical of abiogenic gases formed through Fischer-Tropsch Type synthesis, similar distributions have been observed in natural gases that were formed through the thermal degradation of organic matter (Giggenbach, 1997).

Most studies aiming to distinguish between different sources of hydrocarbon production have primarily focused on methane and C_1-C_5 alkane homologues. There is little data or characterization of organic acids and higher molecular weight hydrocarbons (semi- and non volatiles) at sites of continental serpentinization. This M.Sc. thesis began to bridge this gap in knowledge by focusing on and characterizing a suite of higher molecular weight hydrocarbons discharging from springs at The Cedars and the Tablelands in addition to the conventional low molecular weight hydrocarbons. The application of a 2-component linear mixing model furthered the geochemical understanding of this unique environment and the source of hydrocarbons discharging at serpentinization springs. Hydrocarbon gases discharging at surface springs are difficult to source as migration patterns can alter molecular and isotopic distributions stressing the need for multiple lines of evidence for the souring of hydrocarbons.

1.8 Objectives and Outline of Study

Currently compositional data and isotopic analysis of hydrocarbon gases found at sites of serpentinization are used in an attempt to identify carbon sources and distinguish between different pathways of hydrocarbon formation (Horita and Berndt, 1999; McCollom and Seewald, 2006; Schoell, 1988). However, most geochemical analysis of the hydrocarbon gases are focused on methane and lower molecular weight hydrocarbons, neglecting the longer chained hydrocarbons (e.g. C_{5+}). The characterization and geochemical analysis of the sedimentary organic matter that frequently also exists in ophiolite sequences associated with continental sites of serpentinization has also been unexplored in the context of sourcing hydrocarbons. Furthermore, there is a lack of data and understanding on the macro-nutrients and electron acceptors essential to microbial communities that have been detected in spring fluids associated with continental serpentinization.

This study focused on ultra-basic and highly reducing springs at two continental sites of serpentinization: The Cedars and the Tablelands. The overall aim of this study was to investigate the geochemistry and habitability of these unique fluids as well as characterize the metabolic pathways in this ecosystem and investigate how inorganic and organic pathways interact. The first objective in this investigation was to geochemically characterize the fluids at each site using multiple inorganic geochemical parameters including pH, E_h, conductivity and ionic content. The second objective was to source the hydrocarbons discharging at springs. This was achieved through the analysis of compositional and isotopic distributions of low molecular weight hydrocarbons (C_1-C_6), as well as the identification and composition of semi- and non volatiles including organic

acids. The carbon isotopic signature of sedimentary organic matter from the sedimentary rocks cradling the ultramafics, where springs are discharging was also correlated with observed hydrocarbon gases to further determine potential hydrocarbon sources. Lastly, the third objective was to evaluate the habitability of spring fluids by investigating the macro-nutrients and electron acceptors which can help shed light on how microorganisms are surviving in such an extreme environment (e.g. pH values of >11 and E_h values of <-500 mV) and whether they are contributing to the formation of hydrocarbon gases. All geochemical analysis was put into perspective using a 2-component mixing model (described in Chapter 2) which further aided in the overall understanding of hydrocarbon gas origins and the habitability of spring fluids.

1.9 Contributions to the Field of Natural Science

Subsurface environments such as serpentinizing ultramafic rocks produce substantial reducing power and contain a large reservoir of carbon which has the potential to host a vast microbial diversity and ample biomass; however systems such as these in the subsurface are some of the least understood (Brazelton et al., 2012). The springs in this study are windows into the subsurface biogeochemical cycles of a largely unknown subsurface biosphere (Brazelton et al., 2013). Investigation into the geochemical constraints on habitability of these springs can help put microbiological data from collaborators into perspective and aid in the overall understanding of survival in this harsh environment.

Sites of continental serpentinization are considered analogue sites for both early Earth and Mars (Schulte et al., 2006). Similar to sites of serpentinization the crust and

upper mantle of Mars is comprised of ultra-mafic rock (Boston et al., 1992; Formisano et al., 2004), which has been suggested to be undergoing serpentinization due to the constant detection of putative methane in the atmosphere. Similarly the reducing conditions associated with the alteration of minerals at sites of active serpentinization is thought to be very similar to conditions that were widespread and prevalent on early earth (Schulte et al., 2006; Sleep et al., 2004). The reducing conditions of early Earth suggest that the first microorganisms had to rely on chemical forms of metabolic energy through chemosynthesis reactions (Schulte et al., 2006). Thus studying environments which presently have similar geochemical conditions can have implications for early life. Additionally the lack of detected photosynthetic life on the surface of Mars suggests that if life were to exist on the planet they would also rely on chemosynthesis (Schulte et al., 2006). Therefore the study of serpentinizing systems can have implications for geochemical processes and life on early Earth as well as on Mars.

1.10 Tables and Figures
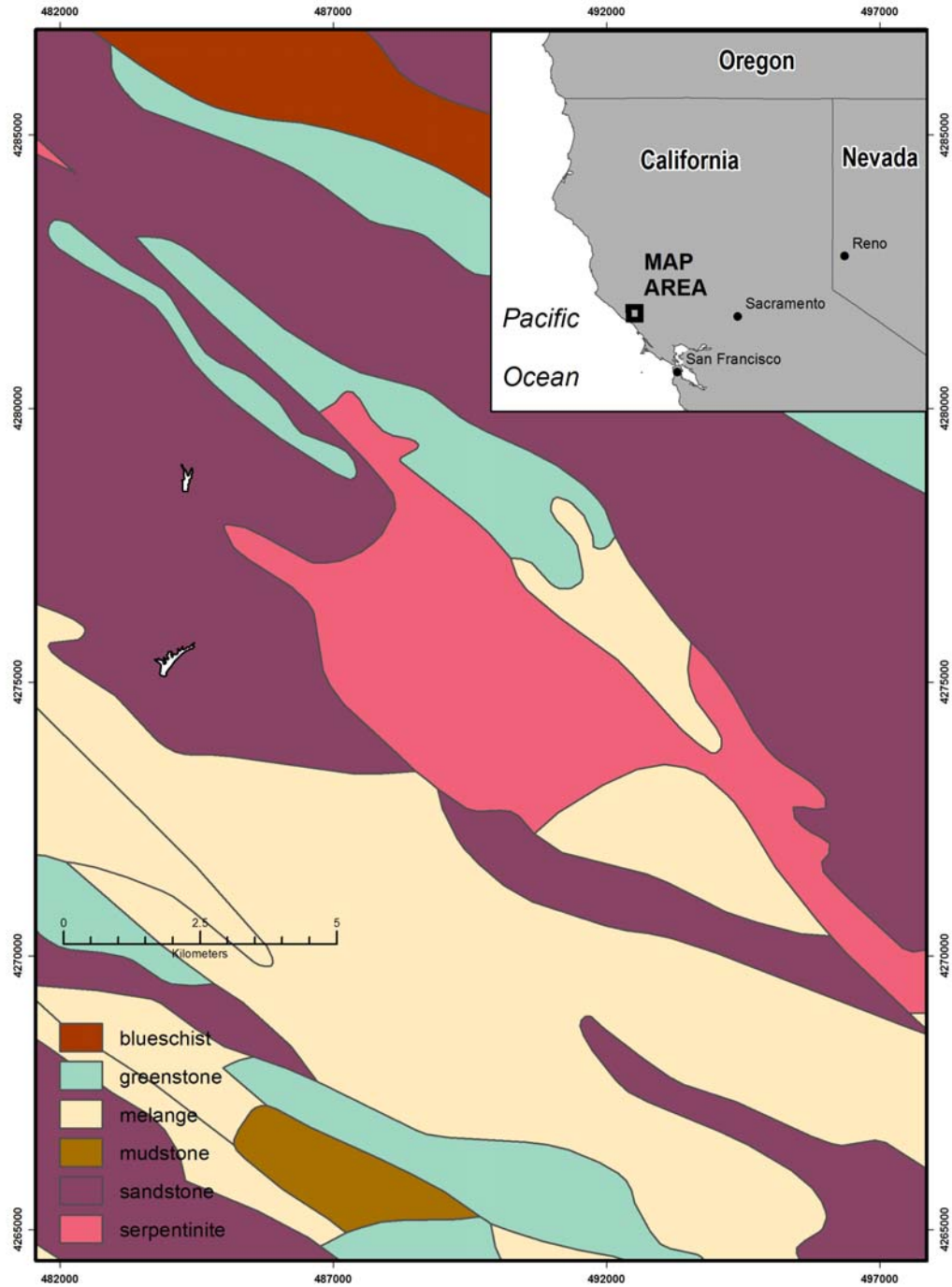
Figure 1.1. Geologic map of The Cedars peridotite showing the surrounding geology within the Franciscan Subduction Complex (FSC) located on the west coast of California, USA. The Cedars peridotite wedge is surrounded and cradled by siliceous and argillaceous marine sediments that originated on the deep seafloor. Source data from USGS (http://geonames.usgs.gov/apex/f?p=132:LOGIN:29910277482038).
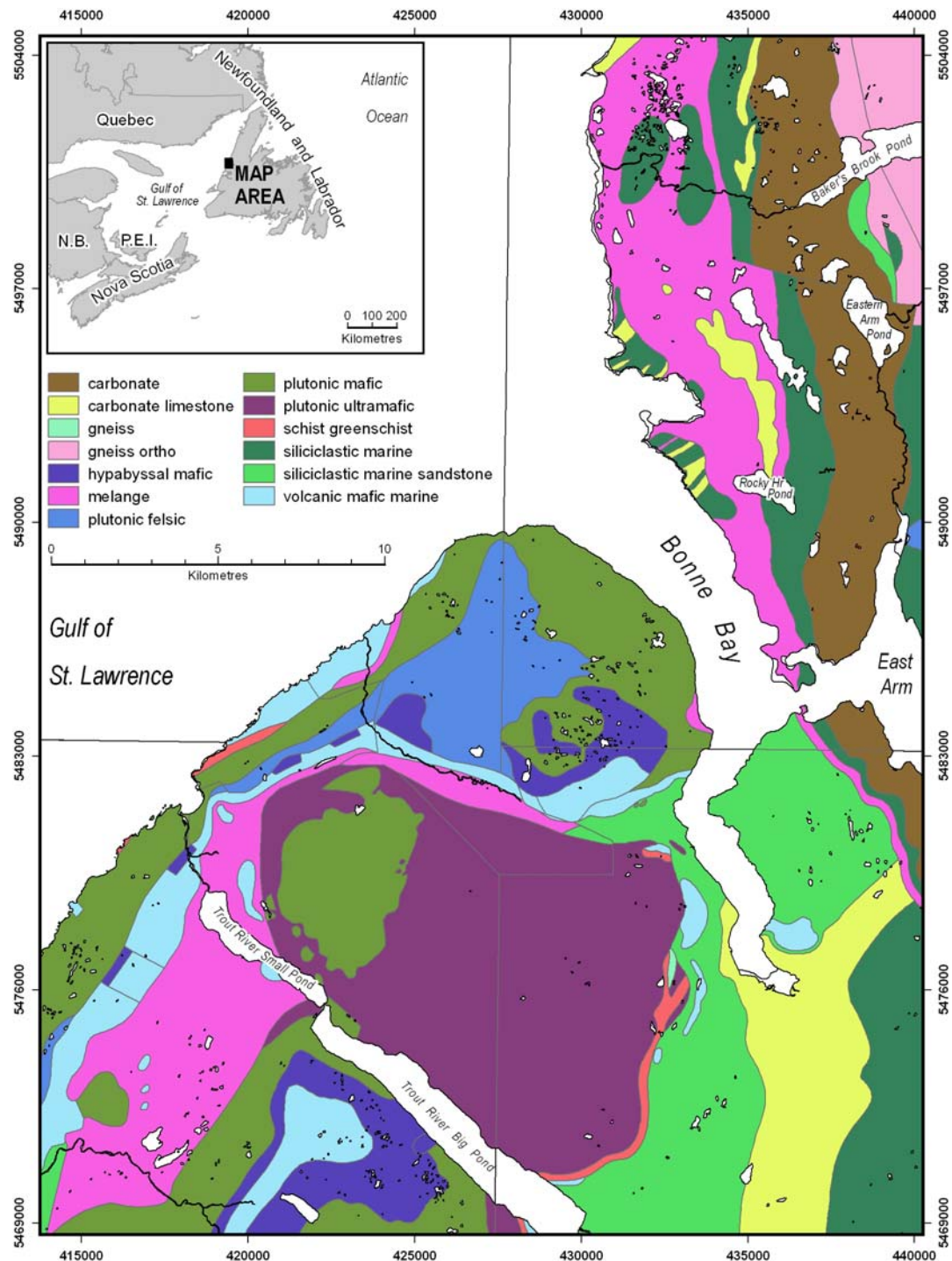
Figure 1.2. Geologic map of the Tablelands showing the surrounding geology of the Humber Arm Allochthon (HAA) located on the west coast of Newfoundland, CAN. The Table Mountain massif is surrounded and cradled by a mélange of argillaceous marine sediments and siliciclastic marine sandstones that originated on the deep seafloor. Source data from NL survey (http://gis.geosurv.gov.nl.ca/) and the federal Department of Natural Resources (http://geogratis.gc.ca/site/eng/extraction?id=2013_51d579a832fb79.569414).
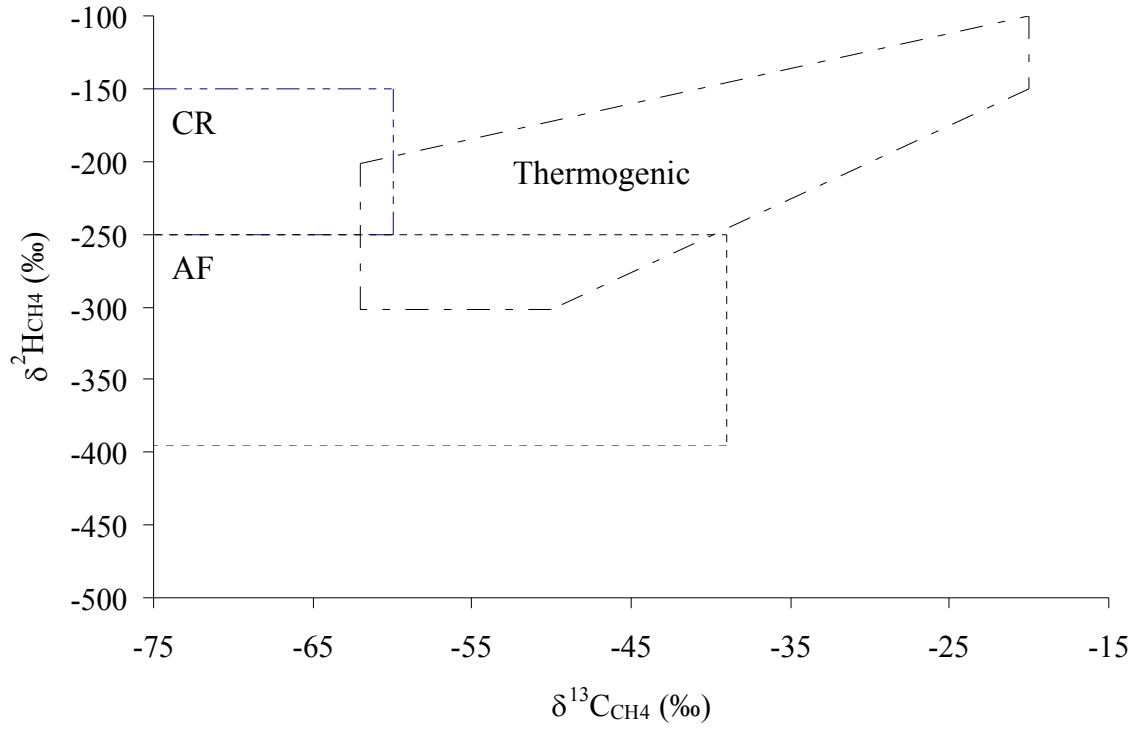
Figure 1.3. A CD diagram (δ^2H_{CH4} versus $\delta^{13}C_{CH4}$) with conventional microbial (CR=CO_2 reduction, AF=acetate fermentation) and thermogenic fields.
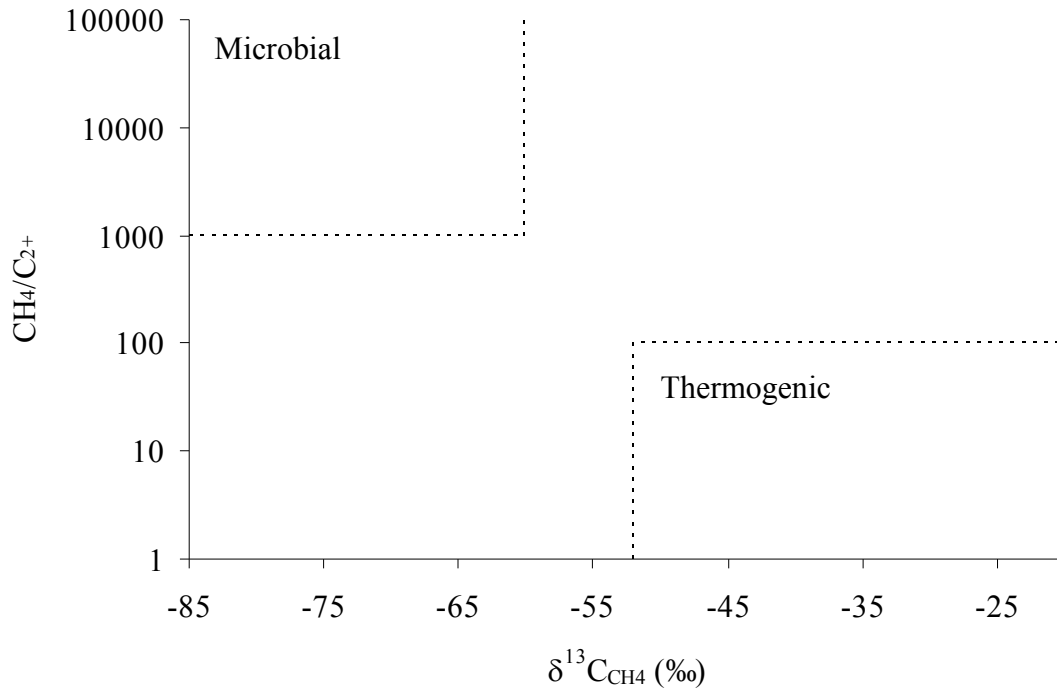
Figure 1.4. A modified Bernard plot of CH_4/C_{2+} ($C_{2+}=C_2+C_3+nC_4$) versus $\delta^{13}C_{CH4}$ with conventional microbial and thermogenic fields.

Chapter 2: Sampling and Analytical Methods

2.1 Sampling Locations and Dates

Three sampling trips to The Cedars and two sampling trips to the Tablelands were taken to ensure that data was consistent throughout the years and to determine any annual changes in aqueous geochemistry. Various springs were sampled on each sampling trip to identify any geochemical differences and to investigate any migratory differences between spring fluids and whether hydrocarbon sources were uniformly distributed within the subsurface.

2.1.1 The Cedars

Highly reducing and ultra-basic springs were discharging from partially serpentinized peridotite rocks located in The Cedars ophiolite located at N 38°37'14.84" W 123°08'02.13" (NAD27 Canada projection was used for all reported co-ordinates) in Northern California close to the Russian River (Figure 2.1). All of the springs sampled for this study were found in the headwaters of Austin Creek which flows through the ultra-mafic peridotite of The Cedars ophiolite (Figure 2.2). Photographs of the ultra-basic springs and all other aqueous sampling locations can be found in Figure 2.3. The Barnes Spring Complex (BSC) which encompassed multiple ultra-basic springs was located in the Main Canyon in a separate tributary (elevation 282 m, N 38°37'17.8" W 123°07'53.5") which flowed into Austin Creek. There were several discharge points in close proximity in the BSC. The ultra-basic springs from the BSC sampled for this study

were BS9, BS5 and BS7 and their orientation within the complex can be seen in Figure 2.3A. The discharge points of the springs in the BSC were located at the bottom of pools of ultra-basic (pH >10) water. The BS5 pool was 38.5 cm deep, the BS7 pool was about 189 cm deep, and the BS9 pool was 12.5 cm deep. The non ultra-basic water for this study was sampled from a branch of Austin Creek (AC) which flowed adjacent to the BSC (Figure 2.3D). Nipple Spring (NS1 and NS2) was located in an upstream tributary located in Mineral Spring Canyon (elevation 321 m, N 38°37'22.2" W 123°08'02.8") that flowed into Austin Creek. There were two discharge points for this spring. One discharge point was found at the top of a carbonate mound (NS1) which stood approximately 40 cm above the adjacent stream. The highly reducing fluid flowed out of a round opening with a diameter of ~1.5 cm. A second discharge point which was sampled for bubbling gases was found at the bottom of a small pool of water (NS2) located next to the mound as seen in Figure 2.3B. The Grotto Pool Spring (GPS1) was located downstream in Austin Creek (elevation 273 m, N 38°37'16.3" W 123°08'01.1") about 65 m from the intersection of the Main Canyon tributary stream. The discharge point of GPS1 was above the adjacent non ultra-basic water flowing from a small opening into the down-stream pool of water (Figure 2.3C).

This study consisted of 3 sampling trips from 2011 to 2013. In October of 2011 the following springs were sampled: BS9, BS5, BS7, NS1, and GPS1 along with non ultra-basic (pH ~9) water from Austin Creek. In June of 2012 springs BS5, NS1, GPS1 and water from Austin Creek were sampled. In June of 2013 springs BS5, NS1 and GPS1, as well as, Austin Creek were sampled. In 2013, *in situ* aqueous measurements were also measured at springs BS7 and BS9 to observe any annual changes. The sampling

campaign in 2013 was based on previous results and was used to collect samples or *in situ* data that were not attained in previous years. GPS1 and NS1 were sampled directly from their points of discharge. Samples for BS9, BS5, and BS7 were collected as close to the discharge point of the ultra-basic fluid as possible, which was identified by low E_h (<-419 mV) readings and where bubbling gas was observed. Water from Austin Creek was sampled from the flowing Creek. Table 2.1 summarizes the sampling seasons, spring sampled, and corresponding analyses for each spring at The Cedars.

2.1.2 The Tablelands

The Tablelands ophiolite in Gros Morne National Park contains ultra-basic reducing fluids discharging from peridotite rocks located at N 49°27'58.9" W 057°57'29.1" (Figure 2.4). Winter House Brook (WHB) flows along the bottom of Winter House Canyon (WHC). The ultra-basic springs sampled in this study are located along the bottom of Winter House Canyon (Figure 2.5). Photographs of the ultra-basic springs and all other aqueous sampling locations can be found in Figure 2.6. Non ultra-basic water was sampled from Winter House Brook (N 49°27'58.9" W 057°57'28.6"). About 5 m down stream from the Winter House Brook sampling site adjacent to the brook was a pool of water labelled WHC2 (N 49°27'58.7" W 057°57'29.2") which had two ultra-basic discharge points. This pool of water was approximately 130 cm wide and 40 cm deep surrounded by travertine deposits and is exposed to the atmosphere at the surface (Figure 2.6B). A more detailed drawing of the WHC2 pool can be seen in Figure 2.7. Within this pool two springs located at the bottom of the pool were identified by low E_h values and were labelled A and B (i.e. WHC2A and WHC2B). An additional sampling location

labelled C (WHC2C) represented a mixing site where water from overland flow was flowing into the highly reducing pool of water. I studied WHC2C to observe the effects of overland flow of non-ultra basic, oxic waters on the geochemistry and microbiology of the ultra-basic reducing fluid discharging from below. Another pool was identified in another travertine deposit only ~ 1.5 m from WHC2 labelled WHC1 (N 49°27'58.9" W 057°57'29.0") (Figure 2.6D). This sampling site was a small oval shaped 5 cm wide and 2 cm deep pool with a recharge rate of 1 mL/min (Szponar et al., 2013). Ultra-basic fluid discharged into the WHC1 pool 6 through the WHC1 travertine deposit and there were no overland flow inputs observed, however the pool of water was oxidized quickly due to its exposure to atmosphere, low flow rate, and small volume.

This study consisted of 2 sampling trips in 2011 and 2012. In June of 2011, the following springs were sampled: WHC2A, WHC2B, and WHC2C along with Winter House Brook for non ultra-basic water. In October of 2012, springs WHC2A, WHC2B, WHC2C, WHC1 and water from Winter House Brook were sampled. In the sampling trip of 2012, a recharge experiment was preformed where the WHC2 pool was emptied and the overland flow was diverted to isolate and sample the ultra-basic reducing fluid discharging from the springs. The ultra-basic water recharging the pool from springs WHC2A and WHC2B were sampled and labelled WHC2A-R and WHC2B-R, respectively. All samples were collected at the identified discharge points of the ultra-basic fluid. Water from Winter House Brook was sampled as non ultra-basic surface water. Table 2.2 summarizes the sampling seasons, springs sampled, and corresponding analyses for each spring at the Tablelands.

2.2 Aqueous Geochemistry

Geochemical characterization of the spring water was completed during every sampling trip (~ one week in duration). The springs and non ultra-basic water were sampled for: pH, E_h, conductivity, total inorganic carbon (TIC), dissolved organic carbon (DOC), $\delta^{18}O_{H2O}$ and $\delta^2 H_{H2O}$ as well as $^3H_{H2O}$, major and trace ions, nutrients, total dissolved nitrogen (TDN), total inorganic nitrogen (TIN) and organic acids. These aqueous geochemical parameters helped me to identify potential reductants, oxidants, and bioactive elements, such as nutrients which resulted in the characterization of fluids within the serpentinization system and identification of potential chemical and biochemical reactions taking place in this environment. Characterizing the fluids helped me determine which metabolic strategies can be supported in this system and helped to determine the overall habitability of these extreme environments. Analyzing serpentinization products also helped me determine whether the serpentinization processes is on going or whether the topographic and mineralogical evidence is due to past serpentinization.

E_h, pH and conductivity. *In situ* field measurements of E_h, pH and conductivity were taken periodically throughout the sampling trips to record changes in the geochemistry as a result of daily fluctuations or rainfall events. The E_h was measured daily using an ORPTestr 10 meter designed by Eutech Instruments (-200mV correction) at the Tablelands and a Thermo Scientific, Orion 5-star pH/ORP/Cond/DO meter (-230 mV correction) at The Cedars. While pH and conductivity were measured using a waterproof handheld IQ180G GLP series meter by IQ Scientific Instruments. These *in situ* field measurements were used to monitor the geochemistry of the springs after

withdrawal of water and precipitation events to determine if the water was diluted in the pools. Collecting the ultra-basic water discharging from the bottom of the pool may cause drawdown of less ultra-basic reducing water from the top of the pool and dilute the fluid of interest. Similarly, precipitation events introduce a larger input of non ultra-basic water into the pool and may cause dilution affects by disrupting the dynamic interactions between the two water sources.

Total inorganic carbon (TIC) and dissolved organic carbon (DOC). Total inorganic carbon and dissolved organic carbon were collected for stable carbon isotopic composition ($\delta^{13}C$), as well as, concentration at springs from The Cedars and the Tablelands. Fluid samples for total inorganic carbon and dissolved organic carbon were collected in acid washed, pre-combusted 40 mL amber vials and spiked with concentrated $HgCl_2$ and 20% H_3PO_4, respectively. Fluids for dissolved organic carbon samples were filtered through 0.7 μm glass microfiber filters (GF/F) which were pre-combusted to remove organic matter. Samples were stored cold and dark until analysis. An OI Analytical AURORA 1030 Total Organic Carbon (TOC) Analyzer coupled to a MAT252 isotope ratio mass spectrometer (IRMS) via a Conflo III interface or a ThermoElectron DeltaVPlus IRMS system was used to determine total inorganic carbon and dissolved organic carbon concentrations and $\delta^{13}C$ values. The Aurora is equipped with a reduction furnace, water trap, and packed gas chromatograph (GC) column and uses phosphoric acid for total inorganic carbon and sodium persulfate for total dissolved organic carbon to extract carbon as CO_2 gas in a wet chemical oxidation process. The accuracy and reproducibility of field replicates for concentration of total inorganic carbon and dissolved organic carbon were ≤ 13.5 % RSD and ≤ 15.7 % RSD (n=3), respectively. For

$\delta^{13}C$ the reproducibility on field replicates for total inorganic carbon and dissolved organic carbon were ± 1.5 ‰ and ± 2.0 ‰ (1σ), respectively. TIC and DOC samples were also analyzed at G.G. Hatch Stable Isotope Laboratory in Ottawa, Ontario on an OI Analytical AURORA 1030 TOC Analyzer interfaced to a ThermoElectron Delta Plus XP IRMS for analysis by continuous flow. The analytical reproducibility for concentration and isotopes was 2% (mg/L) and ± 0.2‰, respectively. The accuracy and reproducibility of field replicates for total inorganic carbon and dissolved organic carbon concentrations were ≤ 6.4 % RSD and ≤ 30.9 % RSD (n=3), respectively. For $\delta^{13}C$ the reproducibility on field replicates for total inorganic carbon and dissolved organic carbon were ± 0.7 ‰ and ± 0.9 ‰ (1σ), respectively. $\delta^{13}C$ values are reported in standard notation (per mil, ‰) relative to the international reference standard Vienna Pee Dee Belemnite (V-PDB). All isotope ratios are reported in delta notation relative to an international standard using (Equation 2.1):

$$\delta^n X = (R_{sample}/R_{standard} - 1) \qquad [2.1]$$

where R is the ratio of the abundance of the heavy to the light isotope, X is the element (i.e. C or H), and n is the heavy isotope (i.e. 13 or 2) (Coplen 2011). The international standards used in this study were Vienna PeeDee Belemnite (V-PDB) and Vienna Standard Mean Ocean Water (V-SMOW).

$\delta^{18}O$ and δ^2H of water. In pre-combusted 4 mL vials water was collected with no headspace for oxygen ($\delta^{18}O_{H2O}$) and hydrogen (δ^2H_{H2O}) isotopes. Samples were stored cold and dark until analysis. Isotopic values were measured at Isotope Tracer Technologies Inc. in Waterloo, Ontario on a Picarro Cavity Ring Down Spectroscopy Analyzer (Model L1102-i). Results are reported relative to the V-SMOW reference

standard (refer to above equation). The reproducibility on $\delta^{18}O$ and δ^2H measurements was ± 0.1 ‰ and ± 0.6 ‰ respectively.

^{3}H of water. Fluid was collected and stored with no headspace in 500 mL Nalgene bottles for electrolytic tritium (^3H) analysis. The samples were stored at room temperature. Analysis took place at Isotope Tracer Technologies Inc, in Waterloo, Ontario using an enrichment technique which passes an electrical current through the water to isolate the tritium and deuterium water molecules while breaking down water into its constituents of hydrogen and oxygen. Tritium was measured using liquid scintillation counting (LSC) which is an analytical technique that measures the activity of radio nuclides from the rate of light photons emitted by the scintillation in a liquid sample and is a common technique for the quantification of β radioactivity. The analytical error associated with this measurement was ± 0.5 Tritium Units (TU) (1σ).

Major and trace ions. Water samples collected to determine the major and trace ion chemistry were filtered through a 0.45 μm (25 mm ID) mixed cellulose esters membrane filter with a sterile 60 mL syringe and collected in 125 mL Trace-Clean bottles. Water samples were kept frozen until analysis. At the time of the analysis the samples were thawed and acidified with 8 N nitric acid before being measured on an ELAN DRCII Inductively Coupled Plasma Mass Spectrometer (ICP-MS). Certified reference materials were used as standards. The total analytical error was ± 10% RSD.

Nutrients. Fluid was filtered through a sterile 0.22 μm (25 mm ID) mixed cellulose esters membrane filter and collected in clean 15 mL test tubes with a sterile 60 mL syringe for the analysis of sodium, potassium, sulphate, nitrate, and phosphate. Samples were kept frozen and dark until analysis. Sodium, potassium, sulfate and nitrate

concentrations were measured by an ion chromatograph (IC) with self-generating

suppression and a conductivity detector (CD) using a Dionex DX-100 IC. Sodium and

potassium were run on an IONPAC CS12A (4 x 250 mm ID) column and sulphate and

nitrate were run on an IONPAC AS4A-SC column (4 x 250 mm ID). To quantify these

compounds the chromatogram peaks were compared to calibration curves of sodium (0,

0.1, 0.5, 1, 2.5, 5, 10 mg/L), potassium (0, 0.05, 0.25, 0.5, 1.25, 2.5, 5 mg/L), sulphate (0,

0.1, 0.25, 0.5, 1, 2.5, 5, 10 mg/L) and nitrate (0.01, 0.05, 0.1 mg/L). The orthophosphate

ion (PO_4^{3-}) was measured on a Lambda 25 UV/VIS Spectrometer by adding ammonium

molybdate, potassium antimonyl-tartrate, and sulphuric acid to the sample, which reacts

with the PO_4^{3-} to form a complex under acidic conditions. This complex is then reduced

by adding ascorbic acid to form a blue complex which is measured by the absorbance of

the 885 nm wavelength on the spectrometer. Absorbance is proportional the concentration

of PO_4^{3-} in the sample. To zero the instrument, nano UV water was used as a blank

periodically throughout the analysis. Sample values were compared to a 4 point (0.2, 0.5,

1, and 2 mg/L) calibration curve ($r^2 \geq 0.99$) for quantification. Standards were run at

regular intervals during analysis to ensure the curve had not changed. Phosphate and

nitrate were also measured using the Lachat QuikChem 8500 FIA Automated Ion

Analyzer and quantified using 9 point (0, 0.025, 0.05, 0.1, 0.25, 0.5, 1, 2.5, 5 mg/L)

calibration curves. The analytical and field replicate error on all nutrients was $\leq 9\%$ RSD.

Total dissolved nitrogen (TDN) and Total inorganic nitrogen (TIN). Water for

total dissolved nitrogen and total inorganic nitrogen was filtered through a sterile 0.22 μm

(25 mm ID) mixed cellulose esters membrane filter using a sterile 60 mL syringe and

stored in clean 15 mL test tubes. Samples were kept frozen and dark until analysis. Total

dissolved nitrogen was measured using a Shimadzu TOC Analyzer (TOC-V$_{CSH}$) equipped with a Total Nitrogen Measuring Unit (TNM-1) using oxidative combustion-chemiluminescence for the quantification of total water-borne nitrogen. Ammonia (NH$_3$) was measured using the Lachat QuikChem 8500 FIA Automated Ion Analyzer and quantified using a 9 point (0, 0.025, 0.05, 0.1, 0.25, 0.5, 1, 2.5, 5 mg/L) calibration curve. Together (NH$_3$ and NO$_3^-$) make up the total inorganic nitrogen (TIN) in the fluid. Total organic nitrogen (TON) was calculated by subtracting the total inorganic nitrogen from the total dissolved nitrogen. The analytical and field replicate error for total dissolved nitrogen was 13% RSD and the error for NH$_3$ and NO$_3^-$ was $\leq$ 9% RSD.

Organic acids. In sterile 50 mL falcon tubes 30 mL of water was collected with a sterile 60 mL syringe and kept frozen and dark for the analysis of formate, acetate, propionate, butyrate and lactate. Concentration values were measured at the Swiss Federal Institute of Technology (ETH) in Zurich, Switzerland on a Surveyor high performance liquid chromatograph (HPLC) with a P1000 pump and a PDA Plus 5 Diode Array Detector with a 50 mm cell path following the method of Albert and Martens (1997) with minor modifications. Adipic acid (20 nmol) was used as an internal standard and was injected into the sample before derivitization. Following derivitization an aliquot of sample (0.4 mL) was injected into a 1.5 cm Prevail Organic Acid C18 guard column (4.6 x 250 mm ID, 5 μm film thickness, Grace Davison Discovery Sciences) using an autosampler equipped with a 1 mL syringe. The mobile phase percolating through the column was varying gradients of two solutions. Solvent A was 2.5% n-butanol, 50 mM sodium acetate, 2 mM tetrabutylammonium hydroxide, 50 mM tetradecyltrimethylammonium bromide with phosphoric acid which was used to adjust the

pH to 4.5. Solvent B was pure methanol (MeOH). The gradient program was as follows: 75:25 (A:B) for 23 minutes, then transitioned to a 50:50 mixture over 5 minutes, held at 50:50 for 5 minutes, then returned to a 75:25 mixture over 5 minutes and equilibrated at 75:25 for 5 minutes. Peaks were detected at 400 nm. The analytical error of individual measurements for acetate and formate was $\pm$ 0.030 mg/L and $\pm$ 0.023 mg/L, respectively. The reproducibility of duplicate analysis ranged from 4 to 48 % RSD.

2.3 H_2, CO_2, and C_1-C_6 Gas Sampling and Analysis

Dissolved and bubbling gas composition and isotopic data was sampled and analyzed to determine potential reactants and products of abiotic and/or biotic reactions and aid in the overall understanding of hydrocarbon production mechanisms in serpentinization environments and consequently the potential habitability of these extreme environments.

2.3.1 Sampling of Gases

Hydrogen (H_2), carbon dioxide (CO_2) and methane (CH_4) gases along with higher molecular weight hydrocarbons (ethane (C_2H_6), propane (C_3H_8), iso- and n-butane (C_4H_{10}), iso- and n-pentane (C_5H_{12}) and n-hexane (C_6H_{14})) were sampled using two different methods – one for dissolved and one for bubbling gases. The ultra-basic water was sampled as close to the source of water discharge as possible for gas concentration and isotopic composition ($\delta^{13}C$).

Sampling for dissolved gas concentrations. For dissolved gases samples were collected using a modified syringe gas phase equilibrium technique by McAuliffe (1971)

and Rudd et al. (1974). Gases were extracted by withdrawing 60 mL of water in three 60 mL sterile syringes (20 mL of water each) filled with an equal amount (20 mL each) of He gas and shaken vigorously for 5 minutes to partition the gases out of the aqueous phase and into the gas phase. The gas phase from the three syringes was then injected into a 30 mL serum vial pre-filled with degassed water which was displaced as the sample gas was injected. A final total gas volume of 60 mL was stored in the serum vial and sealed with a conditioned blue butyl stopper. To prevent the contamination of volatile organic compounds that may be present in the blue butyl stoppers they were conditioned using a method after Oremland et al. (1987). The rubber stoppers were first boiled in 0.1 N NaOH for 1 h followed by 12 h of complete immersion in distilled water. This extraction process was repeated using Ar gas. The samples equilibrated with Ar gas were used to measure hydrogen concentrations while all other gaseous compounds were measured using the bottles equilibrated with He. Samples were collected in triplicates whenever possible. Samples were kept cold and dark until analysis. Samples were fixed with $HgCl_2$ to prevent microbial reactions in the sample after collection.

Sampling for $\delta^{13}C$ of dissolved gases. For $\delta^{13}C$ analysis of dissolved gases 50 mL of water was withdrawn using a sterile 60 mL syringe and injected into a pre-evacuated 125 mL serum vial sealed with a conditioned blue butyl stopper and fixed with concentrated $HgCl_2$ to prevent microbial reactions in the sample after collection. Samples were also collected in triplicates.

Sampling for bubbling gas concentrations, $\delta^{13}C$ and δ^2H. Bubbling gas samples were collected by placing an inverted 1 L Nalgene beaker fitted with a syringe adapter over the exsolving spring (Figure 2.8). The beaker was pre-filled with spring

water. As gas bubbling from the spring accumulated it displaced the spring water in the

beaker. Once a minimum of 50 mLs of gas was collected; the gas was withdrawn with a

sterile syringe through the syringe adapter and directly injected into a pre-combusted, pre-

evacuated 30 mL serum vial and sealed with a conditioned blue butyl stopper. This

process was repeated until the sample bottle contained enough gas to be over-pressurized.

A small amount of spring water was injected into the bottle to enhance the seal of the blue

butyl stopper when stored upside down. The sample was fixed with concentrated $HgCl_2$ to

prevent any microbial activity and kept refrigerated and dark until analysis. Multiple

samples for bubbling springs were collected by this method.

2.3.2 Analysis of Gases

Dissolved and bubbling hydrocarbon gas (C_3-C_6) concentrations were analyzed on

a portable SRI 8610 GC with a Flame Ionization Detector (FID) in the laboratory. The

hydrocarbons were separated on a Q-bond (30 m x 0.32 mm ID, 10 μm film thickness)

column with a temperature program: 40 °C hold for 4 min, ramp at 12 °C/min to 150 °C,

hold for 4 min, ramp at 12 °C/min to 180 °C, hold for 2 min, ramp at 20 °C/min to 225

°C, hold for 3 minutes with helium as the carrier gas. Carbon dioxide (CO_2), methane

(CH_4) and ethane (C_2H_6) were analyzed using a Carboxen 1010 (30 m x 0.32 mm ID, 15

μm film thickness) column with Ar as the carrier gas. The temperature program was as

follows: 35 °C hold for 3.8 min, ramp 25 °C/min to 110 °C, hold for 19 min, ramp at 20

°C/min to 200 °C, hold for 15 minutes. Hydrogen (H_2) was measured on an Agilent

6890A GC equipped with a thermal conductivity detector (TCD) using the Carboxen

1010 column with N_2 as the carrier gas. The oven temperature program was isothermal at 40 °C for 6 min. The analytical error was always within 5% RSD.

A volume of 300 μL was injected for all bubbling and dissolved samples and standards using a gas tight locking syringe. Bubbling gas concentrations were reported as % by mol and all samples and standards were set to atmospheric pressure before being injected into the gas chromatograph. Dissolved gas concentrations were reported as μM. Using the gas tight locking syringe dissolved gas samples were injected at the same pressure as the sample bottle, and the standards were injected at atmospheric pressure. The reproducibility for standards was always <5 % however, the reproducibility on replicate samples ranged from 0.1 to 18% RSD.

Stable carbon isotope values ($\delta^{13}C$) of CO_2 and C_1-C_6 were measured using an Agilent 6890 GC coupled to a Finnigan MAT252 IRMS via combustion Conflo II Interface (GC-C-IRMS). Gas samples were injected directly into the GC-C-IRMS system after being withdrawn from the sample serum vials with a gas tight locking syringe. Injection sizes ranged from 25 μL to 500 μL. The separation of CO_2 was achieved using the Carboxen 1010 column with a temperature program of 35 °C hold for 3.8 min, ramp at 25 °C/min to 110 °C, hold for 5 min with a 10:1 split ratio. Methane and other low molecular weight hydrocarbons (C_2, C_3, iC_4, nC_4, iC_5, nC_5, nC_6) were separated using a GS-CARBONPLOT (30 m x 0.32 mm ID, 3 μm film thickness) column. Methane in the bubbling gas samples was separated using a 60 °C isothermal temperature program with a 100:1 split ratio. Methane in the dissolved gas samples and other hydrocarbons (C_2-C_6) in the both dissolved and bubbling gas samples were separated with a temperature program of 50 °C hold for 3.5 min, ramp 25 °C/min to 260 °C, hold for 10 min with a 10:1 split

ratio. Accuracy and reproducibility of $\delta^{13}C$ values for dissolved and bubbling gases was $\pm$ 0.5 ‰ (1σ) which incorporates both the internal reproducibility on triplicate injections of standards and the analytical error associated with the instrumentation. However, the reproducibility of $\delta^{13}C$ values for triplicate field samples for both dissolved and bubbling gases was $\pm$ 0.7 ‰ (1σ) or better. Results are reported in delta notation relative to the V-PDB standard reference material using Equation 2.1.

Stable hydrogen isotope values (δ^2H) of H_2 and CH_4 were measured using an Agilent 6890 GC interfaced with a pyrolysis furnace in line with a Finnigan MAT252 IRMS via combustion Conflo II Interface. Gas samples were injected directly into the GC-C-IRMS system after being withdrawn from the sample serum vials with a gas tight locking syringe. Injection sizes ranged from 30 µL to 50 µL. The H_2 and CH_4 were separated using the Carboxen 1010 column with a temperature program of 110 °C held for 6 min, ramp 25 °C/min to 260 °C, hold for 2 min with a 10:1 split ratio. Retention times for H_2 and CH_4 were determined with standards. The instrumental accuracy and reproducibility of δ^2H values determined using standards were $\pm$ 5 ‰ (1σ). The reproducibility of δ^2H values for triplicate samples for bubbling gases was $\leq \pm$ 10 ‰ (1σ). Results are reported in delta notation relative to the V-PDB standard reference material using Equation 2.1 written above.

2.4 Volatile and Semi Volatile Organic Compound Sampling and Analysis

Volatile and semi volatile organic compounds were sampled and analyzed for their compositional distribution and identification of biomarkers. Higher molecular weight hydrocarbon data furthered the understanding of hydrocarbon formation

mechanisms at these two sites of continental serpentinization and helped to determine potential abiotic and/or biotic reactions.

2.4.1 Sampling of Volatile and Semi Volatile Organic Compounds

Sampling for volatile and semi volatile organic compounds. Fluids for dissolved high molecular weight hydrocarbons were collected by filtering water through a pre-weighed, pre-combusted GF/F (0.7 μm, 25 mm ID) glass microfibre filter. The fluid was collected using a Cole-Parmer Masterflex E/S 07571-00 Portable Sampling Drive equipped with a Masterflex L/S easy-load pump head and L/S 16 (1/8 in ID) silicon tubing. Tubing was flushed for a few minutes with sample water before collection began. When the pump was unavailable collection and filtering was done manually by using a sterile 60 mL syringe and acid washed filter holder. Filtered fluid was collected into a pre-combusted 1 L glass bottle and sealed with a Teflon lined cap. The samples had minimal headspace and were kept cold and dark until analysis. Replicate bottles were collected when possible.

2.4.2 Analysis of Volatile and Semi Volatile Organic Compounds

The filtered water was divided in the laboratory for various analyses. For volatile organic compound concentrations 3 x 40 mL pre-combusted glass vials were filled and sealed with Teflon lined caps and no headspace. The remaining water was saved for semi volatile organic compound concentrations.

Dissolved volatile organic compounds. Samples were measured on an Agilent 6890A GC equipped with a DB-624 (30 m x 0.25 mm ID, 1.4 μm film thickness) column

and a FID with He as the carrier gas. Volatile organic compounds were extracted and concentrated using a direct headspace technique designed to optimize headspace analysis of trace level dissolved volatile organic compounds adapted from Slater et al. (1999). An aliquot (10 mL) of sample was transferred into a 20 mL glass vial with 6 g of NaCl and sealed with an open aluminum cap with a Teflon septa tightly fitted inside. The samples were saturated with NaCl to increase the ionic strength of the water which reduced the solubility of volatile organic compounds and drove them into the headspace. To further optimize the partitioning of dissolved volatile organic compounds into the headspace the vials were heated to 60°C and simultaneously shaken by an auto sampler for 30 minutes before 300 μL of the headspace was injected into the gas chromatograph. The elevated temperature reduced the solubility of gases and shaking caused an increase in NaCl dissolution which further striped the solution of any gas into the headspace. The standards were prepared and extracted using the same method as described for the samples. The samples were split 5:1 in an Agilent split/splitless injector and the carrier gas flow was constant at 1.3 mL/min. An oven temperature program of 40 °C hold for 5 minutes, ramp 10 °C/min to 260 °C, hold at 260 °C for 3 minutes was used to separate the volatile organic compounds. The auto sampler syringe was flushed with N_2 between every injection to eliminate carryover from one sample to the next. Volatile organic compounds were quantified using a 5 point calibration curve (1000, 500, 100, 50, 10 μg/L) of the following organic compounds: cyclohexane, methylcyclohexane, n-heptane, 1-heptene, benzene, toluene, ethylbenzene, xylene (p, m and o), isopropylbenzene and naphthalene. To identify unknown organic compounds, a selection of samples were also run on an Agilent 6890N GC with a 5975C mass spectrometer detector equipped with the DB-624

column using the same temperature program. To quantify these analytes the calibration curve generated for the standard with the most similar chemical structure were used. The reproducibility on replicate field samples for The Cedars ranged from 1.7 to 47.9 % RSD and for the Tablelands ranged from 8.3 to 12.7 % RSD.

Dissolved semi-volatile organic compounds. To extract semi- and non- volatile organic compounds from aqueous samples a separatory funnel liquid-liquid extraction following the Environmental Protection Agency (EPA) method 3510C was used. The pH of the sample was adjusted to ≥11 using a small amount of a concentrated sodium hydroxide stock solution, unless the sample was already highly basic. The sample was than transferred to a pre-combusted 2 L separatory funnel and extracted three times with 60 mL of dichloromethane. The sample was then acidified to a pH of ≤2 using sulphuric acid and extracted another 3 times with 60 mL of dichloromethane, which gave a total extract volume of 360 mL. With each round of extractions 1 L of nano pure UV water was also extracted as a blank. Extracts were collected in a pre-combusted Erlenmeyer flask and then concentrated down to <1 mL using a ThermoElectron Savant SC250EXP SpeedVac Concentrator. If sample clean up was necessary, then the samples were subjected to gravity-fed solid-liquid chromatography modelled after EPA method 3600C using activated (140 °C, minimum 8hrs) 100-200 mesh silica gel in order to separate organic compounds based on their polarity using different organic solvents. The different fractions were hexane (F1), 2:1 hexane/dichloromethane (F2), and methanol (F3). A consistent amount of internal standard (o-terphenyl and 5α-cholestane) was added to all gas chromatograph vials (standards and samples) before being analyzed. F1 and F2 extracts were analyzed for aliphatic and aromatics, respectively, using an Agilent 6890N

GC with a 5975C MSD equipped with a HP-5MS (30 m x 0.32 mm ID, 0.25 μm film thickness) column or an Agilent 6890N GC with a 5973 inert MSD equipped with a DB-5 (30 m x 0.32 mm ID, 0.25 μm film thickness) column. The oven temperature program was 50 °C hold for 1 min, ramp 8 °C/min to 310 °C, hold for 20 min with He as the carrier gas. Blank chromatograms were subtracted from sample chromatograms after the retention factor (compound area/internal standard area) was calculated for all integrated areas. Sample chromatogram peaks were compared to 4 point calibration curves (r^2>0.99) of aliphatic standard RESTEK 31459 and polycyclic aromatic hydrocarbons standard RESTEK 31011 by using the calibration curve of the standard with the most similar chemical structure. Compounds were identified using Wiley and NIST libraries for references and comparing sample retention times to standards. The reproducibility on replicate field samples for The Cedars ranged from 4.8 to 33.9 % RSD and for the Tablelands ranged from 1.5 to 12.5 % RSD.

2.5 Sedimentary Organic Matter Sampling and Analysis

Sedimentary organic matter was sampled and analyzed to characterize the original organic source. This data was correlated and compared to hydrocarbon products detected in surface springs and furthered the overall understanding of reaction pathways both abiotic and biotic taking place in these environments and more specifically the potential for thermogenic hydrocarbon production at these specific locations.

2.5.1 Sampling for Sedimentary Organic Matter

Fine grained sedimentary rocks were collected from rock units that both underlie and enclose the peridotite body. Locations were selected based on geologic maps and hikes through the area in order to find outcrops in which marine sediments were exposed. The sedimentary rock samples selected are used as proxies to represent the sedimentary organic matter that is buried beneath the peridotite rock. At The Cedars two outcrops revealing the fine grained mudstones from the sedimentary unit of the Franciscan Subduction Complex were exposed along Austin Creek and their location can be found mapped in Figure 2.1. At the Tablelands three outcrops of the sedimentary unit below the peridotite within the Humber Arm Allochthon were identified and sampled. Sampling locations are mapped in Figure 2.4. All rock samples were extracted from the outcrop using gloves and placed in a sterile whirl pak bag.

2.5.2 Analysis of Sedimentary Organic Matter

Sedimentary rocks were scrubbed with distilled water to remove any debris that may be adhering to the outside surface. The rocks were crushed into a fine powder using a cup and mill device which was cleaned thoroughly with ethanol and an air jet in between samples. Samples were stored in sterile plastic containers and kept cold and dark until analysis.

Elemental Analysis (EA). Powdered samples were acidified with concentrated HCl acid in a dessicator for a minimum of 24 hours for the determination of bulk elemental composition and $\delta^{13}C$ ratio of organic compounds. Samples were then stored in pre-combusted glass vials with Teflon lined caps and sent to G.G. Hatch Stable Isotope

Laboratory in Ottawa, Ontario. The isotopic composition of carbon ($\delta^{13}C$) was determined by the analysis of CO_2 gas produced by combustion on the Elementar VarioEL III through on-line analysis by continuous-flow with a DeltaPlus Advantage IRMS coupled with a ConFlo II. $\delta^{13}C$ values are reported in standard notation (per mil, ‰) relative to the international reference standard Vienna Pee Dee Belemnite (V-PDB). The analytical accuracy and reproducibility for this analysis was ± 0.05 ‰ (1σ) and the reproducibility of field replicates was ± 2 ‰ (1σ).

2.6 Mixing Models

A two component mixing model was applied for both sites using the geologic settings and the concentration of conservative ion tracers (Cl^- and Br^-) to reflect the physical mixing of non ultra-basic fluids measured in adjacent streams with the geochemical rich fluids discharging from the springs. This model calculates the fraction of ultra-basic fluid contributing to each sampling location at the time of sampling. A positive correlation of $r^2=1$ of aqueous concentrations of conservative tracers Cl^- and Br^- shows conservative mixing between two fluids with the highest and lowest concentrations of these conservative ions. The fluid with the highest Cl^- concentration represents the ultra-basic end member and the fluid with the lowest Cl^- concentration represents the non ultra-basic end member. The spring chosen as the ultra-basic end member was the best proxy for the ultra-basic end member. The fraction of ultra-basic water (f_{UB}) that was contributing to each individual spring was calculated using the two component mixing model (Equation 2.2):

$$[Cl^-]_{spring} = [Cl^-]_{UB} \times f_{UB} + [Cl^-]_{NUB} \times (1-f_{UB}) \qquad [2.2]$$

where UB is the ultra-basic end member and NUB is the non-ultra-basic end member and [Cl⁻] is the aqueous ion concentration of chloride in the individual spring as well as the two end members.

2.7 Tables and Figures

Table 2.1. Summary of samples collected and analyzed at each spring for three sampling seasons at The Cedars.

	AC			BS9			BS5			BS7			NS1			GPS1		
	2011	2012	2013	2011	2012	2013	2011	2012	2013	2011	2012	2013	2011	2012	2013	2011	2012	2013
In situ Aqueous Geochemistry	x	x	x	x		x	x	x	x	x		x	x	x	x	x	x	x
TIC	x			x			x			x			x			x		x
δ^{13}C TIC	x			x			x			x			x			x		x
DOC			x						x									x
δ^{13}C DOC			x						x									x
δ^{18}O$_{H2O}$ and δD$_{H2O}$	x	x	x	x			x	x	x	x			x	x	x	x	x	x
^{3}H			x						x					x				x
Major and Trace Ions	x	x	x	x			x	x	x	x			x	x	x	x	x	x
Nutrients	x	x		x			x	x		x			x	x		x	x	
TDN	x	x		x			x	x		x			x	x		x	x	
TIN	x	x		x			x	x		x			x	x		x	x	
Organic Acids			x*						x*						x*			x*
H$_2$, CO$_2$ and C$_1$-C$_6$ gas	x		x	x		x	x	x		x			x	x	x	x	x	x
δ^{13}C of CO$_2$ and C$_1$-C$_6$ gas	x			x		x	x	x		x			x	x	x	x	x	

Table 2.1. Continued

	AC			BS9			BS5			BS7			NS1			GPS1		
	2011	2012	2013	2011	2012	2013	2011	2012	2013	2011	2012	2013	2011	2012	2013	2011	2012	2013
δ^2H of H_2 and CH_4 gas				x		x	x	x							x			
VOC	x			x			x	x		x			x			x	x	
S-VOC								x									x	

x = collected and analyzed

x* = collected but not analyzed

Table 2.2. Summary of samples collected and analyzed at each spring for two sampling seasons at the Tablelands.

	WHB		WHC2C		WHC2A		WHC2A-R		WHC2B		WHC2B-R		WHC1	
	2011	2012	2011	2012	2011	2012	2011	2012	2011	2012	2011	2012	2011	2012
In situ Aqueous Geochemistry	x	x	x	x	x	x		x	x	x		x		
TIC		x		x		x		x		x		x		
$\delta^{13}C$ TIC		x		x		x		x		x		x		
DOC														
$\delta^{13}C$ DOC														
$\delta^{18}O_{H2O}$ and δD_{H2O}		x		x		x		x		x		x		x
^3H														
Major and Trace Ions	x	x	x	x	x	x		x	x	x		x		x
Nutrients		x		x		x		x		x		x		x
TDN		x		x		x		x		x		x		x
TIN		x		x		x		x		x		x		x
Organic Acids		x		x		x		x		x		x		
H_2, CO_2 and C_1-C_6 gas		x		x		x		x		x		x		
$\delta^{13}C$ of CO_2 and C_1-C_6 gas	x	x	x	x	x	x		x	x	x		x		
VOC	x	x	x	x	x	x		x	x	x		x		
S-VOC	x	x	x	x	x	x		x		x		x		

x = collected and analyzed
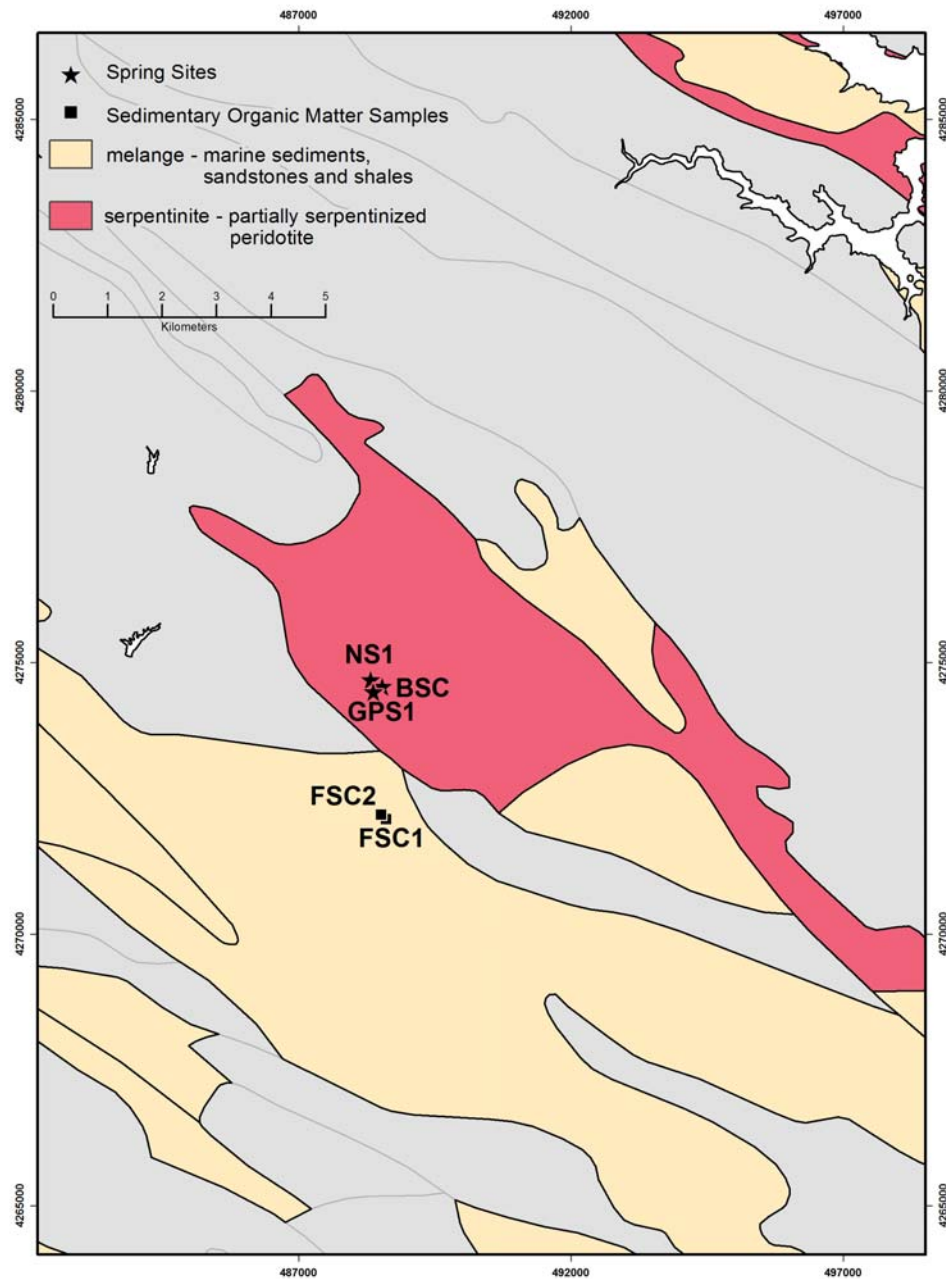
Figure 2.1. Geologic map of The Cedars highlighting the important geologic units and approximate sampling locations. Star symbols represent highly reducing ultra-basic springs discharging from partially serpentinized peridotite. Square symbols represent outcrops of the Late Cretaceous marine sediments and shales that surround and cradle the peridotite body where sedimentary organic matter samples were taken. The BSC location encompasses all the specific springs of the complex sampled for this study (BS5, BS7, and BS9).
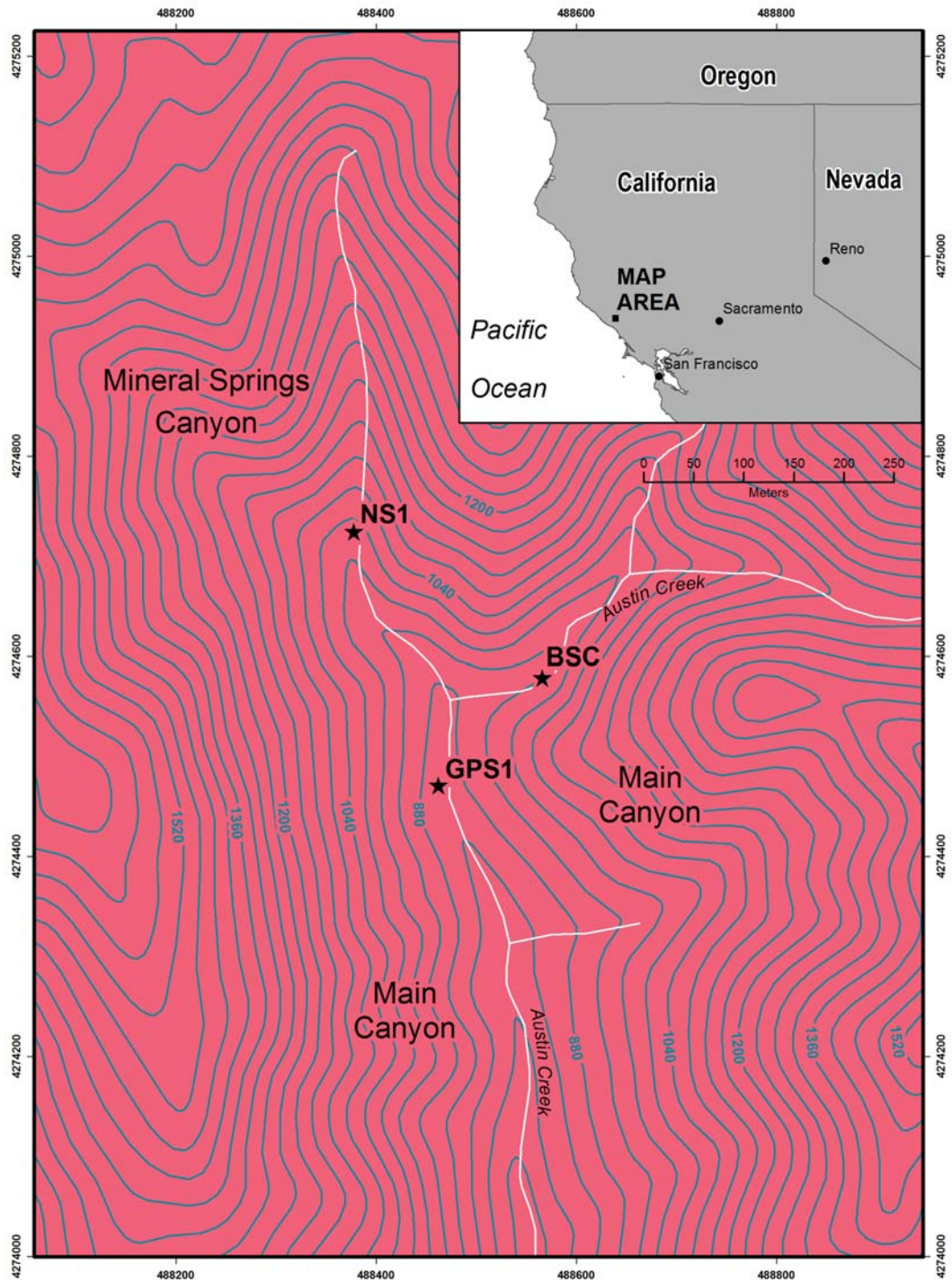
Figure 2.2. Topographic map of The Cedars showing the detailed layout of the spring sampling locations. Springs were found within the headwaters of Austin Creek with GPS1 located below the fork in the creek and NS1 and BSC on separate tributaries above the fork. The BSC location encompasses all the specific springs of the complex sampled for this study (BS5, BS7, and BS9).
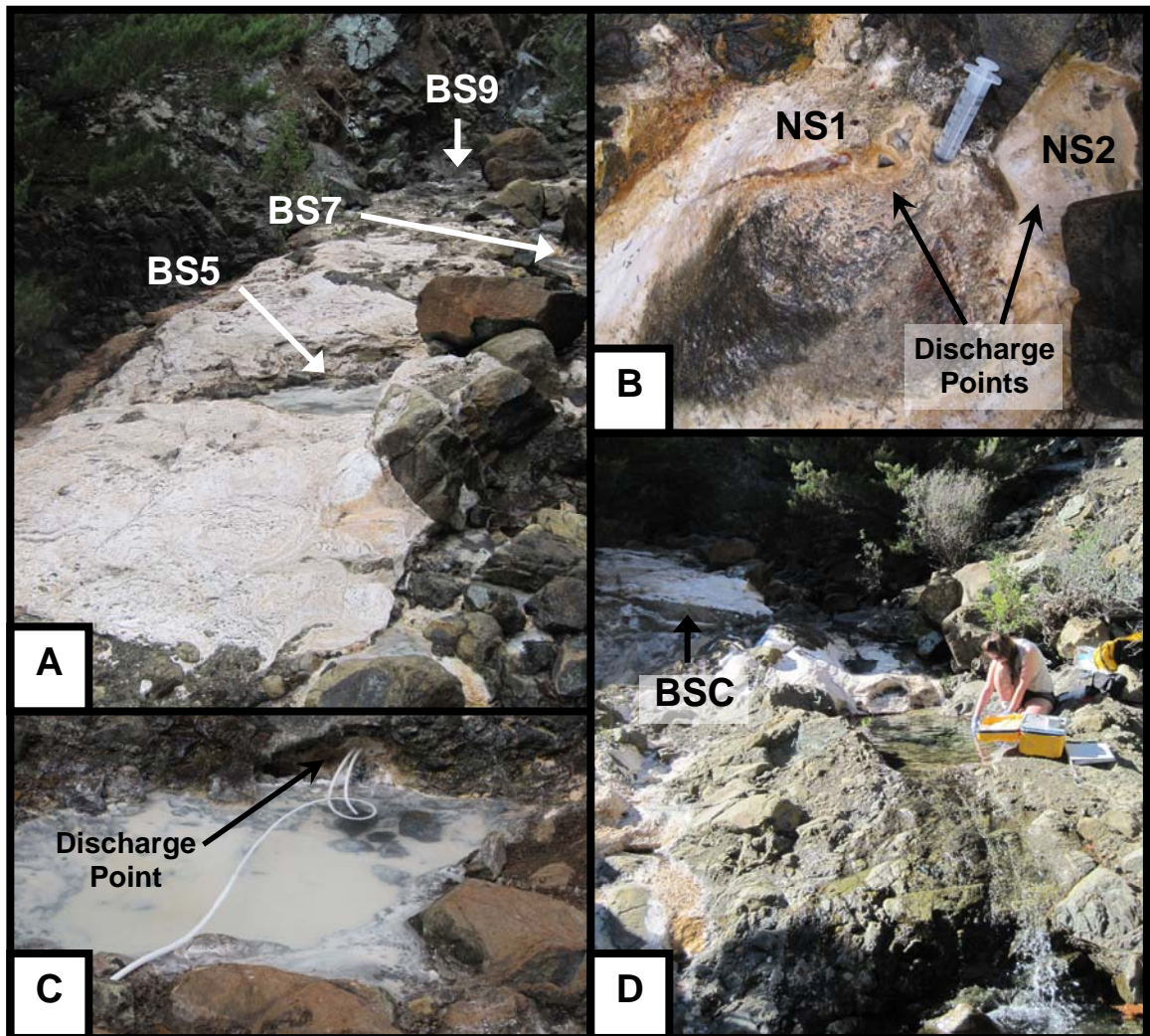
Figure 2.3. Images of springs and travertine deposits at various sampling locations at The Cedars: (A) orientation of the specific springs sampled from the Barnes Spring Complex; (B) discharge points sampled from Nipple Spring; (C) isolated ultra-basic water discharging at GPS1; and (D) orientation of Barnes Spring Complex to Austin Creek sampling location.
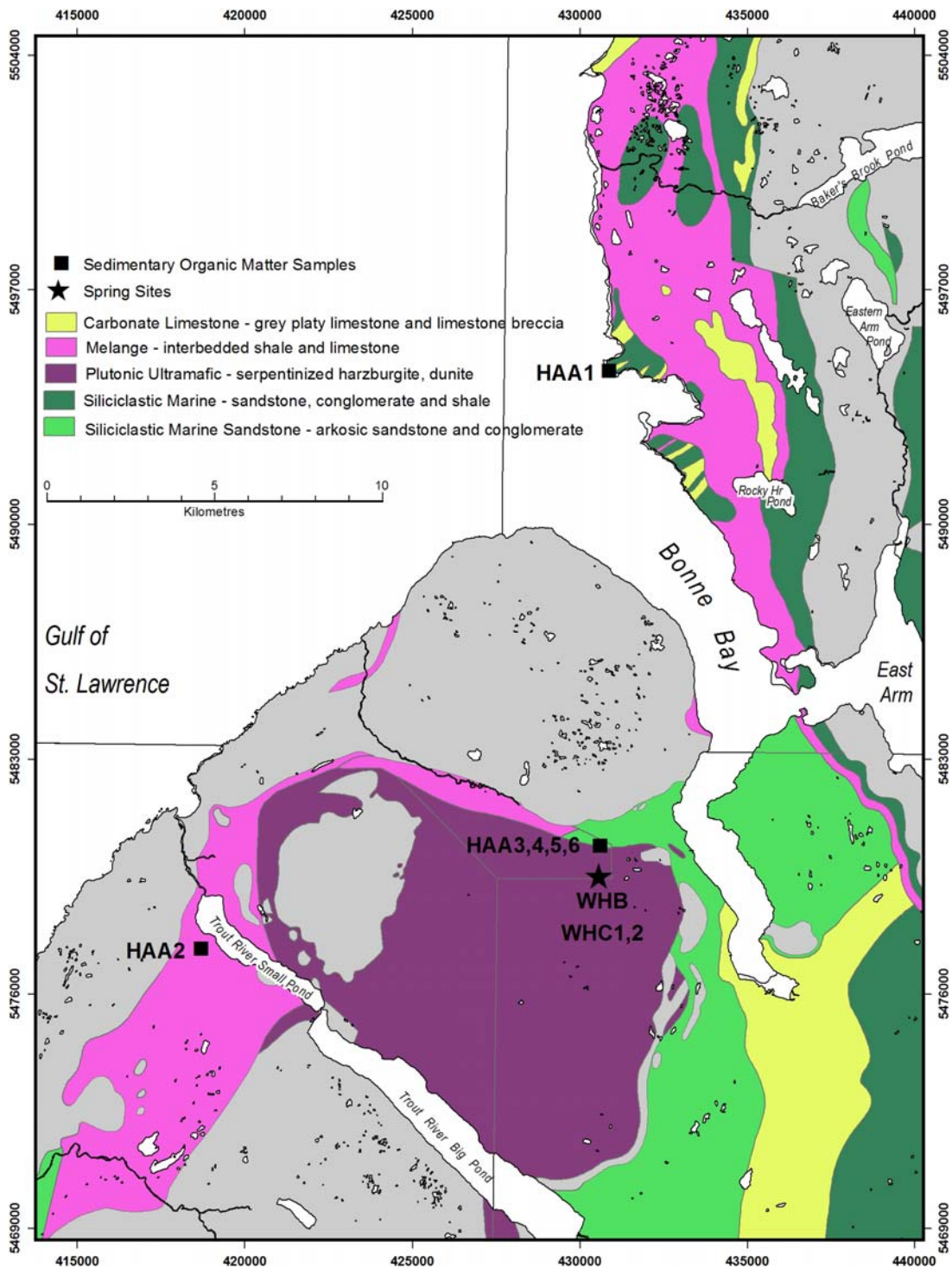
Figure 2.4. Geologic map of the Tablelands highlighting the important geologic units and approximate sampling locations. Star symbols represent highly reducing ultra-basic springs found on the partially serpentinized peridotite. Square symbols represent outcrops of the marine sediments and shales that surround the peridotite body where sedimentary organic matter samples were taken.
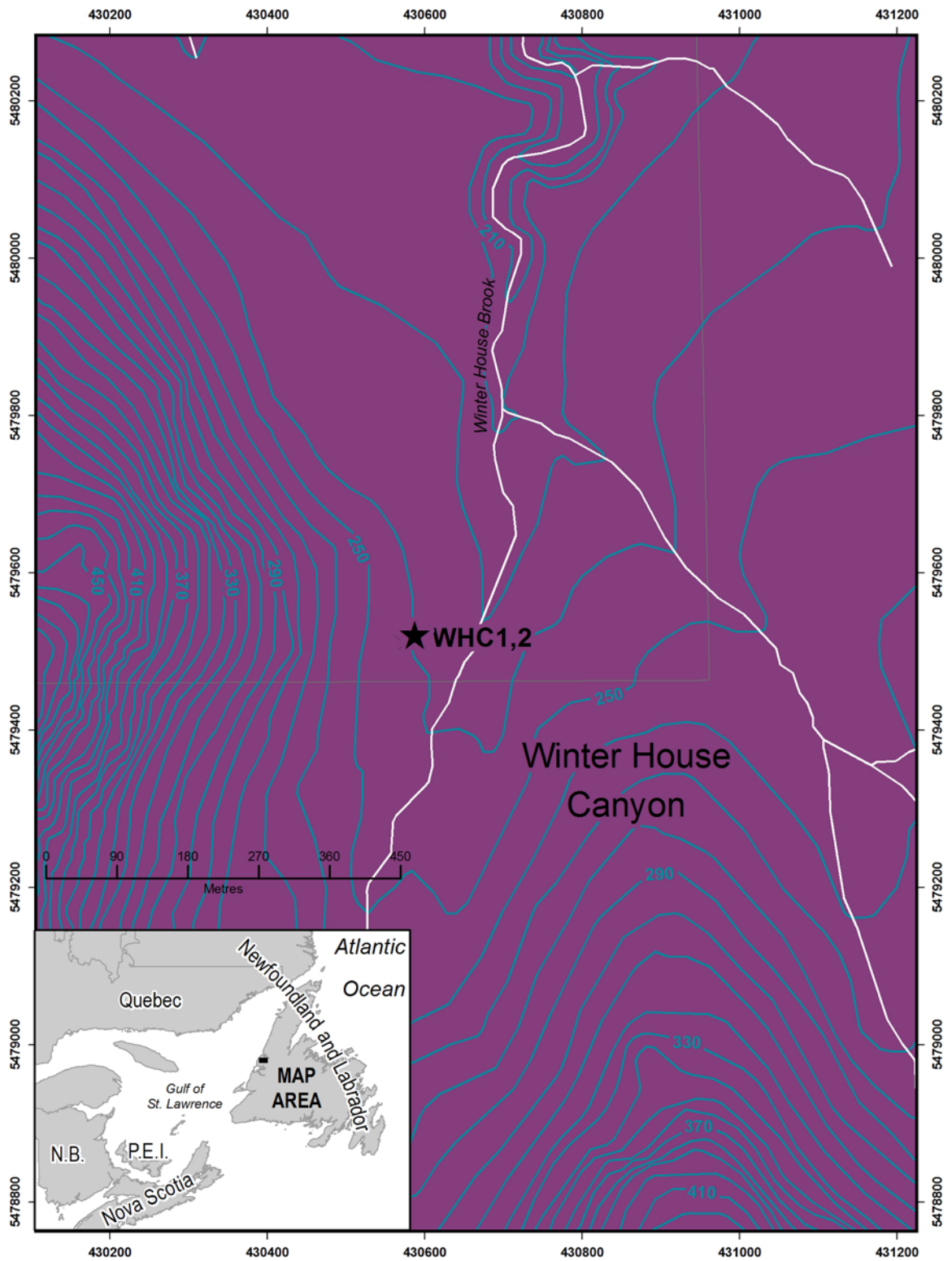
Figure 2.5. Topographic map of the Tablelands showing the detailed layout of the spring sampling area. The springs were found adjacent to Winter House Brook which flows through Winter House Canyon.
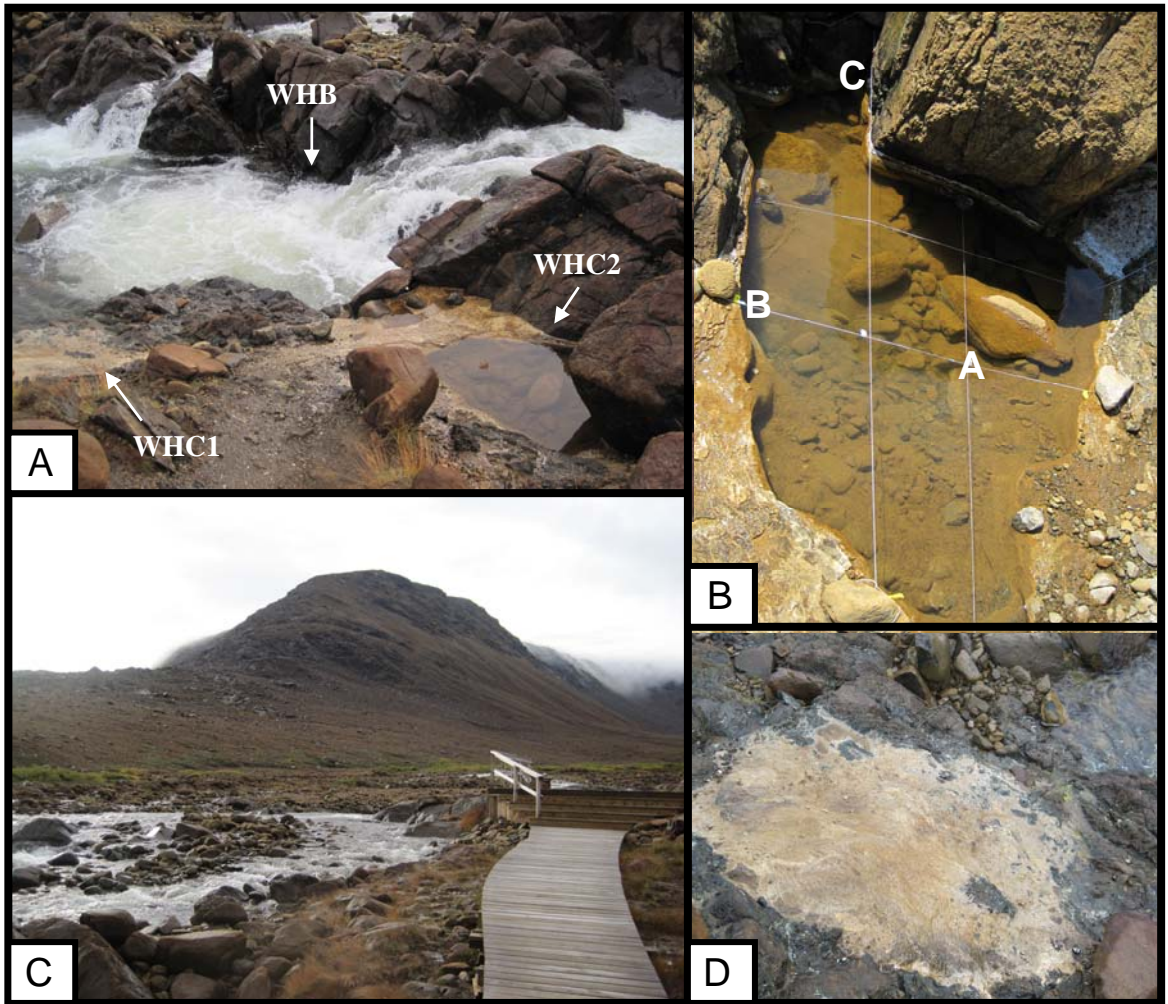
Figure 2.6. Images of springs and travertine deposits at various sampling locations in the Tablelands: (A) orientation of spring sampling locations and Winter House Brook; (B) detailed spring and sampling locations within the WHC2 pool; (C) barren land of Winter House Canyon and WHB a few meters upstream from the spring locations; (D) WHC1 sampling location and the travertine that surrounds pool 6.

WHC2 POOL
Overhead View

Non ultra-basic water input from Winter House Brook (WHB)

C

Boulder

A = WHC2A / WHC2A-R
B = WHC2B / WHC2B-R
C = WHC2C

Cross-Section X-Y

X   B   A   Y

X   Y

0
cm
20
B   A   40

Ultra-basic water discharge points

50 cm
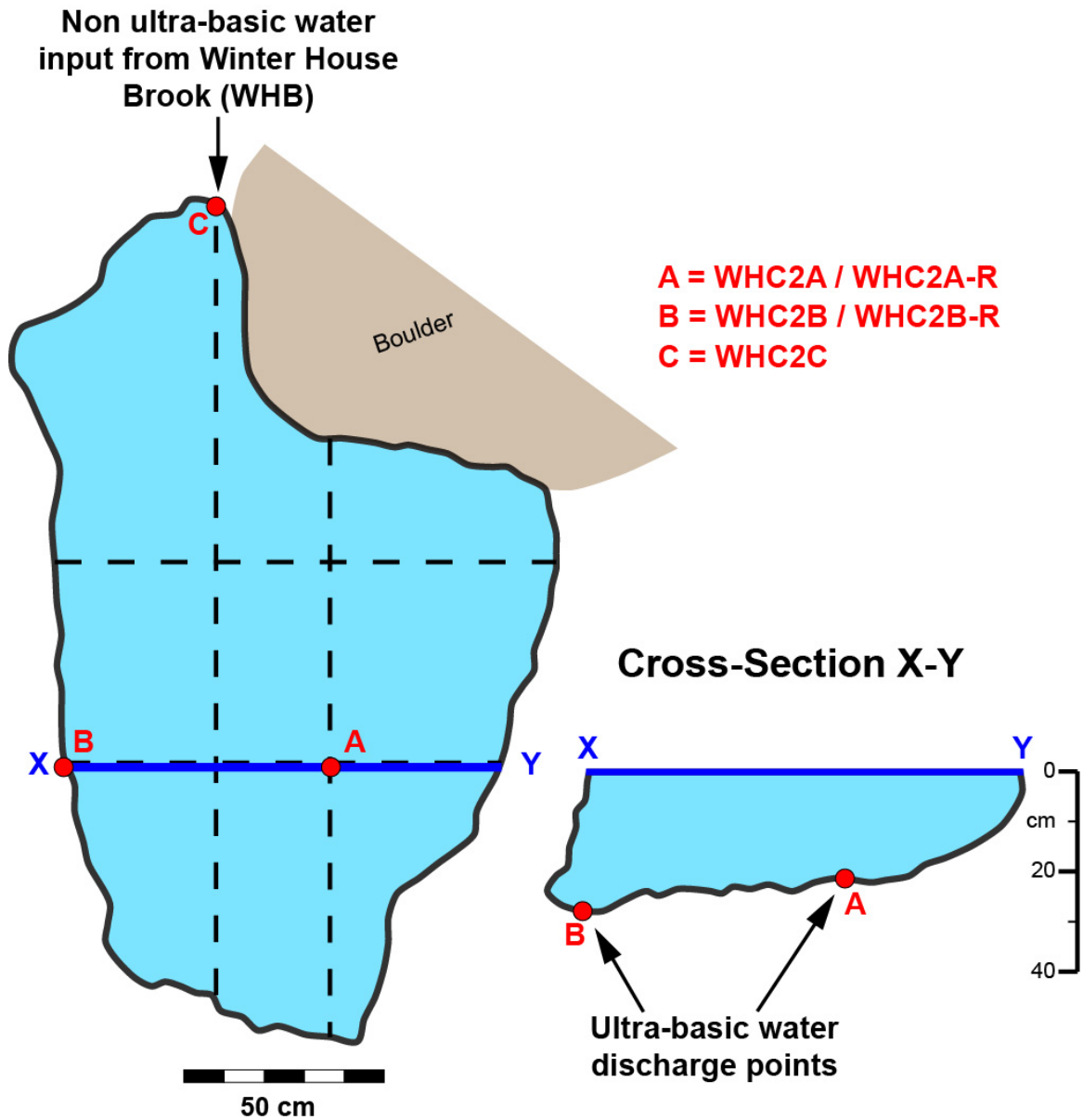
Figure 2.7. Schematic diagrams depicting the various water inputs into the WHC2 pool. Diagram is based on field measurements and field sketches done when profiling the WHC2 pool in 2011.
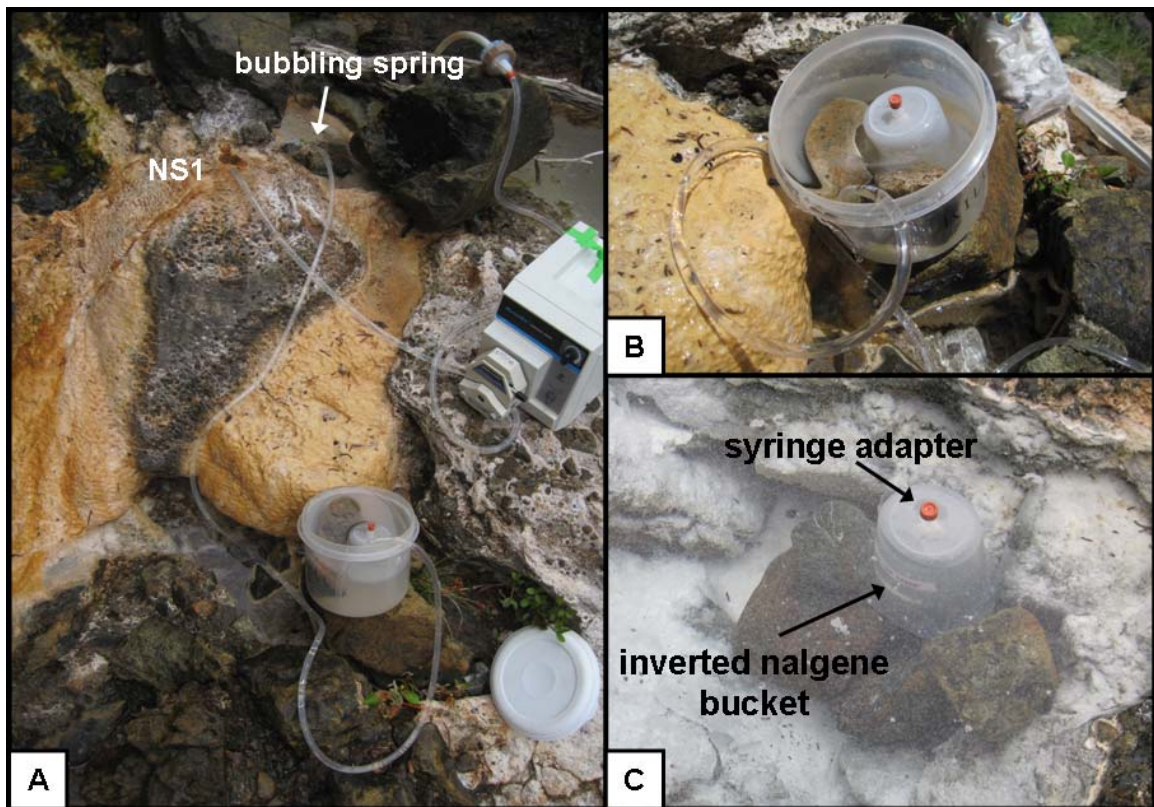
Figure 2.8. Images of bubbling gas collection at The Cedars: (A) The NS2 pool was too shallow for the nalgene bucket, therefore a tygon tube was placed over the bubbling spring and then directed into a larger empty bucket. The bucket was placed at a height where the flow of water and gas was slow enough to not drain the pool but fast enough to effectively collect the bubbling gas; (B) Once the larger bucket was full of ultra-basic water from the spring the nalgene bucket was set up and secured over the tube so that any bubbling gas would be re-directed into the sampling bucket for collection and extraction; (C) A closer look at the inverted nalgene bucket and syringe adapter set up at BS5.

Chapter 3: Results

3.1 The Cedars

3.1.1 Aqueous Geochemistry of Ultra-Basic Springs

The results for aqueous inorganic geochemical parameters (i.e. pH, E_h, and conductivity) for fluids sampled from Austin Creek and springs at The Cedars are reported in Table 3.1 for samples taken in 2011 and Table 3.2 for samples taken in 2012. Geochemical parameters pH and E_h for 2013 are reported in Table 3.3. The fluids discharging from the springs in 2011 were highly basic. GPS1 had the highest pH value (11.9), while Austin Creek had the lowest (9.0). All other springs ranged from 10.0 to 11.8. Similarly in 2012, the highest pH value was measured at GPS1 (12.5) and the lowest at Austin Creek (8.9), while BS5 and NS1 were 11.9 and 11.4, respectively. A similar pattern was found in 2013 with the highest pH measured at GPS1 (12.6) and the lowest at Austin Creek (8.8). All other springs ranged from 10.0 to 12.1. The GPS1 spring was the most basic and increased in pH from 11.9 to 12.6 from 2011 to 2013. The pH of BS9 (10.0) was lower than other springs located within the BSC (11.8 ± 0.1, n=2) in 2011. Similarly in 2013, the pH of BS9 (10.0) was lower than other springs in the BSC (12.1 ± 0.1, n=2). The BS9 and BS7 springs were not sampled in 2012, so a comparison could not be made for that year. In addition to being ultra-basic most springs were also highly reducing. GPS1 had the lowest E_h value (-665 mV), while water sampled from Austin Creek had the highest redox value (+323 mV) in 2011. BS9 had positive E_h values ranging from +120 mV to +304 mV, contrasting the rest of the BSC and NS1 which had

highly negative redox potentials (-618 ± 2 mV, n=3) in 2011. In 2013 the lowest E_h value

was measured at GPS1 (-698 mV) and the highest value was measured at BS9 ($+237$

mV). All other springs ranged from -419 mV to -632 mV and water sampled from Austin

Creek had a positive E_h reading of $+68$ mV. The water measured from the springs in 2011

and 2013 were consistently highly reducing with GPS1 always having the most negative

E_h value. Austin Creek and BS9 always had positive E_h values contrasting with the highly

reducing water sampled at the other spring sites.

In general the ultra-basic springs had a higher conductivity compared to Austin

Creek. In 2011, the highest measured conductivity was 3020 μS/cm at GPS1 and the

lowest conductivity was 163 μS/cm at BS9. NS1 had a conductivity of 752 μS/cm similar

to springs in the BSC (BS5 and BS7) which had a value of 852 ± 40 μS/cm. Austin Creek

had a conductivity of 314 μS/cm. In 2012, GPS1 (1628 μS/cm) had the highest

conductivity value and Austin Creek (206 μS/cm) had the lowest, while BS5 and NS1

were 797 μS/cm and 466 μS/cm, respectively. While GPS1 always had the highest

conductivity value relative to the other springs both in 2011 and 2012, the absolute value

in 2012 was 46% less than the value measured in 2011. The conductivity measured at

NS1 and Austin Creek also decreased between 2011 and 2012 by 38% and 36%,

respectively, while BS5 had a slight increase (10%) from 2011 to 2012. The conductivity

for BS9 and BS7 could not be compared because conductivity was not measured in 2012

for these two springs. Similarly conductivity was not measured in 2013 so no comparison

can be made.

The results for aqueous concentrations of major cations, anions, and nutrients for

fluids sampled from Austin Creek and springs at The Cedars are graphed in Figure 3.1

(raw data in Table A.1) for samples taken in 2011 and Figure 3.2 (raw data in Table A.2) for samples taken in 2012. Major cations and anions for 2013 are graphed in Figure 3.3 (raw data in Table A.3). Over all the concentrations of major anions Cl^-, Br^-, and OH^- were higher in ultra-basic spring fluids compared to Austin Creek. The anion content of the fluids discharging from the springs primarily consisted of Cl^- and OH^- from 2011 to 2013. Non ultra-basic water sampled from Austin Creek consistently had the lowest anion concentration from 2011 to 2013, and ultra-basic water sampled from GPS1 consistently had the highest anion concentration. The concentration of Cl^- was greatest at GPS1 (306.1 mg/L) and the lowest at Austin Creek (11.9 mg/L) in 2011. Springs in the BSC had an average Cl^- concentration of 51.6 ± 6.5 mg/L (n=3) and NS1 measured at 32.5 mg/L. Similarly in 2012, the highest Cl^- concentration was measured at GPS1 (315.5 mg/L) and the lowest was measured at Austin Creek (7.4 mg/L). Comparable to 2011, the Cl^- concentration of BS5 and NS1 were 55.7 mg/L and 30.6 mg/L, respectively in 2012. Once again in 2013, the highest Cl^- concentrations was measured at GPS1 (314.6 mg/L) and the lowest concentration was measured at Austin Creek (8.7 mg/L). The Cl^- concentrations at BS5 and NS1 were 60.8 mg/L and 32.1 mg/L, respectively. Much like Cl^-, the Br^- concentration was highest at GPS1 (0.863 mg/L) and lowest at Austin Creek (0.044 mg/L) in 2011. The BS9 spring had a concentration of 0.164 mg/L while the rest of the springs in the BSC had a concentration of 0.134 ± 0.002 mg/L (n=2) and NS-1 had at concentration of 0.102 mg/L. Similar Br^- concentrations were measured in 2012. GPS1 had the highest Br^- concentration (0.859 mg/L) and Austin Creek had the lowest value (0.027 mg/L). The Br^- concentration at BS5 and NS1 were 0.147 mg/L and 0.080 mg/L, respectively. In 2013, the highest Br^- concentration of 0.954 mg/L was measured at GPS1

and the lowest concentration of 0.025 mg/L was measured at Austin Creek.

Concentrations of Br^- at BS5 and NS1 were 0.202 mg/L and 0.111 mg/L, respectively.

The OH^- concentrations were calculated using the measured *in situ* pH values for that

sampling period and thus have similar patterns as previously discussed for pH.

The cation content of the fluids discharging from the springs primarily consisted

of Ca^{2+} and Na^+ from 2011 to 2012 and high Ca^{2+} concentrations were observed in spring

fluids in 2013. Non ultra-basic water from Austin Creek consistently had the lowest

cation concentration from 2011 to 2013, with the exception of Mg^{2+} which was

consistently the highest at Austin Creek. Mg^{2+} concentrations were highest in Austin

Creek (26.7 mg/L) and lowest at GPS1 (0.028 mg/L) in 2011. All other springs had Mg^{2+}

concentrations that ranged from 0.047 mg/L to 1.96 mg/L. Similarly in 2012, the highest

Mg^{2+} concentration was measured from Austin Creek (25.7 mg/L) and the lowest Mg^{2+}

concentration was measured from GPS1 (0.018 mg/L). The average concentration of all

other springs (BS5 and NS1) was 0.259 ± 0.002 mg/L, n=2. The same pattern was

observed in 2013 with the highest Mg^{2+} concentration measured at Austin Creek (25.7

mg/L) and the lowest at GPS1 (0.212 mg/L). Springs BS5 and NS1 had Mg^{2+}

concentrations of 0.363 mg/L and 0.046 mg/L, respectively. In contrast to the Mg^{2+}

concentrations, Ca^{2+} concentrations were higher in the spring waters compared to Austin

Creek. The highest Ca^{2+} concentration was measured at NS1 (47.3 mg/L) and the lowest

was measured at Austin Creek (8.05 mg/L) in 2011. BS9 had a Ca^{2+} value of 9.77 mg/L,

which was low compared to the Ca^{2+} measured at all the other springs which ranged from

34.1 mg/L to 45.2 mg/L. Similarly in 2012, the highest Ca^{2+} concentration was measured

at NS1 (44.7 mg/L) and the lowest was measured at Austin Creek (3.75 mg/L). BS5 and

GPS1 Ca^{2+} concentrations were 38.5 mg/L and 35.3 mg/L, respectively. In 2013, the highest Ca^{2+} concentration was once again measured at NS1 (45.1 mg/L) and the lowest was measured at Austin Creek (7.35 mg/L). Fluids sampled from springs BS5 and GPS1 had Ca^{2+} concentrations of 34.6 mg/L and 19.2 mg/L, respectively. In 2011, the highest K^+ concentration was measured at BS9 (4.83 mg/L) and the lowest was measured at Austin Creek (0.37 mg/L). All other springs ranged from 1.31 to 4.51 mg/L. In 2012 however, the highest K^+ concentration was measured at GPS1 (3.41 mg/L) and the lowest was measured at Austin Creek (0.08 mg/L). BS5 and NS1 had K^+ concentrations of 1.19 mg/L and 0.46 mg/L, respectively. The Na^+ concentration in 2011 was highest at GPS1 (771 mg/L) and lowest at Austin Creek (17.7 mg/L). The BSC springs (BS5, BS7, and BS9) had an average Na^+ concentration of 94.9 ± 4.1 mg/L (n=3) and NS1 had a Na^+ concentration of 100 mg/L. Similarly in 2012, the highest Na^+ concentration was measured at GPS1 (799 mg/L) and the lowest was measured at Austin Creek (9.08 mg/L). BS5 and NS1 had Na^+ concentration values of 69.2 mg/L and 43.5 mg/L, respectively.

Total inorganic nitrogen (NH_4^+ and NO_3^-) was measured at the ultra-basic highly reducing springs and at Austin Creek in both 2011 and 2012. In 2011, ammonia concentrations were highest at GPS1 (0.777 mg/L) and lowest at BS5 (0.032 mg/L). All other springs ranged from 0.045 to 0.092 mg/L and Austin Creek had an ammonia concentration of 0.040 mg/L. Similarly in 2012, the highest ammonia concentration was at GPS1 (0.766 mg/L), but the lowest concentration was measured at NS1 (0.044 mg/L). BS5 and Austin Creek had concentrations of 0.080 mg/L and 0.062 mg/L, respectively. There was an increase in ammonia concentration from 2011 to 2012 at both BS5 (60% increase) and Austin Creek (35% increase) while NS1 (52% decrease) decreased in

concentration and GPS1 (0.772 ± 0.008 mg/L, n=2) remained consistent. Nitrate

concentrations in 2011 were highest at Austin Creek (0.131 mg/L) and lowest at GPS1

(0.054 mg/L). All other springs ranged from 0.069 mg/L to 0.090 mg/L. Similarly in

2012, the highest nitrate concentration was at Austin Creek (0.111 mg/L) and the lowest

was again at GPS1 (0.061 mg/L). BS5 and NS1 had nitrate concentrations of 0.066 mg/L

and 0.100 mg/L, respectively. The largest change in nitrate concentrations was at NS1

where a 26% increase was observed. All other sampling sites were within 15% from 2011

to 2012. Nitrate concentrations were consistently lowest at GPS1 contrasting the

ammonia concentrations which were consistently highest at GPS1.

Total organic nitrogen was also measured in both 2011 and 2012 at springs and

Austin Creek. In 2011, the only detectable total organic nitrogen was at BS5 (0.091

mg/L) and NS1 (0.252 mg/L). The total organic nitrogen at all other sampling sites were

below the detection limit. In 2012, the highest total organic nitrogen concentration was at

Austin Creek (0.432 mg/L) and the lowest was at NS1 (0.033 mg/L). GPS1 had a total

organic nitrogen concentration of 0.284 mg/L and total organic nitrogen at BS5 was

below the detection limit. The total organic nitrogen concentration measured in the water

at the springs or at Austin Creek from 2011 and 2012 was not consistent.

Phosphate and sulphate concentrations were generally higher at Austin Creek

compared to spring waters in both 2011 and 2012. Phosphate concentration was highest at

BS7 (0.107 mg/L) and lowest at BS5 (0.027 mg/L) in 2011. All other springs ranged from

0.036 mg/L to 0.039 mg/L and Austin Creek had a concentration of 0.047 mg/L. In 2012,

the highest phosphate concentration was measured in fluids sampled from Austin Creek

(0.045 mg/L) and the lowest was measured at NS1 (0.026 mg/L). Water from springs BS5

and GPS1 had phosphate concentrations of 0.029 mg/L and 0.036 mg/L, respectively.

Phosphate concentrations from 2011 and 2012 were consistent (within 5%) with NS1

being the only significant change (33% decrease) from 0.039 mg/L to 0.026 mg/L. In

2011, sulphate concentrations were highest at Austin Creek (0.491 mg/L) and lowest at

GPS1 (0.025 mg/L). All other springs ranged from 0.040 to 0.373 mg/L. In 2012, the

highest sulphate concentration was at Austin Creek (9.40 mg/L) and the lowest was at

NS1 (0.100 mg/L). BS5 and GPS1 had sulphate concentrations of 1.75 mg/L and 2.39

mg/L, respectively.

Trace ion concentrations from The Cedars' ultra-basic fluids discharging from the

springs and non ultra-basic water from Austin Creek are graphed in Figure 3.4 (raw data

in Table A.4.) for 2011 and Figure 3.5 (raw data in Table A.5) for 2012. Alkali metal ions

(Li^+ and Rb^+) were present in trace quantities (≤ 41.7 µg/L) and were more concentrated

in spring waters than the water sampled from Austin Creek in both 2011 and 2012.

Alkaline Earth Metal ions (Sr^{2+} and Ba^{2+}) were detected in both the spring water and

water from Austin Creek at trace levels (≤ 3.8 µg/L) in both 2011 and 2012.

Transition metal ions (Zn^{2+} and Hg^{2+}) were detected in spring waters and water

from Austin Creek in 2011, although in small quantities (≤ 0.37 µg/L for Hg and ≤ 6.2

µg/L for Zn). However in 2012, Zn^{2+} was not detected at any of the sampling locations

and Hg^{2+} was only detected at GPS1 (0.25 µg/L). $Mn^{2+, 3+}$ was detected at BS9, NS1 and

GPS1 ranging from 0.12 to 0.53 µg/L in 2011, but was not detected at Austin Creek. In

2012, $Mn^{2+, 3+}$ was detected at all the springs ranging from 0.14 to 0.51 µg/L as well as

Austin Creek measuring 0.14 µg/L. Other transition metal ion ($Ti^{3+, 4+}$, $Fe^{2+, 3+}$, $Cu^{+, 2+}$)

concentrations were under detection limits in 2011 and 2012 with the exception of $Cu^{+, 2+}$

in 2012 where it was detected ($\leq$ 3.6 µg/L) at NS1, GPS1 as well as Austin Creek. $Cr^{2+, 3+}$ and $Ni^{2+, 3+}$ were detected at Austin Creek and BS9 ($\leq$ 1.4 µg/L for Cr and $\leq$ 0.94 µg/L for Ni), but not at any other spring in 2011. In 2012, $Cr^{2+, 3+}$ was only detected at Austin Creek and BS5 ($\leq$ 1.4 µg/L) and $Ni^{2+, 3+}$ was not detected at any sampling site.

Post transition metal ions (Al^{3+} and $Pb^{2+, 4+}$) were detected in all of the spring waters and at Austin Creek ($\leq$ 2.6 µg/L for Al and $\leq$ 0.07 µg/L for Pb) in 2011 with the exception of Al^{3+} at GPS1 which was undetected. In 2012, $Pb^{2+, 4+}$ was again detected at all the springs and Austin Creek ranging from 0.11 to 0.43 µg/L. Al^{3+} was detected at all the springs ranging from 0.63 µg/L to 10.2 µg/L, but was undetected at Austin Creek. In 2011 $Sn^{2+, 4+}$ was not detected at Austin Creek or BS9, but was detected at all the other springs ranging from 0.27 to 0.42 µg/L. In 2012, $Sn^{2+, 4+}$ was only detected at GPS1 (0.82 µg/L).

Metalloid ions (B, Si, and $Sb^{3+, 5+}$) were all detected in both spring waters and Austin Creek in 2011. B was detected at BS5, NS1, GPS1 and Austin Creek ranging from 0.65 to 1.9 µg/L. Si was detected at BS9, BS7, GPS1 as well as Austin Creek ranging from 0.03 to 2.5 mg/L. $Sb^{3+, 5+}$ was only detected at Austin Creek (0.03 µg/L) and BS9 (0.04 µg/L). In 2012, metalloid ions B and $Sb^{3+, 5+}$ were undetected at all sampling sites and Si was only detected at Austin Creek (0.91 mg/L). Non metal ions S^{2-} and P^{3-} were undetected at all springs and Austin Creek in 2011 and 2012. I^- was detected at Austin Creek and all springs in both 2011 (ranging from 0.02 to 0.92 mg/L) and 2012 (ranging from 0.03 to 1.04 mg/L).

A comparison of the bulk oxidized and reduced pools of carbon (total inorganic carbon (TIC) and dissolved organic carbon (DOC)) in the ultra-basic water discharging

from the springs and non ultra-basic water from Austin Creek are reported in Table 3.4 for 2011 and Table 3.5 for 2013. There were no data for total inorganic carbon and dissolved organic carbon in 2012 due to sampling restrictions. In general total inorganic carbon concentrations were lower in water sampled from the ultra-basic springs compared to the non ultra-basic water sampled from Austin Creek. Furthermore the $\delta^{13}C$ of total inorganic carbon from the springs was more negative than the $\delta^{13}C$ of total inorganic carbon from Austin Creek. In 2011, the highest total inorganic carbon concentration was at Austin Creek (33.3 ± 0.7 mg/L) and the lowest was at NS1 (0.07 ± 0.02 mg/L). The total inorganic carbon in the BS9 pool was higher (10.9 ± 0.4 mg/L) than all the other ultra-basic springs. The other ultra-basic springs total inorganic carbon concentrations ranged from 0.23 to 0.88 mg/L. The $\delta^{13}C$ of total inorganic carbon was the least negative at Austin Creek (-14.5 ± 0.1 ‰) and the most negative at NS1 (-63.5 ± 1.3 ‰). The BSC pools (BS5, BS7, and BS9) had a $\delta^{13}C_{TIC}$ that ranged from -32.5 to -23.0 ‰ and GPS1 had a $\delta^{13}C_{TIC}$ value of -41.1 ‰. In 2013, the total inorganic carbon concentration at GPS1 was 0.55 mg/L and the $\delta^{13}C_{TIC}$ was -24.0 ‰. Unfortunately all other sample bottles for total inorganic carbon broke in transit to the laboratory from the field. Non ultra-basic water sampled from Austin Creek had the highest concentration of total inorganic carbon and the $\delta^{13}C_{TIC}$ at Austin Creek was more enriched in ^{13}C compared to the total inorganic carbon collected from the ultra-basic springs. The NS1 spring which had little to no atmospheric interaction until the point of discharge at the top of a carbonate mound, had the lowest concentration of total inorganic carbon, but the total inorganic carbon was the most depleted in ^{13}C compared to the total inorganic carbon collected from other ultra-basic springs and the non ultra-basic water from Austin Creek. Dissolved organic carbon

samples were compromised in 2011 and therefore not reported. In 2013, the highest

dissolved organic carbon concentration measuring 3.32 ± 1.11 mg/L was at GPS1 and the

lowest concentration measuring 0.34 ± 0.01 mg/L was at Austin Creek. The BS5 spring

had a dissolved organic carbon concentration of 1.53 mg/L. The $\delta^{13}C$ of dissolved organic

carbon was the least negative at BS5 (-17.8 ‰) and the most negative at Austin Creek (-

24.0 $\pm$ 0.2 ‰). The dissolved organic carbon measured at GPS1 had a $\delta^{13}C$ value of -19.2

$\pm$ 7.7 ‰. In general dissolved organic carbon was higher in concentration in the ultra-

basic water discharging from the springs compared to the non ultra-basic water sampled

from Austin Creek. Moreover the dissolved organic carbon measured at the ultra-basic

springs had a less negative $\delta^{13}C$ value compared to dissolved organic carbon measured at

Austin Creek.

The δ^2H_{H2O} and $\delta^{18}O_{H2O}$ values of non ultra-basic fluid collected from Austin

Creek and ultra-basic fluids discharging from the springs from 2011 to 2013 are plotted in

Figure 3.6. The δ^2H_{H2O} and $\delta^{18}O_{H2O}$ data from non ultra-basic fluid from Austin Creek

and ultra-basic fluid from the springs were clustered together with the exception of spring

BS9 in 2011. The BS9 spring however had the least negative δ^2H_{H2O} value of -18.8 ‰

and the least negative $\delta^{18}O_{H2O}$ value of -1.4 ‰ compared to all the other ultra-basic

springs.

Tritium (E^3H_{H2O}) values of fluids sampled from the springs and Austin Creek can

be found in Table 3.3 for 2013. Tritium was only sampled in 2013 during the additional

field campaign. The highest tritium value was measured at BS5 (2.3 TU) and the lowest

was measured at GPS1 (<0.8 TU). NS1 had a tritium concentration of 1.2 TU.

3.1.2 Gaseous Composition of Spring Waters and Austin Creek Water

Dissolved and bubbling gas (H_2, CO_2, and C_1-C_6) concentrations from spring waters and water sampled from Austin Creek at The Cedars can be found in Table 3.6 for 2011, Table 3.7 for 2012 and Table 3.8 for 2013. In general dissolved hydrogen and all dissolved hydrocarbon gases were higher in concentration at the springs compared to water sampled from Austin Creek, while Austin Creek had higher dissolved carbon dioxide concentrations compared to spring waters. GPS1 always had the highest dissolved hydrocarbon concentration compared to all the other springs with the exception of methane where NS1 consistently had the highest concentration and n-pentane in 2012, where again NS1 had the highest concentration. Dissolved methane concentrations were anywhere from 1-4 orders of magnitude greater than higher molecular weight dissolved hydrocarbon gases (ethane, propane, iso-butane, n-butane, iso-pentane, n-pentane, and n-hexane).

Dissolved hydrogen gas was analyzed in 2011 and 2012, but not in 2013. In 2011, dissolved hydrogen concentrations were detected at springs GPS1 (316 ± 1 µM) and NS1 (73.8 ± 24.3 µM), but there was no dissolved hydrogen detected at Austin Creek. In 2012, there was no dissolved hydrogen detected at any of the sampled springs (BS5, NS1, and GPS1), therefore, there was a decrease in dissolved hydrogen concentrations at the springs from 2011 to 2012.

Dissolved carbon dioxide concentrations were analyzed in 2011 and 2013. In 2011, dissolved carbon dioxide was not detected in any of the sampled springs (BS7, NS1 and GPS1) but there was dissolved carbon dioxide detected at Austin Creek (22.6 µM). In 2013, dissolved carbon dioxide was detected at Austin Creek (169 µM) but was not

analyzed for in spring waters. From 2011 to 2013 the carbon dioxide measured at Austin Creek increased substantially from 22.6 to 169 μM.

Dissolved hydrocarbon gases C_1-C_6 were analyzed in 2011, 2012 and in 2013. In 2011, dissolved methane detected in spring waters (BS7, NS1 and GPS1) ranged from 53.6 to 130 μM with the highest concentration detected at NS1. A lower dissolved methane concentration was detected at Austin Creek (10.8 μM). In 2012, the dissolved methane detected in spring waters (BS5, NS1 and GPS1) ranged from 61.7 to 239 μM with NS1 again being the highest in concentration. Similarly in 2013, dissolved methane detected at NS1 (231 ± 1 μM) was the highest and the concentration detected at Austin Creek was the lowest (18.1 μM), while GPS1 had a concentration of 139 ± 8 μM. Dissolved methane concentrations were always highest at NS1 and lowest at Austin Creek from 2011 to 2013.

Dissolved C_2-C_6 concentrations were much lower than dissolved methane concentrations at all springs and Austin Creek from 2011 to 2013. Dissolved ethane concentrations were only quantifiable or detected at GPS1 (0.354 ± 0.136 μM, n=3) from 2011 to 2013. With the exception of BS5 in 2012 which had observable ethane content, all other sampling sites (BS7, NS1 and Austin Creek) from 2011 to 2013 had dissolved ethane concentrations that were below the detection limit. Similarly there was trace to undetected dissolved propane, iso-butane, n-butane, and iso-pentane measured at all sampling locations (BS7, BS5, NS1 and Austin Creek) excluding GPS1 which had concentrations ranging from 0.086 to 0.227 μM in 2011 to 2013. Dissolved n-pentane and n-hexane were also highest at GPS1 ranging from 0.083 to 0.580 μM in 2011 to 2013 compared to all other sampling locations (BS7, BS5, NS1 and Austin Creek). Dissolved

n-hexane concentrations were higher than dissolved C_2-C_5 concentrations at all springs (BS7, BS5, NS1 and GPS1) from 2011 to 2013 with the exception of NS1 in 2012 where the n-pentane and n-hexane concentrations were comparable at 0.139 μM. With the exception of n-pentane in 2012, GPS1 consistently had the highest dissolved C_2-C_6 hydrocarbon concentrations.

In addition to dissolved gases, some springs (BS9, BS5 and NS2) were bubbling with gases that were a mixture of hydrogen, nitrogen and hydrocarbons as previously published in Morrill et al. (2013), which includes data from this thesis. Bubbling gas concentrations can be seen in Table 3.8 for 2011, Table 3.9 for 2012 and Table 3.10 for 2013. In general bubbling gas at the springs from 2011 to 2012 was rich in hydrogen gas ranging from 41.3 to 43.3 %. The concentration of methane in the bubbling gas sampled from the BSC in 2011 to 2013 was also high ranging from 4.2 to 6.4 %; however the highest methane concentration was measured at NS2 with 16.1 % content in 2013. The methane measured at all the springs ranged from 2 to 3 magnitudes greater than higher molecular weight hydrocarbons ethane, propane, butane, pentane and hexane. In 2011, the two springs from the BSC (BS9 and BS5) were very similar to one another in terms of bubbling gas composition.

Bubbling hydrogen gas was analyzed in 2011 and 2012, but not in 2013. The bubbling hydrogen gases detected at the two springs (BS5 and BS9) from the BSC were very similar to one another and stay consistent from 2011 to 2012 (42.3 ± 1.0 %, n=3). Bubbling carbon dioxide was analyzed in 2011, 2012 and 2013 and was consistently below the detection limit at all springs (BS5, BS9 and NS2).

Bubbling hydrocarbon gases (C_1-C_6) were analyzed in 2011, 2012 and 2013. In 2011, the bubbling methane concentration was consistent among the two springs from the BSC with BS9 measuring 5.8 ± 0.8 % and BS5 measuring 6.3 ± 0.2 %. In 2012, the bubbling methane concentration measured at BS5 was 6.4 ± 0.1 %. In 2013, the bubbling methane concentration measured at BS9 was 4.2 ± 1.3 % and the concentration measured at NS2 was 16.1 ± 0.7 %. From 2011 to 2013 the methane bubbling from the BSC springs (BS9 and BS5) were consistent. No comparison can be made at NS2 as bubbling gases were only sampled in 2013.

Similar to dissolved hydrocarbon gas concentrations, bubbling C_2-C_6 concentrations were much smaller than bubbling methane. Bubbling C2-C6 at springs within the BSC ranged from 15.4 to 103 ppm from 2011 to 2013 and NS2 had a range of 10.0 to 105 ppm in 2013. Also similar to dissolved gases, bubbling n-hexane concentrations were greater than bubbling C_2-C_5 concentrations in 2012 and 2013 but in 2011 bubbling ethane concentrations were highest within the C_2-C_6 alkane group.

In 2012, at BS5 dissolved and bubbling gases were sampled. Although there was abundant hydrogen detected in the bubbling gas (~42 %) there was no hydrogen detected in the dissolved gas. In both the bubbling and dissolved gas, methane was the most abundant lower molecular weight (C_1-C_6) hydrocarbon analyzed, by orders of magnitude. Similarly in 2013, dissolved and bubbling gases were sampled for at NS (NS1 and NS2). Methane detected in both the bubbling and dissolved gas from NS was orders of magnitude greater than higher molecular weight hydrocarbons (C_1-C_6) analyzed. Furthermore, methane detected at NS was consistently highest in concentration of all the springs from 2011 to 2013 in both bubbling and dissolved gases.

3.1.3 Isotopic Composition of Gaseous Hydrocarbons

The carbon ($\delta^{13}C$) and hydrogen (δ^2H) isotopic composition of dissolved and bubbling gases at The Cedars can be seen in Table 3.9 for 2011, Table 3.10 for 2012 and Table 3.11 for 2013. $\delta^{13}C$ of CO_2 and hydrocarbons C_1-C_6 were analyzed for in the dissolved gases sampled from 2011 to 2013; however the dissolved gas concentrations were too low for δ^2H analysis. Fortunately, for bubbling gases the δ^2H of both hydrogen gas and methane was measured along with the $\delta^{13}C$ of CO_2 and hydrocarbons C_1-C_6.

For dissolved gases in 2011 and 2012 the $\delta^{13}C$ of CO_2 and hydrocarbons C_1-C_6 were analyzed. The $\delta^{13}C$ of dissolved CO_2 detected at Austin Creek was -11.6 ± 0.5 ‰ in 2011. Carbon dioxide was not detected in any of the spring waters (BS7, NS1 and GPS1) and therefore isotope data for these waters were not reported. In 2012, Austin Creek was not sampled for gases and in spring waters sampled from NS1 and GPS1 the carbon dioxide content was too low for reliable $\delta^{13}C$ values as expected.

In 2011, the $\delta^{13}C$ of dissolved methane was the most negative at NS1 (-67.4 ± 0.5 ‰) and the least negative at GPS1 (-57.2 ± 0.5 ‰). The $\delta^{13}C$ of dissolved methane at Austin Creek and BS7 were very similar to one another at -63.5 ± 0.5‰ and -63.3 ± 0.5 ‰, respectively. Similarly in 2012, the most negative $\delta^{13}C$ of dissolved methane was measured at NS1 (-67.7 ± 0.5 ‰) and the least negative was measured at GPS1 (-56.2 ± 0.5 ‰). At BS5 the $\delta^{13}C$ of dissolved methane was -62.6 ± 0.5 ‰. In 2011, the only $\delta^{13}C$ values for hydrocarbons C_2-C_6 were for ethane (-25.3 ± 0.8 ‰) and hexane (-23.6 ± 0.5 ‰) at GPS1. In 2012, the $\delta^{13}C$ of ethane, propane, n-butane, n-pentane and n-hexane at GPS1 and BS5 ranged from -22.6 to -25.7 ‰. Hydrocarbons C_2-C_6 were too low in concentration at NS1 for $\delta^{13}C$ values. Iso-compounds including iso-butane and iso-

pentane were also too low in concentration at springs BS5, NS1 and GPS1 for $\delta^{13}C$ analysis. Over all there was no significant change in $\delta^{13}C$ of dissolved hydrocarbons from 2011 to 2012 at any of the springs. Furthermore there was no significant difference in $\delta^{13}C$ of hydrocarbons C_2-C_6 between the different springs at the BSC or any of the springs sampled at The Cedars ranging from -22.6 to -25.7 ‰ from 2011 to 2012. The $\delta^{13}C$ of methane had the highest variation between the different springs and was much more negative ranging from -56.2 to -67.7 ‰ from 2011 to 2012 compared to higher molecular weight hydrocarbons.

For bubbling gases sampled from 2011 to 2013 the $\delta^{13}C$ of hydrocarbons C_1-C_6 and the δ^2H of hydrogen and methane were analyzed. . The $\delta^{13}C$ of methane was consistent between the different BSC springs (BS9 and BS5) from 2011 to 2013 averaging -63.1 ± 0.2 ‰, n=4. In 2013, the $\delta^{13}C$ value of methane at NS2 was 3 ‰ more ^{13}C depleted at -66.4 ± 0.5 ‰ compared to methane detected at the springs in the BSC (BS9 and BS5). In 2011, the $\delta^{13}C$ of ethane, propane, iso-butane, n-butane, iso-pentane, n-pentane and hexane were very similar ranging from -23.0 ‰ to -24.1 ‰ at BS9 and -22.6 ‰ to -24.6 ‰ at BS5. Similarly in 2012, the range of $\delta^{13}C$ values for hydrocarbons C_2-C_6 was -23.1 ‰ to -24.3 ‰. Once again the $\delta^{13}C$ value of hydrocarbons remained consistent between the two springs of the BSC (BS9 and BS5) and was consistent from 2011 to 2012. There was a large difference in the $\delta^{13}C$ value of methane compared to the $\delta^{13}C$ value of other low molecular weight hydrocarbons (C_1-C_6) at all the springs measured in both 2011 and 2012.

The $\delta^{13}C$ of dissolved and bubbling methane were within ± 0.3 ‰ error at BS5 and within ± 1.3 ‰ error at NS. Dissolved and bubbling C_2-C_6 hydrocarbons were within

± 1.1 ‰ error at BS5 showing how similar the carbon isotopic composition of dissolved and bubbling gases were. Unfortunately δ^2H could not be obtained for dissolved gases and therefore a comparison between years or between bubbling and dissolved gases could not be made. The δ^2H of hydrogen gas and methane was measured in bubbling gases from 2011 to 2013. The δ^2H of methane at the BSC was comparable from 2011 to 2013 ranging from -350 ‰ to -358 ‰. The δ^2H of methane at NS2 in 2013 was -360 ± 5 ‰. Similarly from 2011 to 2013, the δ^2H of hydrogen gas at the BSC springs (BS9 and BS5) was fairly consistent ranging from -768 ‰ to -775 ‰. In 2013, the δ^2H of hydrogen gas at NS2 was -763 ± 5 ‰. There was no significant difference or change in the δ^2H values of hydrogen gas or methane between the different springs (BS9, BS5 and NS2) or throughout the years from 2011 to 2013.

3.1.4 Volatile and Semi Volatile Organic Compound Composition

Volatile organic compound (VOC) concentrations measured from spring waters and Austin Creek at The Cedars can be found in Table 3.12 for 2011 and Table 3.13 for 2012. There were no volatile organic compounds detected in fluids sampled from Austin Creek or in the spring water sampled from BS9 in 2011. However, in 2011 and in 2012 there were multiple volatile organic compounds detected and quantified in spring waters sampled from BS5, BS7, NS1 and GPS1. For all volatile organic compounds measured in both 2011 and 2012 the highest concentration was always measured at GPS1. In general from 2011 to 2012 there was an increase in concentration observed for all volatile organic compounds measured. The most predominant volatile organic compounds measured in both 2011 and 2012 at BS5 were cyclohexane, methylcyclohexane, toluene and

dimethylcyclohexane compounds. Similarly, with the exception of the toluene content, the most predominant volatile organic compounds measured at NS1 in 2011 were cyclohexane, methylcyclohexane and dimethylcyclohexane compounds. While GPS1 also had high concentrations of these volatile organic compounds there was a stronger presence of BTEX compounds. The most predominant volatile organic compounds measured at GPS1 in both 2011 and 2012 were toluene, cyclohexane, benzene, xylene compounds and methylcyclohexane.

Dissolved concentrations of higher molecular weight alkanes and alkenes detected in the spring waters in both 2011 and 2012 were n-heptane and 1-heptene, however their concentrations were not high enough for quantification. Cyclic alkanes including cyclopentane, cyclohexane, methylcyclopentane, methylcyclohexane, dimethylcyclohexane, and ethylcyclohexane were present in spring waters in both 2011 and 2012. There were no cyclic alkanes detected in waters sampled from Austin Creek or BS9 in 2011 and in 2012 these springs were not sampled for dissolved volatile organic compounds. All cyclic alkanes detected increased in concentration in the spring waters from 2011 to 2012. The highest concentration of cyclic alkanes was always measured at GPS1 in both 2011 and 2012. Cyclohexane was the most concentrated cyclic alkane measured in spring waters in both 2011 and 2012 with methylcyclohexane being the next most concentrated. Cyclopentane was present in trace quantities in spring fluids with the exception of GPS1 in 2012 where the concentration was 0.239 μM. Cyclohexane concentrations ranged from 0.473 to 3.99 μM in spring fluids (BS5, NS1 and GPS1) from 2011 to 2013. The methyl- and dimethyl-substituted cyclic alkanes (methylcyclopentane,

methylcyclohexane, dimethylcyclohexane, and ethylcyclohexane) ranged from 0.156 to 1.48 μM in spring fluids (BS5, NS1 and GPS1) from 2011 to 2013.

Aromatics BTEX (benzene, toluene, ethylbenzene, and xylene) as well as variations of these compounds (isopropylbenzene, propylbenzene, ethyl methyl benzene, and trimethylbenzene) were observed in spring waters (BS5, NS1 and GPS1) sampled in both 2011 and 2012. There were no aromatic compounds detected in waters sampled from Austin Creek and BS9 in 2011. In general all aromatic compounds detected increased in concentration from 2011 to 2012 in the spring waters. GPS1 had the highest concentration of all aromatic compounds detected in both 2011 and 2012 ranging from 0.083 to 4.49 μM. Of all the aromatic compounds detected in spring fluids (BS5, NS1 and GPS1) toluene (0.225 to 4.49 μM) was the most concentrated in both 2011 and 2012 with xylene compounds (0.183 to 3.48 μM) and benzene (0.231 to 2.64 μM) falling closely behind.

The only polycyclic aromatic hydrocarbon (PAH) detected in the spring waters was tetralin (1,2,3,4-tetrahydronaphthalene). Tetralin was not detected in waters sampled from Austin Creek or the BSC (BS9, BS5 and BS7), however it was detected at NS1 (<0.076 μM) and quantified at GPS1 (0.142 μM) in 2011. Like other volatile organic compounds from 2011 to 2012 there was an increase in concentration of tetralin at GPS1 from 0.142 to 0.169 μM. The concentration of tetralin was very low in spring fluids compared to other volatile organic compounds detected in both 2011 and 2012.

Semi volatile organic compound (S-VOC) concentrations detected in spring fluids discharging at BS5 and GPS1 at The Cedars can be found in Table 3.14 for 2012. Semi volatile organic compound samples were compromised in 2011 and were not sampled for in 2013. The two dissolved polycyclic aromatic hydrocarbons (PAH) detected in BS5 and

GPS1 spring waters were tetralin and methyl tetralin. Tetralin concentrations were lower in fluids collected from BS5 with a concentration of $2.5 \times 10^{-3} \pm 1.5 \times 10^{-4}$ μM compared to fluids sampled from GPS1 which had a concentration of $1.0 \times 10^{-2} \pm 3.6 \times 10^{-3}$ μM. Similarly, the methyl tetralin concentration was lower in fluids from BS5 ($3.8 \times 10^{-3} \pm 6.2 \times 10^{-4}$ μM) compared to fluids from GPS1 which had a higher concentration of $4.4 \times 10^{-3} \pm 6.8 \times 10^{-4}$ μM. Alkanes C_{24}, C_{25}, and C_{26} were detected in GPS1 fluids but in concentrations that were too low to quantify. No alkanes were detected in fluids from BS5. Semi volatile organic compound concentrations were consistently higher in GPS1 fluids compared to BS5 fluids in 2012.

3.1.5 Sedimentary Organic Matter Composition

Outcrop and shale sample descriptions from which the sedimentary organic matter (SOM) was extracted can be found in Table 3.15. The outcrops from which the samples were taken were located along Austin Creek in the Franciscan Subduction Complex south of The Cedars peridotite as seen in Figure 2.1. In general shale samples were fine grained, heavily cleaved and dark gray in colour.

The carbon isotopic composition of sedimentary organic matter samples FSC1 and FSC2 collected from The Cedars can be seen in Table 3.16. The $\delta^{13}C$ of bulk carbon in SOM samples were very similar to each other measuring -25.0 ‰ in FSC1 and -24.9 ‰ in FSC2.

3.2 The Tablelands

3.2.1 Aqueous Geochemistry of ultra-basic springs

The results for aqueous inorganic geochemical parameters (i.e. pH, Eh and conductivity) for the Tablelands are reported in Table 3.17 for 2011 and Table 3.18 for 2012. Spring fluids (WHC2A, WHC2B, WHC2A-R and WHC2B-R) and the mixing site (WHC2C) sampled in 2011 and 2012 were ultra-basic, while water sampled from Winter House Brook was neutral. In 2011, Winter House Brook had a neutral pH of 7.8, where as water discharging from the springs (WHC2A and WHC2B) and water collected at the mixing site (WHC2C) had a high average pH value of 12.3 ± 0.1, n=3. In 2012, Winter House Brook had a similar pH of 8.1 and water discharging from the springs (WHC2A and WHC2B) had a similar average pH value of 12.2 ± 0.0, n=2. The pH of WHC2C (11.7) was less than spring fluids in 2012. Additionally in 2012, a recharge experiment, where the WHC2 pool was emptied and overland flow was diverted, isolated fluids from the springs (WHC2A-R and WHC2B-R) which were also sampled. The recharge rate of the WHC2 pool without any overland input was 292 mL/min. Spring recharge fluids (WHC2A-R and WHC2B-R) had a similar average pH value to WHC2A and WHC2B before the WHC2 pool was emptied (12.3 ± 0.1, n=2).

The ultra-basic fluids discharging from the springs were also highly reducing. In 2011, the highest E_h value was detected at Winter House Brook (+382 mV) and the lowest E_h value was detected at WHC2A (-690 mV). WHC2B had a highly negative redox potential much like WHC2A at -618 mV, where as the mixing site, WHC2C, had a redox potential that was less negative (-458 mV).

Depth profiles of both the pH and E_h of the WHC2 pool at our sampling locations

in 2011 are plotted in Figure 3.7. Although the depth of the WHC2 pool varies depending

on the sampling location, there was a clear gradient in both pH and E_h from the bottom of

the pool to the water surface. The pH of the water becomes more ultra-basic with pool

depth at all sampling locations, with the highest pH being measured at the very bottom.

Similarly, at all sampling locations the E_h of the water becomes more reducing with

depth, with the lowest E_h measurement being at the very bottom.

In addition to being ultra-basic and highly reducing the water discharging from the

springs also had significantly higher conductivity compared to the water sampled from

Winter House Brook in both 2011 and 2012. In 2011, the lowest conductivity was at

Winter House Brook (62 μS/cm) and the highest was at WHC2A (3880 μS/cm). The

WHC2B spring also had a high conductivity similar to WHC2A (3830 μS/cm) and

WHC2C had a conductivity of 475 μS/cm. Similarly in 2012, the lowest conductivity was

80 μS/cm at Winter House Brook and the highest conductivity was 2430 μS/cm at

WHC2A. All other springs ranged from 1715 μS/cm to 2080 μS/cm. WHC2C had a

conductivity of 126 μS/cm. Recharge waters WHC2A-R and WHC2B-R were lower in

conductivity than water sampled from WHC2A and WHC2B before the recharge

experiment, but still magnitudes higher than water sampled from Winter House Brook.

The results for aqueous concentrations of major cations, anions, and nutrients for

fluids sampled from Winter House Brook and springs at the Tablelands are graphed in

Figure 3.8 (raw data in Table A.7) for samples taken in 2011 and Figure 3.9 (raw data in

Table A.8) for samples taken in 2012. The concentrations of major anions Cl⁻, Br⁻ and

OH⁻ were consistently higher in the ultra-basic waters discharging from the springs than

in the non-ultra-basic water sampled from Winter House Brook from 2011 to 2012. The dominant anions in the fluids discharging at the springs for 2011 and 2012 were Cl^- and OH^-. In 2011, the Cl^- concentration was lowest at Winter House Brook (7.17 mg/L) and highest at WHC2A (400 mg/L) (in 2011, WHC1was not sampled for ions). The Cl^- concentration of WHC2B (215 mg/L) was less than what was detected at spring WHC2A but it was still higher than WHC2C (67.1 mg/L). In 2012, the lowest Cl^- concentration was detected at Winter House Brook (5.94 mg/L) and the highest was detected at WHC1 (489 mg/L). The Cl^- was more concentrated in the recharge water at spring WHC2A-R measuring 420 mg/L than fluid sampled before the recharge experiment (WHC2A) measuring 138 mg/L, where as the recharge water from spring WHC2B-R remained relatively consistent with the fluid sampled before the experiment (WHC2B) at 408 ± 10 mg/L, n=2. At WHC2C the concentration was 23.2 mg/L. In 2011, the Cl^- concentration of WHC2A was similar to the concentration detected at WHC2A-R, WHC2B and WHC2B-R in 2012 (409 ± 10 mg/L, n=4). In both 2011 and 2012 the same pattern of concentration can be seen for the ion Br^-. In 2011 Br^- concentration was highest at WHC2A (0.957 mg/L) and lowest at Winter House Brook (0.009 mg/L). Br^- concentrations at WHC2B and WHC2C were 0.500 mg/L and 0.156 mg/L, respectively. In 2012, the highest Br^- concentration of 1.19 mg/L was detected at WHC1 and the lowest concentration of 0.027 mg/L was detected at Winter House Brook. WHC2A (0.340 mg/L) had a lower Br^- concentration compared to WHC2A-R, WHC2B and WHC2B-R which had a Br^- concentration of 0.961 ± 0.030 mg/L, n=3, however in 2011 the Br^- concentration of WHC2A was within this error. Hydroxide concentrations were

calculated using the *in situ* pH values and therefore have the same patterns as previously discussed for pH.

In general the major cation (Ca^{2+}, K^+ and Na^+) concentrations were higher in the ultra-basic water discharging at the springs compared to the non ultra-basic water sampled from Winter House Brook with the exception of Mg^{2+} where higher concentrations were detected in the brook and at the mixing site. The cation content in the spring water in 2011 and 2012 primarily consisted of Ca^{2+} and Na^+. Winter House Brook consistently had the lowest cation concentration, with the exception of Mg^{2+}. In 2011, the highest Mg^{2+} concentration was 7.45 mg/L detected at WHC2C, and the lowest concentration of 0.237 mg/L was detected at WHC2A. The Mg^{2+} concentrations at Winter House Brook and WHC2B were 5.64 mg/L and 0.242 mg/L, respectively. Similarly in 2012, the highest Mg^{2+} concentration was detected at WHC2C (12.1 mg/L) and the lowest was detected at WHC2B (0.073 mg/L). Winter House Brook and WHC2A had Mg^{2+} concentrations of 8.65 mg/L and 6.02 mg/L, respectively, while all other springs (WHC2A-R, WHC2B-R and WHC1) ranged from 0.299 to 0.096 mg/L. The water discharging from WHC2A had a high Mg^{2+} concentration (6.02 mg/L) and was not similar to concentrations detected at other ultra-basic water in 2011 nor 2012; however, the Mg^{2+} concentration in WHC2A-R fluids (0.096 mg/L) were significantly lower and were similar to other springs in both 2011 and 2012.

Unlike Mg^{2+}, the Ca^{2+} concentrations were higher in the ultra-basic fluids compared to the non ultra-basic water sampled. In 2011, the highest Ca^{2+} was detected at WHC2A (59.6 mg/L) and the lowest was detected at Winter House Brook (0.388 mg/L). The Ca^{2+} concentration at WHC2C was 9.90 mg/L and the Ca^{2+} concentration at WHC2B

was similar to spring 2A at 58.3 mg/L. In 2012, the highest Ca^{2+} concentration was detected at WHC2B-R (61.0 mg/L) and the lowest was at Winter House Brook (0.771 mg/L). At WHC2C the Ca^{2+} concentration was 3.47 mg/L. All other ultra-basic spring waters (WHC2A, WHC2A-R, WHC2B-R and WHC1) ranged from 4.60 to 60.1 mg/L. There was an increase in the Ca^{2+} concentration at spring 2A after the recharge experiment from 19.0 mg/L (WHC2A) to 58.8 mg/L (WHC2A-R), which was similar to concentrations detected in other spring water in both 2011 and 2012. From 2011 to 2012, with the exception of WHC2A in 2012, the Ca^{2+} concentration of the spring waters at WHC2A and WHC2B including the recharge water WHC2A-R and WHC2B-R were consistent (59.6 ± 1.1 mg/L, n=5). The concentrations detected at Winter House Brook and the mixing site WHC2C also remained consistent from 2011 to 2012.

In 2012, the highest K^+ concentration was detected at WHC2B-R (12.8 mg/L) and the lowest was detected at Winter House Brook (0.16 mg/L). WHC2C had a K^+ concentration of 2.73 mg/L and all other springs ranged from 3.62 to 12.6 mg/L. The highest Na^+ concentration in 2012 was detected at WHC2B (933 mg/L) and the lowest was detected at Winter House Brook (5.82 mg/L). The Na^+ concentration at WHC2C was 95.6 mg/L and all other springs (WHC2A, WHC2A-R, and WHC2B-R) ranged from 129 to 896 mg/L. In 2011, cations K^+ and Na^+ were not analyzed for therefore a comparison between years cannot be made.

Inorganic nitrogen (NH_4^+ and NO_3^-) was analyzed at ultra-basic springs, the mixing site and Winter House Brook in 2011 and 2012. Ammonia concentrations were higher in the ultra-basic spring waters than the water sampled from Winter House Brook in 2012. The lowest concentration of 0.028 mg/L was detected at Winter House Brook

and the highest concentration of 1.70 mg/L was detected at WHC2B. The mixing site WHC2C and WHC2A had similar concentrations of 0.317 mg/L and 0.291 mg/L, respectively. The recharge water from WHC2A-R and WHC2B-R had higher values of 1.20 mg/L and 1.11 mg/L, respectively, more reflective of the concentration seen at WHC2B. Much like other geochemical parameters the concentration detected at WHC2A does not follow the pattern of the other ultra-basic springs (WHC2B, WHC2A-R and WHC2B-R).

Nitrate in 2011 and 2012 was higher in waters sampled from Winter House Brook (0.190 to 0.196 mg/L) and WHC2C (0.172 to 0.750 mg/L) compared to water discharging from the springs. In 2011, spring fluids WHC2A and WHC2B had a nitrate concentration of 0.0145 ± 0.0007 mg/L, n=2. In 2012, spring fluids before the recharge experiment had nitrate concentrations ranging from 0.071 to 0.142 mg/L. The nitrate detected in the recharge waters (0.077 mg/L at WHC2A-R, and 0.085 mg/L at WHC2B-R) were much lower than WHC2A (0.142 mg/L) and comparable to WHC2B (0.071 mg/L). Fluids from WHC2A and WHC2B in 2011 had nitrate concentrations that were in the same order of magnitude as the spring waters from 2012, with the exception of WHC2A in 2012 which was higher and did not follow the mould.

Total organic nitrogen was only calculated for 2012 as there were no ammonia concentrations for 2011 and therefore the calculation could not be made. There was no observable pattern in the total organic nitrogen concentrations at the Tablelands. The total organic nitrogen at Winter House Brook was below the detection limit. In 2012, the highest total organic nitrogen was at WHC2A (0.814 mg/L) and the lowest was at WHC2B (0.029 mg/L). The mixing site (WHC2C) and all other spring fluids (WHC2A-R

and WHC2B-R) ranged from 0.042 to 0.769 mg/L. At WHC2A the total organic nitrogen decreased from 0.814 mg/L to 0.102 mg/L after the recharge experiment and at WHC2B the total organic nitrogen increased from 0.029 mg/L to 0.769 mg/L after the recharge experiment.

Sulphate and phosphate concentrations were analyzed in both 2011 and 2012. In general phosphate concentrations were higher in 2011 compared to 2012 at all sampling locations and there was no significant change in concentration in the spring waters before and after the recharge experiment. Conversely, sulphate concentrations increased from 2011 to 2012 at all sampling locations, but by varying degrees. In 2011, the highest phosphate concentration of 0.76 ± 0.16 mg/L was detected at Winter House Brook and the lowest concentration of 0.08 ± 0.06 mg/L was detected at WHC2A. The concentrations at WHC2C and WHC2B were similar at 0.45 ± 0.21 mg/L and 0.41 ± 0.16 mg/L, respectively. In 2012, the highest concentration was detected at WHC2C (0.070 mg/L) and the lowest was at WHC2A (0.039 mg/L). All other springs (WHC2A-R, WHC2B and WHC2B-R) and Winter House Brook had a similar concentration of 0.046 ± 0.003 (n=4) to that of WHC2A.

In 2011, the highest sulphate concentration was detected at WHC2C (0.92 ± 0.11 mg/L) and the lowest was detected at Winter House Brook (0.250 ± 0.001 mg/L). Springs WHC2A and WHC2B had sulphate concentrations of 0.82 ± 0.01 mg/L and 0.38 ± 0.10 mg/L, respectively. In 2012, the highest sulphate concentration of 1.30 mg/L was detected at WHC2A and the lowest concentration of 0.364 mg/L was detected at WHC2A-R. Similar to WHC2A, Winter House Brook and WHC2C had relatively higher concentrations of sulphate measuring 1.11 mg/L and 1.25 mg/L, respectively. Springs

WHC2B and WHC2B-R had lower concentrations (0.438 mg/L and 0.599 mg/L, respectively) more similar to WHC2A-R. The sulphate content in WHC2A fluids was much higher than the concentration detected at all the other spring sites (WHC2A-R, WHC2B and WHC2B-R).

Trace ion concentrations from all sampling sites at the Tablelands are graphed in Figure 3.10 (raw data in Table A.9) for 2011 and Figure 3.11 (raw data in Table A.10) for 2012. Alkali metal ions (Li^+ and Rb^+) were lower in concentration in the non ultra-basic water from Winter House Brook and at the mixing site WHC2C compared to the ultra-basic water discharging from the springs in both 2011 and 2012. In 2012, there was an increase in alkali metal ion concentration at spring WHC2A after the recharge experiment (from 22.7 to 48.9 µg/L for Li^+ and from 3.23 to 8.71 µg/L for Rb^+), while water from spring WHC2B stayed consistent (64.2 ± 0.4 µg/L, n =2, for Li^+ and 8.86 ± 0.05 µg/L, n=2, for Rb^+).

Alkaline metal ions (Ba^{2+} and Sr^{2+}) were also lower in concentration in the non ultra-basic water from Winter House Brook and at the mixing site WHC2C compared to the ultra-basic water sampled from the springs in both 2011 and 2012. Again there was an increase observed in alkaline metal ion concentration in WHC2A after the recharge experiment (from 0.825 to 1.70 µg/L for Ba^{2+} and from 7.70 to 16.7 µg/L for Sr^{2+}), while water from WHC2B remained consistent (1.97 ± 0.11 µg/L, n=2, for Ba^{2+} and 16.0 ± 0.0 µg/L, n=2, for Sr^{2+}).

In 2011 and 2012 transition metals $Fe^{2+, 3+}$, Hg^{2+}, $Cu^{+, 2+}$ and $Mn^{2+, 3+}$ were detected in trace amounts at Winter House Brook and ranged from 0.076 to 54.2 µg/L in spring fluids (WHC2A, WHC2B, WHC2A-R, WHC2B-R and WHC1) with the exception

of WHC2A in 2012. Conversely, transition metals $Cr^{2+, 3+}$ and $Ni^{2+, 3+}$ were generally

higher in concentration at Winter House Brook (2.09 to 3.53 µg/L) and WHC2C (1.76 to

5.00 µg/L) compared to all springs waters (1.27 to 21.1 µg/L) in 2011 and 2012. In 2011,

Zn^{2+} concentrations were highest at WHC2A (4.36 µg/L) and lowest at WHC2C (0.619

µg/L). The concentration detected at Winter House Brook and WHC2B were 1.71 µg/L

and 0.625 µg/L, respectively. In 2012, Zn^{2+} was below the detection limit in all waters

sampled. Lastly, $Ti^{3+, 4+}$ concentrations detected at WHC2C and WHC2B were 1.05 µg/L

and 0.116 µg/L, respectively and at Winter House Brook and WHC2A $Ti^{3+, 4+}$ was below

the detection limit in 2011. Similar to Zn^{2+}, in 2012 $Ti^{3+, 4+}$ was below the detection limit

in all waters sampled.

Post transition metal ions (Al^{3+}, $Pb^{2+, 4+}$ and $Sn^{2+, 4+}$) were higher in concentration

in 2011 compared to 2012. Al^{3+} was detected at all sampling sites (Winter House Brook,

WHC2C, WHC2A and WHC2B) in 2011 (2.77 ± 0.47 µg/L, n =4) and in 2012 it was

only detected at WHC2A-R (24.5 µg/L). $Sn^{2+, 4+}$ was detected in the ultra-basic water at

springs WHC2A (1.33 µg/L) and WHC2B (2.01 µg/L) as well as the mixing site WHC2C

(0.205 µg/L), but not at Winter House Brook in 2011. In 2012, $Sn^{2+, 4+}$ was not detected at

any sampling site. In 2011, $Pb^{2+, 4+}$ was detected at all sampling sites (Winter House

Brook, WHC2C, WHC2A and WHC2B) but in very small quantities (≤0.054 µg/L). In

2012, $Pb^{2+, 4+}$ was only detected in spring waters (WHC2A-R, WHC2B and WHC2B-R)

at ≤0.307 µg/L.

Metalloid ions (B and Si) were greater in concentration in Winter House brook

and at WHC2C fluids compared to spring fluids in 2011. However, in 2012 B was below

the detection limit at all sampling sites and the Si at WHC2A (4.97 mg/L) was more

similar to the concentration detected at WHB (3.27 mg/L) and WHC2C (7.49 mg/L) which was greater than all other springs sampled (WHC2A-R (1.66 mg/L), WHC2B (0.54 mg/L), WHC2B-R (1.30 mg/L) and WHC1 (0.43 mg/L)). Metalloid ion $Sb^{3+, 5+}$ in 2011 was below the detection limit at all sites except WH2B (0.028 μg/L). In 2012, the highest $Sb^{3+, 5+}$ concentration was detected at WHC1 (0.49 μg/L) and the lower concentrations of 0.048 μg/L and 0.052 μg/L were detected at WHC2A and WHC2B-R, respectively.

Non metals (S^{2-} and P^{3-}) were below detection limits at all sampling sites in 2011. Similarly in 2012, S^{2-} and P^{3-} were below detection limits at all sampling sites with the exception of WHC2B-R which had a sulphur and phosphorus concentration of 9.93 mg/L and 0.03 mg/L, respectively. In 2011, I^- concentrations were 1-2 orders of magnitude greater in spring fluids (128 to 251 μg/L) than fluids sampled from the mixing site (36.5 μg/L) and Winter House Brook (<5.51 μg/L). Iodide was not analyzed in 2012 so no comparison between years could be made.

A comparison of the bulk oxidized and reduced pools of carbon (TIC and DOC) and organic acids in the ultra-basic water discharging from the springs and non ultra-basic water from Winter House Brook are reported in Table 3.19 for 2011 and Table 3.20 for 2012. In both 2011 and 2012, the highest total inorganic carbon concentration was detected at the mixing site, WHC2C, and the non ultra-basic water sampled from the brook had a greater total inorganic carbon concentration compared to the concentration detected at the ultra-basic springs. In 2011, total inorganic carbon was highest at WHC2C (13.5 ± 0.6 mg/L) and lowest at WHC2A (1.13 ± 0.40 mg/L). Non ultra-basic water sampled from Winter House Brook had a total inorganic carbon concentration of 7.14 ± 0.37 mg/L and the ultra-basic spring WHC2B was similar to WHC2A at 1.23 ± 0.35

mg/L. Similarly in 2012, the highest total inorganic carbon concentration was detected at WHC2C (16.9 ± 0.2 mg/L), however the lowest concentration was detected at WHC2B (0.22 ± 0.01 mg/L), instead of at WHC2A. The total inorganic carbon concentration at Winter House Brook was 7.86 ± 0.01 mg/L and all other ultra-basic springs (WHC2A, WHC2A-R and WHC2B-R) ranged from 1.49 to 2.75 mg/L.

Non ultra-basic water from Winter House Brook was the most enriched in ^{13}C compared to the total inorganic carbon collected from the other sites in both 2011 and 2012. The total inorganic carbon detected in the water discharging from the ultra-basic springs was either similar or more depleted in ^{13}C compared to the total inorganic carbon collected from the mixing site. The δ^{13}C of total inorganic carbon was the least negative at Winter House Brook (-2.1 ± 0.1 ‰) and the most negative at WHC2B (-17.6 ± 0.4 ‰) in 2011. The total inorganic carbon detected at WHC2C and WHC2A had a δ^{13}C value of -11.8 ± 0.0 ‰ and -14.7 ± 0.9 ‰, respectively. In 2012, the δ^{13}C of total inorganic carbon was the least negative at Winter House Brook (-4.3 ± 0.2 ‰) and the most negative at WHC2A-R (-23.5 ± 0.3 ‰). All other springs (WHC2A, WHC2B and WHC2B-R) and the mixing site WHC2C ranged from -13.9 to -18.6 ‰.

In 2011, the highest dissolved organic carbon concentration was detected at WHC2C (0.84 ± 0.01 mg/L) and the lowest was detected at WHC2B (0.29 ± 0.03 mg/L). The dissolved organic carbon concentrations at Winter House Brook and WHC2A were 0.30 ± 0.01 mg/L and 0.35 ± 0.20 mg/L, respectively. In 2012, dissolved organic carbon measurements were not attained due to methodical errors. The only reported δ^{13}C value for dissolved organic carbon was for WHC2C at -23.7 ± 0.0 ‰. The dissolved organic carbon concentrations at all other sites were too low for isotopic analysis.

Fluids were not sampled for organic acid analysis in 2011, but in 2012 fluids were collected for the analysis of formate, acetate, propionate, butyrate and lactate. Only acetate and formate were detected in the non ultra-basic water from Winter House Brook and the ultra-basic water discharging from the springs. In general the acetate and formate concentrations were greater in the ultra-basic water sampled from the springs compared to the water sampled from Winter House Brook and WHC2C. The highest acetate concentration was detected at WHC2B (4.49 ± 0.24 mg/L) and the lowest was detected at Winter House Brook (0.124 ± 0.037 mg/L). All other springs (WHC2A, WHC2A-R and WHC2B-R) and the mixing site WHC2C ranged from 0.311 to 3.67 mg/L. The highest formate concentration was detected at WHC2A-R (1.30 ± 0.052 mg/L) and the lowest was detected at WHC2C (0.047 ± 0.023 mg/L). The formate concentration at Winter House Brook was below the detection limit. All other springs (WHC2A, WHC2B and WHC2B-R) ranged from 0.051 to 0.593 mg/L.

The δ^2H_{H2O} and $\delta^{18}O_{H2O}$ values of non ultra-basic fluid collected from Winter House Brook and ultra-basic fluids discharging from the springs in 2012 are plotted in Figure 3.12. There were two distinct clusters of the Tablelands data. The first cluster consisting of WHB, WHC2C and the two ultra-basic springs before the recharge experiment (WHC2A and WHC2B) had a more enriched δ^2H_{H2O} and $\delta^{18}O_{H2O}$ signature compared to the second cluster consisting of WHC1 and the two ultra-basic springs after the recharge experiment (WHC2A-R and WHC2B-R). The recharge water from springs were more depleted in both ^2H and ^{18}O compared to the original isotopic values observed before the pool was emptied and then allowed to recharge with only the ultra-basic water discharging from these two springs.

3.2.2 Gaseous Composition of Spring Waters and Winter House Brook Waters

The dissolved gaseous composition (H_2, CO_2, and C_1-C_6) of waters sampled from the Tablelands can be seen in Table 3.21 for 2011 and Table 3.22 for 2012. Dissolved gases were sampled at all springs, with the exception of WHC1 where the recharge rate of the shallow pool did not allow for this sampling technique, as well as at the mixing site and Winter House Brook. Over all, dissolved hydrogen gas and low molecular weight hydrocarbons (C_1-C_6) were higher in ultra-basic fluids sampled from the springs than in fluids sampled from Winter House Brook and the mixing site where overland flow from Winter House Brook mixes with the ultra-basic water discharging from the springs below. The dissolved gases detected in the ultra-basic fluids discharging from the springs were primarily composed of hydrogen and methane. Methane and hydrogen were 1-4 orders of magnitude greater than higher molecular weight hydrocarbons C_2-C_6.

In both 2011 and 2012, there was a higher concentration of dissolved hydrogen in spring fluids compared to fluids sampled from Winter House Brook and WHC2C. In 2011, the highest dissolved concentration of hydrogen was detected at WHC2A (584 ± 25 μM) and the lowest was detected at the mixing site WHC2C (34.7 ± 5.0 μM). The second ultra-basic spring WHC2B had a dissolved hydrogen concentration of 515 ± 59 μM. In 2012, dissolved hydrogen was below the limit of detection in fluids sampled from Winter House Brook and WHC2C. The dissolved hydrogen concentrations detected from the springs before (WHC2A and WHC2B) and after (WHC2A-R and WHC2B-R) the recharge experiment were very similar at 481 ± 35 μM (n=4) with WHC2B being the highest at 529 μM. Dissolved carbon dioxide was analyzed in 2012 for fluids sampled from Winter House Brook and WHC2C. The dissolved carbon dioxide concentration at

WHC2C was 108 ± 41 μM, while the concentration at Winter House Brook was below the quantification limit (<16.8 μM).

Dissolved hydrocarbon gases C_1-C_6 were analyzed in 2012, but only methane was analyzed in 2011. In 2011 the highest dissolved methane concentration of 20 ± 0.6 μM was detected at both WHC2A and WHC2B and the lowest concentration of 1.87 ± 0.00 μM was detected at WHC2C. In 2012, WHC2B had the highest dissolved methane concentration (36.8 μM) and WHC2C had the lowest (13.4 ± 0.5 μM). No dissolved methane was detected in fluids sampled from Winter House Brook. All other springs (WHC2A, WHC2A-R and WHC2B-R) ranged from 25.8 to 36.3 μM. The dissolved methane concentrations detected in spring fluids before and after the recharge experiment were very similar. In fluids sampled from the ultra-basic springs (WHC2A and WHC2B) and the mixing site the dissolved methane increased in concentration from 2011 to 2012.

Dissolved hydrocarbons C_2-C_6 (ethane, propane, iso-butane, n-butane, iso-pentane, n-pentane, and n-hexane) were analyzed in all fluids sampled in 2012. Dissolved C_2-C_6 hydrocarbon concentrations were quantified in spring fluids (WHC2A, WHC2B, WHC2A-R and WHC2B-R), where as in fluids sampled from Winter House Brook and the mixing site (WHC2C) C_2-C_6 hydrocarbon concentrations were below the detection or quantification limit. Dissolved ethane detected at the springs before (WHC2A and WHC2B) and after (WHC2A-R and WHC2B-R) the recharge experiment were similar in concentration (1.25 ± 0.04 μM, n =4). Hydrocarbons C_3-C_6 were highest in concentration at WHC2B-R (ranging from 0.152 to 1.04 μM) and lowest at WHC2A (ranging from 0.086 to 0.499 μM). Recharge fluids (WHC2A-R and WHC2B-R) always had higher C_3-C_6 concentrations compared to fluids sampled before the pool was emptied (WHC2A and

WHC2B). The branched alkanes (iso-butane and iso-pentane) were always less in concentration than the straight alkanes (n-butane and n-pentane) for all of the springs sampled (WHC2A, WHC2A-R, WHC2B and WHC2B-R).

3.2.3 Isotopic Composition of Gaseous Hydrocarbons

The carbon isotopic composition ($\delta^{13}C$) of gases sampled at Winter House Brook, the mixing site as well as the springs can be seen in Table 3.23 for 2011 and Table 3.24 for 2012. In 2011, the $\delta^{13}C$ of carbon dioxide was least negative at Winter House Brook (-3.5 ‰) and most negative at WHC2C (-14.1 ± 4.7 ‰). Similarly in 2012, the $\delta^{13}C$ of carbon dioxide was least negative at Winter House Brook (-10.2 ‰) and most negative at WHC2C (-19.2 ‰). The concentrations of carbon dioxide in spring fluids (WHC2A, WHC2A-R, WHC2B and WHC2B-R) were too low for $\delta^{13}C$ analysis in 2011 and 2012.

Carbon isotope values for low molecular weight hydrocarbons (C_1-C_6) were analyzed at WHC2C and the springs WHC2A and WHC2B in both 2011 and 2012. The range of $\delta^{13}C$ values for methane in both years was -27.7 to -25.9 ‰ and the range for other low molecular weight hydrocarbons (C_2-C_6) was-32.4 to -29.7 ‰. There was little variation in the carbon isotopic values of C_1-C_6 between all springs sampled from 2011 to 2012 (≤1.8 ‰ error). The only isotope value reported for WHC2C was methane as hydrocarbons C_2-C_6 were too low in concentration for $\delta^{13}C$ analysis in both 2011 and 2012.

In 2011, the $\delta^{13}C$ of methane was least negative at WHC2C (-25.9 ‰) and most negative at WHC2B (-27.4 ‰). The $\delta^{13}C$ of methane detected at WHC2A was very similar to WHC2B at -27.1 ‰. In 2012, the $\delta^{13}C$ of methane was least negative at

WHC2A (-25.9 ‰) and most negative at WHC2A-R (-27.7 ‰). The $\delta^{13}C$ of methane at WHC2B and WHC2B-R were -27.0 ‰ and -27.5 ‰, respectively and at WHC2C the value was -26.2 ‰. Both springs had a slight depletion of ^{13}C in methane in the recharge waters (WHC2A-R and WHC2B-R) compared to water sampled before the experiment (WHC2A and WHC2B).

In 2011, the $\delta^{13}C$ of ethane, propane and butane at WHC2A and WHC2B ranged from -29.8 to -31.9 ‰. Hydrocarbons iso-butane, iso-pentane, n-pentane and n-hexane were too low in concentration for isotope measurements. Similarly in 2012, the $\delta^{13}C$ of ethane, propane and butane at WHC2A-R, WHC2B and WHC2B-R ranged from -29.7 to 32.4 ‰. Once again iso-butane, iso-pentane, n-pentane and n-hexane were too low in concentration for $\delta^{13}C$ analysis. At WHC2A in 2012 and there were no isotope values for any hydrocarbon other than methane due to low concentrations.

3.2.4 Volatile and Semi Volatile Organic Compound Composition

Volatile organic compounds analyzed at the springs, the mixing site and Winter House Brook at the Tablelands can be found in Table 3.25 for 2011 and Table 3.26 for 2012. In general, no volatile organic compounds were detected at Winter House Brook or at WHC2C in both 2011 and 2012. In 2011 the concentrations of volatile organic compounds that were quantified (cyclohexane and methylcyclohexane) at the springs (WHC2A and WHC2B) were very similar to one another. In 2012, the recharge water (WHC2A-R and WHC2B-R) had higher volatile organic compound concentrations than water sampled before the experiment (WHC2A and WHC2B). WHC2B-R always had the highest volatile organic compound concentrations followed by WHC2A-R. Waters

sampled from both springs after the recharge (WHC2A-R and WHC2B-R) were very similar in volatile organic compound composition and concentration to one another. The concentration of cyclohexane and methylcyclohexane was higher at WHC2A and WHC2B in 2011 compared to 2012; however the concentration of these compounds at WHC2A-R and WHC2B-R in 2012 was higher than fluids sampled at the springs in 2011. From 2011 to 2012 there was more volatile organic compounds detected, although the majority of the concentrations were below the limit of quantification. Overall, spring fluid volatile organic compound compositions were dominated by cyclic compounds from 2011 to 2012.

In 2011, volatile compounds including higher molecular weight alkanes and alkenes (n-heptane and 1-heptene) and aromatic compounds were below the detection limit in fluids sampled from WHC2A, WHC2B, WHC2C and Winter House Brook. Only cyclohexane and methylcyclohexane were quantifiable in spring fluids (WHC2A and WHC2B) with concentrations ranging from 0.382 to 0.696 μM. The cyclohexane and methylcyclohexane concentrations between the two springs were comparable. Trace amounts of methylcyclopentane was also detected in spring fluids (<0.119 μM).

In 2012, the only high molecular weight alkane or alkene detected in spring fluids was 1-heptane (<0.102 μM) at WHC2B-R. Similarly volatile aromatic compounds including the group BTEX were either not detected or present in trace quantities in spring fluids sampled. There were multiple cyclic alkanes detected in the spring fluids (WHC2A, WHC2B, WHC2A-R and WHC2B-R) including cyclohexane, methylcyclopentane, methylcyclohexane, dimethylcyclohexane and ethylcyclohexane, however, only cyclohexane (from 0.388 to 0.747 μM) and methylcyclohexane (from 0.187 to 0.475 μM)

were quantifiable. All quantifiable volatile organic compounds were greater in concentrations in spring fluids sampled after the recharge experiment (WHC2A-R and WHC2B-R) compared to spring fluids sampled before the recharge experiment (WHC2A and WHC2B).

Dissolved semi volatile organic compound (S-VOC) concentrations analyzed at the springs, the mixing site and Winter House Brook at the Tablelands can be found in Table 3.27 for 2012. Semi volatile organic compound samples were compromised in 2011 and are not reported. No dissolved semi volatile organic compounds were detected in fluids from Winter House Brook and WHC2C in 2012. In spring fluids dissolved straight chained alkanes including C_{17}, C_{24-28}, C_{30} and C_{31} were detected but there were no dissolved polycyclic aromatic hydrocarbons (PAH) detected. There were no branched alkanes detected in any fluid sampled from the Tablelands. Fluids collected from WHC2A-R had the widest range of high molecular weight alkanes and consistently had the highest concentration of any semi volatile organic compounds detected. Alkane C_{17} concentrations were detected in recharge spring waters WHC2A-R (7.1×10^{-3} μM) and WHC2B-R (6.2×10^{-3} μM) but not in spring fluids before the recharge experiment (WHC2A and WHC2B). Alkane C_{24} was also detected in WHC2A-R fluids ($3.7 \times 10^{-3} \pm 5.9 \times 10^{-5}$ μM) but not in any other spring fluids. Similarly, alkanes C_{26} (3.5×10^{-3} μM), C_{28} ($3.9 \times 10^{-3} \pm 2.8 \times 10^{-4}$ μM), C_{30} ($3.5 \times 10^{-3} \pm 7.1 \times 10^{-5}$ μM), and C_{31} (3.3×10^{-3} μM) were detected in WHC2A-R fluids but not in any other fluid sampled from the Tablelands. Alkane C_{27} on the other hand was detected at WHC2A (4.2×10^{-3} μM), WHC2A-R ($4.2 \times 10^{-3} \pm 2.4 \times 10^{-4}$ μM), and WHC2B (4.0×10^{-3} μM) and alkane C_{25} was detected at WHC2A (3.5×10^{-3} μM) and WHC2A-R (3.7×10^{-3} μM).

3.2.5 Sedimentary Organic Matter Composition

Outcrop and shale sample descriptions from which the sedimentary organic matter (SOM) was extracted can be found in Table 3.28 and sampling locations can be found in Figure 2.4. The Tablelands peridotite undergoing serpentinization is part of a group of ophiolitic rocks that form the high structural slices of the Humber Arm Allochthon (HAA). HAA1 was sampled in Lobster Cove from the Green Point Formation of the Cow Head Group which are sedimentary rocks that are part of the lower structural slices of the Humber Arm Allochthon. HAA2 was sampled by the Trout River Small Pond from the Crolly Cove mélange which are sedimentary and ophiolitic rocks that are part of the higher structural slices of the Humber Arm Allochthon and likely to be the sedimentary rocks that are directly cradling the Tablelands peridotite. HAA3-6 were sampled along the shoreline of Winter House Brook from the Blow Me Down Brook Formation which are sedimentary and volcanic rocks that are part of the intermediate structural slices of the Humber Arm Allochthon. This formation may also be in direct contact with the Tablelands peridotite or underlying sedimentary and ophiolitic rocks from higher structural slices such as the Crolly Cove mélange. A more detailed description of rock formations and the geologic context of the different slices in the Humber Arm Allochthon can be found on the Williams and Cawood Humber Arm Allochthon map (1989). In general samples HAA1-4 were heavily cleaved fine grained shale rocks that were dark gray in colour. HAA5 was identified as limestone and HAA6 was identified as a fine to medium grained siltstone or sandstone.

The carbon isotopic composition of sedimentary organic matter samples (HAA1-6) collected from the Tablelands can be seen in Table 3.19. The $\delta^{13}C$ of bulk carbon in

sedimentary organic matter samples varied greatly among samples ranging from -4.9 ‰

to -31.6 ‰. The most negative δ^{13}C of the fine grained shale samples was -31.6 ‰ at

HAA2 and the least negative was -16.3 ‰ at HAA4. The δ^{13}C of HAA1 and HAA3 were

-27.4 ‰ and -22.4 ‰, respectively. The limestone sample (HAA5) had a δ^{13}C value of

-4.9 ‰ and the medium grained sedimentary sample (HAA6) had a δ^{13}C value of

-23.6 ‰.

3.3 Tables and Figures

Table 3.1. A comparison of aqueous, inorganic geochemical parameters of waters sampled at The Cedars in 2011.

	AC	BS9	BS5	BS7	NS1	GPS1	r^2
pH	9.0	10.0	11.8	11.7	11.4	11.9	nc
E_h (mV)	+323	+120 to +304	-616	-618	-620	-655	nc
Cond (µS/cm)	314	163	880	823	752	3020	0.91
Ca^{2+}/Mg^{2+}	0.3	5	216	389	1004	1231	0.48
E^3H_{H2O} (TU)[a]	-	-	-	-	-	-	nc
f_{UB}[b]	0.00	0.16	0.13	0.12	0.07	1.00	

- = not analyzed/not sampled; n/a = calculation not available; nc = indicates that there were not enough data points to confidently do the r^2 calculation or the parameter (e.g. pH) is not on a linear scale. The r^2 is a correlation co-efficient of the regression analysis of the concentration and f_{UB}, which depicts how well the parameter is described by the two component mixing model. The r^2 was calculated when there were at minimum 3 data points and no more than half of the data points were an end member.
[a] Electrolytic tritium (^3H) of water
[b] The f_{UB} is the calculated fraction of ultra-basic water contributing to that particular spring during that sampling period using Equation 2.2.

Table 3.2. A comparison of aqueous, inorganic geochemical parameters of waters sampled at The Cedars in 2012.

	AC	BS9	BS5	BS7	NS1	GPS1	r^2
pH	8.9	-	11.9	-	11.4	12.5	nc
E_h (mV)	-	-	-	-	-	-	nc
Cond (μS/cm)	206	-	797	-	466	1628	0.93
Ca^{2+}/Mg^{2+}	0.1	-	148	-	174	2015	0.99
E^3H_{H2O} (TU)[a]	-	-	-	-	-	-	nc
f_{UB}[b]	0.00	-	0.16	-	0.08	1.00	

- = not analyzed/not sampled; n/a = calculation not available; nc = indicates that there were not enough data points to confidently do the r^2 calculation or the parameter (e.g. pH) is not on a linear scale. The r^2 is a correlation co-efficient of the regression analysis of the concentration and f_{UB}, which depicts how well the parameter is described by the two component mixing model. The r^2 was calculated when there were at minimum 3 data points and no more than half of the data points were an end member.
[a] Electrolytic tritium (^3H) of water
[b] The f_{UB} is the calculated fraction of ultra-basic water contributing to that particular spring during that sampling period using Equation 2.2.

Table 3.3. A comparison of aqueous, inorganic geochemical parameters of waters sampled at The Cedars in 2013.

	AC	BS9	BS5	BS7	NS1	GPS1	r^2
pH	8.8	10.0	12.1	12.0	12.0	12.6	nc
E_h (mV)	+68	+237	-602	-419	-632	-698	nc
Ca^{2+}/Mg^{2+}	0.3	-	95	-	972	90	0.08
E^3H_{H2O} (TU)[a]	-	-	2.3	-	1.2	<0.8	0.43
f_{UB}[b]	0.00	-	0.17	-	0.08	1.00	

- = not analyzed/not sampled; nc = indicates that there were not enough data points to confidently do the r^2 calculation or the parameter (e.g. pH) is not on a linear scale. The r^2 is a correlation co-efficient of the regression analysis of the concentration and f_{UB}, which depicts how well the parameter is described by the two component mixing model. The r^2 was calculated when there were at minimum 3 data points and no more than half of the data points were an end member.

[a] Electrolytic tritium (^3H) of water
[b] The f_{UB} is the calculated fraction of ultra-basic water contributing to that particular spring during that sampling period using Equation 2.2.

Table 3.4. Bulk aqueous carbon pools and organic acids measured from waters sampled at The Cedars in 2011.

	AC	BS9	BS5	BS7	NS1	GPS1	r^2
TIC (mg/L)	33.26 (± 0.74)	10.85 (± 0.41)	0.88 (± 0.11)	0.68 (± 0.03)	0.07 (± 0.02)	0.23 (± 0.03)	0.14
$\delta^{13}C_{TIC}$ (‰)	-14.5 (± 0.1)	-23.0 (± 0.1)	-32.5 (± 1.5)	-33.0 (± 0.8)	-63.5 (± 1.3)	-41.1 (± 0.1)	nc
DOC (mg/L)	-	-	-	-	-	-	nc
$\delta^{13}C_{DOC}$ (‰)	-	-	-	-	-	-	nc
Acetate (mg/L)	-	-	-	-	-	-	nc
Formate (mg/L)	-	-	-	-	-	-	nc
f_{UB}[a]	0.00	0.16	0.13	0.12	0.07	1.00	

- = not analyzed/not sampled; nc = indicates that there were not enough data points to confidently do the r^2 calculation or the parameter (e.g. pH) is not on a linear scale. The r^2 is a correlation co-efficient of the regression analysis of the concentration and f_{UB}, which depicts how well the parameter is described by the two component mixing model. The r^2 was calculated when there were at minimum 3 data points and no more than half of the data points were an end member.

[a] The f_{UB} is the calculated fraction of ultra-basic water contributing to that particular spring during that sampling period using Equation 2.2.

The error reported is the standard deviation of replicate samples.

Table 3.5. Bulk aqueous carbon pools and organic acids measured from waters sampled at The Cedars in 2013.

	AC	BS9	BS5	BS7	NS1	GPS1	r^2
TIC (mg/L)	-	-	-	-	-	0.55	nc
$\delta^{13}C_{TIC}$ (‰)	-	-	-	-	-	-24.0	nc
DOC (mg/L)	0.34 (± 0.01)	-	1.53	-	-	3.32 (± 1.11)	nc
$\delta^{13}C_{DOC}$ (‰)	-24.0 (± 0.2)	-	-17.8	-	-	-19.2 (± 7.7)	nc
Acetate (mg C/L)	-	-	-	-	-	-	nc
Formate (mg C/L)	-	-	-	-	-	-	nc
f_{UB}[a]	0.00	-	0.17	-	0.08	1.00	

- = not analyzed/not sampled; nc = indicates that there were not enough data points to confidently do the r^2 calculation or the parameter (e.g. pH) is not on a linear scale. The r^2 is a correlation co-efficient of the regression analysis of the concentration and f_{UB}, which depicts how well the parameter is described by the two component mixing model. The r^2 was calculated when there were at minimum 3 data points and no more than half of the data points were an end member.

[a] The f_{UB} is the calculated fraction of ultra-basic water contributing to that particular spring during that sampling period using Equation 2.2.

The error reported is the standard deviation of replicate samples.

Table 3.6. Gaseous composition of ultra-basic spring waters and water sampled from Austin Creek at The Cedars in 2011.

	Bubbling (% mol)		Dissolved (µM)				r^2
	BS9	BS5	AC	BS7	NS1	GPS1	
H_2	41.3 (± 5.2)	43.3 (± 1.3)	<d.l.	-	73.8 (± 24.3)	316 (± 1)	nc
CO_2	<d.l.	<d.l.	22.6	<d.l.	<d.l.	<d.l.	nc
CH_4	5.8 (± 0.8)	6.3 (± 0.2)	10.8	53.6	130 (± 42)	91.8 (± 2.3)	0.09
	(ppm mol)						
C_2H_6	52.6 (± 7.5)	64.8 (± 1.9)	<d.l.	<d.l.	<d.l.	0.299 (± 0.013)	nc
C_3H_8	32.7 (± 4.4)	38.9 (± 1.3)	<d.l.	<0.068	<0.068	0.113 (± 0.007)	nc
iC_4H_{10}	19.7 (± 2.6)	21.8 (± 0.8)	<d.l.	<0.069	<d.l.	<0.069	nc
nC_4H_{10}	38.9 (± 5.3)	45.7 (± 2.1)	<d.l.	<0.069	<0.069	0.103 (± 0.007)	nc
iC_5H_{12}	32.2 (± 4.6)	35.7 (± 2.4)	<d.l.	<0.069	<0.069	0.097 (± 0.008)	nc
nC_5H_{12}	37.6 (± 5.3)	42.4 (± 3.1)	<d.l.	<0.069	<0.069	0.097 (± 0.008)	nc
nC_6H_{14}	50.6 (± 7.5)	58.2 (± 1.6)	<0.070	0.139	0.139 (± 0.001)	0.499 (± 0.081)	0.99
C_1/C_{2+}	464	413	-	-	-	178	nc
f_{UB}[a]	0.16	0.13	0.00	0.12	0.07	1.00	

- = not analyzed/not sampled; <d.l. = analyte was below detection limits of the analytical method used; nc = indicates that there were not enough data points to confidently do the r^2 calculation or the parameter (e.g. pH) is not on a linear scale. The r^2 is a correlation co-efficient of the regression analysis of the concentration and f_{UB}, which depicts how well the parameter is described by the two component mixing model. The r^2 was calculated when there were at minimum 3 data points and no more than half of the data points were an end member.

[a] The f_{UB} is the calculated fraction of ultra-basic water contributing to that particular spring during that sampling period using Equation 2.2.

The standard deviation associated with the concentration values are the error on replicate field samples (1σ). The quantification limit of an analyte was reported if the concentration was observed but too low to quantify. In C_1/C_{2+} calculation the C_{2+} represents the sum of C_2, C_3, and nC_4.

Table 3.7. Gaseous composition of ultra-basic spring waters at The Cedars in 2012.

	Bubbling (% mol)	Dissolved (μM)			
	BS5	BS5	NS1	GPS1	r^2
H_2	42.4 (± 0.3)	<d.l.	<d.l.	<d.l.	nc
CO_2	<d.l.	-	-	-	nc
CH_4	6.4 (± 0.1)	61.7 (± 8.0)	239 (± 13)	105 (± 12)	0.13
	(ppm mol)				
C_2H_6	64.0 (± 1.1)	<0.067	<d.l.	0.333 (± 0.033)	nc
C_3H_8	39.0 (± 1.1)	<0.068	<0.068	0.136 (± 0.045)	nc
iC_4H_{10}	22.9 (± 0.5)	<0.069	<0.069	<0.069	nc
nC_4H_{10}	48.7 (± 1.8)	<0.069	<0.069	0.120 (± 0.034)	nc
iC_5H_{12}	42.6 (± 1.4)	<0.069	<0.069	0.180 (± 0.042)	nc
nC_5H_{12}	55.6 (± 2.2)	0.111 (± 0.014)	0.139 (± 0.055)	0.083 (± 0.028)	0.81
nC_6H_{14}	103 (± 3.0)	0.337 (± 0.081)	0.139 (± 0.081)	0.522 (± 0.058)	0.80
C_1/C_{2+}	421	-	-	178	nc
f_{UB}[a]	0.16	0.16	0.08	1.00	

- = not analyzed/not sampled; <d.l. = analyte was below detection limits of the analytical method used; nc = indicates that there were not enough data points to confidently do the r^2 calculation or the parameter (e.g. pH) is not on a linear scale. The r^2 is a correlation co-efficient of the regression analysis of the concentration and f_{UB}, which depicts how well the parameter is described by the two component mixing model. The r^2 was calculated when there were at minimum 3 data points and no more than half of the data points were an end member.

[a] The f_{UB} is the calculated fraction of ultra-basic water contributing to that particular spring during that sampling period using Equation 2.2.

The standard deviation associated with the concentration values are the error on replicate field samples (1σ). The quantification limit of an analyte was reported if the concentration was observed but too low to quantify. In C_1/C_{2+} calculation the C_{2+} represents the sum of C_2, C_3, and nC_4.

Table 3.8. Gaseous composition of ultra-basic spring waters and water sampled from Austin Creek at The Cedars in 2013.

	Bubbling (% mol)		Dissolved (µM)			r^2
	BS9	NS2	AC	NS1	GPS1	
H_2	-	-	-	-	-	nc
CO_2	<d.l.	<d.l.	169	-	-	nc
CH_4	4.2 (± 1.3)	16.1 (± 0.7)	18.1	231 (± 1)	139 (± 8)	nc
	(ppm mol)					
C_2H_6	36.7 (± 12.1)	25.3 (± 2.2)	<d.l.	<d.l.	0.499 (± 0.033)	nc
C_3H_8	23.0 (± 0.3)	10.0 (± 0.4)	<d.l.	<0.068	0.227 (± 0.000)	nc
iC_4H_{10}	15.4 (± 0.1)	12.0 (± 0.6)	<d.l.	<0.069	0.086 (± 0.005)	nc
nC_4H_{10}	32.0 (± 1.1)	24.1 (± 1.7)	<d.l.	<0.069	0.224 (± 0.005)	nc
iC_5H_{12}	32.2 (± 1.3)	36.5 (± 2.4)	<d.l.	<0.069	0.166 (± 0.000)	nc
nC_5H_{12}	42.0 (± 2.9)	34.2 (± 2.9)	<0.069	0.069 (± 0.004)	0.180 (± 0.004)	nc
nC_6H_{14}	84.9 (± 8.0)	105 (± 11)	<0.070	0.081	0.580 (± 0.046)	nc
C_1/C_{2+}	457	2729	-	-	146	nc
f_{UB}[a]	-	0.08	0.00	0.08	1.00	

- = not analyzed/not sampled; <d.l. = analyte was below detection limits of the analytical method used; nc = indicates that there were not enough data points to confidently do the r^2 calculation or the parameter (e.g. pH) is not on a linear scale. The r^2 is a correlation co-efficient of the regression analysis of the concentration and f_{UB}, which depicts how well the parameter is described by the two component mixing model. The r^2 was calculated when there were at minimum 3 data points and no more than half of the data points were an end member.

[a] The f_{UB} is the calculated fraction of ultra-basic water contributing to that particular spring during that sampling period using Equation 2.2.

The standard deviation associated with the concentration values are the error on replicate field samples (1σ). The quantification limit of an analyte was reported if the concentration was observed but too low to quantify. In C_1/C_{2+} calculation the C_{2+} represents the sum of C_2, C_3, and nC_4.

Table 3.9. Hydrogen and carbon isotopic composition of gases measured in spring waters and Austin Creek at The Cedars in 2011.

	Bubbling		Dissolved			
	BS9	BS5	AC	BS7	NS1	GPS1
$\delta D\ H_2$ (‰)	-775 (± 7)	-772	-	-	-	-
$\delta D\ CH_4$ (‰)	-350 (± 10)	-355	-	-	-	-
$\delta^{13}C\ CO_2$ (‰)	-	-	-11.6	<d.l.	<d.l.	<d.l.
$\delta^{13}C\ CH_4$ (‰)	-63.0	-62.9	-63.5	-63.3	-67.4	-57.2
$\delta_{13}C\ C_2H_6$ (‰)	-24.0	-24.6	<d.l.	<q.l.	<q.l.	-25.3 (± 0.8)
$\delta^{13}C\ C_3H_8$ (‰)	-23.3	-23.5	<d.l.	<q.l.	<q.l.	<q.l.
$\delta^{13}C\ iC_4H_{10}$ (‰)	<q.l.	<q.l.	<d.l.	<q.l.	<q.l.	<q.l.
$\delta^{13}C\ nC_4H_{10}$ (‰)	-23.0	-23.7	<d.l.	<q.l.	<q.l.	<q.l.
$\delta^{13}C\ iC_5H_{12}$ (‰)	<q.l.	<q.l.	<d.l.	<q.l.	<q.l.	<q.l.
$\delta^{13}C\ nC_5H_{12}$ (‰)	-23.7	-22.6 (± 0.7)	<d.l.	<q.l.	<q.l.	<q.l.
$\delta^{13}C\ nC_6H_{14}$ (‰)	-24.1	- 23.1	<d.l.	<q.l.	<q.l.	-23.6
f_{UB}[a]	0.16	0.13	0.00	0.12	0.07	1.00

- = not analyzed/not sampled; <d.l. = analyte was below detection limits of the analytical method used; <q.l. = analyte was observed but peak too small to be reliable.

[a] The f_{UB} is the calculated fraction of ultra-basic water contributing to that particular spring during that sampling period using Equation 2.2.

The standard deviation associated with the isotope values are the error on replicate field samples (1σ). If no error is reported than the error on replicate samples was less than the analytical error, which was ± 0.5 ‰ for $\delta^{13}C$ and ± 5 ‰ for δD.

Table 3.10. Hydrogen and carbon isotopic composition of gases measured in spring waters at The Cedars in 2012.

	Bubbling	Dissolved		
	BS5	BS5	NS1	GPS1
$\delta D\ H_2$ (‰)	-768	-	-	-
$\delta D\ CH_4$ (‰)	-352	-	-	-
$\delta^{13}C\ CO_2$ (‰)	-	-	<d.l.	<d.l.
$\delta^{13}C\ CH_4$ (‰)	-62.9	-62.6	-67.7	-56.2
$\delta_{13}C\ C_2H_6$ (‰)	-24.3	-24.4	<d.l.	-25.7
$\delta^{13}C\ C_3H_8$ (‰)	-23.8	-25.2	<d.l.	-23.7
$\delta^{13}C\ iC_4H_{10}$ (‰)	<q.l.	<q.l.	<d.l.	<q.l.
$\delta^{13}C\ nC_4H_{10}$ (‰)	-23.1	-23.0	<d.l.	-22.7
$\delta^{13}C\ iC_5H_{12}$ (‰)	<q.l.	<q.l.	<d.l.	<q.l.
$\delta^{13}C\ nC_5H_{12}$ (‰)	-23.7	-23.0	<d.l.	-22.6
$\delta^{13}C\ nC_6H_{14}$ (‰)	-23.3	-23.6	<d.l.	-23.8
f_{UB}[a]	0.16	0.16	0.08	1.00

- = not analyzed/not sampled; <d.l. = analyte was below detection limits of the analytical method used; <q.l. = analyte was observed but peak too small to be reliable.
[a] The f_{UB} is the calculated fraction of ultra-basic water contributing to that particular spring during that sampling period using Equation 2.2.
The standard deviation associated with the isotope values are the error on replicate field samples (1σ). If no error is reported than the error on replicate samples was less than the analytical error, which was ± 0.5 ‰ for $\delta^{13}C$ and ± 5 ‰ for δD.

Table 3.11. Hydrogen and carbon isotopic composition of gases measured in spring waters at The Cedars in 2013.

	Bubbling	
	BS9	NS2
δD H_2 (‰)	-771	-763
δD CH_4 (‰)	-358	-360
$\delta^{13}C$ CH_4 (‰)	-63.4	-66.4
f_{UB}[a]	-	0.08

- = not analyzed/not sampled

[a] The f_{UB} is the calculated fraction of ultra-basic water contributing to that particular spring during that sampling period using Equation 2.2.

The standard deviation associated with the isotope values are the error on replicate field samples (1σ). If no error is reported than the error on replicate samples was less than the analytical error, which was $\pm$ 0.5 ‰ for $\delta^{13}C$ and $\pm$ 5 ‰ for δD.

Table 3.12. Volatile organic compounds extracted and measured from spring waters and Austin Creek at The Cedars in 2011.

Probable structure	AC	BS9	BS5	BS7	NS1	GPS1	r^2
1-heptene	<d.l.	<d.l.	<0.120	<d.l.	<0.120	<0.120	nc
n-heptane	<d.l.	<d.l.	<d.l.	<d.l.	<d.l.	<d.l.	nc
cyclopentane	<d.l.	<d.l.	<d.l.	<d.l.	<d.l.	<0.143	nc
cyclohexane	<d.l.	<d.l.	<0.119	<d.l.	0.473	3.41	nc
methylcyclopentane	<d.l.	<d.l.	<0.119	<d.l.	<0.119	0.422	nc
methylcyclohexane	<d.l.	<d.l.	<0.102	<d.l.	0.269	0.937	nc
dimethylcyclohexane*	<d.l.	<d.l.	<0.089	<0.089	0.211	0.219	nc
ethylcyclohexane	<d.l.	<d.l.	<d.l.	<d.l.	<0.089	<0.089	nc
benzene	<d.l.	<d.l.	<0.128	<0.128	<0.128	2.04	nc
toluene	<d.l.	<d.l.	0.225	<0.109	<0.109	3.21	nc
ethylbenzene	<d.l.	<d.l.	<0.094	<d.l.	<0.094	0.633	nc
p,m-xylene*	<d.l.	<d.l.	<0.094	<d.l.	<0.094	1.35	nc
o-xylene	<d.l.	<d.l.	<0.094	<d.l.	<0.094	1.23	nc
isopropylbenzene	<d.l.	<d.l.	<d.l.	<d.l.	<d.l.	<0.083	nc
propylbenzene	<d.l.	<d.l.	<d.l.	<d.l.	<d.l.	0.262	nc
ethyl methyl benzene*	<d.l.	<d.l.	<0.083	<d.l.	<d.l.	0.321	nc
trimethylbenzene*	<d.l.	<d.l.	<0.083	<0.083	<0.083	0.216	nc
tetralin	<d.l.	<d.l.	<d.l.	<d.l.	<0.076	0.142	nc
f_{UB}[a]	0.00	0.16	0.13	0.12	0.07	1.00	

* = value reported is the sum of all isomers quantified; <d.l. = analyte was below detection limits of the analytical method used; nc = indicates that there were not enough data points to confidently do the r^2 calculation or the parameter (e.g. pH) is not on a linear scale. The r^2 is a correlation co-efficient of the regression analysis of the concentration and f_{UB}, which depicts how well the parameter is described by the two component mixing model. The r^2 was calculated when there were at minimum 3 data points and no more than half of the data points were an end member.

[a] The f_{UB} is the calculated fraction of ultra-basic water contributing to that particular spring during that sampling period using Equation 2.2.

The quantification limit of an analyte was reported if the concentration was observed but too low to quantify.

Table 3.13. Volatile organic compounds extracted and measured from spring waters and Austin Creek at The Cedars in 2012.

Probable structure	Concentration (µM)		
	BS5	GPS1	
			r^2
1-heptene	<0.120	<0.120	nc
n-heptane	<0.100	<0.100	nc
cyclopentane	<0.143	0.239	nc
cyclohexane	0.992	3.99	nc
methylcyclopentane	0.183	0.585	nc
methylcyclohexane	0.694	1.48	nc
dimethylcyclohexane*	0.396	0.436	nc
ethylcyclohexane	<0.089	0.156	nc
benzene	0.231	2.64	nc
toluene	0.530	4.49	nc
ethylbenzene	<0.094	0.870	nc
p,m-xylene*	0.183	1.94	nc
o-xylene	<0.094	1.54	nc
isopropylbenzene	<0.083	0.083	nc
propylbenzene	<0.083	0.376	nc
ethyl methyl benzene*	<0.083	0.434	nc
trimethylbenzene*	<0.083	0.270	nc
tetralin	<0.076	0.169	nc
f_{UB}[a]	0.16	1.00	

* = value reported is the sum of all isomers quantified; nc = indicates that there were not enough data points to confidently do the r^2 calculation or the parameter (e.g. pH) is not on a linear scale. The r^2 is a correlation co-efficient of the regression analysis of the concentration and f_{UB}, which depicts how well the parameter is described by the two component mixing model. The r^2 was calculated when there were at minimum 3 data points and no more than half of the data points were an end member.
[a] The f_{UB} is the calculated fraction of ultra-basic water contributing to that particular spring during that sampling period using Equation 2.2.
The quantification limit of an analyte was reported if the concentration was observed but too low to quantify.

Table 3.14. Semi volatile organic compounds extracted and measured from spring waters at The Cedars in 2012.

| Probable structure | Concentration (μM) | | r^2 |
	BS5	GPS1	
tetralin	2.50E-03 (± 1.51E-04)	1.03E-02 (± 3.56E-03)	nc
methyl tetralin*	3.76E-03 (± 6.15E-04)	4.38E-03 (± 6.84E-04)	nc
n-tetracosane (C_{24})	<d.l.	<1.48E-03	nc
n-pentacosane (C_{25})	<d.l.	<1.42E-03	nc
n-hexacosane (C_{26})	<d.l.	<1.36E-03	nc
f_{UB}[a]	0.16	1.00	

* = value reported is the sum of all isomers quantified; <d.l. = analyte was below detection limits of the analytical method used; nc = indicates that there were not enough data points to confidently do the r^2 calculation or the parameter (e.g. pH) is not on a linear scale. The r^2 is a correlation co-efficient of the regression analysis of the concentration and f_{UB}, which depicts how well the parameter is described by the two component mixing model. The r^2 was calculated when there were at minimum 3 data points and no more than half of the data points were an end member.

[a] The f_{UB} is the calculated fraction of ultra-basic water contributing to that particular spring during that sampling period using Equation 2.2.

The standard deviation associated with the concentration values are the error on replicate field samples (1σ). The quantification limit of an analyte was reported if the concentration was observed but too low to quantify. Calibration curves for C_{24} and C_{26} only had two data points while lower alkanes (C_{10}-C_{22}) had calibration curves with 3 or more data points. All compounds above C_{26} were quantified using the C_{26} calibration curve. Odd chained hydrocarbons were quantified by rounding up and using the closest even chained hydrocarbon standard.

Table 3.15. Sedimentary organic matter sample descriptions for The Cedars.

CEDARS		
Outcrop Description: Location: N 38°35'58.0" W 123°07'51.0" ~2.5 m high outcrop composed of dark gray shale (1.5 m) underlying a light gray sandstone (1 m).	**FSC1**	Sample Description: Fine grained dark gray shale sample which was heavily cleaved and crumbled out from the outcrop fairly easily.
Outcrop Description: Location: N 38°36'00.3" W 123°07'54.5" ~4.5 m high outcrop dominantly composed of dark gray shale.	**FSC2**	Sample Description: Very fine grained dark shale loosely held into outcrop. Some loose crumbly shale was collected from behind more compacted shale samples, as seen in the picture.

Table 3.16. Carbon isotopic value of sedimentary organic matter samples from The Cedars and the Tablelands.

| | CEDARS | | TABLELANDS | | | | | |
	FSC1	FSC2	HAA1	HAA2	HAA3	HAA4	HAA5	HAA6
$\delta^{13}C$ (‰)	-25.0	-24.9	-27.4	-31.6	-22.4	-16.3	-4.9	-23.6

Table 3.17. A comparison of aqueous, inorganic geochemical parameters of waters sampled at the Tablelands in 2011.

	WHB	WHC2C	WHC2A	WHC2A-R	WHC2B	WHC2B-R	WHC1	r^2
pH*	7.8	12.2	12.4	-	12.3	-	-	nc
E_h (mV)*	+382	-458	-690	-	-618	-	-	nc
Cond (μS/cm)	62	475	3880	-	3830	-	-	0.82
Ca^{2+}/Mg^{2+}	0.07	1	252	-	241	-	-	0.82
f_{UB}^a	0.00	0.15	1.00	-	0.53	-	-	

- = not analyzed/not sampled; nc = indicates that there were not enough data points to confidently do the r^2 calculation or the parameter (e.g. pH) is not on a linear scale. The r^2 is a correlation co-efficient of the regression analysis of the concentration and f_{UB}, which depicts how well the parameter is described by the two component mixing model. The r^2 was calculated when there were at minimum 3 data points and no more than half of the data points were an end member.
^{a} The f_{UB} is the calculated fraction of ultra-basic water contributing to that particular spring during that sampling period using Equation 2.2.
* Data from Szponar 2012

Table 3.18. A comparison of aqueous, inorganic geochemical parameters of waters sampled at the Tablelands in 2012.

	WHB	WHC2C	WHC2A	WHC2A-R	WHC2B	WHC2B-R	WHC1	r^2
pH	8.1	11.7	12.2	12.3	12.2	12.2	-	nc
E_h (mV)	-	-	-	-	-	-	-	nc
Cond (μS/cm)	80	126	2430	1838	2080	1715	-	0.51
Ca^{2+}/Mg^{2+}	0.09	0.3	3	614	827	204	16	0.32
f_{UB}[a]	0.00	0.04	0.27	0.86	0.85	0.82	1.00	

- = not analyzed/not sampled; n/a = calculation not available; nc = indicates that there were not enough data points to confidently do the r^2 calculation or the parameter (e.g. pH) is not on a linear scale. The r^2 is a correlation co-efficient of the regression analysis of the concentration and f_{UB}, which depicts how well the parameter is described by the two component mixing model. The r^2 was calculated when there were at minimum 3 data points and no more than half of the data points were an end member.
[a] The f_{UB} is the calculated fraction of ultra-basic water contributing to that particular spring during that sampling period using Equation 2.2.

Table 3.19. Bulk aqueous carbon pools and organic acids measured from waters sampled at the Tablelands in 2011.

	WHB	WHC2C	WHC2A	WHC2B	r^2
TIC (mg/L)	7.14 (± 0.37)*	13.52 (± 0.61)*	1.13 (± 0.40)*	1.23 (± 0.35)*	0.55
$\delta^{13}C_{TIC}$ (‰)	-2.1 (± 0.1)*	-11.8 (± 0.0)*	-14.7 (± 0.9)*	-17.6 (± 0.4)*	nc
DOC (mg/L)	0.30 (± 0.01)*	0.84 (± 0.01)*	0.35 (± 0.20)*	0.29 (± 0.03)*	0.11
$\delta^{13}C_{DOC}$ (‰)	<d.l.*	-23.7 (± 0.0)*	<d.l.*	<d.l.*	nc
Acetate (mg/L)	-	-	-	-	nc
Formate (mg/L)	-	-	-	-	nc
f_{UB}[a]	0.00	0.15	1.00	0.53	

- = not analyzed/not sampled; <d.l. = analyte was below detection limits of the analytical method used; nc = indicates that there were not enough data points to confidently do the r^2 calculation or the parameter (e.g. pH) is not on a linear scale. The r^2 is a correlation co-efficient of the regression analysis of the concentration and f_{UB}, which depicts how well the parameter is described by the two component mixing model. The r^2 was calculated when there were at minimum 3 data points and no more than half of the data points were an end member.

[a] The f_{UB} is the calculated fraction of ultra-basic water contributing to that particular spring during that sampling period using Equation 2.2.

* = Data from Szponar (2012)

The error reported is the standard deviation of replicate samples.

Table 3.20. Bulk aqueous carbon pools and organic acids measured from waters sampled at the Tablelands in 2012.

	WHB	WHC2C	WHC2A	WHC2A-R	WHC2B	WHC2B-R	r^2
TIC (mg/L)	7.86 (± 0.01)	16.87 (± 0.21)	2.75 (± 2.07)	1.49 (± 0.07)	0.22 (± 0.01)	1.53 (± 0.25)	0.62
$\delta^{13}C_{TIC}$ (‰)	-4.3 (± 0.2)	-14.2 (± 0.1)	-17.1 (± 0.7)	-23.5 (± 0.3)	-13.9 (± 0.1)	-18.6 (± 0.1)	nc
DOC (mg/L)	-	-	-	-	-	-	nc
$\delta^{13}C_{DOC}$ (‰)	-	-	-	-	-	-	nc
Acetate (mg/L)	0.124 (± 0.037)	0.311 (± 0.051)	1.50 (± 0.07)	3.67 (± 0.37)	4.49 (± 0.24)	3.26 (± 0.19)	0.96
Formate (mg/L)	<d.l.	0.047 (± 0.023)	0.051 (±0.022)	1.30 (± 0.05)	0.121 (± 0.023)	0.593 (± 0.260)	0.39
f_{UB}[a]	0.00	0.04	0.27	0.86	0.85	0.82	

- = not analyzed/not sampled; <d.l. = analyte was below detection limits of the analytical method used; nc = indicates that there were not enough data points to confidently do the r^2 calculation or the parameter (e.g. pH) is not on a linear scale. The r^2 is a correlation co-efficient of the regression analysis of the concentration and f_{UB}, which depicts how well the parameter is described by the two component mixing model. The r^2 was calculated when there were at minimum 3 data points and no more than half of the data points were an end member.

[a] The f_{UB} is the calculated fraction of ultra-basic water contributing to that particular spring during that sampling period using Equation 2.2.

The error reported is the standard deviation of replicate samples.

Table 3.21. Gaseous composition of ultra-basic spring waters and water sampled at the mixing site at the Tablelands in 2011.

	Dissolved (µM)			
	WHC2C	WHC2A	WHC2B	r^2
H_2	34.7 (± 5.0)*	584 (± 25)*	515 (± 59)*	0.80
CO_2	-	-	-	nc
CH_4	1.87 (± 0.00)*	20.0 (± 0.6)*	20.0 (± 0.6)*	0.70
C_2H_6	-	-	-	nc
C_3H_8	-	-	-	nc
iC_4H_{10}	-	-	-	nc
nC_4H_{10}	-	-	-	nc
iC_5H_{12}	-	-	-	nc
nC_5H_{12}	-	-	-	nc
nC_6H_{14}	-	-	-	nc
C_1/C_{2+}	-	-	-	nc
f_{UB}[a]	0.15	1.00	0.53	

- = not analyzed/not sampled; nc = indicates that there were not enough data points to confidently do the r^2 calculation or the parameter (e.g. pH) is not on a linear scale. The r^2 is a correlation co-efficient of the regression analysis of the concentration and f_{UB}, which depicts how well the parameter is described by the two component mixing model. The r^2 was calculated when there were at minimum 3 data points and no more than half of the data points were an end member.

[a] The f_{UB} is the calculated fraction of ultra-basic water contributing to that particular spring during that sampling period using Equation 2.2.

* = Data from Szponar 2012

The standard deviation associated with the concentration values are the error on replicate field samples (1σ). In C_1/C_{2+} calculation the C_{2+} represents the sum of C_2, C_3, and nC_4.

Table 3.22. Gaseous composition of ultra-basic spring waters, non ultra-basic water sampled from Winter House Brook as well as the mixing site at the Tablelands in 2012.

	WHB	WHC2C	WHC2A	WHC2A-R	WHC2B	WHC2B-R	r^2
			Dissolved (µM)				
H_2	<d.l.	<d.l.	472 (± 49)	475 (± 49)	529	446 (± 2)	0.35
CO_2	<16.8	108 (± 41)	-	-	-	-	nc
CH_4	<d.l.	13.4 (± 0.5)	26.0 (± 1.2)	25.8 (± 0.4)	36.8	36.3 (± 1.4)	0.76
C_2H_6	<d.l.	<d.l.	1.20 (± 0.03)	1.23 (± 0.03)	1.30	1.26 (± 0.07)	0.03
C_3H_8	<d.l.	<0.068	0.499 (± 0.091)	0.907 (± 0.113)	0.748 (± 0.159)	1.04 (± 0.09)	0.47
iC_4H_{10}	<d.l.	<d.l.	0.086 (± 0.017)	0.155 (± 0.017)	0.138 (± 0.034)	0.189 (± 0.017)	0.70
nC_4H_{10}	<d.l.	<0.069	0.155 (± 0.034)	0.292 (± 0.034)	0.241 (± 0.052)	0.344 (± 0.034)	0.52
iC_5H_{12}	<d.l.	<0.069	<0.069	0.125 (± 0.014)	0.097 (± 0.028)	0.152 (± 0.014)	0.51
nC_5H_{12}	<0.069	<0.069	0.097 (± 0.004)	0.180 (± 0.014)	0.194 (± 0.042)	0.236 (± 0.014)	1.00
nC_6H_{14}	<d.l.	<0.070	0.116 (± 0.012)	0.232 (± 0.035)	0.186 (± 0.070)	0.278 (± 0.046)	0.52
C_1/C_{2+}	-	-	14.0	10.6	16.1	13.7	0.10
f_{UB}[a]	0.00	0.04	-	0.86	0.85	0.82	

- = not analyzed/not sampled; <d.l. = analyte was below detection limits of the analytical method used; nc = indicates that there were not enough data points to confidently do the r^2 calculation or the parameter (e.g. pH) is not on a linear scale. The r^2 is a correlation co-efficient of the regression analysis of the concentration and f_{UB}, which depicts how well the parameter is described by the two component mixing model. The r^2 was calculated when there were at minimum 3 data points and no more than half of the data points were an end member.

[a] The f_{UB} is the calculated fraction of ultra-basic water contributing to that particular spring during that sampling period using Equation 2.2.

The standard deviation associated with the concentration values are the error on replicate field samples (1σ). The quantification limit of an analyte was reported if the concentration was observed but too low to quantify. In C_1/C_{2+} calculation the C_{2+} represents the sum of C_2, C_3, and nC_4.

Table 3.23. Carbon isotopic compositions of gases measured in spring waters, Winter House Brook as well as the mixing site at the Tablelands in 2011.

| | Dissolved | | | |
	WHB	WHC2C	WHC2A	WHC2B
$\delta^{13}C$ CO_2 (‰)	-3.5	-14.1 (± 4.7)	-	-
$\delta^{13}C$ CH_4 (‰)	-	-25.9	-27.1	-27.4
$\delta^{13}C$ C_2H_6 (‰)	-	<q.l.	-30.1	-29.8
$\delta^{13}C$ C_3H_8 (‰)	-	<q.l.	-31.7	-31.9
$\delta^{13}C$ iC_4H_{10} (‰)	-	<q.l.	<q.l.	<q.l.
$\delta^{13}C$ nC_4H_{10} (‰)	-	<q.l.	-31.6	-30.9
$\delta^{13}C$ iC_5H_{12} (‰)	-	<q.l.	<q.l.	<q.l.
$\delta^{13}C$ nC_5H_{12} (‰)	-	<q.l.	<q.l.	<q.l.
$\delta^{13}C$ nC_6H_{14} (‰)	-	<q.l.	<q.l.	<q.l.
f_{UB}[a]	0.00	0.15	1.00	0.53

- = not analyzed/not sampled; <d.l. = analyte was below detection limits of the analytical method used; <q.l. = analyte was observed but peak too small to be reliable.
[a] The f_{UB} is the calculated fraction of ultra-basic water contributing to that particular spring during that sampling period using Equation 2.2.
The standard deviation associated with the isotope values are the error on replicate field samples (1σ). If no error reported than the error on replicate samples was less than the analytical error (± 0.5 ‰).

Table 3.24. Carbon isotopic compositions of gases measured in spring waters, Winter House Brook as well as the mixing site at the Tablelands in 2012.

	Dissolved					
	WHB	WHC2C	WHC2A	WHC2A-R	WHC2B	WHC2B-R
$\delta^{13}C$ CO_2 (‰)	-10.2	-19.2	-	-	-	-
$\delta^{13}C$ CH_4 (‰)	-	-26.2	-25.9	-27.7	-27.0	-27.5
$\delta^{13}C$ C_2H_6 (‰)	-	<q.l.	<q.l.	-30.3	-29.7	-30.0
$\delta^{13}C$ C_3H_8 (‰)	-	<q.l.	<q.l.	-32.4	-31.7	-32.1
$\delta^{13}C$ iC_4H_{10} (‰)	-	<q.l.	<q.l.	<q.l.	<q.l.	<q.l.
$\delta^{13}C$ nC_4H_{10} (‰)	-	<q.l.	<q.l.	-31.6 (± 0.8)	-31.3	-30.9
$\delta^{13}C$ iC_5H_{12} (‰)	-	<q.l.	<q.l.	<q.l.	<q.l.	<q.l.
$\delta^{13}C$ nC_5H_{12} (‰)	-	<q.l.	<q.l.	<q.l.	<q.l.	<q.l.
$\delta^{13}C$ nC_6H_{14} (‰)	-	<q.l.	<q.l.	<q.l.	<q.l.	<q.l.
f_{UB}[a]	0.00	0.04	-	0.86	0.85	0.82

- = not analyzed/not sampled; <d.l. = analyte was below detection limits of the analytical method used; <q.l. = analyte was observed but peak too small to be reliable.
[a] The f_{UB} is the calculated fraction of ultra-basic water contributing to that particular spring during that sampling period using Equation 2.2.
The standard deviation associated with the isotope values are the error on replicate field samples (1σ). If no error reported than the error on replicate samples was less than the analytical error (± 0.5 ‰).

Table 3.25. Volatile organic compounds extracted and measured from spring waters, Winter House Brook as well as the mixing site at the Tablelands in 2011.

	Concentration (μM)				
	WHB	WHC2C	WHC2A	WHC2B	
Probable structure					r^2
1-heptene	<d.l.	<d.l.	<d.l.	<d.l.	nc
n-heptane	<d.l.	<d.l.	<d.l.	<d.l.	nc
cyclopentane	<d.l.	<d.l.	<d.l.	<d.l.	nc
cyclohexane	<d.l.	<d.l.	0.696	0.654	nc
methylcyclopentane	<d.l.	<d.l.	<0.119	<0.119	nc
methylcyclohexane	<d.l.	<d.l.	0.382	0.367	nc
dimethylcyclohexane*	<d.l.	<d.l.	<d.l.	<d.l.	nc
ethylcyclohexane	<d.l.	<d.l.	<d.l.	<d.l.	nc
benzene	<d.l.	<d.l.	<d.l.	<d.l.	nc
toluene	<d.l.	<d.l.	<d.l.	<d.l.	nc
ethylbenzene	<d.l.	<d.l.	<d.l.	<d.l.	nc
p,m-xylene*	<d.l.	<d.l.	<d.l.	<d.l.	nc
o-xylene	<d.l.	<d.l.	<d.l.	<d.l.	nc
isopropylbenzene	<d.l.	<d.l.	<d.l.	<d.l.	nc
propylbenzene	<d.l.	<d.l.	<d.l.	<d.l.	nc
ethyl methyl benzene*	<d.l.	<d.l.	<d.l.	<d.l.	nc
trimethylbenzene*	<d.l.	<d.l.	<d.l.	<d.l.	nc
tetralin	<d.l.	<d.l.	<d.l.	<d.l.	nc
f_{UB}[a]	0.00	0.15	1.00	0.53	

* = value reported is the sum of all isomers quantified; <d.l. = analyte was below detection limits of the analytical method used; nc = indicates that there were not enough data points to confidently do the r^2 calculation or the parameter (e.g. pH) is not on a linear scale. The r^2 is a correlation co-efficient of the regression analysis of the concentration and f_{UB}, which depicts how well the parameter is described by the two component mixing model. The r^2 was calculated when there were at minimum 3 data points and no more than half of the data points were an end member.
[a] The f_{UB} is the calculated fraction of ultra-basic water contributing to that particular spring during that sampling period using Equation 2.2.
The quantification limit of an analyte was reported if the concentration was observed but too low to quantify.

Table 3.26. Volatile organic compounds extracted and measured from spring waters, Winter House Brook as well as the mixing site at the Tablelands in 2012.

Probable structure	Concentration (µM)						r^2
	WHB	WHC2C	WHC2A	WHC2A-R	WHC2B	WHC2B-R	
1-heptene	<d.l.	<d.l.	<d.l.	<d.l.	<d.l.	<0.102	nc
n-heptane	<d.l.	<d.l.	<d.l.	<d.l.	<d.l.	<d.l.	nc
cyclopentane	<d.l.	<d.l.	<d.l.	<d.l.	<d.l.	<d.l.	nc
cyclohexane	<d.l.	<d.l.	0.388	0.637	<0.119	0.747	nc
methylcyclopentane	<d.l.	<d.l.	<0.119	<0.119	<d.l.	<0.119	nc
methylcyclohexane	<d.l.	<d.l.	0.187	0.415	<0.102	0.475	nc
dimethylcyclohexane*	<d.l.	<d.l.	<d.l.	<0.089	<d.l.	<0.089	nc
ethylcyclohexane	<d.l.	<d.l.	<d.l.	<0.089	<d.l.	<0.089	nc
benzene	<d.l.	<d.l.	<d.l.	<d.l.	<d.l.	<d.l.	nc
toluene	<d.l.	<d.l.	<d.l.	<0.109	<d.l.	<0.109	nc
ethylbenzene	<d.l.	<d.l.	<d.l.	<d.l.	<d.l.	<d.l.	nc
p,m-xylene*	<d.l.	<d.l.	<d.l.	<d.l.	<d.l.	<d.l.	nc
o-xylene	<d.l.	<d.l.	<d.l.	<d.l.	<d.l.	<d.l.	nc
isopropylbenzene	<d.l.	<d.l.	<d.l.	<d.l.	<d.l.	<d.l.	nc
propylbenzene	<d.l.	<d.l.	<d.l.	<d.l.	<d.l.	<d.l.	nc
ethyl methyl benzene*	<d.l.	<d.l.	<d.l.	<d.l.	<d.l.	<d.l.	nc
triemthylbenzene*	<d.l.	<d.l.	<d.l.	<0.083	<d.l.	<d.l.	nc
tetralin	<d.l.	<d.l.	<d.l.	<d.l.	<d.l.	<d.l.	nc
f_{UB}[a]	0.00	0.04	-	0.86	0.85	0.82	

* = value reported is the sum of all isomers quantified; <d.l. = analyte was below detection limits of the analytical method used; nc = indicates that there were not enough data points to confidently do the r^2 calculation or the parameter (e.g. pH) is not on a linear scale. The r^2 is a correlation co-efficient of the regression analysis of the concentration and f_{UB}, which depicts how well the parameter is described by the two component mixing model. The r^2 was calculated when there were at minimum 3 data points and no more than half of the data points were an end member.
[a] The f_{UB} is the calculated fraction of ultra-basic water contributing to that particular spring during that sampling period using Equation 2.2.
The quantification limit of an analyte was reported if the concentration was observed but too low to quantify.

Table 3.27. Semi volatile organic compounds extracted and measured from spring waters, Winter House Brook as well as the mixing site at the Tablelands in 2012.

	Concentration (μM)						
	WHB	WHC2C	WHC2A	WHC2A-R	WHC2B	WHC2B-R	
Probable structure							r^2
n-heptadecane (C_{17})	<d.l.	<d.l.	<d.l.	7.11E-03	<d.l.	6.15E-03	nc
n-tetracosane (C_{24})	<d.l.	<d.l.	<d.l.	3.72E-03 (± 5.91E-05)	<d.l.	<d.l.	nc
n-pentacosane (C_{25})	<d.l.	<d.l.	3.54E-03	3.74E-03	<d.l.	<d.l.	nc
n-hexacosane (C_{26})	<d.l.	<d.l.	<d.l.	3.49E-03	<d.l.	<d.l.	nc
n-heptacosane (C_{27})	<d.l.	<d.l.	4.18E-03	4.23E-03 (± 2.36E-04)	3.99E-03	<d.l.	nc
n-octacosane (C_{28})	<d.l.	<d.l.	<d.l.	3.90E-03 (± 2.79E-04)	<d.l.	<d.l.	nc
n-triacontane (C_{30})	<d.l.	<d.l.	<d.l.	3.52E-03 (± 7.10E-05)	<d.l.	<d.l.	nc
n-hentriacontane (C_{31})	<d.l.	<d.l.	<d.l.	3.25E-03	<d.l.	<d.l.	nc
f_{UB}[a]	0.00	0.04	-	0.86	0.85	0.82	

<d.l. = analyte was below detection limits of the analytical method used; nc = indicates that there were not enough data points to confidently do the r^2 calculation or the parameter (e.g. pH) is not on a linear scale. The r^2 is a correlation co-efficient of the regression analysis of the concentration and f_{UB}, which depicts how well the parameter is described by the two component mixing model. The r^2 was calculated when there were at minimum 3 data points and no more than half of the data points were an end member.

[a] The f_{UB} is the calculated fraction of ultra-basic water contributing to that particular spring during that sampling period using Equation 2.2.

The standard deviation associated with the concentration values are the error on replicate field samples (1σ). The quantification limit of an analyte was reported if the concentration was observed but too low to quantify. Calibration curves for C_{24} and C_{26} only had two data points while lower alkanes (C_{10}-C_{22}) had calibration curves with 3 or more data points. All compounds above C_{26} were quantified using the C_{26} calibration curve. Odd chained hydrocarbons were quantified by rounding up and using the closest even chained hydrocarbon standard.

Table 3.28. Sedimentary organic matter sample descriptions for the Tablelands.

TABLELANDS		
Outcrop description: Location: N 49°36'06.84" W 057°57'23.52" ~1.5 m high outcrop, homogeneous dark gray shale.	**HAA1** 	Sample description: Dark gray shale that was heavily cleaved.
Outcrop description: Location: N 49°26'43.46" W 058°07'17.59" ~35 m high outcrop, fairly homogeneous, dominantly dark gray/black shaley melange morphed around entrained blocks and cobbles (0.1-1.5m size).	**HAA2** 	Sample description: Shale is heavily cleaved and very fine grained. Shale collected fell apart very easily and was dark grey in colour.
Outcrop description: Location: N 49°28'28.40" W 057°57'27.85" ~10 m high outcrop exposure, running 50 m along shoreline of Winter House Brook. Outcrop dominantly fine grained black shale/mudstone (4 m thick) interbedded with massive limestone and sandstone (10-40 cm thick). Mudstone was penetratively cleaved and contained many angular fragments of limestone and siltstone. The cleaved shale unit varied from a dark gray to a coal black colour. The shale units cleavage was wavy but bedding was mostly parallel.	**HAA3** 	Sample description: Shale was heavily cleaved and very fine grained (1 mm scale). Shale is coal black in colour.
	HAA4 	Sample description: Shale was very fine grained and heavily cleaved. Shale is dark grey in colour.
	HAA5 	Sample description: Limestone taken from a thick limestone bed.
	HAA6 	Sample description: Fine to medium grained siltstone/sandstone sample taken from a thick sedimentary bed.
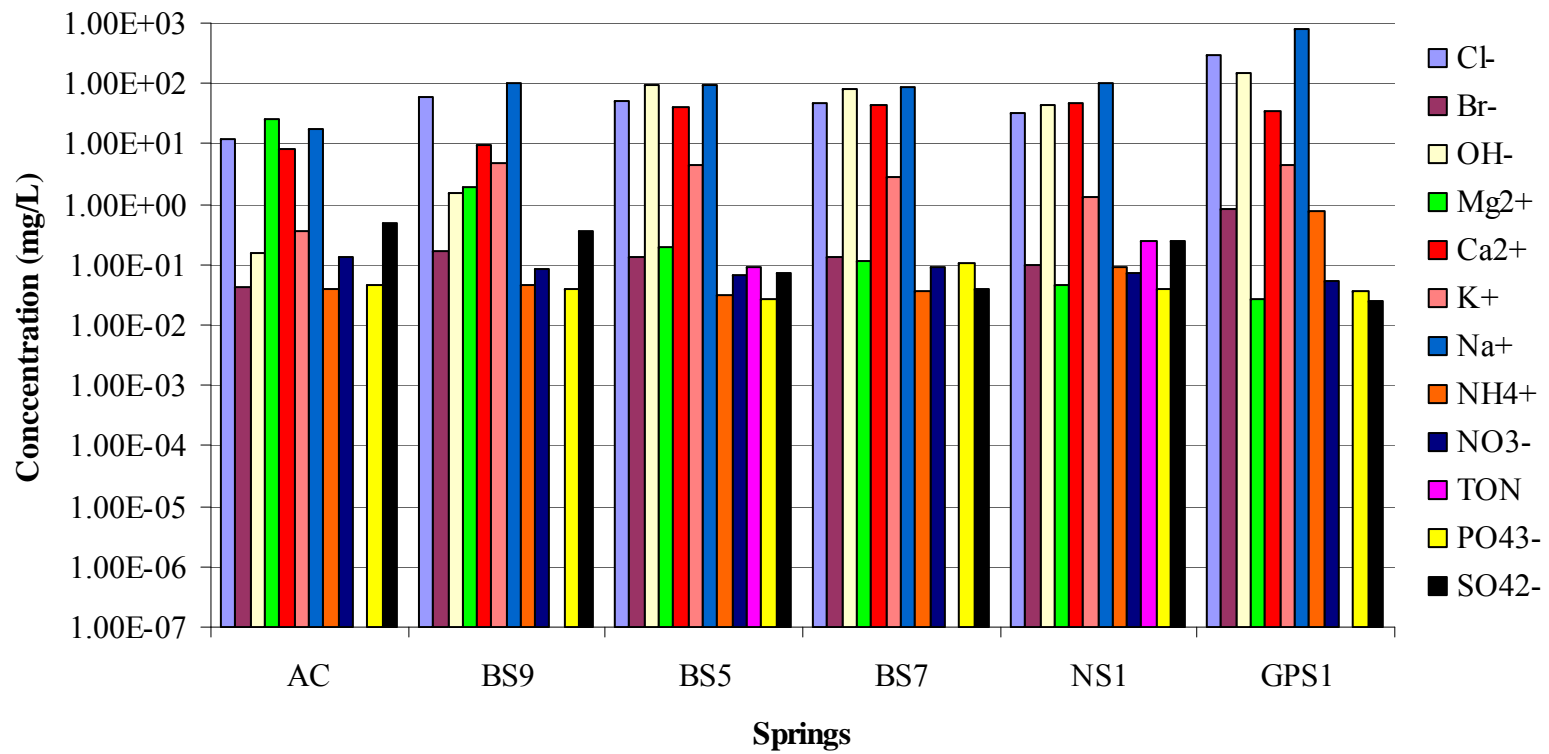
Figure 3.1. Aqueous concentrations of major cations, anions and nutrients in waters sampled at The Cedars in 2011. Raw data can be found in A.1.
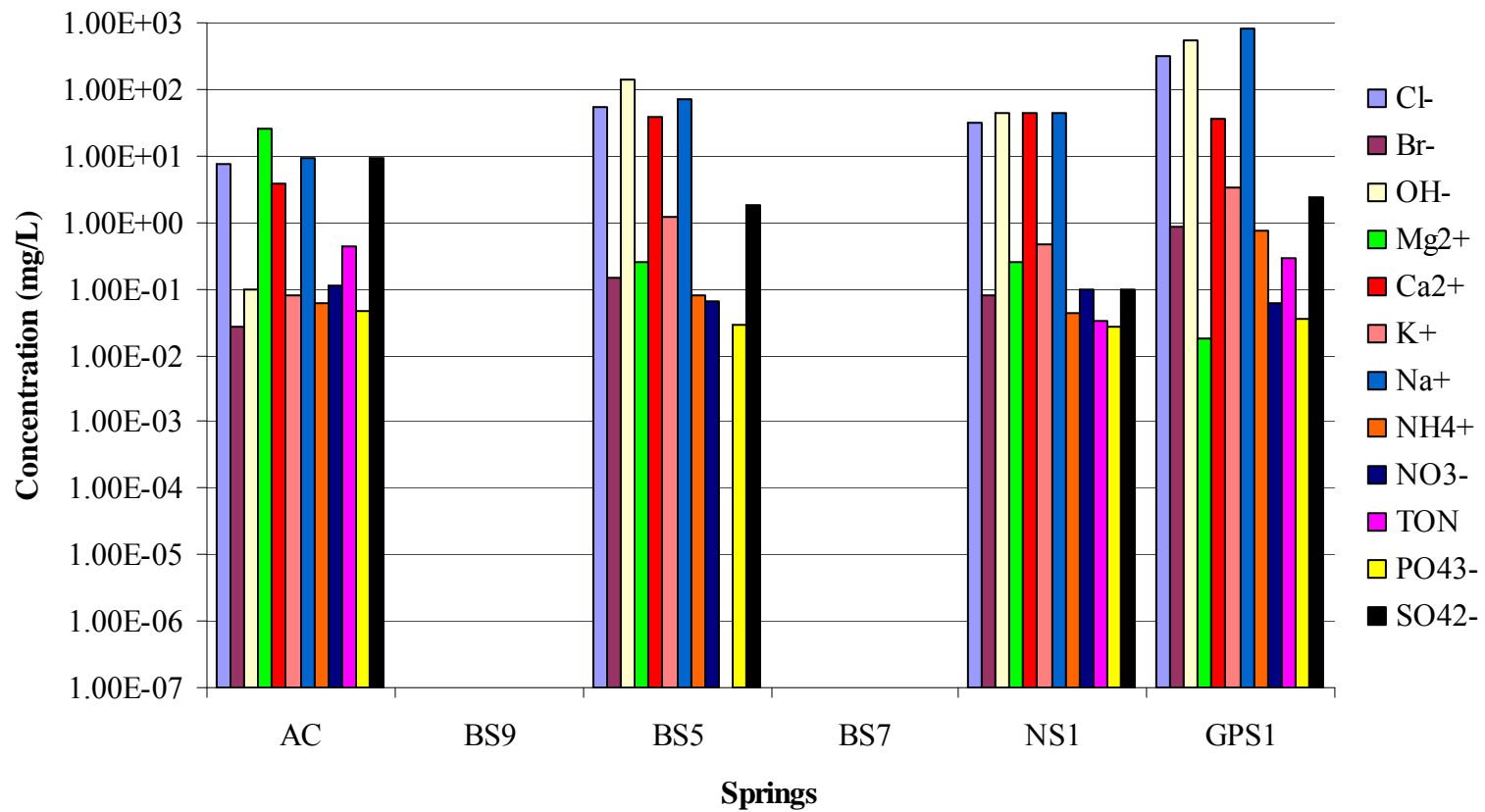
Figure 3.2. Aqueous concentrations of major cations, anions and nutrients in waters sampled at The Cedars in 2012. Raw data can be found in A.2.
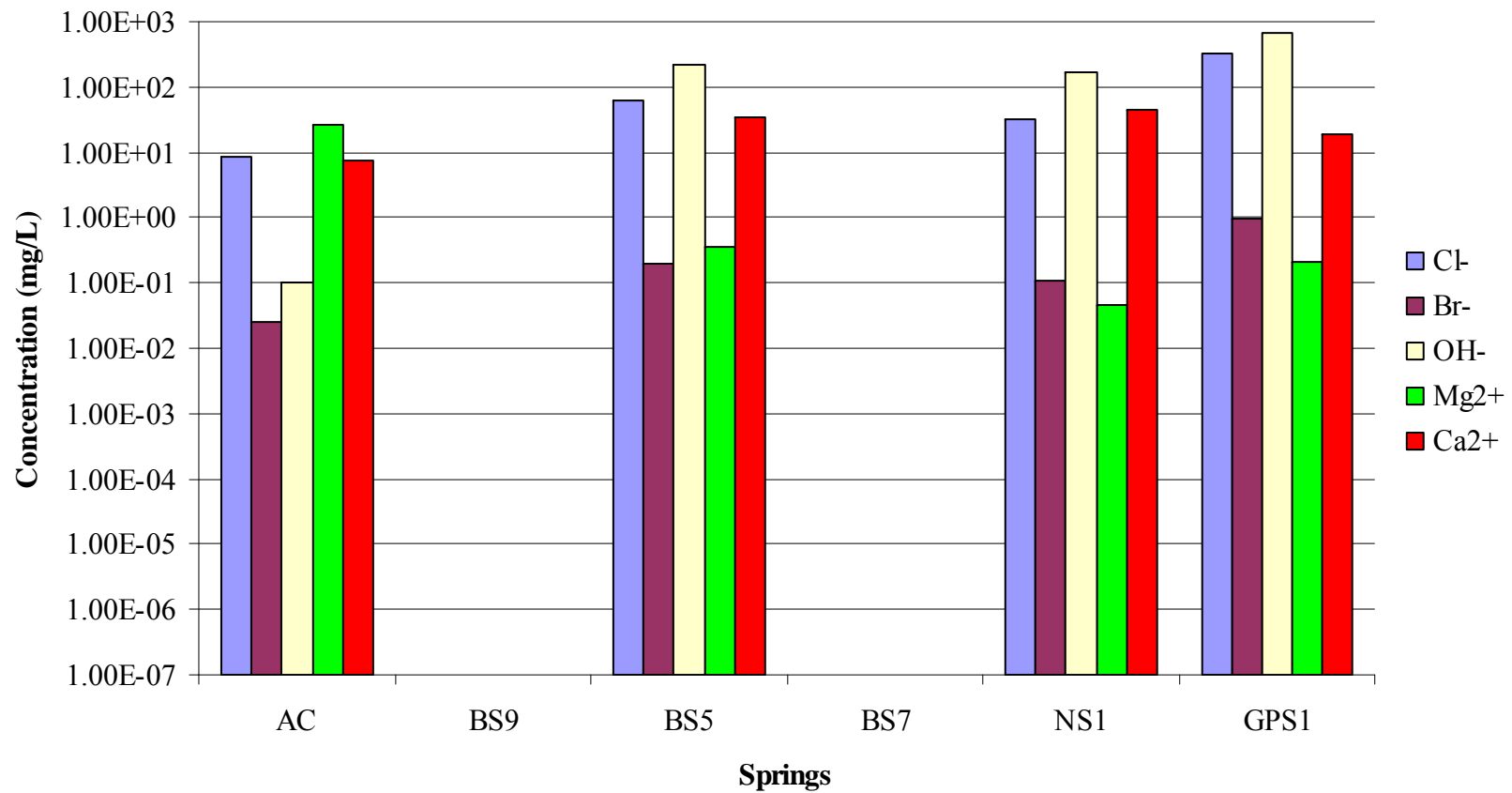
Figure 3.3. Aqueous concentrations of major cations, anions and nutrients in waters sampled at The Cedars in 2013. Raw data can be found in A.3.
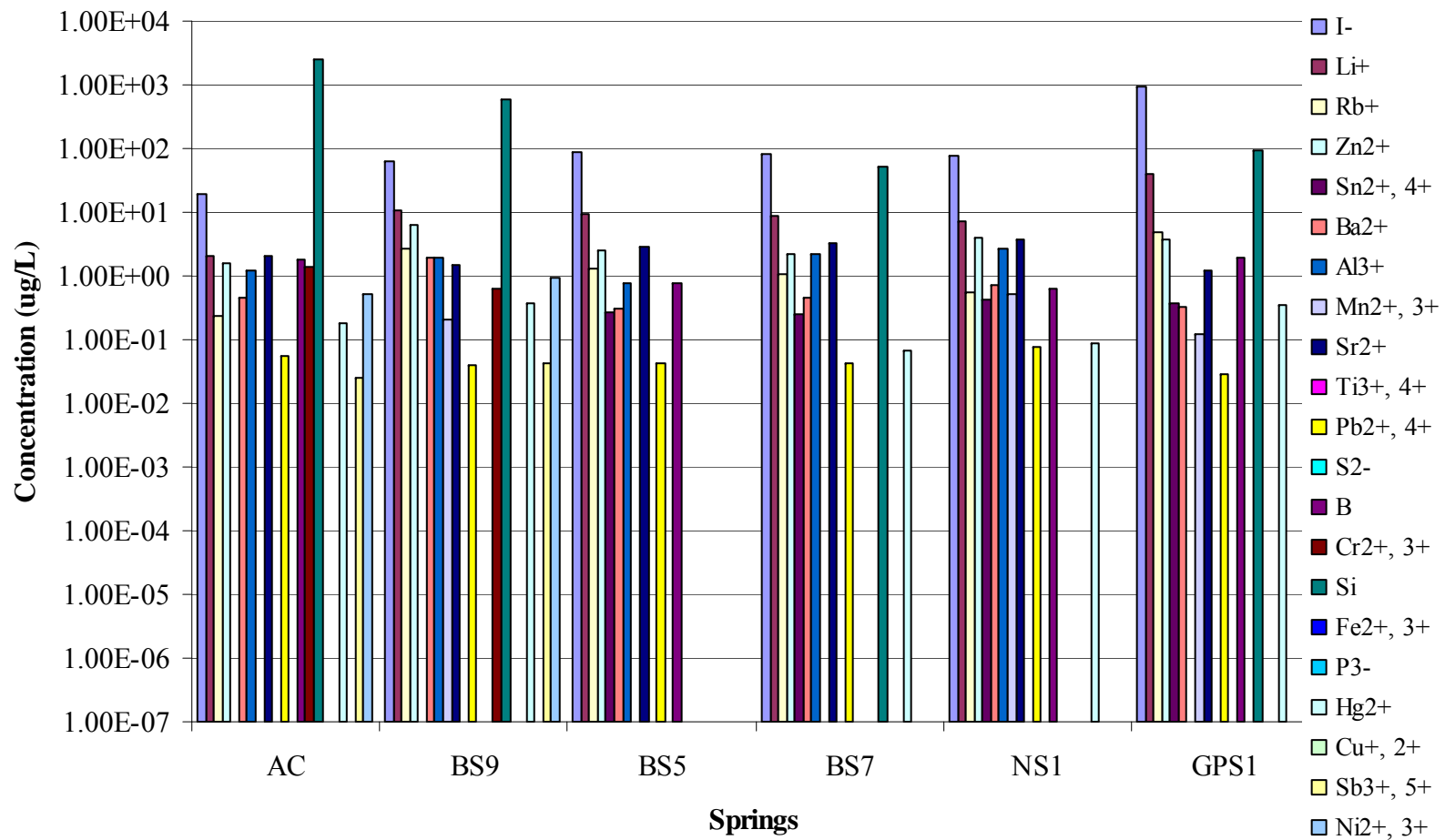
Figure 3.4. Ion concentrations of ultra-basic spring water and non ultra-basic Austin Creek water at The Cedars in 2011. Raw data can be found in A.4.
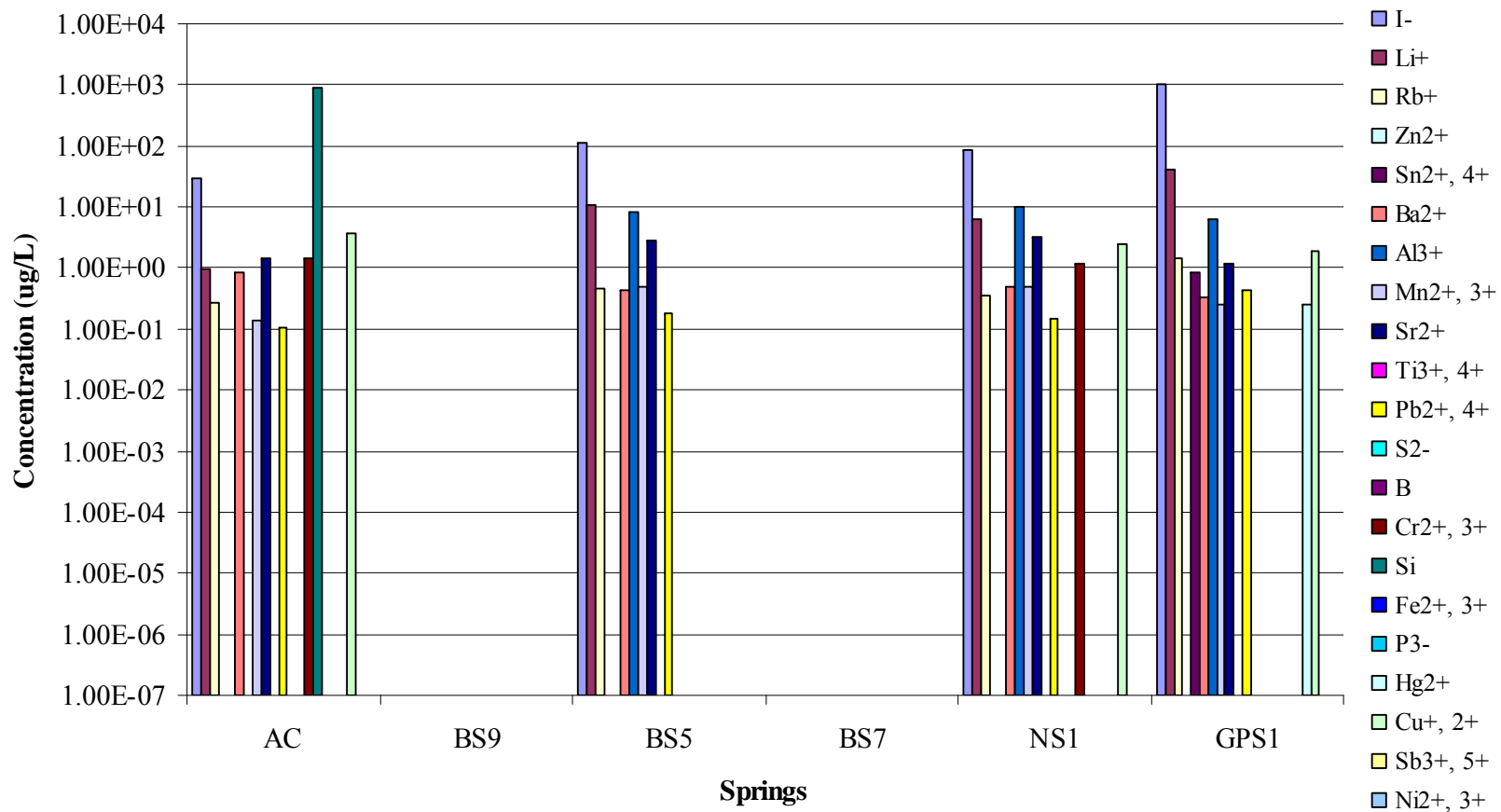
Figure 3.5. Ion concentrations of ultra-basic spring waters and non ultra-basic Austin Creek water at The Cedars in 2012. Raw data can be found in A.5.

Figure 3.6. δ^2H and δ^{18}O of fluids sampled from all sites from 2011 to 2013, as well as data from Morrill et al. (2013) for The Cedars. The solid line represents the local meteoric water line (y=7.8x+5.4, r^2=0.98) calculated by Coplen and Kendall (2000) using data sampled from the Russian River, CA, USA. The dotted line represents The Cedars local meteoric water line (y=3.9x-13.7, r^2=0.98) calculated by the linear regression of the δ^2H and δ^{18}O isotopes measured from water sampled from Austin Creek and springs from 2011 to 2013 and data from Morrill et al. (2013). Note that error bars are equal or smaller than the plotted symbols. δ^2H$_{H2O}$ and δ^{18}O$_{H2O}$ raw data can be found in A.6.

Figure 3.7. Depth profile looking at the change in (a) pH and (b) E_h with increasing depth in the WHC2 pool located at the Tablelands in 2011. Depth of the pool varied at all sampling locations but the entire water column from the surface to the rocky bottom was measured for these profiles.
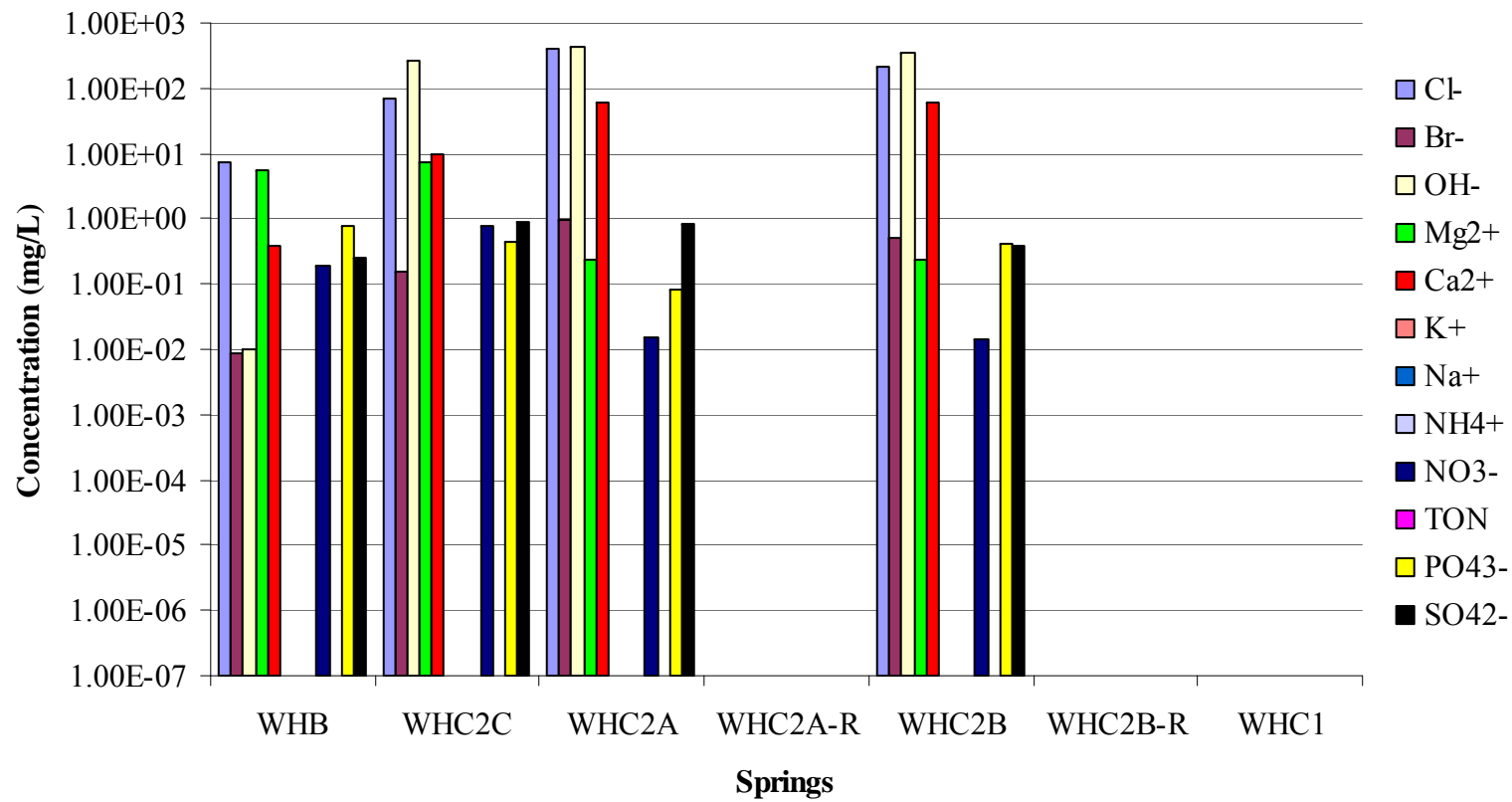
Figure 3.8. Aqueous concentrations of major cations, anions and nutrients in waters sampled at the Tablelands in 2011. Raw data can be found in A.7.
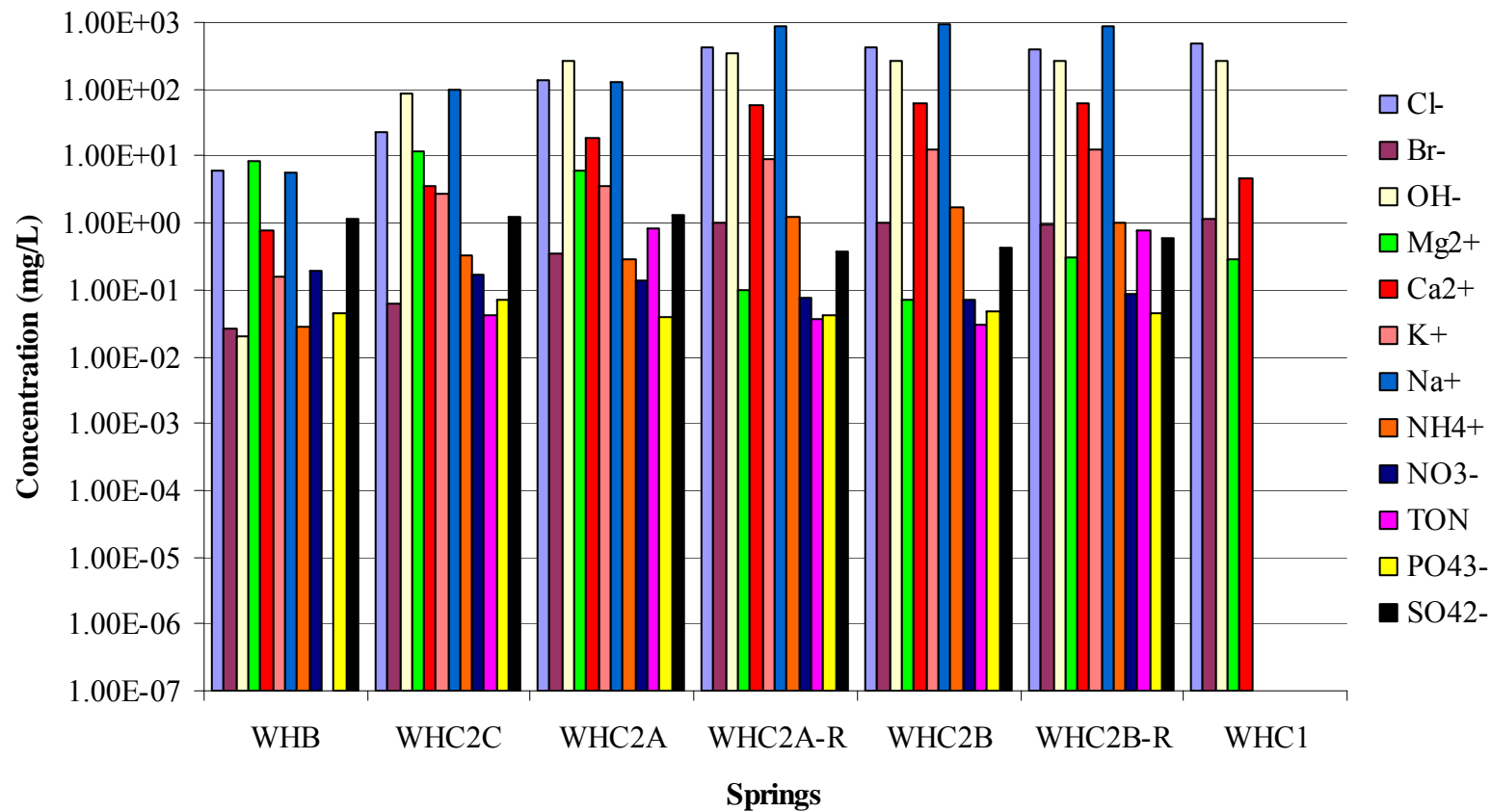
Figure 3.9. Aqueous concentrations of major cations, anions and nutrients in waters sampled at the Tablelands in 2012. Raw data can be found in A.8.
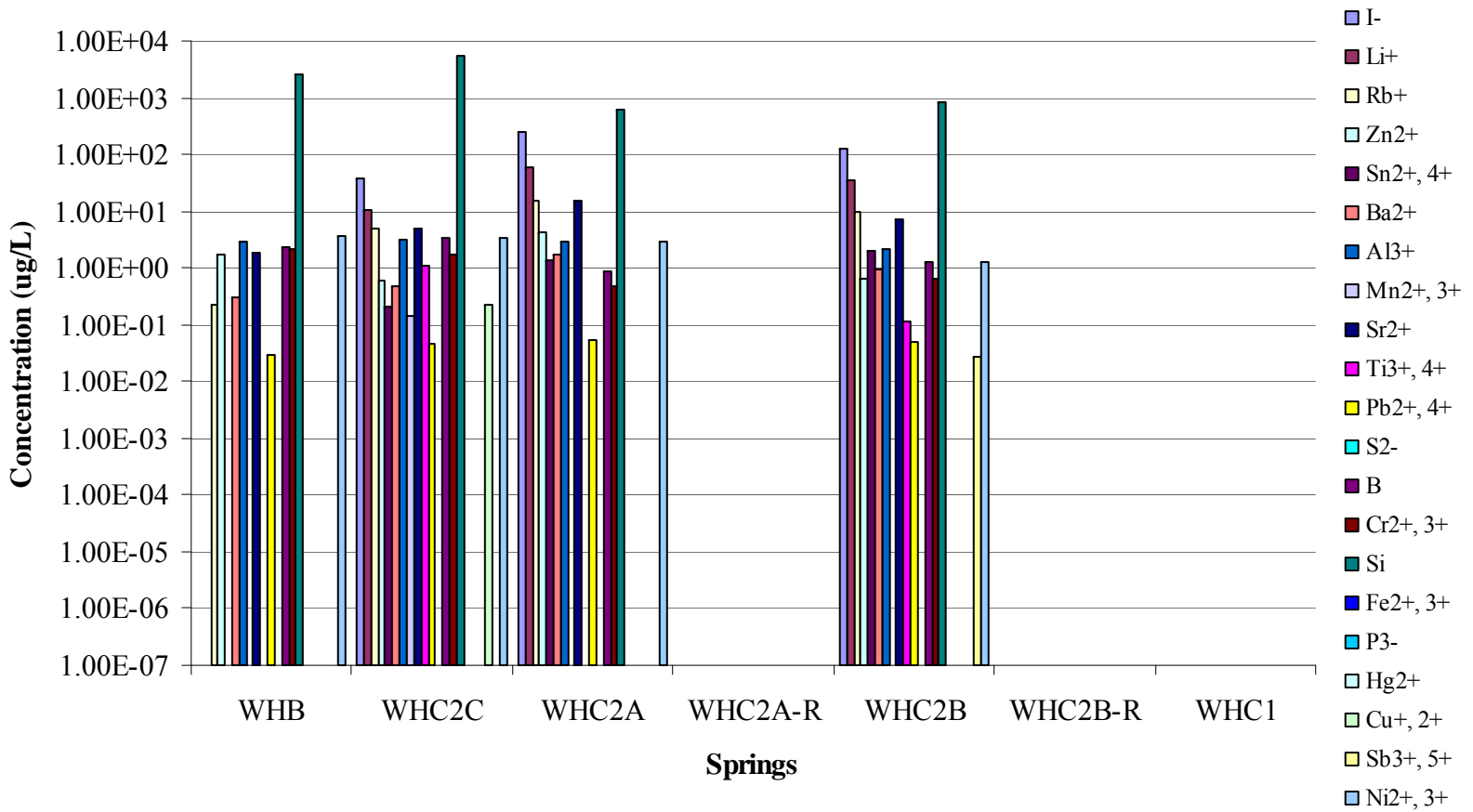
Figure 3.10. Ion concentrations (µg/L) of ultra-basic spring water and non ultra-basic Winter House Brook water at the Tablelands in 2011. Raw data can be found in A.9.
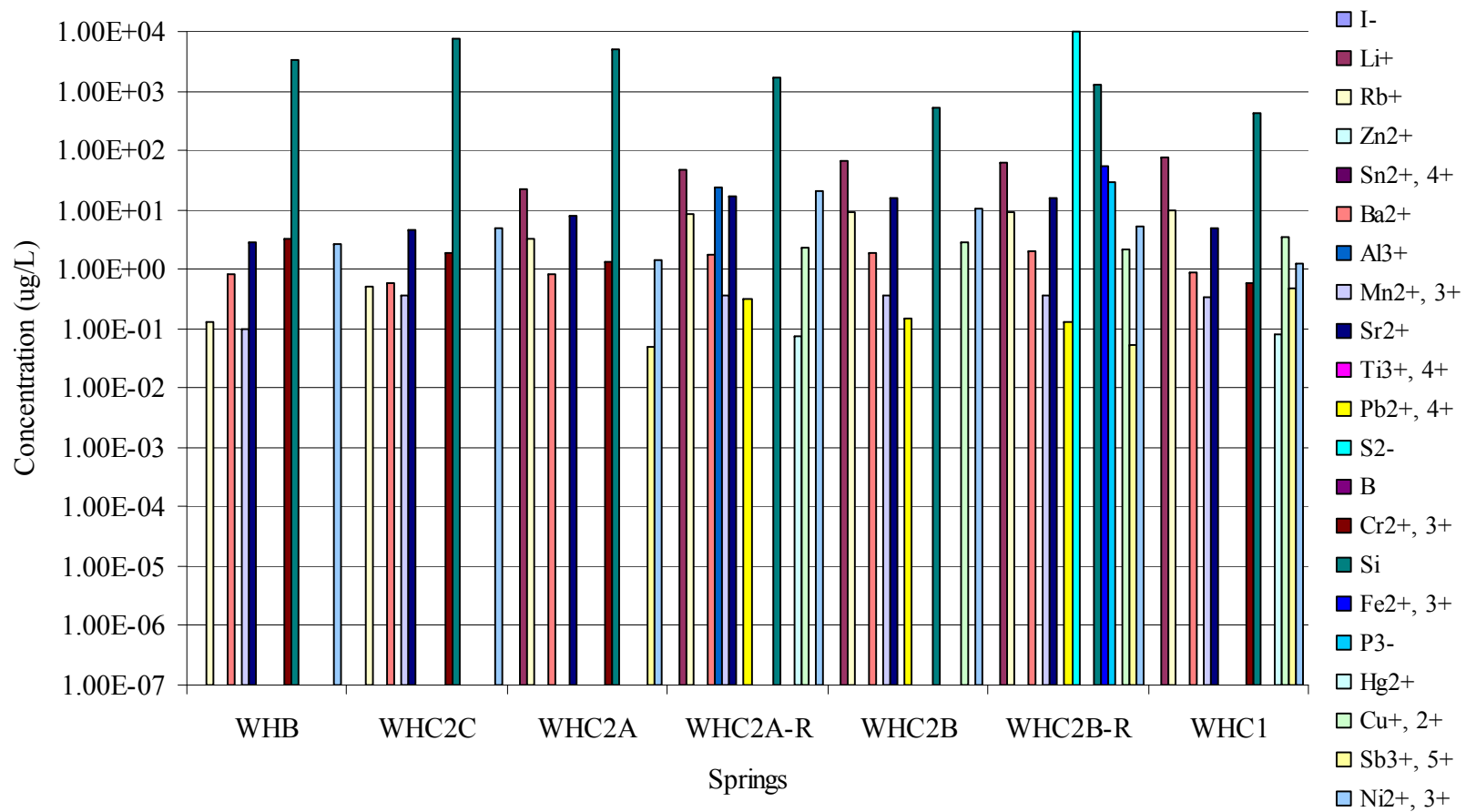
Figure 3.11. Ion concentrations (µg/L) of ultra-basic spring water and non ultra-basic Winter House Brook water at the Tablelands in 2012. Raw data can be found in A.10.

158
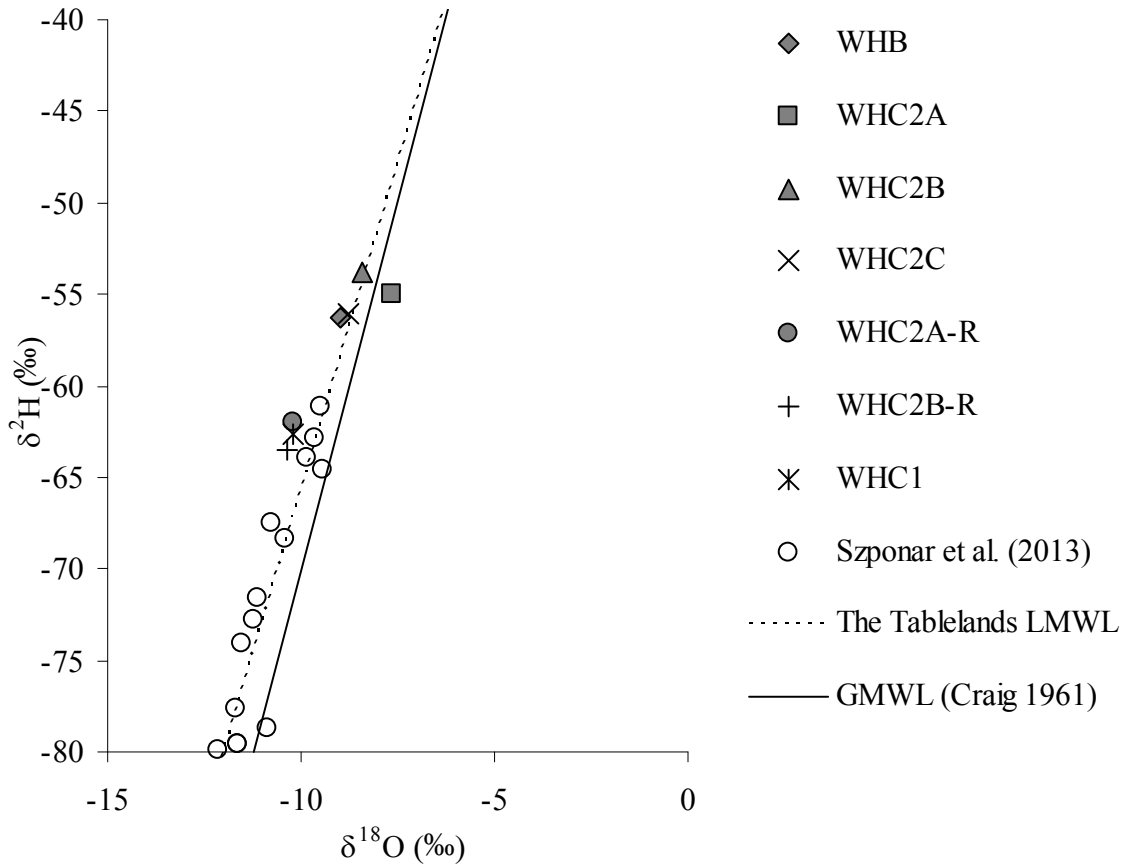
Figure 3.12. δ^2H and $\delta^{18}O$ of fluids sampled from all sites in 2011 and 2012 as well as data from Szponar et al. (2013) for the Tablelands. The solid line represents the global meteoric water line (y=8x+10) calculated by Craig (1961) from precipitation data collected in various locations world wide. The dotted line represents the Tablelands local meteoric water line (y=7.1x+5.8, r^2=0.90) calculated by the linear regression of the δ^2H and $\delta^{18}O$ isotopes measured in water sampled from Winter House Brook and spring fluids in both 2011 and 2012 and data from Szponar et al (2013). Note that error bars are equal or smaller than the plotted symbols. δ^2H_{H2O} and $\delta^{18}O_{H2O}$ raw data can be found in A.6.

Chapter 4: Discussion

4.1 Evidence of Serpentinization

Continental serpentinization reactions produce distinct geochemical indicators. The hydration reaction results in groundwater fluids that are ultra-basic (pH >11) and highly reducing (Eh < -400 mV) with high Ca^{2+}/Mg^{2+} ratios and substantial H_2 gas. The ultra-basic condition of the water is due to the partial dissolution of OH-bearing minerals such as brucite ($Mg(OH)_2$) which is formed when the Mg-end member (forsterite Mg_2SiO_4) in olivine reacts with water in the serpentinization reaction. The release of Mg^{2+} ions into solution is also due to the dissolution of brucite and other Mg-bearing minerals. An additional source of OH^- is due to the dissolution of CaO in solution during the hydration of clinopyroxene in the serpentinization process (Frost and Beard 2007). Multiple analyses of serpentine minerals have shown that CaO is not readily incorporated into serpentine-group minerals and thus Ca^{2+} ions remain in aqueous solution during the alteration of minerals in the serpentinization reaction (Barnes et al., 1967). The abundance of Ca^{2+} ions is concomitant with the production of OH^- ions (Palandri and Reed 2004) creating fluids with high pH that are rich in Ca^{2+} through the following reaction:

$$CaO + 2H_2O \rightarrow Ca^{2+} + 2OH^- \hspace{3cm} [4.1]$$

Mg^{2+} ions on the other hand are readily accommodated into serpentine-group minerals and will therefore remain in the mineral structure during alteration (Barnes et al., 1967). As a result serpentinizing systems typically have a high Ca^{2+}/Mg^{2+} ratio. Another product

of the serpentinization reaction is the formation of hydrogen gas which is produced as the reduced iron ($Fe(OH)_2$) formed from the alteration of the Fe-end member (fayalite Fe_2SiO_4) of olivine is oxidized to form magnetite (Fe_3O_4). Due to the substantial H_2 gas production the water becomes highly reducing with E_h values typically ranging from -400 to -700 mV. Therefore all of these aqueous geochemical (high pH, low E_h, high Ca^{2+}/Mg^{2+}, and H_2 gas) parameters detected in groundwater flowing through peridotite and/or serpentinite are indicators of ongoing serpentinization.

4.1.1 Cedars

Fluids discharging from the springs at The Cedars were geochemically unique compared to waters sampled from near-by Austin Creek. Some of the most distinct properties of the spring waters include high pH, low E_h, high Ca^{2+}/Mg^{2+} ratios and the presence of H_2 gas bubbling out of the springs, all of which were evidence of active serpentinization. The Cedars is part of a peridotite body that originated from the mantle and was emplaced up onto the continent as part of the Franciscan Subduction Complex 170-164 MA by tectonic activity (Coleman 2000). The ultramafic rock chemistry at The Cedars is well described by Coleman (2000) and consists primarily of olivine and pyroxenes. It has been well documented that the ultramafic body has been partially altered along its outer edges as well as throughout the interior to form serpentine and other secondary minerals including lizardite, antigorite, chlorite, magnetite and brucite (Coleman 2004; Oze et al., 2004; Hostetler et al., 1966). As groundwater continues to flow through the peridotite and comes in contact with unaltered ultramafic minerals the potential for serpentinization in the subsurface still exists today.

The waters discharging from the springs were ultra-basic with high pH values ranging from 11.4 to 12.6 with the exception of BS9 which consistently measured less basic at a pH of 10.0. The ultra-basic water discharging from the springs was consistent with the production of hydroxide ions during the serpentinization reactions. The serpentinization reactions also produce substantial amounts of hydrogen gas. At The Cedars, hydrogen gas was detected in spring waters, but not in waters sampled from Austin Creek. The hydrogen gas made up 41.3 to 43.3 % of the total gas bubbling out of the springs (BS5 and BS9) in both 2011 and 2012. In springs where bubbling gases were not observed (GSP1 and NS1) the hydrogen gas dissolved in the ultra-basic fluid ranged from 73.8 to 316 μM in 2011. The hydrogen gas measured in the spring waters was present in a highly reducing environment with negative redox values ranging from -419 to -698 mV with the exception of BS9 which had positive E_h values (+120 to +304 mV). While the hydrogen measured from the bubbling gas was consistent at all springs where bubbles were observed (BS5 and BS9), the highest dissolved hydrogen concentration was measured at the most reducing site (GPS1) and lesser amounts of hydrogen were measured at sites that were less reducing (NS1). It is unclear whether this loss of dissolved hydrogen measured at NS1 is due to uptake or oxidation. Sampled gas bubbling from BS9 had considerable hydrogen gas but the fluid discharging from the spring was not reducing which may be a function of the pools size whereby the water may be oxidizing due to its contact with the atmosphere more rapidly. Overall the spring waters contained significant concentrations of hydrogen gas and were highly reducing.

During serpentinization the dissolution of CaO (Equation 4.1) releases Ca^{2+} ions, and the dissolution of secondary Mg-bearing minerals formed through this process release

Mg^{2+} ions. A high Ca^{2+}/Mg^{2+} ion ratio in groundwater fluids discharging from ultramafic rocks is indicative of active serpentinization. At The Cedars the Ca^{2+}/Mg^{2+} ratios measured were much higher in the ultra-basic spring waters compared to the non ultra-basic water sampled from Austin Creek. Furthermore, the Ca^{2+}/Mg^{2+} ratio of the fluids sampled increased with decreasing E_h values in 2011 (Table 3.1), however this pattern was not observed in 2013 (Table 3.3).

As mentioned earlier Mg^{2+} ions are readily incorporated into serpentine minerals while Ca^{2+} ions preferentially remain in solution which produces a high Ca^{2+}/Mg^{2+} ratio within the fluids associated with the serpentinization reaction. Furthermore it has been demonstrated through geochemical modeling that Ca-silicates are unstable in serpentinizing environments which are low in aluminum or ferric iron resulting in an increase of Ca^{2+} in fluids at lower temperatures (Frost and Beard 2007). In spring waters from The Cedars there was little to no Al and Fe measured in spring waters. The overall result is elevated Ca^{2+} concentrations and low Mg^{2+} concentrations which were observed in ultra-basic fluids discharging from the springs at The Cedars giving a high Ca^{2+}/Mg^{2+} ion ratio. The fluids discharging from the springs were rich in Ca^{2+} and highly basic which drove the precipitation of Ca^{2+} ions in the form of carbonates in the presence of an inorganic carbon source through the following reaction:

$$Ca^{2+} + CO_3^{2-} \rightarrow CaCO_{3\ (s)} \qquad\qquad\qquad [4.2]$$

Carbonate deposits in the form of travertine, which are formed through the rapid precipitation of calcium carbonate ($CaCO_3$), were found surrounding the ultra-basic springs at The Cedars as seen in Figure 2.3. Precipitated calcium carbonate sediment was observed floating on the surface and deposited at the bottom of the pools of water within

the BSC, as well as, at GPS1. At NS1 the discharging point for the highly basic fluid was through the top of a carbonate mound.

4.1.2 Tablelands

Similarly at the Tablelands the fluids discharging from the springs were geochemically distinct from waters sampled from near-by Winter House Brook with high pH values, low E_h measurements, high Ca^{2+}/Mg^{2+} ratios and relatively high concentrations of dissolved H_2 . The rocks found at the Tablelands are primarily peridotites that originated from the mantle and were obducted onto the continent as part of an ophiolite complex about 500 Ma (Suhr 1992). Although the extent of alteration to the Tablelands rocks is unknown there was evidence of alteration throughout the formation. The volume expansion associated with the serpentinization reaction has caused the peridotite to be highly fractured and has resulted in mountainous talus slopes. Furthermore serpentine minerals were found on the faces of loose peridotite rocks. As groundwater continues to flow through the ultramafic rocks the serpentinization reaction has the potential to take place in the subsurface in modern times.

The waters discharging from the springs were ultra-basic ranging from a pH value of 12.2 to 12.4. This ultra-basic property suggests the presence of hydroxide ions in the fluid which is a product of the serpentinization process. Serpentinization reactions and the weathering of secondary minerals release Ca^{2+} and Mg^{2+} ions into the surrounding fluids. With high pH and these ions present in the water, carbonates will precipitate provided there is an inorganic carbon source. At the Tablelands travertine ($CaCO_3$) was found surrounding the spring waters (Figure 2.7). Travertine is the expected precipitated

carbonate to form in this environment considering that the spring water is rich in dissolved aqueous Ca^{2+} ions and with pH values >11.0 the dominant dissolved carbonate species was CO_3^{2-}. Szponar (2012), through X-ray Diffraction (XRD) analyses determined the composition of the travertine surrounding the springs and confirmed that >90% of the carbonate was calcite. Furthermore the total inorganic carbon measured within the spring fluids was determined to be the inorganic carbon source required for the precipitation (Szponar 2012).

In addition to being ultra-basic the spring waters were highly reducing and contained dissolved hydrogen gas, which as previously mentioned is another product of the serpentinization reaction. The concentration of dissolved hydrogen gas ranged from 446 to 584 μM in waters sampled from the springs (WHC2A, WHC2A-R, WHC2B and WHC2B-R). Lesser amounts of dissolved hydrogen were measured at WHC2C where overland flow is mixing with the spring waters and no dissolved hydrogen gas was detected in waters sampled from Winter House Brook.

The high Ca^{2+}/Mg^{2+} ratio measured in spring waters at the Tablelands is characteristic of groundwater associated with serpentinization. In 2011 (Table 3.17), the highest Ca^{2+}/Mg^{2+} ratio was 252 measured at WHC2A and the lowest ratio of 0.07 was measured at Winter House Brook. The ratio at WHC2B was similar to WHC2A at 241 and the ratio at the mixing site WHC2C was much lower at 1. Similar relationships were observed in 2012 (Table 3.18). In general for both 2011 and 2012 the Ca^{2+}/Mg^{2+} ratio is higher in ultra-basic fluid discharging from the springs than the non ultra-basic water sampled from the brook. This is a result of Ca^{2+} ions remaining in solution as Mg^{2+} ions were incorporated into serpentine mineral structures during the alteration process.

Moreover the lower Ca^{2+}/Mg^{2+} ratios measured in waters sampled from Winter House Brook and WHC2C maybe related to the weathering of Mg-bearing serpentine minerals and phases in locations of inactive or incomplete serpentinization (Barnes et al., 1967).

4.1.3 Summary and Comparison

Geochemically, the water discharging from the springs at The Cedars and the Tablelands were very similar to each other and very different from the non ultra-basic Austin Creek and Winter House Brook, respectively. Spring waters were rich in hydrogen gas, ultra-basic, and highly reducing with high Ca^{2+}/Mg^{2+} ratios. Predominant ions in spring waters at The Cedars and the Tablelands include OH^- and Ca^{2+} which were emblematic of serpentinizing peridotite environments. Similarly the lack of Mg^{2+} suggests its incorporation into serpentine-group minerals during the alteration process. The serpentinization and subsequent reactions result in high Ca^{2+}/Mg^{2+} ion ratios that were observed for the ultra-basic spring waters at The Cedars and the Tablelands. Higher ratios were measured at The Cedars ranging from 90 to 2015 from 2011 to 2013 compared to the Tablelands with ratios ranging from 3 to 827 from 2011 to 2012. Furthermore, calcium carbonate deposits were found within and surrounding spring discharge points at both sites. The hydrogen content of dissolved gases collected from the Tablelands (446 to 584 μM) were greater than dissolved gases measured at The Cedars (73.8 to 316 μM), however, hydrogen gas was bubbling at some of the springs at The Cedars (41.3 to 43.3 % by mol) whereas all gas was dissolved at the Tablelands.

4.2 Groundwater End members and Their Relative Mixing

The geochemically unique waters associated with serpentinization described above act as portals into subsurface systems and were used as proxies for subsurface biogeochemistry processes. At both continental systems, The Cedars and the Tablelands, fluids discharging from springs were geochemically unique compared to fluids measured in Austin Creek and Winter House Brook. It is possible that fluids discharging from springs were a mixture of subsurface fluids associated with serpentinization and fluids associated with surface processes from Austin Creek or Winter House Brook. Therefore before using the water discharging at springs as proxies for these subsurface systems, we must first consider all the possible water inputs of the springs. We must also consider any physical mixing of the two geochemically distinct fluids at or before the point of discharge.

To determine the relative mixing of these two water sources at our sampling locations a 2-component mixing model was applied. The two water end members were chosen by considering both the geochemical properties of the waters, as well as, the geologic setting in which they are found. Spectator cations and anions, which completely disassociate in water, and rarely react in these types of systems, such as Cl^- and Br^-, are conservative tracers, which can be used to model physical mixing of fluids. A linear regression of Cl^- and Br^- concentrations with an $r^2=0.999$ for each field site (Figure 4.1 and 4.2) demonstrated that these ions can be used as conservative tracers in these systems. End members were established based on the highest and lowest Cl^- and Br^- concentrations.

Once end members were established, the fraction of ultra-basic water (f_{UB})

contributing to each individual sampling location was calculated using Equation 2.2.

$$[Cl^-]_{spring} = [Cl^-]_{UB} \times f_{UB} + [Cl^-]_{NUB} \times (1-f_{UB}) \qquad [2.2]$$

The calculated f_{UB} gave us a representation of the relative mixing between the two

water end members at each individual spring and sampling location. Furthermore, a

regression analysis of various measurements, including aqueous ions and hydrocarbon

concentrations, detected at the springs and the calculated f_{UB} demonstrated whether the

observed concentrations were a result of simple physical mixing of the two water end

members. For example, a regression analysis of Mg^{2+} and f_{UB} that yielded a result of $r^2=1$

meant that the concentration of Mg^{2+} was well described by the mixing model and the

measured concentrations were attributed to physical mixing of groundwater end

members. Poor correlation coefficients indicate that one or more processes in addition to

physical mixing was occurring and that observed concentrations were not solely due to

the physical mixing of these two water end members. Therefore, this mixing model

deciphered whether concentrations measured at various sampling locations are solely

attributed to subsurface processes, in addition to determining the relative mixing of the

two distinct water end members at individual sampling locations.

4.2.1 The Cedars

There were two distinct freshwater types measured at The Cedars. Ultra-basic and

highly reducing water that was associated with serpentinization was Ca^{2+} and OH^- rich

and found discharging at the springs. A second more abundant freshwater type that was

moderately basic, oxidizing and rich in Mg^{2+} was measured in Austin Creek. These two

water types are consistent with those identified in Barnes et al (1967). The two waters are distinct from one another in many inorganic geochemical parameters including pH, E_h, conductivity as well as dissolved ion concentrations (Tables 3.1 to 3.3 and Figures 3.1 to 3.3). The geochemistry of the spring water, which is summarized in section 4.1.1, contrasts the geochemical conditions measured in waters sampled from Austin Creek. Austin Creek fluids were characterized by moderately basic pH values averaging 8.9 ± 0.1 and oxidizing redox values from +68 to +323 mV from 2011 to 2013. Conductivity measured in Austin Creek waters were lower ranging from 206 to 314 µS/cm compared to the higher conductivity of spring waters which ranged from 466 to 3020 µS/cm. The spring waters were characterized by high concentrations of Ca^{2+}, Na^+, and K^+ cations and high concentrations of Cl^- and OH^- anions. The ion concentrations measured in the spring waters at the Cedars are comparable to those measured at other continental sites of serpentinization including Oman and New Caledonia (Barnes and O'Neil, 1978), Maqarin, Jordan (Pederson et al., 2004) and Newfoundland, Canada (Szponar et al., 2013). In contrast to the spring waters the fluid measured from Austin Creek had low concentrations of all these aqueous ions and higher concentrations of Mg^{2+}, phosphate and sulphate. Based on the inorganic geochemical difference between fluids measured at The Cedars two distinct freshwater types within this site of continental serpentinization were identified.

Dissolved concentrations of conservative tracers Cl^- and Br^- were used to model the physical mixing between these two distinct water types. The positive correlation between Cl^- and Br^- seen in Figure 4.1 for 2011 to 2013 suggested that there is mixing between two consistent water end members. Fluid samples with the lowest aqueous

concentration of Cl$^-$ and Br$^-$ were the moderately basic waters measured from Austin

Creek, therefore, water sampled from Austin Creek represents our non ultra-basic end

member in the mixing model. Fluid samples with the highest aqueous concentration of Cl$^-$

and Br$^-$ were GPS1, which were the most reducing fluids measured at The Cedars. The

GPS1 spring also had the highest pH and conductivity value from 2011 to 2013. In

addition to the geochemistry, the geologic setting of GPS1 further supports its selection as

the ultra-basic end member. The GPS1 spring has the lowest elevation of all the springs

and the fluids were sampled directly from discharging location before contact with the

atmosphere (see Methods 2.1.1 for sampling method of this spring). Therefore fluids

sampled from the GPS1 spring represent our ultra-basic end member in the mixing model.

These end members and their geochemical conditions support the conceptual

model of springs published in Morrill et al. (2013), a paper which incorporates data from

this thesis, and that I co-authored. This conceptual model identifies Austin Creek as a

shallow groundwater end member and GPS1 as a deep groundwater end member. GPS1

had the highest conductivity from 2011 to 2013 suggesting a higher interaction with fine

grained marine sedimentary rocks which contain material that ionizes (dissolves into

ionic components) in water resulting in higher conductivity values (Spellman 2008). Such

fine grained sedimentary rocks were found in the argillaceous marine sediments of the

Franciscan Subduction Complex that are cradling the peridotite rock where GPS1 and

other springs are discharging from. Marine shales tend to have high chlorine content

which is predominantly water soluble, consequently, when groundwater comes into

contact with these rocks their is an observable reduction in the chlorine content of the

shales (Billings and Williams 1967). This results in an increase of dissolved Cl$^-$ ions in

the groundwater fluids. From 2011 to 2013, GPS1 had the highest dissolved Cl^- concentration which further suggests its interaction with the deeper marine shales of the Franciscan Subduction Complex. Actual deep groundwater in contact with the sedimentary rocks below is unattainable; therefore, fluids discharging from GPS1 best represent ultra-basic and highly reducing deep groundwater.

The relative mixing of these two groundwater end members was calculated using a 2-component mixing model which determines the f_{UB} contributing to each individual sampling location using Equation 2.2. Table 4.1 summarizes the calculated f_{UB} from 2011 to 2013. The f_{UB} of all springs was consistent from 2011 to 2013 with the BSC pools ranging from 0.12 to 0.17 and NS1 ranging from 0.07 to 0.08. All springs have a greater input from the non ultra-basic end member than the ultra-basic end member. The NS1 spring had the lowest contribution of deep ultra-basic groundwater compared to all other springs most likely due to its elevation. The regression analysis of the conservative ion tracer Br^- with the f_{UB} calculated yielded a correlation coefficient (r^2) of 1.00 in 2011 (Table A.1, Figure 4.3a) indicating that the observed concentration of this particular ion is due to the physical mixing of our two water end members. This also indicated that this model could be used to predict the concentrations of various ions and compounds due to physical mixing as Br^- is a spectator ion that can be used as a conservative mixing tracer. A similar result for the Br^- ion is seen in both 2012 and 2013 (Table A.2 and A.3). Table A.1, A.2 and A.3 report the correlation coefficient of major ions within this serpentinizing continental system. An extended list of ion concentrations and their corresponding correlation coefficients can be seen in Table A.4 for 2011 and Table A.5 for 2012.

Ca^{2+} ion concentrations were under predicted by the mixing model, with the exception of BS9, illustrated in Figure 4.3b, suggesting chemical or biological production in spring fluids. Serpentinizing systems are Mg rich environments where Ca minerals are unstable, thus resulting in the dissolution of Ca^{2+} into the surrounding fluids via Equation 4.1 during the alteration of ultramafic minerals such as clinopyroxene (Frost and Beard, 2007). This suggests that spring fluids first flowed through fresh peridotite where Ca-bearing clinopyroxene minerals such as diopside were being altered to Mg-bearing secondary minerals resulting in the dissolution of Ca^{2+} into the fluids before being discharged. The water contribution to the springs was primarily shallow groundwater originating from precipitation that percolated through the unsaturated zone and eventually flowed through peridotite fractures where serpentinization was occurring before being discharged at the springs. The instability of Ca-silicates and the proposed reaction was demonstrated through geochemical modeling by Frost and Beard (2007) using the following equation:

$$3CaMgSi_2O_6 + 6H^+_{(aq)} \rightarrow Mg_3Si_2O_5(OH)_4 + 3Ca^{2+}_{(aq)} + H_2O + 4SiO_{2(aq)} \qquad [4.3]$$

   diopside   serpentine
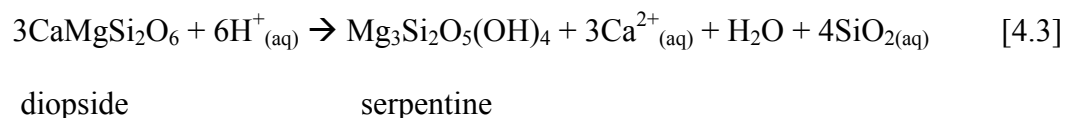
At lower temperatures, and in the absence of substantial amounts of ferric iron or Al, this reaction proceeds to the right resulting in an abundance of Ca^{2+}. The geologic setting as well as elevated dissolved Ca^{2+} concentrations and low iron and Al concentrations measured at The Cedars supports this reaction and the proposed mechanism for the deviation of Ca^{2+} in spring waters from the mixing model.

Dissolved Mg^{2+} and OH^- concentrations had poor correlation coefficient values and were not well described by the mixing model. The dissolved Mg^{2+} concentrations

were lower than predicted (Figure 4.3c) suggesting they were being consumed by a process other than physical mixing of the two water end members. As described above the serpentinization process readily incorporates Mg into the crystal structures of various secondary minerals. As shallow groundwater flows through peridotite fractures where serpentinization is occurring dissolved aqueous Mg^{2+} can be incorporated into secondary minerals resulting in the reduction of Mg^{2+} ions in groundwater fluids. The concentrations of OH^- ions were greater than predicted by the model (Figure 4.3d). The dissolution of OH-bearing secondary minerals such as brucite release OH^- ions into solution. This causes an increase in pH which was observed in the spring fluids. Additionally the dissolution of CaO during the serpentinization process is associated with the production of OH^- ions in congruence with Equation 4.1 described above. The dissolved aqueous Ca^{2+}, Mg^{2+} and OH^- concentrations observed further suggests that shallow groundwater fluids have come into contact with serpentinizing peridotite before being discharged at ultra-basic springs.

Much like Cl^- and Br^- concentrations, other ions that form strong acids and bases such as I^-, Li^+, and Rb^+ were well described by the two component mixing model with r^2 ≥ 0.83 for 2011 (Table A.4) and r^2 ≥ 0.99 for 2012 (Table A.5). Other spectator ions including Ba^{2+} and Sr^{2+} have a low r^2 suggesting there were other processes either biological or chemical affecting the ion concentrations. Non-conservative ions have low r^2 values and were not well described by the mixing model, with the exception of Pb in 2012 which has an r^2 of 1.00.

4.2.2 The Tablelands

At the Tablelands there were two distinct freshwater types sampled. Ultra-basic
and highly reducing fluids with ample Ca^{2+} and OH^- associated with serpentinization
were sampled from spring waters, and overland flow (Winter House Brook) that was
neutral, oxidizing and rich in Mg^{2+}. Multiple inorganic geochemical parameters including
pH, E_h, conductivity and ion concentrations measured in these two water types were
distinct from each other. Characterization of the ultra-basic water associated with
serpentinization discharging from the springs can be found in section 4.1.2. Winter House
Brook fluids were neutral to moderately basic, with pH values ranging from 7.8 to 8.1,
and oxidizing, with Eh values ranging from +227 to +382 mV from 2011 to 2012. The
lower conductivity ranging from 62 to 80 μS/cm measured from Winter House Brook
fluids further contrasted the high conductivity of the spring waters which ranged from
1715 to 3880 μS/cm. Spring waters were dominated by dissolved aqueous Ca^{2+}, Na^+, and
K^+ cations and Cl^- and OH^- anions. Similar ion concentrations were measured in other
serpentine waters including The Cedars (Morrill et al., 2013; and this thesis Table 3.20
and 3.21), Cabeco de Vide (Tiago et al., 2004), Oman and New Caledonia (Barnes et al,
1978). Fluids measured from Winter House Brook were not rich in any of these ions and
had higher concentrations of Mg^{2+} compared to spring waters similar to Austin Creek at
The Cedars. Given the inorganic geochemistry of these two waters two distinct water
types at this site were identified.

These two types of water were simultaneously contributing to the WHC2 pool,
which can be seen in Figure 2.7. Non ultra-basic overland water from a tributary of
Winter House Brook trickled down into the WHC2 pool at the WHC2C sampling

location. Two springs at the bottom of the pool (sampling location WHC2A, WHC2A-R, WHC2B, and WHC2B-R) were simultaneously discharging highly reducing and ultra-basic fluids associated with serpentinization at a rate of 290 mL/min. Depth profiles of both the pH and E_h of the WHC2 pool at our sampling locations in 2011 (Figure 3.7) show a clear gradient in both pH and E_h from the bottom of the pool to the water surface. Due to the mixing of the two water inputs into the WHC2 pool it is important to determine the extent of mixing at sampling locations when interpreting geochemical measurements.

Ideal water end members for all sampling locations within the WHC2 pool would be located outside the pool where we have established there is mixing among two geochemically distinct types of water. Considering the geologic setting of the pool in Figure 2.6, there were other sampling locations within close proximity. Winter House Brook, which provides the overland flow into the WHC2 pool, flows adjacent to the pool and would be my best representative of the non ultra-basic water trickling down into the pool. Similarly, WHC1 pool 6 located 1.5 m from the WHC2 pool is a tiny pool of water that is recharged through the WHC1 travertine and is isolated from the atmosphere until the point of discharge. Because of its close proximity and geologic setting it would be the best representation for the ultra-basic and highly reducing water that is recharging the WHC2 pool from the two springs located along the bottom.

Dissolved aqueous concentrations of conservative tracers Cl^- and Br^- were used to model the physical mixing between the two distinct water inputs to the WHC2 pool. The positive correlation between Cl^- and Br^- seen in Figure 4.2 for 2011 and 2012 suggested mixing between two water end members; however, the ultra-basic end member is not

consistent from 2011 to 2012. Unfortunately in 2011, the WHC1 pool 6 was not sampled. As a result in 2011 the fluid with the highest Cl^- and Br^- concentration was measured at WHC2A. In 2012, the fluid with the highest Cl^- and Br^- concentration was sampled from WHC1 pool 6. For the 2-component physical mixing model, fluids from WHC2A were used as the ultra-basic end member in 2011 and fluids from WHC1 pool 6 were used as the ultra-basic end member in 2012. The fluids with the lowest Cl^- and Br^- concentrations in both 2011 and 2012 were sampled from Winter House Brook; therefore, fluids from Winter House Brook represented our non ultra-basic end member in the mixing model for both years.

Fluids that are discharged from the springs had all the geochemical characteristics of serpentine water as discussed above. Among those geochemical characteristics was high conductivity. The bedrock geology can be a key factor in the conductivity of groundwater fluids (Spellman 2008). Fluids with high conductivity often indicate clay like bedrock, which contains material that ionizes when dissolved into water. The conductivity of the spring waters was generally high ranging from 1715 to 3880 μS/cm in 2011 and 2012. This suggests interaction with fine grained sedimentary rocks that are buried underneath the serpentinizing peridotite where the spring discharge points are located. The highly reducing and ultra-basic groundwater that is associated with serpentinization may have had contact with these sediments and also represent deeper groundwater. Similarly the high Cl^- content of the spring water also indicates extended interaction with marine shales which have a high chlorine content that is largely soluble (Billings and Williams 1967). If groundwater was in contact with the argillaceous marine sediments underlying the peridotite, Cl^- ions would dissolve into the fluids and result in a

high Cl$^-$ ion concentration. This high Cl$^-$ ion concentration was reflected in the ultra-basic

fluids discharging from the springs further suggesting its flow into the deeper subsurface.

Fluids sampled from Winter House Brook lacked these geochemical characteristics. The

elevated Mg^{2+} concentrations however, reflect weathering of Mg-bearing phases in the

bedrock of the near surface and possibly soil (Barnes et al., 1967), suggesting shallow and

overland flow of this water.

The relative mixing of these two water end members at each sampling location

was calculated using Equation 2.2. The f$_{UB}$ calculated for the Tablelands in both 2011 and

2012 are reported in Table 4.1. The f$_{UB}$ calculated in 2011 and 2012 were not consistent

with each other which may in part be a function of the changing ultra-basic end member

between years. As expected in both 2011 and 2012 sampling location WHC2C had a

higher contribution of non ultra-basic overland flow than the water associated with

serpentinization discharging from the springs. Fluids sampled from WHC2A had a low

f$_{UB}$ of 0.27 in 2012 suggesting this sampling location was diluted. Ion, nutrient, and bulk

aqueous carbon pool data taken at the same location reflect this dilution when comparing

concentrations measured at WHC2A to WHC2A-R, WHC2B and WHC2B-R.

Gaseous data measured at WHC2A, on the other hand, had comparable results to

other spring fluids and do not reflect this dilution. The discrepancy between ion and gas

data at WHC2A may be attributed to the inconspicuous location of the spring which made

repeated sampling at the exact same location difficult, especially with 2 or more samplers.

I propose that gaseous samples were taken as close to the discharge point as possible and

ion data was taken at a shallower depth. The E$_h$ vs. depth provided in Figure 3.7b

demonstrates how quickly the geochemistry can change with distance from the spring

source in the WHC2 pool. Therefore, calculated r^2 values for gaseous compounds did not include WHC2A datum in 2012. In 2011 WHC2A had similar geochemical results to WHC2A-R, WHC2B and WHC2B-R in 2012, therefore, this dilution was not measured in 2011 and we were able to isolate the ultra-basic fluid and therefore the results are comparable. Spring waters WHC2A-R, WHC2B, and WHC2B-R in 2012 and WHC2A in 2011 had a high contribution of ultra-basic water which was expected given the steep pH and E_h gradient with pool depth seen in the 2011 profiling (Figure 3.7).

Regression analysis of Br^- and the calculated f_{UB} yielded a correlation coefficient of 1.00 for both years which indicated that its concentration at all sampling locations was a result of simple physical mixing of the water end members for that particular year (Figure 4.4a). The correlation co-efficient of key inorganic ions and compounds are reported in Table A.7 for 2011 and Table A.8 for 2012. An extended list of ion concentrations and their corresponding r^2 values can be found in Table A.9 for 2011 and Table A.10 for 2012. Dissolved aqueous Ca^{2+} and OH^- concentrations were under-predicted by the mixing model at all sampling locations as illustrated in Figure 4.4b and d. This suggests that spring fluids flowed through fractures within the peridotite where serpentinization was occurring and now geochemically reflect the alteration process. Mg^{2+} concentrations were over predicted by the model (Figure 4.4c), with the exception of WHC2C, the mixing site, which could also be attributed to the serpentinization process. The ion concentrations observed in the spring waters as well as in Winter House Brook support the theory that spring water was groundwater that has flowed into peridotite fractures undergoing serpentinization and possibly come into contact with the marine shales buried beneath the serpentinizing unit.

Similar to Cl^- and Br^- spectator ions such as I^-, Li^+, Rb^+, Ba^{2+} and Sr^{2+} were well described by the mixing model with $r^2 \geq 0.97$ in 2011 (Table A.9). Similar r^2 values (≥ 0.87) were calculated in 2012 (Table A.10) with the exception of Ba^{2+} and Sr^{2+} which had low r^2 values and I^- which was not analyzed for. Other ions such as sulphate and nitrate were poorly described by the mixing model in 2011 (Table A.7) suggesting other processes either chemical and/or biological were also affecting the concentrations observed. In 2012 (Table A.8) however, these ions were well described by the mixing model ($r^2 \geq 0.86$). Ions that do actively participate in chemical or biological reactions generally displayed a low r^2 in both 2011 and 2012.

4.2.3 Summary and Comparison

At both The Cedars and the Tablelands there were two distinct fresh water types identified. A neutral to moderately basic water was measured in Austin Creek at The Cedars and in Winter House Brook at the Tablelands. Similarly, an ultra-basic and highly reducing fluid associated with serpentinization was measured discharging from multiple springs at both sites. The spring water measured at both sites was geochemically similar to one another and to other sites of serpentinization (Pederson et al., 2004; Barnes et al., 1978). The non ultra-basic members identified at both sites were also geochemically similar to one another. At both The Cedars and the Tablelands conservative tracers Cl^- and Br^- were successfully implemented in the development and validity of the 2-component mixing model created to determine the extent of physical mixing between two water end members. Springs located at The Cedars had a higher contribution of the non ultra-basic end member, while at the Tablelands the springs had a higher contribution of

the ultra-basic water associated with serpentinization. At both locations however, the Ca^{2+}

and OH^- concentrations were under-predicted by the model and could be explained by the

geochemical changes a fluid experiences when involved in the alteration process of

serpentinization. Similarly, the observed Mg^{2+} concentrations were also attributed to the

serpentinization process occurring within the subsurface. At both The Cedars and the

Tablelands the ultra-basic water end member associated with serpentinization had high

conductivity values and a high Cl^- content suggesting contact with buried marine shales.

As a result the ultra-basic end member at both sites was associated with deeper

groundwater, where as the non ultra-basic waters showed characteristics of overland flow

and shallower groundwater flow. The f_{UB} calculated using the mixing model will be

compared to geochemical measurements throughout this thesis to help distinguish the

origin of observed concentrations. It will also aid in deciphering between subsurface and

surface reactions.

4.3 Source of Groundwater

Hydrogen and oxygen isotopic values of groundwater were used as unique

geochemical tools to source and evaluate groundwater. Most commonly groundwater

isotopic composition reflects local precipitation and recharge water that has recently been

in contact with the hydrological cycle (Sharp 2007). However, in some cases water can

become trapped and isolated from the hydrological cycle for extended periods on the

geologic time scale. In general there are three different types of groundwater: meteoric,

connate, and juvenile water (Pielou 1998). Meteoric water is groundwater that circulates

as part of the hydrological cycle and is by far the most abundant kind of groundwater on

Earth. Connate water, also referred to as fossil water, is water that has been trapped in ancient sediments that have subsequently been transformed into sedimentary rocks. Lastly, juvenile or magmatic water is groundwater that was partitioned from molten rock (magma) during solidification and subsequently trapped within the subterranean. Connate and juvenile water are forms of non-cycling water, and do not participate in the circulation of the hydrological cycle. However, given enough time these rocks will be exposed and eroded and the groundwater will eventually become integrated into the global water cycle. Differentiating between these sources of water is possible with hydrogen and oxygen isotopic analysis.

A plot of δ^2H_{H2O} and $\delta^{18}O_{H2O}$ is often used as a tool to identify water that has recently been in contact with the atmosphere (i.e. meteoric in origin) (Craig 1961). The source of groundwater discharged from the springs at The Cedars and the Tablelands was determined using the δ^2H_{H2O} and $\delta^{18}O_{H2O}$ composition of fluids sampled. For further clarification concentrations of radioactive tritium (^3H) were measured to determine the source of groundwater at The Cedars. ^3H consists of two neutrons and one proton with a half life of 12.43 years, in groundwater and can provide a date in which the water was last in contact with the atmosphere and therefore provide a relative age to the groundwater (Clark and Fritz 1997).

4.3.1 The Cedars

The δ^2H_{H2O} and $\delta^{18}O_{H2O}$ values of non ultra-basic fluid collected from Austin Creek and ultra-basic fluids discharging from the springs from 2011 to 2013 and data from Morrill et al., 2013 are plotted in Figure 3.6 along with the local meteoric water line

(LMWL) generated by Coplen and Kendall (2000) using data sampled from the Russian River, CA, USA. Although data collected from The Cedars did not plot directly on the water line generated with the Russian River data, it did plot close suggesting the groundwater was meteoric in origin. This plot further suggests that groundwater measured at The Cedars both discharging from springs and flowing in Austin Creek has had recent contact with the atmosphere as precipitation, excluding connate or magmatic water as possible sources.

The fractionation of δ^2H_{H2O} and $\delta^{18}O_{H2O}$ is a function of temperature which is dependent on seasonality causing greater fractionation with decreasing temperature resulting in more depleted δ^2H_{H2O} and $\delta^{18}O_{H2O}$ values. The data used to generate the local meteoric water line for the Russian River were influenced by local meteoric conditions including temperature and seasonality which govern the δ^2H_{H2O} and $\delta^{18}O_{H2O}$ relationship. The local meteoric water line generated by The Cedars data, by using a linear line of regression of all freshwater samples collected, is also a function of local meteoric conditions which may explain the discrepancy between the two water lines. Fluids measured from Austin Creek and spring waters at The Cedars were very similar, with the exception of BS9, and forms a line with a linear regression correlation coefficient of $r^2=0.98$. The enriched δ^2H_{H2O} and $\delta^{18}O_{H2O}$ values measured at the BS9 spring may be a function of pool size and subsequent evaporation. The pool surface area to depth ratio is largest for the BS9 pool which makes it more susceptible to the affects of evaporation. Lighter isotopologues of water preferentially escape the liquid water surface to become water vapour leaving heavier isotopologues within the pool (Sharp 2007), which would be reflected by enriched δ^2H_{H2O} and $\delta^{18}O_{H2O}$ values. The similar δ^2H_{H2O} and $\delta^{18}O_{H2O}$

values of fluids from Austin Creek and spring waters suggest that although the geochemical properties of the groundwater drastically change as they travel through serpentinizing peridotite fractures, the δ^2H_{H2O} and $\delta^{18}O_{H2O}$ values remain intact contrary to the prediction of Wenner (1971), who expected ^{18}O enrichment in fluids associated with serpentinization. This may be a function of the large water-rock ratio and/or the low temperature of serpentinizing systems, as suggested by Morrill et al., 2013. Transit time of the groundwater may also have an affect.

Relative groundwater ages of spring fluids were estimated using the semi-quantitative technique of tritium analysis and are reported in Table 3.3. Fluids from the GPS1 spring, the ultra-basic deep groundwater end member, had the lowest value of <0.8 TU which is below the detection limit (~1 TU) of tritium indicative of submodern groundwater (Clark and Fritz 1997). The minimal level of tritium measured in GPS1 fluids further suggests that this groundwater fluid originated prior to the 1950's when the atmospheric nuclear bomb testing from 1951 to 1976 began. Mixing sites BS5 and NS1 had values of 2.3 and 1.2 TU, respectively, which was indicative of groundwater with a mixture of submodern and modern waters (Clark and Fritz 1997). This was consistent with the calculated f_{UB} values for NS1 and BS5 using the 2-component mixing model (Table 4.1). The expected range of values for Austin Creek was 5-15 TU indicating modern water (<5 to 10 years).

4.3.2 The Tablelands

The δ^2H_{H2O} and $\delta^{18}O_{H2O}$ values of non ultra-basic fluid collected from Winter House Brook and ultra-basic fluids discharging from the springs in 2012 and data from

Szponar et al., 2013 are plotted in Figure 3.12 along with the global meteoric water line (GMWL) calculated by Craig (1961) using precipitation data from various locations around the world since no local meteoric water line is available for this location. Although the δ^2H_{H2O} and $\delta^{18}O_{H2O}$ data from the Tablelands did not plot directly on the global meteoric water line, they did plot very close suggesting the fluids sampled from the Tablelands were meteoric in origin, eliminating magmatic or connate water as possible sources. Fluids collected from the springs after the recharge experiment (WHC2A-R and WHC2B-R) and WHC1 were more depleted and similar to fluids collected by Szponar in 2009 and 2010, compared to fluids collected at the spring before the recharge (WHC2A and WHC2B), WHC2C and Winter House Brook which were slightly more enriched.

Local differences, such as vapour pressures and temperature control, the fractionation and δ^2H_{H2O} and $\delta^{18}O_{H2O}$ relationship (Sharp 2007), causing the deviation of the local derived water line compared to the global meteoric water line developed by Craig (1961). Similar to The Cedars the geochemical properties of the spring waters were changed drastically by the serpentinization process; however, the $\delta^{18}O_{H2O}$ isotopic signature was unaltered.

4.3.3 Summary and Comparison

At both serpentinizing systems the groundwater fluids sampled from the springs were meteoric in origin suggesting recent interaction with the atmosphere and the hydrological cycle. Fluids measured from Austin Creek and Winter House Brook did not have significantly different δ^2H_{H2O} and $\delta^{18}O_{H2O}$ values than their respective spring fluids

also suggesting meteoric origin. Both locally derived water lines were not identical to water lines previously generated by other studies due to local temperature and vapour pressure variances. Fluids measured from the Tablelands were more depleted in both δ^2H_{H2O} and $\delta^{18}O_{H2O}$ compared to fluids from the Cedars which were more enriched. The Tablelands, located farther north than The Cedars, has a colder climate which leads to greater fractionation of δ^2H_{H2O} and $\delta^{18}O_{H2O}$ and more depleted isotopic values. Tritium concentrations measured at The Cedars revealed that GPS1 fluids were dated to sometime before the 1950's (submodern water) and all other spring fluids (BS5 and NS1) were a mixture of modern and submodern water as the mixing model suggested. In both serpentinizing systems the $\delta^{18}O_{H2O}$ was not affected as Wenner (1971) predicted by the water-rock reactions in the alteration process. It is common for fluids associated with serpentinization to retain their $\delta^{18}O_{H2O}$ signatures as observed in the Zambales ophiolite study conducted in the Philippines (Abrajano et al., 1990).

4.4 Source of higher molecular weight hydrocarbons

Dissolved higher molecular weight hydrocarbons (volatile organic compounds and semi volatile organic compounds) were observed in spring fluids sampled from The Cedars and the Tablelands. The 2-component mixing model, as well as, the identification and compositional distribution of higher molecular weight hydrocarbons were used to determine their likely origin. Observed concentrations may not represent the true composition at the time of formation due to secondary processes and migration processes along the groundwater flow path, so caution must be taken when interpreting hydrocarbons discharging at surface springs.

The identification of biological markers (hydrocarbon products exclusive to biological activity) and hydrocarbon compositional data was used to determine potential sources of hydrocarbons. Saturated alkanes (nC_{16+}) produced through Fischer-Tropsch Type synthesis will decrease in abundance with increasing carbon number (McCollom and Seewald, 2007). Conversely, major saturated alkanes present in plants, algae, and pollen grains are generally odd carbon numbered with specific dominant ranges for a terrestrial (C_{25}-C_{31}) source (Hunt 1996). Correlating observed hydrocarbons with sedimentary organic matter characteristics described above also aided in the understanding of the high molecular weight origin of measured hydrocarbons in spring fluids.

4.4.1 The Cedars

No volatile organic compounds were detected in fluids sampled from Austin Creek and BS9 in 2011, but they were detected in all other spring fluids in 2011 (Table 3.12) and 2012 (Table 3.13), suggesting that these organic compounds were being produced within the subsurface. Unfortunately, the mixing model could not be used to describe the observed concentrations as there were not enough data points to confidently calculate the mixing correlation coefficient. Similarly, the mixing model could not be used to describe the concentrations of semi volatile organic compounds detected in spring fluids from BS5 and GPS1 in 2012 (Table 3.14) due to a lack of data. As a result it can not be determined if the concentrations of these compounds are due to simple mixing of groundwater end members or if they were produced or consumed after mixing.

The identification of organic compounds exclusive to biological processes suggests that these compounds were not formed exclusively through abiogenic processes. For example, cycloalkanes measured in spring fluids have not been detected in hydrothermal Fischer-Tropsch Type experiments thus far in the literature. However, they are common constituents of petroleum. Moreover, the cycloalkanes detected in spring fluids, methyl- and dimethyl- substituted cyclopentane and cyclohexane, are the most common cyclic alkanes associated with petroleum (Hunt, 1996).

The thermogenic removal of hydrogen from these cyclic alkanes results in the production of aromatic compounds. Tetralin and other branched aromatic compounds measured in spring fluids have been detected in petroleum but have not been detected in Fischer-Tropsch Type processes thus far (McCollom 2003; Hunt 1996). Other aromatics including benzene, toluene, ethylbenzene, and xylene (BTEX compounds) that were measured in spring fluids are also common products of thermogenic processes. Of the BTEX compounds measured in spring fluids, toluene and xylenes (methyl substituted aromatics) were more concentrated compared to benzene (unsubstituted aromatic ring) which is a characteristic distribution measured in petroleum (Hunt 1996). BTEX compounds however, have been shown to form abiogenically through the decomposition of siderite ($FeCO_3$) with a similar distribution as thermogenically produced BTEX (McCollom 2003). Thus the presence and molecular distribution of these compounds can not alone distinguish between thermogenic and abiogenic sources.

Dissolved high molecular weight alkanes (C_7, C_{24}, C_{25}, and C_{26}) were below the quantification limit in spring fluids in 2012. As a result, no pattern could be observed and no inference of source could be determined as n-alkanes are common products of both

thermogenic and/or abiogenic (up to C_{24}) processes. In general, n-alkanes have a lower solubility compared to alkylated aromatic compounds and therefore may have come out of solution during migration as fluid temperature cooled. Additionally they can be more biologically available and may have been consumed before fluids reached the surface and therefore were not quantified or detected in spring fluids. Biological markers involving the repetitive condensation of isoprene (C_5) measured in sedimentary organic matter of the Franciscan Subduction Complex were also not detected in any spring fluids.

The concentrations of all high molecular weight hydrocarbons measured in spring fluids were consistently the highest in GPS1 fluids, which represents the deepest groundwater that has been in contact with the underlying mature kerogen of the Subduction Complex. Cycloalkanes and aromatic compounds were more prevalent in the high molecular weight hydrocarbon distribution compared to n-alkanes. This is consistent with thermogenic gases produced by kerogen within the oil generation stage where the chemical structure of petroleum shifts from straight alkanes to cyclic alkanes to aromatic compounds (increasing aromaticity) with increasing temperature and kerogen maturity seen in some studies. Furthermore, a study by Morrill et al. (2013) determined that BTEX compounds measured in the same spring fluids used for this study were well described by a 2-component mixing model based on the same groundwater end members. The potential for thermogenic hydrocarbon production demonstrated through the molecular distribution of volatile and semi volatile organic compounds suggests that higher molecular weight compounds were likely produced by thermogenic processes although an abiogenic contribution can not be ruled out.

4.4.2 The Tablelands

There were no volatile organic compounds detected in fluids from Winter House Brook or WHC2C, but there were volatile organic compounds detected and measured in spring fluids in both 2011 (Table 3.25) and 2012 (Table 3.26), suggesting that these organic compounds originated within the subsurface. Volatile organic compound concentrations were greater in recharge fluids compared to fluids sampled before the recharge experiment. Similarly, no semi volatile organic compounds were detected in fluids from Winter House Brook or WHC2C, but there were semi volatile organic compounds measured in spring fluids in 2012 (Table 3.27), again suggesting production of high molecular weight hydrocarbons in the subsurface. There were no calculated r^2 values for high molecular weight hydrocarbons due to the lack of data; therefore it was not determined if observed concentrations were due to physical mixing of groundwater end members or if compounds were produced or consumed after mixing.

Compounds unique to biological activity such as methyl substituted or unsubstituted cyclopentane and cyclohexane measured in spring fluids suggests that higher molecular weight hydrocarbons were a result of thermal decomposition of underlying sedimentary organic matter in the Humber Arm Allochthon. Cycloalkanes have not been formed in hydrothermal Fischer-Tropsch Type laboratory experiments thus far but are common constituents of petroleum. The presence of toluene although unquantifiable in recharge waters (WHC2A-R and WHC2B-R) could have been formed through thermogenic or abiogenic processes. However, trimethylbenzene has yet to be identified as formed through Fischer-Tropsch Type synthesis, although it was detected in only one spring fluid and at quantities too low to quantify.

A regular decrease in alkane abundance is observed with increasing carbon number after the nC_{16} alkane with abiotic synthesis (McCollom 2013). This pattern was not observed in spring fluids. The sum of odd alkanes was higher than the sum of even alkanes in all spring fluids which can be indicative of plant hydrocarbon production; however, alkanes were not accompanied by even chained alcohols and acids as expected with biological activity (Hunt 1996). Alkanes C_{17}, C_{25}, and C_{27} are measured in more than one spring fluid and at relatively high concentrations and are some of the most common odd alkanes produced by plants (marine and terrestrial) (Hunt 1996).

Acetate and formate concentrations were higher in spring fluids compared to fluids from Winter House Brook (Table 3.25), suggesting that organic acids also originated from the subsurface. Acetate concentrations were well described by the mixing model ($r^2=0.96$), while formate concentrations were not well described ($r^2=0.39$) suggesting additional process(es) beyond physical mixing have affected the formate concentrations. Elevated acetate content compared to formate measured in spring fluids is a typical thermogenic distribution suggesting that organic acids were formed through the decomposition of more complex organic compounds within the sedimentary organic matter in the Humber Arm Allochthon. Conversely, acetate and formate measured at the marine serpentinizing system of the Lost City Hydrothermal Field (LCHF) were proposed to be abiogenic in origin due to elevated formate over acetate concentrations (Lang et al., 2010) and estimated enriched $\delta^{13}C$ values (~4.5 to 11 ‰), however this pattern was not observed at the Tablelands. While the $\delta^{13}C$ of acetate and formate were not directly measured in this study the $\delta^{13}C$ of dissolved organic carbon (DOC) ranged from -17.7 ‰ to -23.7 ‰ from 2009 to 2011 (Szponar 2012) and can represent organic acid isotopic

data. If organic acids were a result of biomass degradation the $\delta^{13}C$ of dissolved organic carbon should be similar to the $\delta^{13}C$ signature of the starting material. The $\delta^{13}C$ of organic matter in the fine grained sedimentary source rocks ranged from -16.3 ‰ to -31.6 ‰ which were consistent with dissolved organic carbon isotopic values; however these are bulk values and starting material may have had a different isotopic signature.

Acetate and formate could have been formed by acetogenic bacteria as metabolites, however it is unlikely due to the large fractionation (-58.6 ± 0.7 ‰) associated with microbial formation (Zerkle et al., 2005), which was not observed in dissolved organic carbon isotopic data. This large fractionation however, is dependent upon the completion of the reaction; therefore, the values measured from the field are dependent upon the degree of reaction which may not have reached completion. Moreover, a metagenomic survey of spring fluids published by Brazelton et al. (2012) found that acetogenesis is not a prevalent anaerobic metabolic pathway; therefore a microbial origin for these organic acids is unlikely. Alternatively, ultra-basic fluids with elevated H_2 concentrations thermodynamically favour the formation of formate from dissolved inorganic carbon and H_2 abiotically as shown by McCollom and Seewald (2003). Although acetate is also more thermodynamically stable than dissolved inorganic carbon in these conditions it has yet to be produced in similar experiments, therefore it is unlikely that abiotic reactions are the sole source for organic acids. The compositional distribution of organic acids and the $\delta^{13}C$ of dissolved organic carbon measured in spring fluids suggest subsurface thermal degradation as the primary source of organic acids, however due to the presence of putative abiogenic organic acids in fluids from the Lost City Hydrothermal Field serpentinizing system and the thermodynamically favoured

conditions of fluids associated with serpentinization an abiogenic contribution can not be ruled out at the Tablelands. To further investigate the source of organic acids $\delta^{13}C$ of acetate and formate should be analyzed.

4.4.3 Summary and Conclusion

All high molecular weight hydrocarbons measured in spring fluids from The Cedars and the Tablelands originated from the subsurface. Spring fluids from The Cedars had higher concentrations and a wider variety of volatile hydrocarbons compared to spring fluids from the Tablelands. Conversely, spring fluids from the Tablelands had a higher abundance of saturated alkanes (nC_{17+}) compared to spring fluids at The Cedars. Compositional data suggest that the primary source for high molecular weight hydrocarbons measured in spring fluids from The Cedars is thermogenic, with a possible abiogenic contribution. Similarly for the Tablelands, compositional and isotopic data suggest that thermogenic processes are responsible for the majority of measured hydrocarbons in spring fluids, however, an abiogenic contribution can not be ruled out. At both The Cedars and the Tablelands the measured hydrocarbons are consistent with the sedimentary organic matter characterization of the underlying sedimentary complexes further suggesting thermal degradation of sedimentary organic matter as the primary hydrocarbon production mechanism.

4.5 Source of low molecular weight alkanes (C_2-C_6)

Low molecular weight alkanes (C_2, C_3, iC_4, nC_4, iC_5, nC_5, and nC_6) were measured in spring fluids at the Tablelands and The Cedars. These gases have the

potential to be produced through microbial, thermogenic or abiogenic processes or possibly a mixture of two or more mechanisms. The concentrations and carbon isotopic composition of these alkanes were evaluated using the mixing model and applied to various models to determine their origin.

A Schulz-Flory distribution (log mole fraction versus carbon number) and a plot of carbon isotope values ($\delta^{13}C$) versus carbon number for the straight chain alkanes C_1-C_6 were used to determine potential hydrocarbon gas sources. Surface gas springs like at The Cedars and the Tablelands may not reflect the original hydrocarbon composition as secondary chemical/biological processes and/or segregate migration can alter the molecular composition as it travels towards the surface. In addition, secondary fractionation processes such as diffusion or mixing of various alkane sources can alter the observed isotopic trends of alkane gases measured in spring waters, so caution must be taken when interpreting these models. For additional lines of evidence correlation with the maturity of underlying sedimentary organic matter and the mixing model were used to further delineate potential hydrocarbon sources.

4.5.1 Cedars

Higher concentrations of alkanes C_2-C_6 were measured in spring fluids compared to fluids collected from Austin Creek (Table 3.6 for 2011, 3.7 for 2012, and 3.8 for 2013), suggesting that C_2-C_6 alkanes were being produced in the subsurface along the groundwater flow path. A study (Morrill et al., 2013) that took place from 2005 to 2011 that included data from this thesis, showed that C_2-C_6 concentrations of bubbling springs were well described by a mixing model ($r^2 \geq 0.95$) based on the same groundwater end

members which calculated similar f_{UB} values reported in this thesis. In addition, the C_2-C_6 concentrations measured from bubbling springs in this study were comparable to concentrations measured in the published study (Morrill et al. 2013). Since geochemical data collected through this study is similar to those found in Morrill et al. (2013) it is reasonable to assume C_2-C_6 concentrations were well described during the duration of this study (2011 to 2013) as well. This suggests that the observed C_2-C_6 concentrations were a product of physical mixing between ground water end members and that they were not being produced along the groundwater flow path after the mixing of the two ground waters. Instead, C_2-C_6 alkanes must have been produced along the flow path of the deep ground water only before mixing with the shallow groundwater.

Highest dissolved C_2-C_6 concentrations were measured in deep groundwater fluids measured from GPS1 which have contact with the argillaceous marine sediments of the Franciscan Subduction Complex below, suggesting a possible thermogenic origin, however, abiogenic production can not be ruled out as these fluids also flow through serpentinizing peridotite which creates conditions that are amenable for Fischer-Tropsch Type synthesis. Higher bubbling and dissolved concentrations of C_6 compared to C_2 and C_3 alkanes, with the exception of bubbling gases in 2011 where C_6 concentrations were slightly lower compared to C_2 concentrations, suggests a thermogenic origin. A general abiogenic trend of alkanes as observed with field samples of putative abiogenic gases (Sherwood Lollar et al., 2008; Potter and Konnerup-Madsen, 2003) and laboratory experiments of Fischer-Tropsch Type synthesis (McCollom and Seewald, 2006) is a decrease in alkane homologues abundance with an increase in carbon number. This relationship is reflected in a Schulz-Flory distribution where a typical abiogenic

dominated gas yields a correlation coefficient of $r^2 > 0.99$ (Etiope and Sherwood Lollar, 2013). A Schulz-Flory distribution of C_1-C_5 gases measured in spring fluids from The Cedars yielded r^2 values ranging from 0.46 to 0.66 (Figure 4.5), suggesting these alkanes were not predominantly abiogenic or that their concentrations have been affected by secondary reactions (e.g. oxidation or segregative migration). C_2 and C_3 alkanes produced through abiotic reactions in some experimental studies had similar relative abundances (Fu et al., 2007; Taran et al., 2007); however the abundant C_6 detected in spring fluids has not yet been observed for abiogenic hydrocarbon production through Fischer-Tropsch Type synthesis.

The δ^{13}C isotopic composition of C_2-C_6 alkanes ranged from -25.7 to -22.6 ‰ which is within range of both thermogenic and abiogenic field gas data (Etiope and Sherwood Lollar, 2013). The δ^{13}C of ethane produced through bacteriogenesis in two near surface aquifers in western Canada ranged from -73.9 to -45.4 ‰ (Taylor et al., 2000), which is much more depleted than the C_2-C_6 alkanes measured in spring fluids at The Cedars and therefore unlikely to be producing the observed gas. Natural gases that are associated with the transformation of kerogen are isotopically depleted in ^{13}C relative to their organic precursors (Whiticar 1996) due to ^{12}C forming slightly weaker terminal carbon chemical bonds compared to ^{13}C. This creates a difference in reaction rates between molecules containing ^{12}C atoms versus ^{13}C atoms (Clayton 1991). The δ^{13}C of the bulk organic carbon measured from marine shales of the Franciscan Subduction Complex was -25.0 ‰, similar to the δ^{13}C value of C_2-C_6 gases discharging from springs. This may be an indication of extensive thermal decay of the sedimentary organic carbon in the Franciscan Subduction Complex underlying the peridotite resulting in the

dissolution of thermogenic alkane gases into deep groundwater and subsequent transportation and discharge at the springs, much like the higher molecular weight hydrocarbons discussed above.

Alternatively, these alkanes could have formed through abiogenic processes. A natural gas plot of C_1-C_6 alkanes shows that the carbon isotopic values do not follow the abiogenic polymerization model proposed by Sherwood Lollar et al. (2008) (Figure 4.6). The significant fractionation between methane and ethane seen in the abiogenic model mimicking actual data was forced due to the fractionation factor between methane and ethane which is calculated based on average $\delta^{13}C$ values of observed C_1 and C_2 measurements. Subsequent hydrocarbon production (C_3-C_6) did not follow the abiogenic model likely due to the incorporation of $\delta^{13}C$ of methane into every succeeding alkane calculation in the polymerization model. Methane measured at The Cedars was primarily microbial (see below) and has a depleted $\delta^{13}C$ signature influencing the behaviour of the model and causing it to deviate from observed values, therefore, if alkanes C_2-C_6 were being formed through abiogenic polymerization they were not using the microbial methane as their precursor. A thermogenic isotopic trend of $\delta^{13}C$ enrichment with increasing carbon number was also not observed in the C_1-C_6 carbon isotopic data. Not all abiogenic and thermogenic gases can be described using carbon isotopic trends like the C_1-C_6 data collected from The Cedars. Fractionation processes related to secondary alteration processes such as oxidation or mixing of sources may have caused The Cedars data to be unrecognizable compared to established isotopic trends.

4.5.2 Tablelands

Dissolved alkane gases C_2-C_6 were higher in concentration ranging from 0.086 to 1.30 μM in spring fluids compared to fluids collected from Winter House Brook where the concentrations were below the detection limit or below the quantification limit (Table 3.22). This suggests that alkanes were being produced within the subsurface and transported to the WHC2 pool with ultra-basic spring waters. Dissolved C_2-C_6 concentrations were not well described by the mixing model, with the exception of nC_5 (r^2=1.00), suggesting processes other than physical mixing are affecting the observed alkane concentrations along the groundwater flow path of spring fluids.

A Schulz-Flory distribution of alkanes C_1-C_5 at all springs in 2012 yielded correlation coefficient values ranging from 0.82 to 0.89 (Figure 4.5), suggesting that these alkanes were not quasi-pure abiogenic gas, or that secondary processes were affecting the molecular distribution during migration. Thermogenic gases are typically characterized by a distribution coefficient of r^2<0.9 as seen with Tablelands C_2-C_5 data (Etiope and Sherwood Lollar, 2013). Although an abiogenic input can not be ruled out by this plot it does suggest that the alkanes were not dominantly abiogenic and more likely a mixture of thermogenic and abiogenic gases. Alternatively, migration fractionation of gases could have affected the distribution of alkanes resulting in a molecular composition that is uncharacteristic of abiotic production. Ethane/propane ratios which range from 0.83 to 1.64 further suggest a possible mixture of thermogenic gas with another source. As seen in hundreds of natural gas wells in the United States thermogenic gases typically display ethane/propane ratios greater than 1 (Mines, 1979).

The $\delta^{13}C$ range of C_2-C_6 gases was -32.4 to -29.7 ‰ which is within range of both thermogenic and abiogenic gas, but too enriched to be attributed to bacteriogenesis. The $\delta^{13}C$ of the bulk organic carbon in fine grained sedimentary rocks sampled from the underlying marine mélange ranged from -31.6 to -16.3 ‰ which is within range of the gases measured at the Tablelands.

A plot of carbon isotope values versus carbon number for C_1-C_6 alkanes from the Tablelands did not follow the abiogenic polymerization model (Figure 4.6) which suggests gases were not dominantly abiogenic, but many abiotic gases do not follow this model (Morrill et al., submitted) so an abiogenic contribution can not be ruled out. A saw-tooth pattern proposed by Sherwood Lollar et al. (2008) where an isotopic depletion between methane and ethane followed by an isotopic enrichment from ethane to propane is observed assuming rapid abiogenic polymerization chain growth also does not match measured $\delta^{13}C$ alkanes from the Tablelands. Low molecular weight hydrocarbons from the Lost City Hydrothermal Field that have been proposed to be produced through Fischer-Tropsch Type synthesis (Proskurowski et al., 2008), however, had similar $\delta^{13}C$ trends as the Tablelands data. Dissolved C_2-C_6 alkanes in spring fluids at the Tablelands were not consistently well described by abiogenic or thermogenic $\delta^{13}C$ trends suggesting either mixing of varying sources or secondary alteration and fractionation processes.

4.5.3 Summary and Comparison

Low molecular weight alkanes (C_2-C_6) measured at The Cedars and the Tablelands were more concentrated in spring fluids compared to Austin Creek and Winter House Brook, respectively, suggesting alkane production within the subsurface. Alkane

concentrations were well described by the mixing model at The Cedars, suggesting production in groundwater fluids that flow deep within the subsurface before mixing. Conversely, at the Tablelands the C_2-C_6 alkanes were not well described by the mixing model, suggesting that changes in alkane concentrations could have transpired before or after the mixing of the two groundwater end members. Elevated C_6 concentrations at The Cedars could not be explained through Fischer-Tropsch Type synthesis and a Schulz-Flory distribution was not typical of abiogenic dominated gas, suggesting a thermogenic source or mixing of thermogenic and abiogenic sources. Similarly at the Tablelands, the distribution coefficient was indicative of a thermogenic source or possible mixing of different sources and the ethane/propane ratios also suggested a mixture of sources.

Alkanes measured at The Cedars were slightly more enriched with $\delta^{13}C$ values ranging from -25.7 to -22.6 ‰ compared to the Tablelands where gases ranged from -32.4 to -29.7 ‰. The carbon isotopic values for both sites were in range of thermogenic and abiogenic production but outside the range associated with bacteriogenesis. The alkane carbon isotopic values were in range of $\delta^{13}C$ for sedimentary organic matter sampled from formations that underlie the serpentinizing systems at both locations. The natural gas plots of C_1-C_6 for The Cedars and the Tablelands did not follow any thermogenic or abiogenic trends, suggesting secondary fractionation processes or mixing of different sources.

Low molecular weight alkane (C_2-C_6) gas measured at The Cedars and the Tablelands were not dominated by an abiogenic source. At The Cedars gases were likely formed by thermogenic processes however an abiogenic contribution could not be ruled out. At the Tablelands there was evidence of possible thermogenic and abiogenic

contributions suggesting a possible mixture of alkane sources. Further research and

analyses, such as δ^2H of alkanes C_2-C_6, can further distinguish between thermogenic and

abiogenic processes and aid in the sourcing of low molecular weight alkanes. It is

important to note that alkane (C_1-C_6) data can not be applied blindly to these different

plots and models as circumstance and different sources can influence the behaviour of

observed data and calculated models. Great caution must be taken when interpreting the

data and the generated models that are based on measured data or similar field samples.

4.6 Source of Methane

At these terrestrial serpentinization sites, where low-temperature gas-water-rock

reactions are occurring at shallow depths, methane can be produced through biogenic

(microbial and thermogenic) and/or abiogenic processes. To decipher between these three

methane formation pathways at The Cedars and the Tablelands the concentration and

isotopic composition of hydrocarbon gases, including methane and other low molecular

weight hydrocarbons, was evaluated using the two component mixing model and applied

to various methane sourcing plots to form multiple lines of evidence.

The 2-component mixing model of groundwater was used to determine whether

methane is being produced along the flow path of mixing springs, but could not be used

to distinguish between different sources. A modified Bernard plot, a plot of CH_4/C_{2+} ratio

versus $\delta^{13}C$ of the methane (Hunt 1996), was used as a first step in distinguishing

between sources of methane. A second plot of δ^2H_{CH4} versus $\delta^{13}C_{CH4}$ (a CD diagram) was

used to distinguish between different biogenic sources (microbial and thermogenic).

Lastly the relationship between $\alpha C_{DIC-CH4}$ and $\alpha H_{H2O-CH4}$ was used to distinguish between

methane sources. Correlating geochemical data obtained through this thesis and microbiological work done by collaborators at The Cedars (Suzuki et al., 2013, Suzuki et al., 2014) and the Tablelands (Brazelton et al., 2012, Brazelton et al., 2013) further constrained potential methane sources. Using aforementioned plots and measured data from The Cedars and the Tablelands multiple lines of evidence will be employed to source the observed methane.

4.6.1 The Cedars

Dissolved methane concentrations were higher in spring fluids ranging from 53.6 to 239 μM compared to Austin Creek which had low concentrations averaging 14.5 ± 5.2 μM of dissolved methane. Fluids collected for Austin Creek were taken below the BSC therefore the creek fluids used for this study may have BSC methane contributing to it resulting in the low observed methane concentration. Supporting this theory is the similar $\delta^{13}C$ values of bubbling and dissolved methane measured in BSC spring fluids (-63.1 ± 0.2 ‰, n=3) and Austin Creek fluids (-63.5 ‰) in 2011 suggesting the same methane origin. Additionally, the spring CS1 in Morrill et al. (2013) was bubbling in the middle of the creek, therefore, other bubbling sources could be located along the bottom of the creek and contributing methane. Methane is often associated with the serpentinization process (Schrenk et al., 2013; Proskurowski 2010) so it is likely that the methane being discharged in spring fluids is being produced within the subsurface. Dissolved methane concentrations measured at the mixing sites (NS1 and BSC springs) were under-predicted by the mixing model (Table 3.6 for 2011 and 3.7 for 2012), indicating that methane was being produced by either biological or chemical processes in fluids along the ground

water flow path before being discharged at the springs. In addition to the dissolved

methane observed within spring fluids, gases bubbling from mixing springs (BS5, BS9

and NS2) were also rich in methane ranging from 4.2 to 16.1 %. This suggests a

substantial amount of methane was produced along the ground water flow path after the

deep groundwater mixes with the shallow groundwater.

A modified Bernard plot (Figure 4.7) was used as a first approach in determining

the primary source of this observed methane (both dissolved and bubbling). Methane gas

bubbling from the NS2 spring plots within the traditional microbial field with a high

CH_4/C_{2+} ratio of 2.72 x 10^3 and a depleted $\delta^{13}C_{CH4}$ value of -66.4 ‰. Bubbling gas from

various BSC springs and dissolved gas from GPS1 had a lower CH_4/C_{2+} and more

enriched $\delta^{13}C_{CH4}$ values plotting between fields, with dissolved methane from GPS1

plotting closest to the thermogenic traditional field and abiogenic CH_4/C_{2+}. This plot

suggests that methane in the NS spring is dominated by microbial methane where as

methane in the BSC and GPS1 springs, which trend towards a thermogenic/abiogenic

source, were a mixture of microbial and non microbial methane. The observed trend may

also be a result of anaerobic methane oxidation along the groundwater flow path within

the peridotite which causes a decrease in the alkane ratio and more enriched $\delta^{13}C_{CH4}$

values as ^{12}C is preferentially utilized by methane oxidizers (Wiese and Kvenvolden

1993). The occurrence of anaerobic methanotrophic archaea phylotypes and associated

genes at other serpentinizing systems (Schrenk et al., 2013) is evidence for potential

methane oxidation in similar conditions, such as The Cedars. Total inorganic carbon

(TIC) measured in spring fluids in 2011 (Table 3.4) ranged from -63.5 to -23.0 ‰

supporting the proposed organic and methane oxidation; however the corresponding

$\delta^2 H_{CH4}$ enrichment of gases measured at the BSC springs compared to NS2 is not observed. Also, if CH_4 oxidation was occurring than the mixing model would have over-predicted the CH_4 concentrations instead of under-predicted the concentrations as observed. Therefore, the observed trend on the modified Bernard plot is most likely due to the mixing of a microbial and non microbial methane source in the BSC and GPS1 springs.

In support of these findings the $\delta^2 H_{CH4}$ and $\delta^{13} C_{CH4}$ values of bubbling methane from NS2, BS9 and BS5 were within range of microbial derived methane and plot within the acetate fermentation field on a CD diagram (Figure 4.8). Traditional fields of the CD diagram have been expanded through subsequent studies and a more detailed updated version can be seen in a review paper by Etiope and Sherwood Lollar (2013). Even in the updated CD diagram bubbling methane measured at The Cedars plots within the microbial methyl fermentation zone. This plot further suggests a primary microbial source to the bubbling methane generated at The Cedars. Dissolved methane concentrations were too low for $\delta^2 H_{CH4}$ analysis and therefore I could not constrain specific data points, but the range of $\delta^{13} C$ for dissolved methane could potentially plot in any of the three traditional fields on the CD diagram. The carbon and hydrogen fractionation factors calculated for bubbling methane measured at springs BS5 ($\alpha C_{DIC-CH4}$=1.03, $\alpha H_{H2O-CH4}$=1.49) and BS9 ($\alpha C_{DIC-CH4}$=1.04, $\alpha H_{H2O-CH4}$=1.51) in 2011 however plot within or very close to the aceticlastic pathway field originally outlined by Whiticar et al. (1986) on a $\alpha C_{DIC-CH4}$ versus $\alpha H_{H2O-CH4}$ plot further suggesting a primary microbial source to the methane measured at The Cedars.

The limited total inorganic carbon in spring fluids (0.07 to 10.85 mg/L) present a challenge to autotrophic microbial populations despite the chemical disequilibria and thermodynamically favourable conditions created by the serpentinization process. In addition to low inorganic carbon concentrations, inorganic carbon in high pH conditions, as seen in spring fluids, is predominantly carbonate (CO_3^{2-}), which requires unknown biological transport mechanisms for microbial utilization, therefore, it is unlikely that an autotrophic methanogenic pathway is responsible for the observed microbial methane at The Cedars. Acetotrophic methanogenesis, as suggested by the CD diagram and calculated fractionation factors above, is a heterotrophic pathway that may have produced the microbial methane measured. Elevated formate and acetate concentrations were observed in the marine serpentinizing system at the Lost City hydrothermal field (Lang et al., 2010) and were measured in spring fluids at the Tablelands. It is likely that such organic acids also exist in The Cedars system and were acting as the carbon substrate for methanogenesis.

Based on DNA sequencing published in Suzuki et al. (2013) one identical archaeal sequence (*Euryarchaeota*) was detected over the span of 3 years and is closely related to the order *Methanosarcinales*. This methanogen was measured in fluids collected from the BS5, NS1 and GPS1 springs, where we observe the depleted $\delta^{13}C_{CH4}$ values indicative of microbial methane. Multiple lines of evidence suggest that methane measured in fluids discharging from springs at The Cedars was primarily microbial. Secondary processes such as anaerobic oxidation of methane may also be occurring within the subsurface and mixing with methane formed from the decomposition of

Franciscan Subduction Complex sediments or through abiogenic reactions within the subsurface is likely occurring at mixing springs.

4.6.2 The Tablelands

Dissolved methane concentrations were higher in spring fluids ranging from 20.0 to 36.8 μM compared to fluids measured from Winter House Brook where methane was below the detection limit. This suggests that methane was being produced within the subsurface and brought to the pool with deep groundwater discharging at springs. The methane detected at the Tablelands in 2012 was not well described by the mixing model (r^2=0.76). The more concentrated methane measured in WHC2B (CH_4=36.8 μM, f_{UB}=0.85) and WHC2B-R (CH_4=36.3 μM, f_{UB}=0.82) fluids compared to WHC2A-R (CH_4=25.8 μM, f_{UB}=0.86) fluids and their associated calculated f_{UB} suggests that methane was either being consumed in fluids from WHC2A-R or produced in fluids from springs WHC2B and WHC2B-R. The $\delta^{13}C$ of total inorganic carbon from WHC2A-R (-23.5 ‰) is more depleted compared to WHC2B-R (-18.6 ‰) suggesting possible methane oxidation as a consumption mechanism at WHC2A-R, however only a small amount of methane oxidation is required to change the $\delta^{13}C$ of total inorganic carbon by 5 ‰. Therefore even if methane oxidation was occurring only a small amount of methane would have been consumed at WHC2A-R through this mechanism. Additionally, neither aerobic or anaerobic methanotrophic bacteria have been identified at the Tablelands (Brazelton et al., 2012; Brazelton et al., 2013) and the $\delta^{13}C$ of total inorganic carbon from WHC2A-R is not as depleted as expected with methane oxidation (<-30 ‰), thus it is

unlikely to be occurring. More likely methane was being produced along the ground

water flow path or at the discharge point of springs WHC2B and WHC2B-R.

A previous microbiological study conducted by Brazelton et al. (2012) found that

the presence of methanogens in WHC2B fluids were extremely rare comprising only

0.2% of the full metagenomic dataset. However, genomic results from the recharge fluids

obtained through the recharge experiment designed and executed through this study

showed an increase in the presence of methanogen genes compared to fluids collected

before the recharge experiment suggesting that methanogens were present in spring fluids

(Brazelton, pers com) and that some methane could potentially be microbial. The

speciation of limited inorganic carbon (CO_3^{2-}) in spring fluids suggests that the microbes

would be heterotrophic and rely on organic carbon such as acetate and/or formate, which

were both measured in spring fluids, for a carbon source (Table 3.20). Acetate ($r^2=0.96$) is

well described by the mixing model but formate ($r^2=0.31$) is not well described

suggesting additional chemical or microbial processes were affecting the formate

concentrations. Formate concentrations were lower in fluids from springs WHC2B (0.121

± 0.023 mg/L) and WHC2B-R (0.593 ± 0.260 mg/L) compared to fluids from WHC2A-R

(1.303 ± 0.052 mg/L). It is possible that fermentation a methanogenic process was

occurring in spring fluids from WHC2B and WHC2B-R and causing the observed

consumption of formate and production of methane. Although acetate is the dominant

substrate used for fermentation in natural environments, about half of the known

methanogen species can reduce formate to create methane (Wiese and Kvenvolden 1993).

Furthermore, feeding upon formate gives more energy per mol (-127 KJ/mol) compared

to acetate (-28 KJ/mol) which would make formate a more energetically favourable substrate to consume compared to acetate (Wiese and Kvenvolden 1993).

On the modified Bernard plot (Figure 4.7) methane measured in spring fluids collected before (WHC2A and WHC2B) and after (WHC2A-R, WHC2B-R) the recharge experiment plotted within the traditional thermogenic field in a cluster. This suggests that the methane was primarily non microbial and either thermogenic and/or abiogenic in origin. Similarly, the range of $\delta^{13}C_{CH4}$ for all spring fluids overlaps the thermogenic field but not the microbial fields on a CD diagram (Figure 4.8) although without δ^2H_{CH4} the Tablelands data can not be plotted. The range of $\delta^{13}C_{CH4}$ also overlaps putative abiogenic gases measured from deep bore holes in crystalline igneous rocks in Sudbury-Canada and Juuka-Finland (Sherwood Lollar et al., 1993), and is very close to putative abiogenic gases in terrestrial settings including serpentinized ultra-mafic rocks in Happo-Japan (Suda 2013) and Othrys-Greece (Etiope et al., 2013), all of which have a more ^{13}C-^2H depleted signature indicative of a crustal carbon source. The carbon isotope fractionation factors ($\alpha C_{DIC-CH4}$) calculated for dissolved methane measured at springs WHC2A, WHC2A-R, WHC2B, and WHC2B-R ranged from 1.00 to 1.01 in 2011 and 2012 which could potentially plot within the aceticlastic pathway field originally outlined by Valentine et al. (2004), but was also within range of putative abiogenic methane from the Precambrian shield on a $\alpha C_{DIC-CH4}$ versus $\alpha H_{H2O-CH4}$ plot (Sherwood Lollar et al., 2008). The $\delta^{13}C$ signature of methane ranges from -25.9 ‰ to -27.7 ‰ in spring fluids which strongly suggests a non microbial source.

The geochemical evidence suggests that methane measured in spring fluids from the Tablelands is primarily non-microbial with a possible minor microbial contribution. An isotopic mass balance equation of methane:

$$\delta^{13}C_{CH4mix} \times [CH_4]_{mix} = \delta^{13}C_{CH4nm} \times [CH_4]_{nm} + \delta^{13}C_{CH4m} \times [CH_4]_m \qquad [4.4]$$

where nm refers to the non microbial contribution and m refers to the microbial contribution can be used to predict the $\delta^{13}C$ of mixed methane. Based on the microbial reaction:

$$4CHOO^- + 4H^+ \rightarrow CH_4 + 3CO_2 + 2H_2O \qquad [4.5]$$
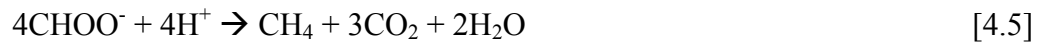
and the difference in predicted formate concentrations based on physical mixing alone using the mixing model and actual formate concentrations measured, the concentration of methane produced through this reaction can be calculated and used in the isotopic mass balance equation as the concentration of microbial methane ($[CH_4]_m$). Using this concentration and the range of $\delta^{13}C_{CH4}$ values associated with fermentation we can predict the range of $\delta^{13}C_{CH4}$ values expected for a mixture of microbial and non microbial methane. Observed $\delta^{13}C_{CH4}$ values in spring fluids were in the predicted range for a mixture of microbial (fermentation mechanism) and non microbial methane using the isotopic mass balance equation suggesting that the amount of methane produced through fermentation may not be enough to change the $\delta^{13}C$ signature of the methane measured. Additional data such as the $\delta^{13}C$ of formate would further constrain the expected carbon isotopic value of methane and aid in the understanding of the different mechanisms that were occurring within spring fluids. The overwhelming geochemical data suggests that methane measured in spring fluids was predominantly non microbial, however, a possible minor microbial contribution of methane could not be ruled out.

4.6.3 Summary and Comparison

At The Cedars, methane measured in spring fluids from NS was primarily microbial; while methane measured in fluids from mixing sites (BS5, BS9 and GPS1) were most likely a mixture of microbial and non microbial methane. At sites of serpentinization organic carbon is typically more biologically available than inorganic carbon unlike most environments. These organic compounds can support heterotrophic fermentative archaea and bacteria (Schrenk et al., 2013) despite the harsh conditions created by the serpentinization process. The proposed microbial methane measured at The Cedars is thought to be produced through fermentative metabolic pathways. Similarly at the Tablelands, there is evidence of possible fermentation of formate to produce methane; however, additional geochemical and genomic evidence is required to validate this theory. Unlike The Cedars, the Tablelands methane is dominantly thermogenic or abiogenic or possibly a mixture of the two in origin.

4.7 Habitability of springs

There are numerous challenges for life to exist in the harsh environment of terrestrial serpentinizing systems including high pH, limitations of carbon fixation, and a lack of electron acceptors and macro-nutrients. Survival in serpentinizing systems is dependent on the balance of energy gained through metabolic processes and energy expelled for biosynthesis and activity in addition to the energetic costs of maintenance and coping strategies needed for this extreme environment (Hoehler 2007). Geochemical data collected in this study aids in the overall understanding of the survival of microorganisms that have been detected in this extreme environment at both The Cedars

(Morrill et al., 2013; Suzuki et al., 2013; Suzuki et al., 2014) and the Tablelands

(Brazelton et al., 2013; Brazelton et al., 2012).

4.7.1 The Cedars

Suspended cell densities in spring fluids (10^2-10^4 cells/ml) and incubated glass

slides (10^6-10^7 cells/cm^2) suggest that microbial life does exist within the subsurface in

these extreme conditions at The Cedars (Morrill et al., 2013). A culture independent

geomicrobiological study of spring fluids (BS5, NS1, and GPS1) found that the microbial

communities present in mixing springs (NS1 and BS5) were similar to those measured at

other terrestrial serpentinization sites and were dominated by phylotypes in classes

Betaproteobacteria and *Clostridia* (Suzuki et al., 2013). The microbial communities

present in spring fluids from GPS1 on the other hand were unique compared to other

studies and were dominated by phyla *Chloroflexi* and *Firmicutes*, along with a few

undefined phyla in the SILVA database (Suzuki et al., 2013). One identical archaeal

sequence was identified in all springs and places close to the order *Methanosarcinales*,

suggesting possible methanogenesis (Suzuki et al., 2013).

Fluids discharging from springs were ultra-basic (≥ 11.4) which would have

required a robust pH homeostasis mechanism or the use of alternative gradients for the

synthesis of adenosine triphosphate (ATP) in microbes. Ions Na^+ and K^+ can be pumped

across the membrane instead of protons to generate adenosine triphosphate and are the

most common ionic gradients used by alkaliphiles. In spring fluids, Na^+ and K^+ were low

in concentration ranging from 44 to 799 mg/L and from 0.46 to 4.83 mg/L, respectively.

Generating adenosine triphosphate from these low concentrations would have been

difficult for microbes suggesting that alternative ions were being exploited, however this hypothesis is unexplored and it is not known whether other ions can be used by their membrane transport mechanisms (Schrenk et al., 2013).

Typical of serpentinization environments the total inorganic carbon content (0.07 to 0.88 mg/L) is low compared to the dissolved organic carbon content (1.53 to 3.32 mg/L) in spring fluids thus making organic carbon more biologically available for carbon fixation. The $\delta^{13}C_{TIC}$ of spring fluids ranged from -63.5 to -32.5 ‰, which suggests bacterial organic oxidation and the presence of heterotrophic microbes. The total inorganic carbon isotopic compositions support the identification of heterotrophic phylotypes in spring fluids at The Cedars (Suzuki et al., 2013). Alkaliphilic heterotrophs have also been observed in high pH waters from springs in Oman and Portugal (Bath et al., 1987; Tiago et al., 2005). In contrast to other springs, BS9 fluids had a larger total inorganic carbon concentration of 10.85 mg/L and a more enriched $\delta^{13}C_{TIC}$ value of -23.0 ‰ most likely due to the lower pH (10.0) and interactions with the atmosphere. The highly depleted $\delta^{13}C_{TIC}$ value at NS1 (-63.5 ‰) where methane was the most abundant was likely due to methane oxidation by methanotrophic bacteria, although methanotrophic microorganisms have not yet been indentified in spring fluids. Even though methanotrophs have not been identified, $\delta^{13}C_{TIC}$ values <-30 ‰ observed in all spring fluids suggests a methane oxidation contribution.

All macro-nutrients (P, N, and S) required for growth in the forms phosphate, nitrate, ammonium and sulphate in spring fluids were low in concentration. There were also no obvious or abundant electron acceptors making spring fluids nutrient and electron acceptor limiting. Ammonium was well described by the mixing model in 2011 and 2012,

but nitrate concentrations were not well described suggesting consumption of nitrate at mixing springs (BSC and NS1). While N_2 gas was not measured in this study it has been measured in great quantities ($\geq$36.6 % by vol) bubbling from springs at The Cedars (Morrill et al., 2013), which may suggest that nitrate is being reduced as the electron acceptor to form N_2 gas (denitrification). However, it is unclear whether nitrogen was being reduced as an electron acceptor or biologically assimilated with the data obtained in this study.

Sulphate concentrations were also over-predicted by the mixing model suggesting consumption in mixing spring fluids. Similar to nitrate, it is unclear whether sulphate was being reduced as an electron acceptor to form H_2S or biologically assimilated for growth purposes. Dehalogenated microorganisms were detected in spring fluids indicating that electron acceptors which produce more energy per mol including oxygen, Mn and Fe oxides, nitrate, and sulphate must be limiting or used up so it is no surprise that sulphate and nitrate would be used as electron acceptors and be consumed in this highly reducing environment. As expected the species richness was greater in mixing spring fluids (BS5 and NS1) compared to GPS1 fluids (Suzuki et al., 2013). Shallow groundwater brings a whole new suite of electron acceptors and macro-nutrients that can be utilized by microorganisms to deep groundwater at mixing sites which increases the chance for survival.

4.7.2 The Tablelands

Suspended cell densities in spring fluids (10^4-10^6 cells/ml) as well as cell densities associated with carbonate sediments (10^8-10^9 cells/g) suggests that microbial life does

exist in the extreme conditions of the subsurface at the Tablelands (Szponar 2012). Phospholipid fatty acid (PLFA) analysis and carbon isotopic data suggest that both autotrophic and heterotrophic metabolisms were present in spring fluids from the Tablelands (Szponar 2012). A metagenomic study of the microbial ecology of spring fluids found *Betaproteobacteria* within the order *Burkholderials* associated with near-surface mixing zones and *Firmicutes* or *Clostridiales*-like organisms associated with deeper anoxic subsurface habitats (Brazelton et al., 2013). Genes associated with methanogens were rare in the full metagenomic dataset but sequences related to methanogenesis were present in spring fluids from the Tablelands (Brazelton et al., 2012).

Fluids discharging from springs were ultra-basic ($\geq$12.2) making it very difficult to maintain a pH gradient and pump protons across the membrane in order to generate adenosine triphosphate. Alternatively, alkaliphiles use ionic gradients involving Na^+ and K^+, however in spring fluids the concentrations of Na^+ (129 to 933 mg/L) and K^+ (3.6 to 12.8 mg/L) were low. Like the Cedars, this suggests that other ions were being pumped across the membrane however it is not known whether membrane transport mechanisms could function using alternative ions (Schrenk et al., 2013).

Typical of serpentinization environments the total inorganic carbon content (0.07 to 0.88 mg/L) is lower compared to the dissolved organic carbon content (1.53 to 3.32 mg/L) in spring fluids suggesting heterotrophic metabolic pathways will dominate the ground water associated with serpentinization. The $\delta^{13}C_{TIC}$ of spring fluids ranged from -23.5 to -13.9 ‰ suggesting bacterial organic oxidation and the presence of heterotrophic microbes. Organic acids acetate and formate were present in spring fluids and may support fermentative archaea and bacteria in spring fluids and act as the organic substrate

that was reduced during organic oxidation. Despite the abundance of dissolved methane in spring fluids methane oxidation was likely not primarily contributing to the total inorganic carbon pool as evidenced by the more enriched $\delta^{13}C_{TIC}$ values (>-30 ‰) observed in fluids. This is consistent with metagenomic studies which found no methanotrophic bacteria in spring fluids (Schrenk et al., 2013).

All macro-nutrients (P, N, and S) required for growth in the forms phosphate, nitrate, ammonium and sulphate in spring fluids were low in concentration and there were also no obvious or abundant electron acceptors making spring fluids limited in both nutrients and electron acceptors (Table A.7 for 2011 and Table A.8 for 2012). In 2011 nitrate was not well described by the mixing model (r^2=0.34). Nitrate measured in the highly mixed WHC2C fluids were under-predicted by the model suggesting possible nitrogen fixation where nitrate was being biologically produced. Nitrate measured in WHC2B fluids which were primarily deep groundwater on the other hand were over predicted by the model which suggests nitrogen was being reduced as an electron acceptor or reduced during biological assimilation. In 2012 however, the N-sources ammonium and nitrate were both fairly well described by the mixing model suggesting that they were not being biologically assimilated at any great rate or used as the primary electron acceptors.

In 2011, sulphate concentrations were under predicted by the mixing model at WHC2C and over predicted at WHC2B. This suggests that at sites of more mixing (lower f_{UB}) sulphate was being produced and at sites dominated by deeper groundwater associated with serpentinization (higher f_{UB}) sulphate was being consumed. The deeper groundwater is highly reducing (≤-618 mV) so it is not surprising to have sulphate

reduced as an electron acceptor in these anoxic conditions. In 2012 however, sulphate concentrations were fairly well described by the mixing model suggesting that sulphate was not being used at a great rate and was most likely not the primary electron acceptor being utilized.

4.7.3 Summary and Conclusion

At both The Cedars and the Tablelands spring fluids were ultra-basic with low Na^+ and K^+ concentrations suggesting possible unknown membrane transport mechanisms of alternative ions. The organic carbon content in spring fluids was greater compared to the inorganic carbon content at both locations suggesting a dominantly heterotrophic metabolic community. The $\delta^{13}C_{TIC}$ values at The Cedars suggest that organic oxidation was occurring in spring fluids and more specifically there was evidence of methane oxidation. The $\delta^{13}C_{TIC}$ values at the Tablelands also suggest organic oxidation and possible methane oxidation although the amount was minimal if any. Concentrations of macro-nutrients which are essential for biomass production and growth were low at both The Cedars and the Tablelands. Available electron acceptors were also low in spring fluids at The Cedars however; there was evidence of nitrate and sulphate reduction. Similarly, at the Tablelands there was evidence of nitrate and sulphate reduction however the data was not consistent. Microbial communities observed in the mixing spring at The Cedars (BS5 and NS1) were similar to those measured at the Tablelands and other sites of terrestrial serpentinization including the Cabeço de Vide aquifer in Portugal (Tiago and Verissimo 2013) and borehole water from Outokumpu in Finland (Itävaara et al., 2011). This microbial community consists of three related *Betaproteobacteria* strains whose

physiological and genomic features are described in Suzuki et al. (2014). A new genus called 'Serpentinomonas' has been proposed to encompass these alkaliphiles associated with terrestrial serpentinization environments (Suzuki et al., 2014). The microbial community observed in GPS1 fluids however, were not similar to the Tablelands and were unique from other terrestrial serpentinizing communities. DNA sequencing at The Cedars and the Tablelands have identified archaeal genes associated with methanogenesis although the gene was more predominant in Cedars springs compared to Tablelands springs.

4.8 Tables and Figures

Table 4.1 Calculated f_{UB} using Equation 2.2 for The Cedars and the Tablelands from 2011 to 2013.

	f_{UB}		
Cedars	2011	2012	2013
AC	0.00	0.00	0.00
BS9	0.16	-	-
BS7	0.12	-	-
BS5	0.13	0.16	0.17
NS1	0.07	0.08	0.08
GPS1	1.00	1.00	1.00

	f_{UB}		
Tablelands	2011	2012	2013
WHB	0.00	0.00	-
WHC2C	0.15	0.04	-
WHC2A	1.00	0.27	-
WHC2A-R	-	0.86	-
WHC2B	0.53	0.85	-
WHC2B-R	-	0.82	-
WHC1	-	1.00	-

\- = no Cl⁻ data exists to calculate f_{UB}

a)

y = 356.74x - 1.46
r^2 = 0.999

Legend:
- AC 2011
- BS5 2011
- BS7 2011
- BS9 2011
- NS1 2011
- GPS1 2011
- Regression Line

Cl$^-$ (mg/L) vs Br$^-$ (mg/L)

b)

y = 367.97x - 0.13
r^2 = 0.999

Legend:
- AC 2012
- BS5 2012
- NS1 2012
- GPS1 2012
- Regression Line

c)

y = 332.43x - 3.35
r^2 = 0.999

Legend:
- AC 2013
- BS5 2013
- NS1 2013
- GPS1 2013
- Regression Line
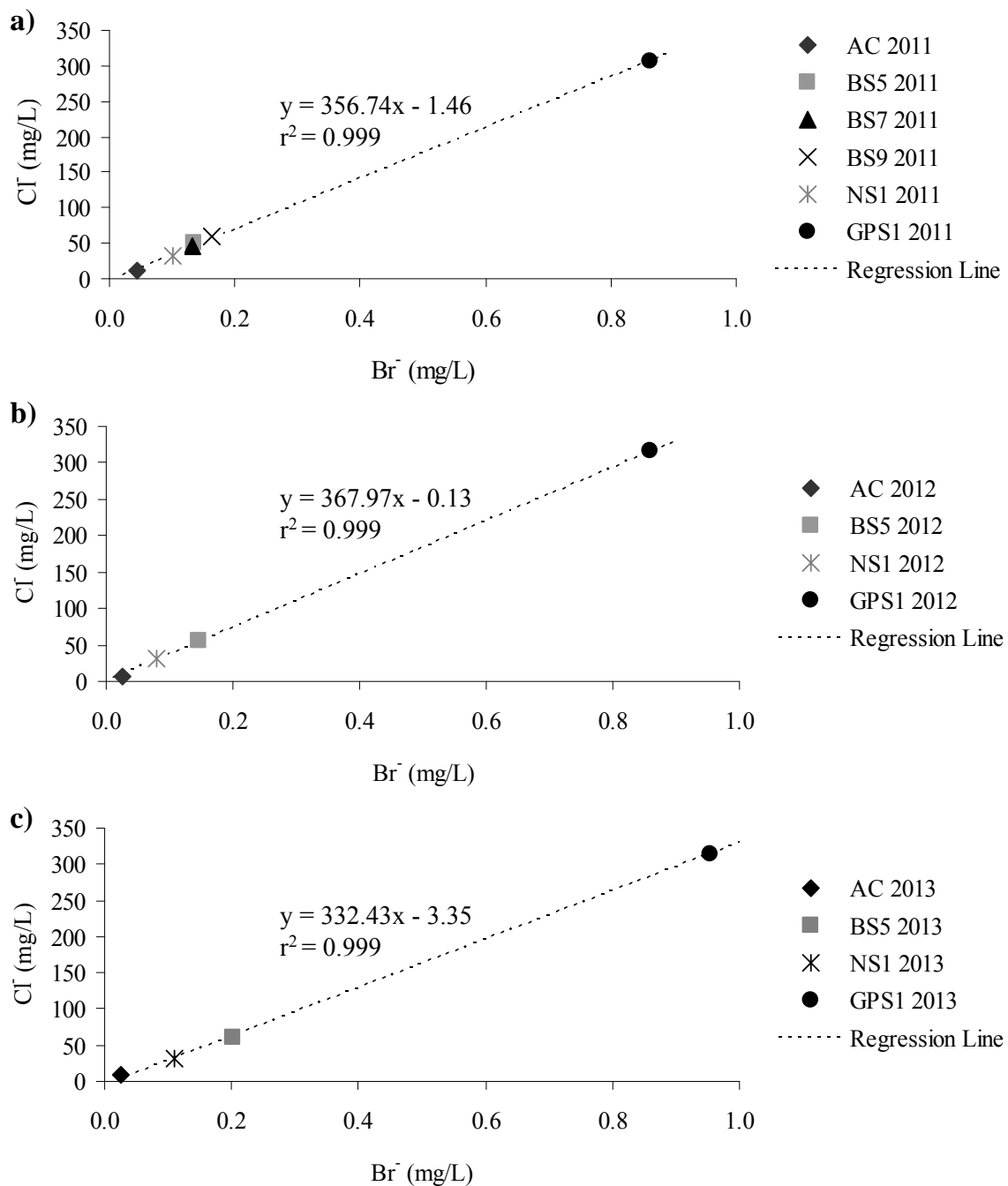
Figure 4.1. Dissolved aqueous concentrations of conservative tracers Cl$^-$ and Br$^-$ for fluids sampled from The Cedars in (a) 2011, (b) 2012, and (c) 2013. The dotted line representing the regression line of plotted data suggests conservative mixing between moderately basic water sampled from Austin Creek and ultra-basic water sampled from the GPS1 spring in all years. Error bars of ± 10 % for Cl$^-$ and Br$^-$ may appear smaller than plotted symbols.
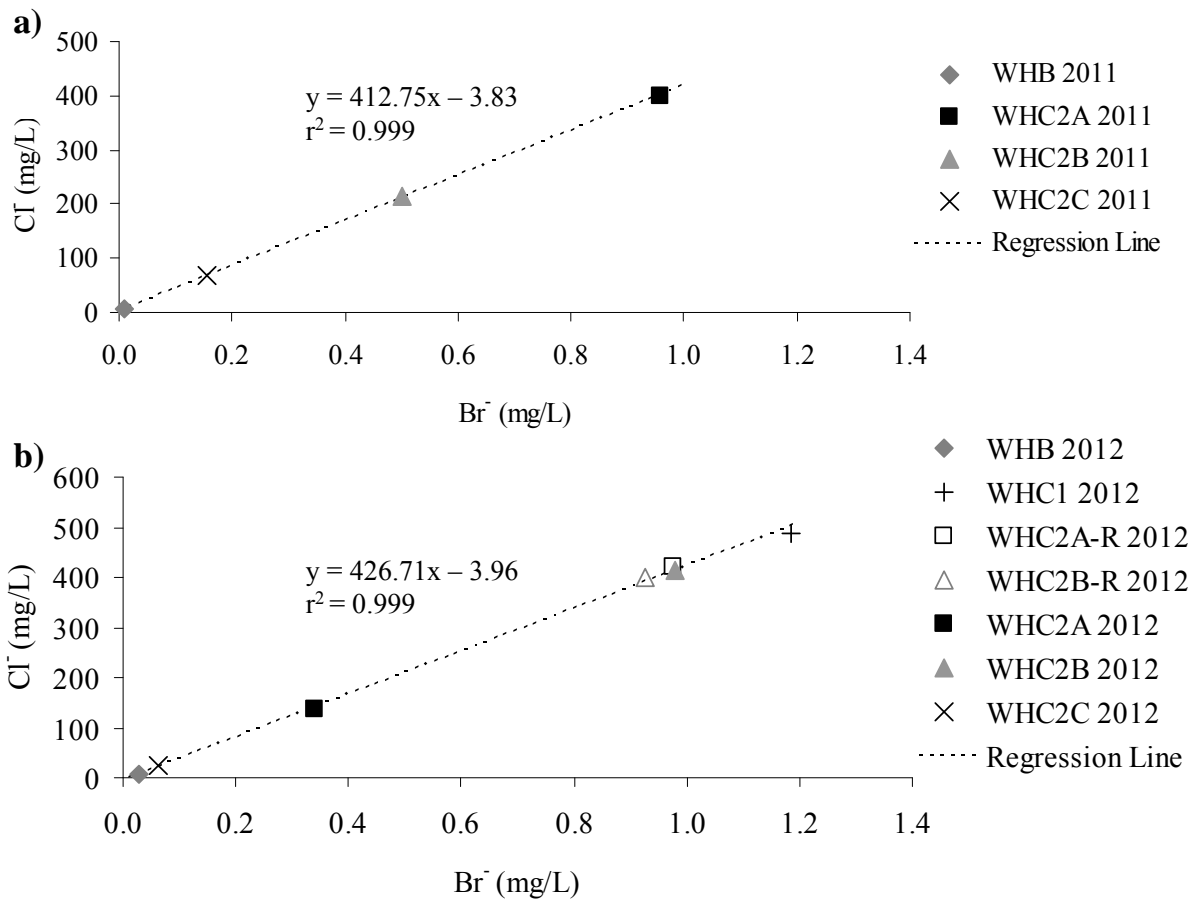
Figure 4.2. Dissolved aqueous concentrations of conservative tracers Cl⁻ and Br⁻ for fluids sampled from the Tablelands in (a) 2011 and (b) 2012. The dotted line representing the regression line of the plotted data suggests conservative mixing between non ultra-basic water sampled from Winter House Brook and ultra-basic water sampled from the WHC2A spring in 2011 and the WHC1 spring in 2012. Note that WHC2A-R had a higher concentration of both Cl⁻ and Br⁻ similar to WHC2B and WHC2B-R compared to WHC2A in 2012. Error bars of ± 10 % for Cl⁻ and Br⁻ may appear smaller than plotted symbols.
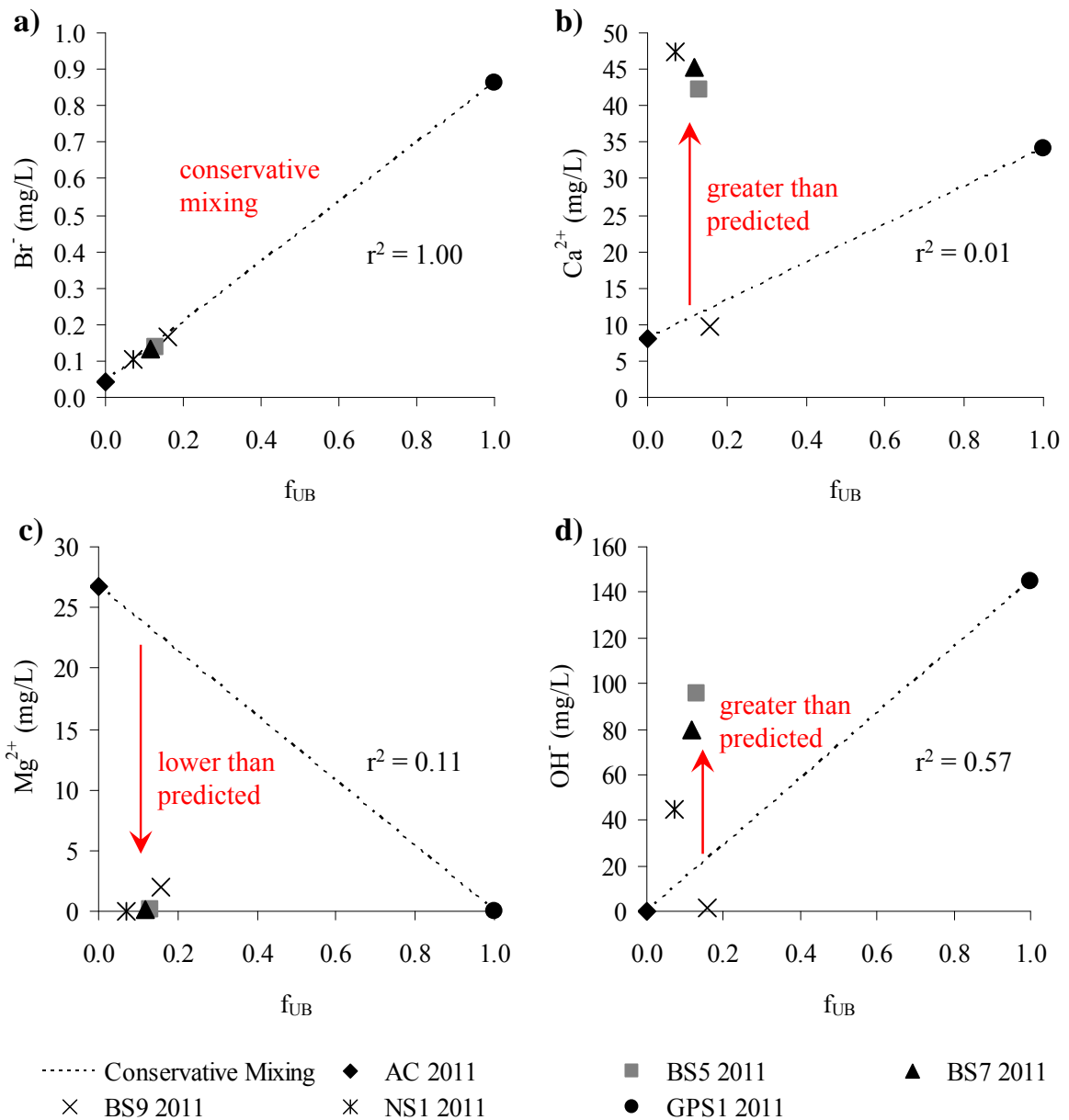
Figure 4.3. Predicted (a) Br$^-$, (b) Ca^{2+}, (c) Mg^{2+}, and (d) OH$^-$ concentrations based on physical mixing alone using the 2-component mixing model and actual measured data at The Cedars in 2011. The dashed line represents the predicted concentrations using the mixing model which is solely based upon physical mixing of water end members. Correlation coefficients (r^2) describe the accuracy of the model to the actual observed data. Note that similar deviations were seen in plots for 2012 and 2013 (data available in Tables 3.2 and 3.3). Error bars may appear smaller than plotted symbols.
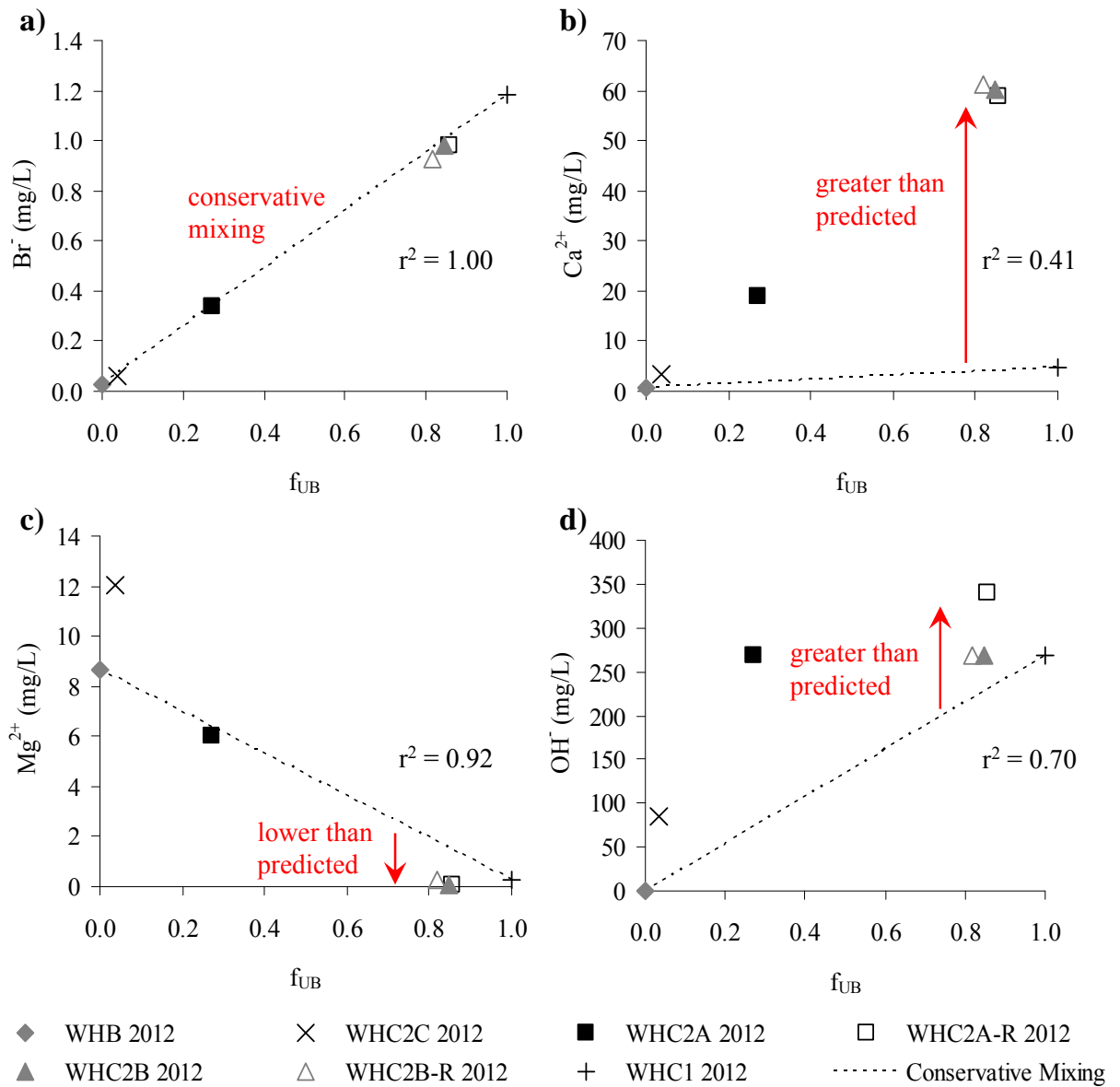
Figure 4.4. Predicted (a) Br⁻, (b) Ca²⁺, (c) Mg²⁺, and (d) OH⁻ concentrations based on physical mixing alone using the 2-component mixing model and actual measured data at the Tablelands in 2012. The dashed line represents the predicted concentrations using the mixing model which is solely based upon physical mixing of water end members. Correlation coefficients (r^2) describe the accuracy of the model to the actual observed data. Note that similar deviations were seen in plots for 2011 (data available in Table 3.21). Error bars may appear smaller than plotted symbols.
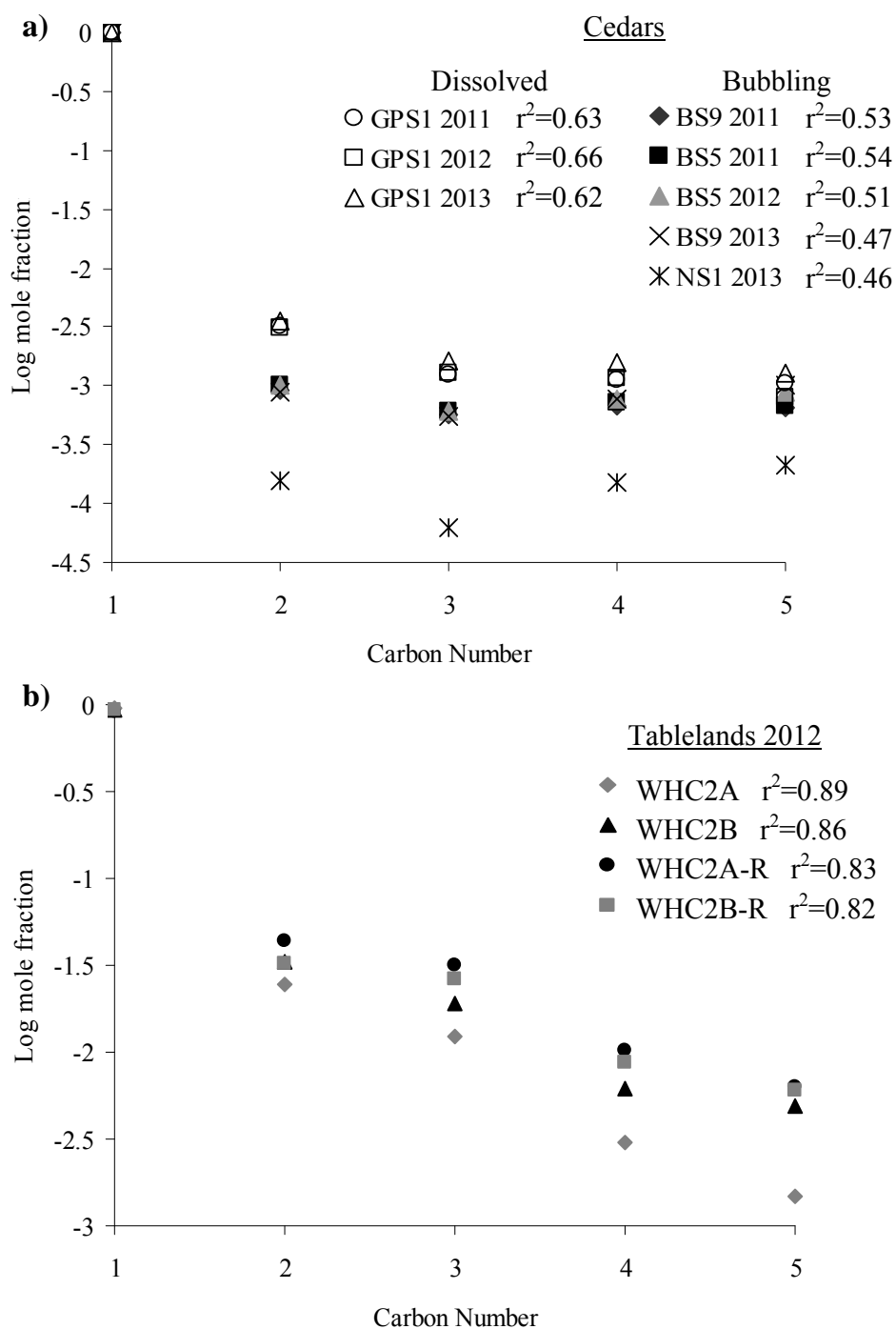
Figure 4.5. Shulz-Flory distributions with compositional alkane data from (a) The Cedars and (b) the Tablelands. Data from (a) The Cedars and (b) the Tablelands do not fit a Shulz-Flory distribution with calculated distribution coefficients r^2 <0.90, suggesting these are not exclusively abiogenic gas samples. Only nC_4 and nC_5 data were used for carbon numbers 4 and 5.
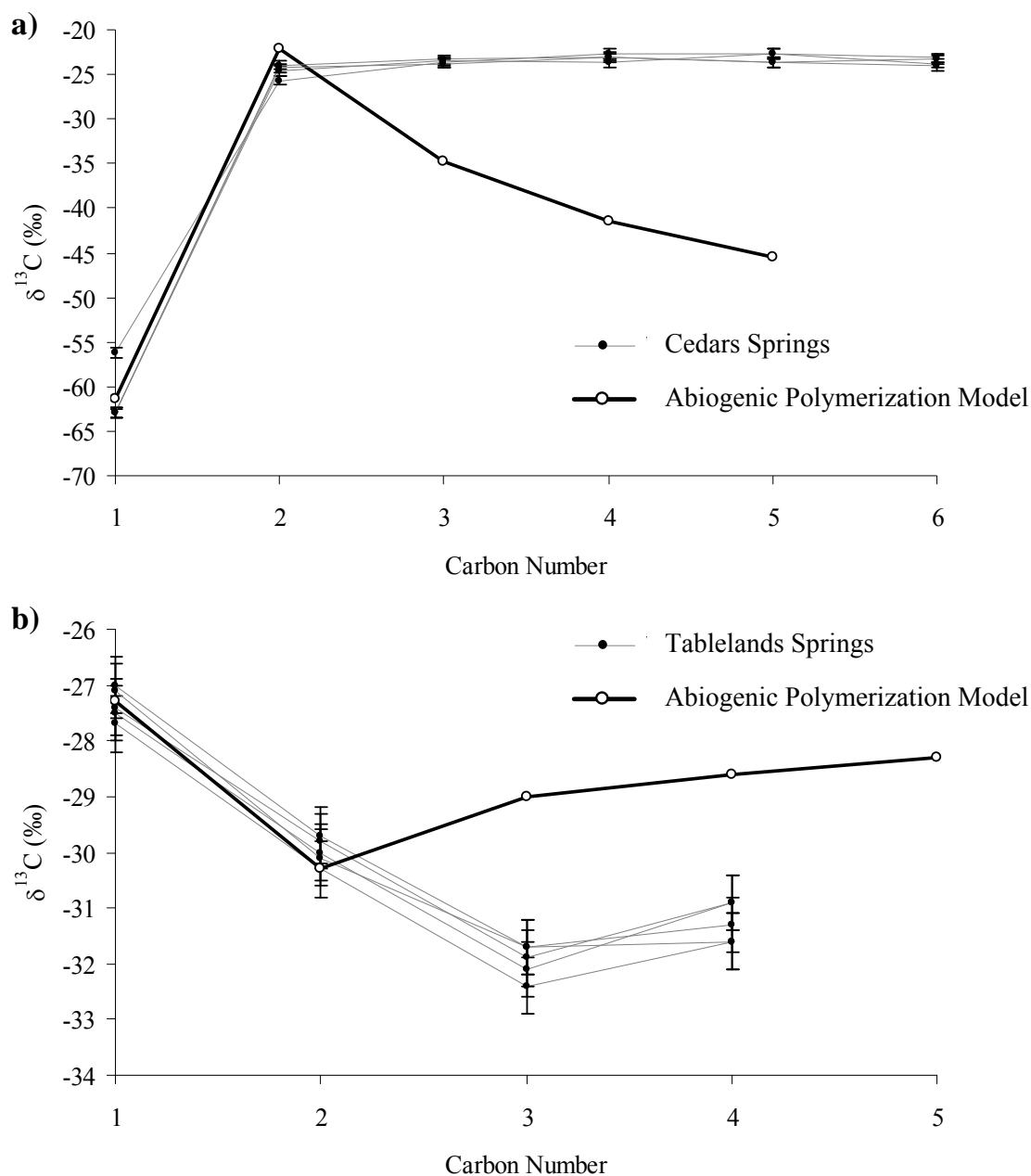
Figure 4.6. Carbon isotope values plotted versus carbon number of hydrocarbons C_1-C_6 sampled from (a) The Cedars (2011 and 2012) and (b) the Tablelands (2012). Only nC_4 and nC_5 data were used for carbon numbers 4 and 5. Thick black line represents the calculated abiogenic model using equations: $\delta^{13}C_{C2}=1000\ln\alpha+\delta^{13}C_{CH4}$ [4.6], $\delta^{13}C_{C3}=0.33\delta^{13}C_{CH4}+0.66\delta^{13}C_{C2}$ [4.7], $\delta^{13}C_{nC4}=0.25\delta^{13}C_{CH4}+0.75\delta^{13}C_{C3}$ [4.8], $\delta^{13}C_{nC5}=0.2\delta^{13}C_{CH4}+0.8\delta^{13}C_{C4}$ [4.9], where $\alpha=(1000+\delta^{13}C_{C2})/(1000+\delta^{13}C_{CH4})$ [4.10], developed by Sherwood Lollar et al. (2008). Initial $\delta^{13}C$ inputs of methane and ethane to equations 13 and 9 were the average carbon isotopic values measured at (a) The Cedars and (b) the Tablelands.
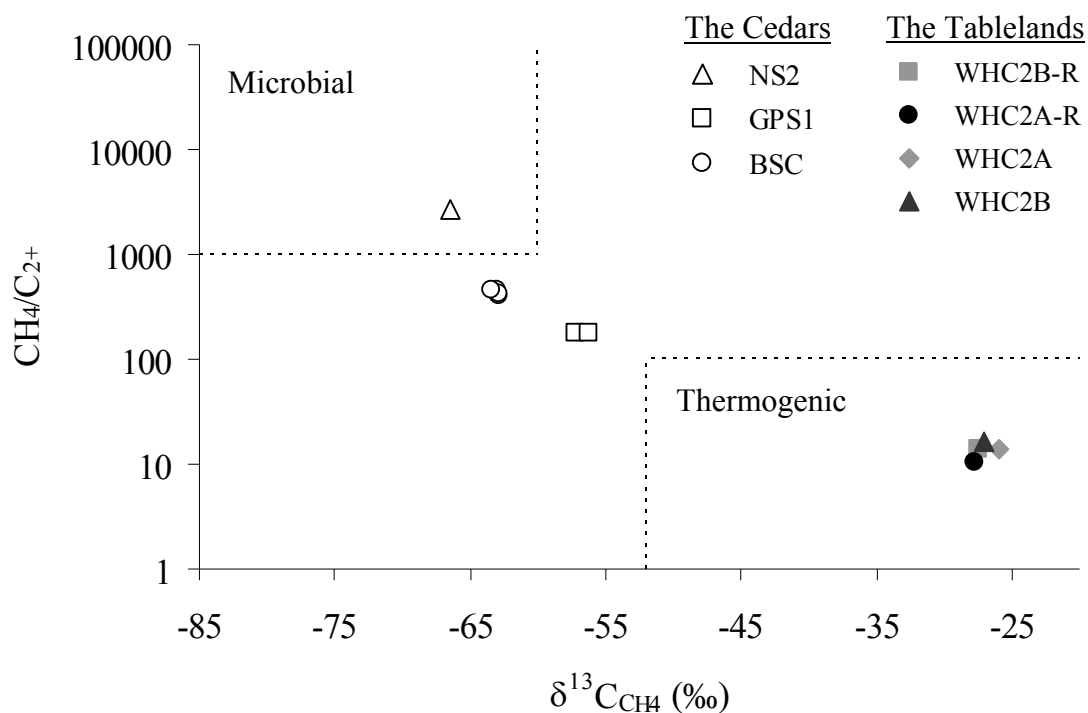
Figure 4.7. A modified Bernard plot of CH_4/C_{2+} ($C_{2+}=C_2+C_3+nC_4$) versus $\delta^{13}C_{CH4}$ measured in spring fluids from The Cedars and the Tablelands compared to conventioal microbial and thermogenic fields adapted from Hunt (1996). Cedars data plots in microbial field and trends towrads a thermogenic/abiogenic signature suggesting mixing of methane sources at BSC springs and GPS1. Bubbling gas measurements were used for NS1 and BSC (BS5 and BS9) datums and dissolved gas measurements were used for GPS1 datum. Tablelands data plots in the thermogenic field suggesting a thermogenic and/or abiogenic source. All gases measured at the Tablelands were dissolved. Error bars may appear smaller than plotted symbols.
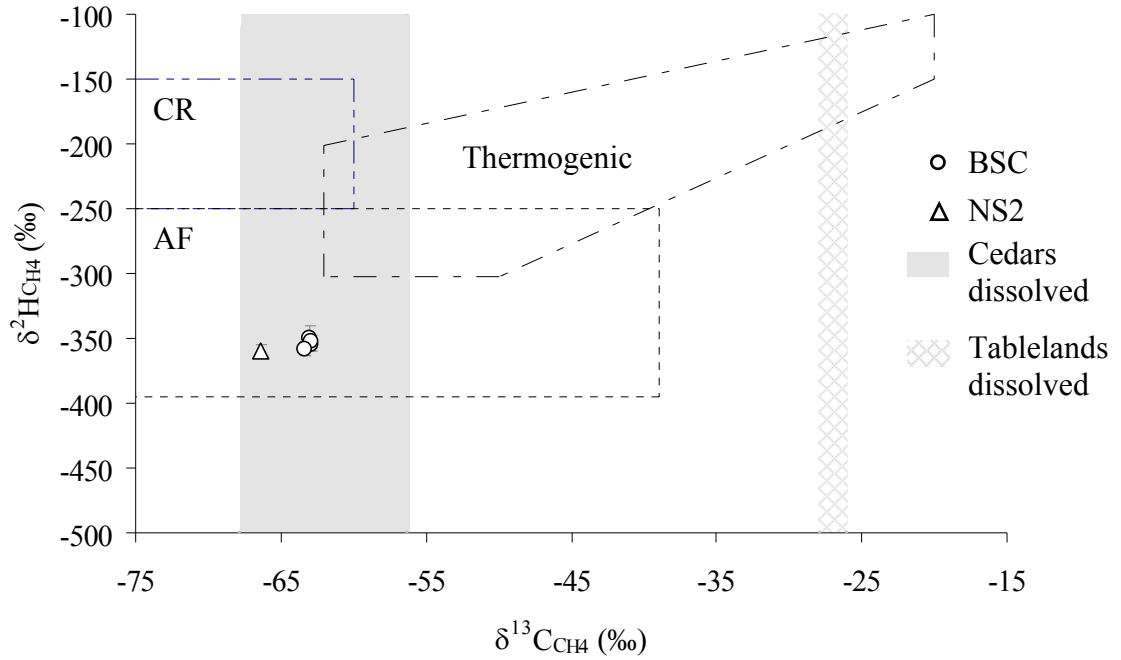
Figure 4.8. A CD diagram ($\delta^2 H_{CH4}$ versus $\delta^{13} C_{CH4}$) with conventional microbial (CR=CO_2 reduction, AF=acetate fermentation) and thermogenic fields. Data plotted for the Cedars was bubbling methane measured from NS1 and the BSC springs (BS5 and BS9). Dissolved methane concentrations were too low for $\delta^2 H_{CH4}$ analysis and therefore only the $\delta^{13} C_{CH4}$ could be measured and a field of possible solutions is plotted. Error bars may appear smaller than potted symbols all error is included in fields of possible solutions for dissolved gases.

Chapter 5: Conclusion

5.1 Summary and Future Work

Serpentinization is a highly exothermic reaction which involves the hydration of ultramafic minerals converting them into secondary minerals including magnetite, brucite and serpentine. The serpentinization process creates characteristic fluids and conditions amenable for microbial and abiogenic hydrocarbon production within the subsurface. There is also the potential for thermogenic hydrocarbons at continental ophiolites undergoing serpentinization such as The Cedars and the Tablelands where organic rich sediments are buried beneath the ultramafic portion of the ophiolite complex. Due to the multiple potential sources of hydrocarbons at sites of active continental serpentinization further investigation into the geochemistry and habitability of these geologic settings was the overall aim of this project. This investigation was achieved through 3 broad objectives which include: 1) geochemically characterizing spring fluids, 2) sourcing the hydrocarbons, and 3) determining the habitability of spring fluids and the subsurface environment through geochemical means.

The first objective of this thesis was to geochemically characterize the fresh water fluids at both The Cedars and the Tablelands. Typical of serpentinizing environments spring fluids were ultra-basic (>11), highly reducing (<-400 mV) and rich in H_2 gas with high Ca^{2+}/Mg^{2+} ratios at The Cedars and the Tablelands. Further emblematic of serpentinizing environments were Cl^-, OH^- and Ca^{2+} ions in spring fluids. Contrasting the spring fluids at both The Cedars and the Tablelands neutral to moderately basic fluids that

were oxidizing with trace to no H_2 or hydrocarbon gases were identified in the near by

Austin Creek and Winter House Brook.

Using conservative tracers Cl^- and Br^- a 2-component mixing model was applied

and groundwater end members were established at both The Cedars and the Tablelands.

The geologic context of these sites and ionic compositional data suggested that fluids

discharging from GPS1 at The Cedars and WHC1 at the Tablelands represent

groundwater that has contact with peridotite and potentially underlying marine sediments,

while fluids from Austin Creek and Winter House Brook represent overland flow and

shallow groundwater. Other springs sampled at The Cedars (BSC and NS) and the

Tablelands (WHC2C, WHC2A, WHC2B, WHC2A-R, and WHC2B-R) were a mixture of

the two end members. While these end members were geochemically distinct from one

another their isotopic composition (δ^2H and $\delta^{18}O$) revealed that they are both meteoric in

origin.

At The Cedars and the Tablelands fluids discharging at springs had variable

concentrations of methane, other low molecular weight hydrocarbons (C_2-C_6) and high

molecular weight hydrocarbons including alkanes (C_{7+}), cyclic alkanes and aromatic

compounds which were all sourced to be originating from the subsurface. The second

objective of this thesis was to determine the mechanisms for hydrocarbon synthesis at

The Cedars and the Tablelands using various compositional and isotopic analyses on the

hydrocarbons discharging at springs. At The Cedars the abundance of substituted and

unsubstituted cyclopentane and cyclohexane and aromatic compounds detected in spring

fluids suggested that sedimentary organic matter was within the oil window and

hydrocarbons were thermogenic origin. At the Tablelands, on the other hand, the low

abundance of volatile organic compounds observed in spring fluids suggested that sedimentary organic matter was over mature and past the stage of petroleum generation resulting in the dry thermogenic gas observed. Therefore, higher molecular weight hydrocarbons (C_{7+}) at both locations were likely produced through thermogenic processes although an abiogenic contribution could not be entirely ruled out.

At The Cedars alkane gases C_2-C_6 were well described by the mixing model suggesting they originated in the groundwater fluids which have been in contact with the mature sedimentary organic matter of the Franciscan Subduction Complex, which suggests a thermogenic origin. Compositional and isotopic data also suggest a thermogenic source to C_2-C_6 gases; however, a possible thermogenic and abiogenic mixture should also be considered. Similarly at the Tablelands, the C_2-C_6 gases were not dominated by an abiogenic source and most likely were a mixture of thermogenic and abiogenic in origin. At both locations it is likely that secondary fractionation processes and migratory segregation has altered the compositional and isotopic composition of these low molecular weight alkanes.

The compositional and isotopic signatures of methane detected at The Cedars suggested the primary source of methane at NS to be microbially produced through fermentative metabolic pathways. At other springs (BSC and GPS1) this microbial methane is most likely mixed with a non-microbial source. To further validate this theory the concentrations and isotopic composition of organic acids in spring fluids collected in this study should be analyzed. The Cedars is the first and only continental serpentinizing system where methane is suggested to primarily be microbial in origin. While there is the potential for microbial methane at the Tablelands the geochemical evidence strongly

suggests that the primary source of methane is likely thermogenic and possibly abiogenic or possibly a mixture of the two. Isotopic analysis of organic acids detected at the Tablelands would further support the proposed potential for methanogenesis in spring fluids. Overall the δ^2H of dissolved methane and C_2-C_6 gases both bubbling and dissolved can further aid in the sourcing of these low molecular weight hydrocarbons detected in spring fluids at both The Cedars and the Tablelands.

Lastly, the third objective of this study was to investigate the habitability of these ophiolite serpentinizing systems. Geochemical data suggested that spring fluids were limited in electron acceptors, nutrients, and inorganic carbon but were rich in H_2 gas and organic carbon. The $\delta^{13}C_{TIC}$ values suggested that organic oxidation was occurring in spring fluids at both the Cedars and the Tablelands providing evidence for a heterotrophic pathway. There was also evidence of possible nitrate and sulphate reduction in spring fluids at The Cedars and the Tablelands; however it is not clear whether these compounds were used for biomass assimilation or as an electron acceptor. The high pH and low Na^+ and K^+ concentrations suggest unknown membrane transportation of alternative ions that is not understood with our current geomicrobiological knowledge. It has been suggested that microbes aggregate onto precipitated $CaCO_3$ and create a microenvironment by changing the surrounding conditions to be more favourable (Suzuki et al., 2014). However, with limited electron acceptors and nutrients in spring fluids further investigation is required to understand how microbes are surviving in such a harsh environment and how they are potentially contributing to hydrocarbon production at sites of active continental serpentinization.

This study investigates the potential sources of hydrocarbons and the habitability of spring fluids associated with active continental serpentinization at two different ophiolite complexes that were emplaced onto the continent in different geologic time periods. Hydrocarbons C_{2+} detected in spring fluids hosted by the younger ophiolite complex (The Cedars ~ 170 MA) were most likely thermogenic in origin with potential abiogenic inputs. C_{2+} hydrocarbons detected in spring fluids hosted by the older ophiolite complex (the Tablelands ~500 MA) were likely a mixture of both thermogenic and abiogenic sources. Distinguishing between non-microbial sources would require further investigation and more distinct geochemical parameters that have yet to be constrained for field abiogenic hydrocarbons. Geochemical data at The Cedars suggested a dominant microbial source for methane unlike any other continental site of serpentinization to date, where as methane at the Tablelands was dominated by non-microbial sources. Although microorganisms have been detected in this harsh environment further investigation is required in order to fully understand the metabolic and physiological functions that these microorganisms possess in order to grow and sustain life in such a limited and extreme environment.

5.2 References

Abrajano T. A., Sturchio N. C., Bohlke J. K., Lyon G. L., Poreda R. J., and Stevens C. M., (1988) Methane-hydrogen gas seeps, Zambales Ophiolite, Philippines: deep or shallow origin? *Chemical Geology* **71**, 211-222.

Abrajano T. A., Sturchio N., Kennedy B. M., Lyon G. L., Muehlenbachs K., and Bohlke J. K., (1990) Geochemistry of reduced gas related to serpentinization of the Zambales ophiolite, Philippines. *Applied Geochemistry* **5**, 625-630.

Barnes I., LaMarche V. C., and Himmelberg G., (1967) Geochemical evidence of present-day serpentinization. *Science* **156**, 830-832.

Barnes, I. and O'Neil, J. R., (1969) The relationship between fluids in some fresh alpine-type ultramafics and possible modern serpentinization, Western United States. *Geological Society of American Bulletin* **80**.

Barnes I., O'Neil J. R., and Trescases J. J., (1978) Present day serpentinization in New-Caledonia, Oman and Yugoslavia. *Geochimica et Cosmochimica Acta* **42**.

Bath A. H., Christofi N., Philp J. C., Cave M. R., McKinley I. G., and Berner U., (1987) Trace element and microbiological studies of alkaline groundwaters in Oman, Arabian Gulf: A natural analog for cement pore-waters. FLPU Report 87-2. *British Geological Survey*.

Billings D. K. and Williams H. H., (1967) Distribution of chlorine in terrestrial rocks (a discussion). *Geochimica et Cosmochimica Acta* **31**, 2247.

Boston P. M., Ivanov M. V., and McKay C. P., (1992) On the possibility of chemosynthetic ecosystems in subsurface habitats on Mars. *Icarus* **95**, 300-308.

Brazelton W. J., Morrill P. L., Szponar N., and Schrenk M. O., (2013) Bacterial communities associated with subsurface geochemical processes in continental serpentinite springs. *Applied and Environmental Microbiology* **79**, 3906-3916.

Brazelton W. J., Nelson B., and Schrenk M. O., (2012) Metagenomic evidence for H2 oxidation and H2 production by serpentinite-hosted microbial communities. *Frontiers in Microbiology* **2**, 1-16.

Cipolli F., Gambardella B., Marini L., Ottonello G., and Zuccolini M. V., (2004) Geochemistry of high-pH waters from serpentinites of the Gruppo di Voltri (Genova, Italy) and reaction path modeling of CO2 sequestration in serpentinite aquifers. *Appl Geochem* **19**, 787-802.

Clark I. and Fritz P., (1997) *Environmental Isotopes in Hydrogeology*. Lewis Pubishers, New York.

Clayton C., (1991) Carbon isotope fractionation during natural gas generation from kerogen. *Marine and Petroleum Geology* **8**, 232-240.

Coleman R. G., (2000) Prospecting for ophiolites along the California continental margin. In: Dilek Y., Moores E. M., Elthon D., and Nicolas A. Eds.), *Ophiolites and Oceanic Crust: New Insights from Field Studies and the Ocean Drilling Program:*. Geological Society of America, Boulder, Colorado.

Coleman R. G., (2004) Geologic nature of the Jasper Ridge Biological Preserve, San Francisco Peninsula, California. *Int. Geol. Rev.* **46**, 629-637.

Coplen T. B., (2011) Guidelines and recommended terms for expression of stable-isotope-ratio and gas-ratio measurement results. *Rapid Communications in Mass Spectrometry* **25**, 2538-2560.

Coplen T.B., and Kendall C., (2000) Stable Hydrogen and Oxygen Isotope Ratios for Selected Sites of the U.S. Geological Survey's NASQAN and Benchmark Surface-water Networks. USGS, Reston, Virginia.

Craig H., (1961) Isotopic variations in meteoric waters. *Science* **133**, 1702-1703.

Delacour A., Fruh-Green G. L., Bernasconi S. M., Schaeffer P., and Kelley D. S., (2008) Carbon geochemistry of serpentinites in the Lost City Hydrothermal System (30N, MAR). *Geochimica et Cosmochimica Acta* **73**, 3681-3702.

DesMarais D. J., Donchin J. H., Nehring N. L., and Truesdell A. H., (1981) Molecular carbon isotopic evidence for the origin of geothermal hydrocarbons. *Nature* **292**, 826-828.

Dick J. B., Lin J., and Schouten H., (2003) An ultraslow-spreading class of ocean ridge. *Nature* **426**, 405-412.

Dilek Y. and Furnes H., (2011) Ophiolitic genesis and global tectonics: Geochemical and tectonic fingerprinting of ancient oceanic lithosphere. *Geol Soc Am Bull* **123**, 387-411.

Edmonds H. N., Michael P. J., Baker E. T., Connelly D. P., Snow J. E., Langmuir C. H., Dick J. B., Muhe R., German C. R., and Graham D. W., (2003) Discovery of abundant hydrothermal venting on the ultraslow-spreading Gakkel ridge in the Arctic Ocean. *Nature* **421**, 252-256.

Ehlmann B. L., Mustard J. F., and Murchie S. L., (2010) Geologic setting of serpentine deposits on Mars. *Geophysical Research Letters* **37:L06201**.

Etiope G. and Sherwood Lollar B., (2013) Abiotic Methane on Earth. *Reviews of Geophysics* **51**, 276-299.

Etiope G., Tsikouras B., Kordella S., Ifandi E., Christodoulou D., and Papatheodor.ou G., (2013) Methane flux and origin in the Othrys ophiolite hyperalkaline springs, Greece. *Chemical Geology* **347**, 161-174.

Flanagan F. J., (1969) US Geological Survey standards .2. first compilation for data for new USGS rocks *Geochimica et Cosmochimica Acta* **33**, 81-120.

Formisano V., Atreya S., Encrenaz T., Ignatiev N., and Giuranna M., (2004) Detection of methane in the atmosphere of Mars. *Science* **306**, 1758 - 1761.

Foustoukos D. I. and Seyfried W. E. J., (2004) Hydrocarbons in hydrothermal vent fluids: the role of chrome-bearing catalysts. *Science* **304**, 1002-1005.

Fritz P., Clark I. D., Fontes J.-C., Whiticar M. J., and Faber E., (1992) Deuterium and ^{13}C evidence for low temperature production of hydrogen and methane in a highly alkaline groundwater environment in Oman. In: Maest K. (Ed.),*Water-rock Interaction*, Rotterdam.

Frost B. R. and Beard J. S., (2007) On silica activity and serpentinization. *Journal of Petrology* **48**, 1351-1368.

Fruh-Green G. L., Connolly J. A. D., Plas A., Kelley D. S., and Grobety B., (2004) *Serpentinization of oceanic peridotites: Implications for geochemical cycles and biological activity*. American Geophysical Union, Washington, DC.

Fryer P., Wheat C. G., and Mottl M. J., (1999) Mariana bluschist mud volcanism: Implications for conditions within the subduction zone. *Geology* **27**, 103-106.

Fu Q., Sherwood Lollar B., Horita J., Lacrampe-Couloume G., and Seyfried J., W.E., (2007) Abiotic formation of hydrocarbons under hydrothermal conditions:

Constraints from chemical and isotope data. *Geochimica et Cosmochimica Acta* **71**, 1982-1998.

Gigggenbach W. F., (1997) Relative importance of thermodynamic and kinetic processes in governing the chemical and isotopic composition of carbon gases in high-heatflow sedimentary basins. *Geochimica et Cosmochimca Acta* **61**, 3763-3785.

Hinrichs K., Hayes J. M., Spivack A. J., Hmelo L. R., Holm N. G., Johnson C. J., and Sylva S. P., (2006) Biological formation of ethane and propane in the deep marine subsurface. *Proceedings of the National Academy of Sciences* **103**, 14684-14689.

Hoehler T., (2007) An energy balance concept for habitability. *Astrobiology* **7**, 824-838.

Horita J. and Berndt M. E., (1999) Abiogenic methane formation and isotopic fractionation under hydrothermal conditions. *Science* **285**, 1055-1057.

Hosgormez H., (2007) Origin of the natural gas seep of Cirali (Chimera), Turkey: Site of the first Olympic fire. *Journal of Asian Earth Sciences* **30**, 131-141.

Hostetler P. B., Coleman R. G., Mumpton F. A., and Evans W. B., (1966) Brucite in alpine serpentinites. *The American Mineralogist* **51**, 75-98.

Hunt J. M., (1996) *Petroleum Geochemistry and Geology*. W.H. Freeman and Company, New York.

Itävaara M., Nyyssönen M., Bomberg M., Kapanen A., Nousiainen A., Ahonen L., Hultman J., Paulin L., Auvinen P., and Kukkonen I. T., (2011) Microbiological sampling and analysis of the Outokumpu Deep Drill Hole biosphere in 2007-2009*Special Paper of the Geological Survey of Finland*.

James A. T., (1983) Correlation of natural gas by use of carbon isotopic distribution between hydrocarbon components. *American Association of Petroleum Geologists Bulletin* **67**, 1176-1191.

Karson J. A., (1998) *Internal Structure of Oceasnic Lithosphere: A Perspective from Tectonic Windows*. American Geophysical Union.

Kavanagh H., (2012) Aqueous Geochemistry and Substrate Utilization by Microorganisms at Active Sites of Serpentinization: Tablelands Ophiolite, Newfoundland and Cedars Complex, California, Memorial University.

Kelley D. S., Karson J. A., Fruh-Green G. L., Yoerger D. R., Shank T. M., Butterfield D. A., Hayes J. M., Schrenk M. O., Olson E. J., Proskurowski G., Jakuba M., Bradley A., Larson B., Ludwig K., Glickson D., Buckman K., Bradley A. S., Brazelton W. J., Roe K., Elend M. J., Delacour A., Bernasconi S. M., Lilley M. D., Baross J. A., Summons R. T., and Sylva S. P., (2005) A serpentinite-hosted ecosystem: The lost city hydrothermal field. *Science* **307**, 1428-1434.

Konn C., Charlou J. L., Donval J. P., Holm N., Dehairs F., and Bouillon S., (2009) Hydrocarbons and oxidized organic compounds in hydrothermal fluids from Rainbow and Lost City ultramafic-hosted vents. *Chemical Geology* **258**, 299-314.

Krulwich T. A., (1995) Alkaliphiles: "basic" molecular problems of pH tolerance and bioenergetics. *Mol Microbiol* **15**, 403-410.

Lagabrielle Y., Bideau D., Cannat M., Karson J. A., and Mevel C., (1998) *Ultramafic-Mafic Plutonic Rock Suites Exposed Along the Mid-Atlantic Ridge (10 N-30 N). Symmetrical-Asymmentrical Distribution and Implications for Seafloor Spreading Processes*. American Geophysial Union.

Lancet H. S. and Anders E., (1970) Carbon isotope fractionation in the Fischer-Tropsch synthesis of methane. *Science* **170**, 980-982.

Lang S. Q., Butterfield D. A., Schulte M., Kelley D. S., and Lilley M. D., (2010) Elevated concentrations of formate, acetate and dissolved organic carbon found at the Lost City hydrothermal field. *Geochimica et Cosmochimica Acta* **74**, 941-952.

Longhi J., Knittle E., Holloway J. R., and Wanke H., (1992) *The bulk composition, mineralogy and internal structure of Mars*. University of Arizona Press, Tuscon.

Marques J. M., Carreira P. M., Carvalho M. R., Matias M. J., Goff F. E., Basto M. J., Graca R. C., Aires-Barros L., and Rocha L., (2008) Origins of high pH mineral waters from ultramafic rocks, Central Portugal. *Appl Geochem* **23**, 3278-3289.

McAuliffe C., (1971) GC determination of solutes by multiple phase equilibration. *Chemical Technology* **1**, 46-51.

McCollom T. M., (2003) Formation of meteorite hydrocarbons from thermal decomposition of siderite (FeCO3). *Geochimica et Cosmochimica Acta* **67**, 311-317.

McCollom T. M., (2013) Laboratory Simulations of Abiotic Hydrocarbon Formation in Earth's Deep Subsurface. *Reviews in Mineralogy & Geochemistry* **75**, 467-494.

McCollom T. M. and Seewald J. S., (2001) A reassessment of the potential for reduction of dissolved CO_2 to hydrocarbons during serpentinization of olivine. *Geochimica et Cosmochimica Acta* **65**, 3769-3778.

McCollom T. M. and Seewald J. S., (2003) Experimental constraints on the hydrothermal reactivity of organic acids and acid anions: I. Formic acid and formate. *Geochimica et Cosmochimica Acta* **67**, 3625-3644.

McCollom T. M. and Seewald J. S., (2006) Carbon isotope composition of organic

compounds produced by abiotic synthesis under hydrothermal conditions. *Earth*

and Planetary Science Letters **243**, 74-84.

McCollom T. M. and Seewald J. S., (2007) Abiotic Synthesis of Organic Compounds in

Deep-Sea Hydrothermal Environments. *Chemical Reviews* **107**, 382-401.

Mines U. S. B. o., (1979) Analyses of natural gases, 1978. United Stated Bureau of

Mines.

Morrill P. L., Kuenen J. G., Johnson O. J., Suzuki S., Rietze A., Sessions A. L., Fogel M.

L., and Nealson K. H., (2013) Geochemistry and geobiology of a present-day

serpentinization site in California: The Cedars. *Geochimica et Cosmochimica Acta*

109, 222-240.

Morrill P. L., Weinberger D. S., Foustoukos D. I., Sherwood Lollar B., Fogel M. L., and

Cody G. D., (Submitted) Carbon and Hydrogen Isotopic Fractionation During

Abiotic Hydrocarbon Formation Under Hydrothermal Conditions. *Chemical*

Geology.

Neal C. and Stanger G., (1983) Hydrogen generation from mantle source rocks in Oman.

Earth and Planetary Science Letters **66**, 315-321.

Oremland R. S., Miller L. G., and Whiticar M. J., (1987) Sources and flux of natural

gases from Mono Lake, California. *Geochimica et Cosmochimica Acta* **51**, 2915-

2929.

Oze C., Fendorf S., Bird D. K., and Coleman R. G., (2004) Chromium geochemistry in

serpentinized ultramafic rocks and serpentine soils from the Franciscan complex

of California. *American Journal of Science* **304**, 67-101.

Palandri J. L. and Reed M. H., (2004) Geochemical models of metasomatism in

  ultramafic systems: Serpentinization, rodingitization, and sea floor carbonate

  chimney precipitation. *Geochimica et Cosmochimica Acta* **68**, 1115-1133.

Pedersen K., Nilsson E., Arlinger J., Hallbeck L., and O'Neill A., (2004) Distribution,

  diversity and activity of microorganisms in the hyper-alkaline spring waters of

  Maqarin in Jordan. *Extremophiles* **8**, 151-164.

Pielou E. C., (1998) *Fresh Water*. University of Chicago Press.

Potter J. and Konnerup-Madsen J., (2003) A review of the occurrence and origin of

  abiogenic hydrocarbons in igneous rocks. In: Petford N. and McCaffrey K. J. W.

  Eds.), *Hydrocarbons in Crystalline Rocks*. Geological Society London, London.

Proskurowski G., (2010) Abiogenic Hydrocarbon Production at the Geosphere-Biosphere

  Interface via Serpentinization Reactions. In: Timmis K. N. (Ed.), *Handbook of

  Hydrocarbon and Lipid Microbiology*. Springer-Verlag Berlin Heidelberg.

Proskurowski G., Lilley M. D., Seewald J. S., Früh-Green G. L., Olson E. J., J.E. L.,

  Sylva S. P., and Kelley D. S., (2008) Abiogenic hydrocarbon production at Lost

  City Hydrothermal Field. *Science* **319**, 604-607.

Raiche R., (2009) The Cedars: Sonoma County's hidden treasure. *Fremontia Journal of

  the California Native Plant Society* **37**, 3-15.

Rudd J. W. M., Hamilton R. D., and Campbell N. E. R., (1974) Measurement of

  microbial oxidation of methane in lake water. *Limnology and Oceanography* **19**,

  519-524.

Schoell M., (1988) Multiple origins of methane in the earth. *Chemical Geology* **71**, 1-10.

Schrenk M. O., Brazelton W. J., and Lang S. Q., (2013) Serpentinization, carbon and deep life. *Rev. Mineral. Geochem.* **75**, 575-606.

Schulte M., Blake D., Hoehler T., and McMcCollom T., (2006) Serpentinization and its implications for life on the early Earth and Mars. *Astrobiology* **6**, 364-376.

Schulz H., (1999) Short history and present trends of Fischer-Tropsch synthesis. *Applied Catalysis A: General* **186**, 3-12.

Sharp Z., (2007) *Principles of Stable Isotope Geochemistry*. Pearson Education, Inc.

Sherwood Lollar B., Lacrampe-Couloume G., Slater G. F., Ward J. A., Moser D. P., Gihring T. M., Lin L.-H., and Onstott T. C., (2006) Unravelling abiogenic and biogenic sources of methane in the Earth's deep subsurface. *Chemical Geology* **226**, 328-339.

Sherwood Lollar B., Frape S. K., Weise S. M., Fritz P., Macko S. A., and Welhan J. A., (1993) Abiogenic methanogenesis in crystalline rocks. *Geochimica et Cosmochimica Acta* **57**, 5087-5097.

Sherwood Lollar B., Lacrampe-Couloume G., Voglesonger K., Onstott T. C., Pratt L. M., and Slater G. F., (2008) Isotopic signatures of CH4 and higher hydrocarbon gases from Precambrian Shield sites: A model for abiogenic polymerization of hydrocarbons. *Geochimica et Cosmochimica Acta* **72**, 4778-4795.

Sherwood Lollar B., Westgate T. D., Ward J. A., Slater G. F., and Lacrampe-Couloume G., (2002) Abiogenic formation of gaseous alkanes in the Earth's crust as a minor source of global hydrocarbon reservoirs. *Nature* **416**, 522-524.

Slater G. F., Dempster H. S., Sherwood Lollar B., and Ahad J., (1999) Headspace
analysis: a new application for isotopic characterization of dissolved organic
contaminants. *Environmental Science & Technology* **33**, 190-194.

Sleep N. H., Meibom A., Fridriksson T., Coleman R. G., and Bird D. K., (2004) H2-rich
fluids from serpentinization: Geochemical and biotic implications. *PNAS* **101**,
12818 -12823.

Spellman F. R., (2008) *Handbook of water and wastewater treatment plant operations*.
CRC Press.

Suda K., (2013) Origin of CH4 in serpentinite-hosted hydrothermal system: the CH4-H2-
H2O hydrogen isotope systematics of the Hakuba Happo hot spring, Tokyo
Institute of Technology.

Sudarikov S. M. and Roumiantsev A. B., (2000) Structure of hydrothermal plumes at the
Logatchev vent field, 14 45'N, Mid-Atlanic Ridge: evidence from geochemical
and geophysical data. *Journal of Volcanology and Geothermal Research* **101**,
245-252.

Suhr G., (1992) Upper mantle peridotites in the Bay of Islands Ophiolite, Newfoundland:
Formation during the final stages of a spreading centre? *Tectonophysics* **206**, 31-
53.

Suhr G. and Cawood P. A., (1993) Structural history of ophiolite obduction, Bay of
Islands, Newfoundland. *Geological Society of America Bulletin* **105**, 399-410.

Suzuki S., Ishii S., Wu A., Cheung A., Tenney A., Wanger A., Kuenen J. G., and Nealson
K. H., (2013) Microbial diversity in The Cedars, an ultrabasic, ultrareducing, and
low salinity serpentinizing ecosystem. *PNAS* **110**, 15336-15341.

Suzuki S., Kuenen J. G., Schipper K., van der Velde S., Ishii S., Wu A., Sorokin D. Y., Tenney A., Meng X., Morrill P. L., Kamagata Y., Muyzer G., Wanger A., and Nealson K. H., (2014) Physiological and genomic features of highly alkaliphilic hydrogen-utilizing Betaproteobacteria from a continental serpentinizing site. *Nature Communications*.

Szponar N., (2012) Carbon Cycling at a Site of Present-Day Serpentinization: The Tablelands, Gros Morne National Park. Thesis - paper based, Memorial University.

Szponar N., Brazelton W. J., Schrenk M. O., Bower D. M., Steele A., and Morrill P. L., (2013) Geochemistry of a Continental Site of Serpentinization in the Tablelands Ophiolite, Gros Morne National Park: a Mars Analogue. *ICARUS* **224**, 286-296.

Taran Y. A., Kliger G. A., Cienfuegos E., and Shuykin A. N., (2010) Carbon and hydrogen isotopic compositions of products of open-system catalytic hydrogenation of CO2: Implications for abiogenic hydrocarbons in Earth's crust. *Geochimica et Cosmochimica Acta* **74**, 6112-6125.

Taran Y. A., Kliger G. A., and Sevastianov V. S., (2007) Carbon isotope effects in the open-system Fischer–Tropsch synthesis. *Geochimica et Cosmochimica Acta* **71**, 4474-4487.

Taylor S., Sherwood Lollar B., Wassenaar L., and Hendry J. M., (2000) Bacteriogenic Ethane in Near-Surface Aquifers: Implications for Leaking Hydrocarbon Well Bores. *Environmental Science & Technology*.

Tazaz A. M., Bebout B. M., Kelley C. A., Poole J., and Chanton J. P., (2013) Redefining the isotopic boundaries of biogenic methane: Methane from endoevaporites. *Icarus* **224**, 268-275.

Tiago I., Chung A. P., and Verissimo A., (2004) Bacterial diversity in a nonsaline alkaline environment: Heterotrophic aerobic populations. *Applied and Environmental Microbiology* **70**, 7378-7387.

Tiago I., Pires C., Mendes P. V., Costa M. D., and Verissimo A., (2005) A Gram-negative alkaliphilic bacterium isolated from a nonsaline alkaline groundwater. *Syst. Appl. Microbiol.* **28**, 479-487.

Tiago I. and Verissimo A., (2013) Microbial and fuctional diversity of a subterrestrial high pH groundwater associated to serpentinization. *Environmental Microbiology* **15**, 1687-1706.

Tissot B., Califet-Debyser Y., Deroo G., and Oudin J. L., (1971) Origin and evolution of hydrocarbons in early Toarcian shales, Paris Basin, France. *American Association of Petroleum Geology Bulletin* **55**, 2177-2193.

Tissot B. P. and Welte D. H., (1984) *Petroleum formation and occurrence*. Springer-Verlaq, Federal Republic of Germany.

Valentine D. L., Chidthaisong A., Rice R., Reeburgh W. S., and Tyler S. C., (2004) Carbon and hydrogen isotope fractionation by moderately thermophilic methanogens. *Geochimica et Cosmochimica Acta* **68**, 1571-1590.

Vance S., Harnmeijer J., Kimura J., Hussmann H., Demartin B., and Brown J. M., (2007) Hydrothermal systems in small ocean planets. *Astrobiology* **7**, 987-1005.

Weaver F. J. and Macko S. A., (1988) Source rocks of Western Newfoundland. *Organic Geochemistry* **13**, 411-421.

Wenner D. B., (1971) Hydrogen and oxygen isotopic studies of serpentinization of ultramafic rocks, California Institute of Technology.

Whiticar M. J., (1996) Stable isotope geochemistry of coals, humic kerogens and related natural gases. *International Journal of Coal Geology* **32**, 191-215.

Whiticar M. J., (1999) Carbon and hydrogen isotope systematics of bacterial formation and oxidation of methane. *Chemical Geology* **161**, 291-314.

Whiticar M. J., Faber E., and Schoell M., (1986) Biogenic methane formation in marine and freshwater environments: CO_2 reduction *vs* acetate fermentation--Isotope evidence. *Geochimica et Cosmochimica Acta* **50**, 693-709.

Wiese K. and Kvenvolden K. A., (1993) Introduction to Microbial and Thermal Methane. *U.S. Geological Survey Professional Paper* **1570**, 13-20.

Williams H., and Cawood P.A., 1989: Geology, Humber Arm Allochthon, Newfoundland; Geological Survey of Canada, Map 1678A, scale 1:250 000.

Zerkle A. L., House C. H., and Brantley S. L., (2005) Biogeochemical signatures through time as inferred from whole microbial genomes. *American Journal of Science* **305**, 467-502.

Appendix A: Raw Data

TAble A.1. A comparison of aqueous, inorganic geochemical parameters of waters sampled at The Cedars in 2011.

	AC	BS9	BS5	BS7	NS1	GPS1	r^2
Cl^- (mg/L)	1.19E+01	5.87E+01	4.99E+01	4.61E+01	3.25E+01	3.06E+02	1.00
Br^- (mg/L)	4.36E-02	1.64E-01	1.36E-01	1.32E-01	1.02E-01	8.63E-01	1.00
OH^- (mg/L)[a]	1.60E-01	1.50E+00	9.56E+01	7.95E+01	4.47E+01	1.45E+02	0.57
Mg^{2+} (mg/L)	2.67E+01	1.96E+00	1.96E-01	1.16E-01	4.71E-02	2.77E-02	0.11
Ca^{2+} (mg/L)	8.05E+00	9.77E+00	4.22E+01	4.52E+01	4.73E+01	3.41E+01	0.01
K^+ (mg/L)	3.70E-01	4.83E+00	4.35E+00	2.92E+00	1.31E+00	4.51E+00	0.26
Na^+ (mg/L)	1.77E+01	9.78E+01	9.66E+01	9.02E+01	1.00E+02	7.71E+02	0.99
NH_4^+ (mg/L)	4.00E-02	4.50E-02	3.15E-02	3.70E-02	9.20E-02	7.77E-01	0.97
NO_3^- (mg/L)	1.31E-01	8.40E-02	6.90E-02	9.00E-02	7.40E-02	5.40E-02	0.41
TON (mg/L)[b]	n/a	n/a	9.07E-02	n/a	2.52E-01	n/a	nc
PO_4^{3-} (mg/L)	4.70E-02	3.90E-02	2.70E-02	1.07E-01	3.90E-02	3.60E-02	0.05
SO_4^{2-} (mg/L)	4.91E-01	3.73E-01	7.00E-02	4.00E-02	2.54E-01	2.50E-02	0.28
f_{UB}[c]	0.00	0.16	0.13	0.12	0.07	1.00	

- = not analyzed/not sampled; n/a = calculation not available; nc = indicates that there were not enough data points to confidently do the r^2 calculation or the parameter (e.g. pH) is not on a linear scale. The r^2 is a correlation co-efficient of the regression analysis of the concentration and f_{UB}, which depicts how well the parameter is described by the two component mixing model. The r^2 was calculated when there were at minimum 3 data points and no more than half of the data points were an end member.
[a] Calculated OH^- concentrations based on measured pH values
[b] Calculated TON based on measured TDN and TIN (NH_4^+ and NO_3^-)
[c] The f_{UB} is the calculated fraction of ultra-basic water contributing to that particular spring during that sampling period using Equation 2.2.

Table A.2. A comparison of aqueous, inorganic geochemical parameters of waters sampled at The Cedars in 2012.

	AC	BS9	BS5	BS7	NS1	GPS1	r^2
Cl^- (mg/L)	7.38E+00	-	5.57E+01	-	3.06E+01	3.16E+02	1.00
Br^- (mg/L)	2.69E-02	-	1.47E-01	-	8.04E-02	8.59E-01	1.00
OH^- (mg/L)[a]	1.00E-01	-	1.41E+02	-	4.47E+01	5.50E+02	0.99
Mg^{2+} (mg/L)	2.57E+01	-	2.60E-01	-	2.57E-01	1.75E-02	0.20
Ca^{2+} (mg/L)	3.75E+00	-	3.85E+01	-	4.47E+01	3.53E+01	0.08
K^+ (mg/L)	8.00E-02	-	1.19E+00	-	4.60E-01	3.41E+00	0.97
Na^+ (mg/L)	9.08E+00	-	6.92E+01	-	4.35E+01	7.99E+02	0.99
NH_4^+ (mg/L)	6.20E-02	-	8.00E-02	-	4.40E-02	7.66E-01	0.99
NO_3^- (mg/L)	1.11E-01	-	6.60E-02	-	1.00E-01	6.10E-02	0.53
TON (mg/L)[b]	4.32E-01	-	n/a	-	3.27E-02	2.84E-01	0.01
PO_4^{3-} (mg/L)	4.50E-02	-	2.90E-02	-	2.60E-02	3.60E-02	0.00
SO_4^{2-} (mg/L)	9.40E+00	-	1.75E+00	-	1.00E-01	2.39E+00	0.07
f_{UB}[c]	0.00	-	0.16	-	0.08	1.00	

- = not analyzed/not sampled; n/a = calculation not available; nc = indicates that there were not enough data points to confidently do the r^2 calculation or the parameter (e.g. pH) is not on a linear scale. The r^2 is a correlation co-efficient of the regression analysis of the concentration and f_{UB}, which depicts how well the parameter is described by the two component mixing model. The r^2 was calculated when there were at minimum 3 data points and no more than half of the data points were an end member.

[a] Calculated OH^- concentrations based on measured pH values
[b] Calculated TON based on measured TDN and TIN (NH_4^+ and NO_3^-)
[c] The f_{UB} is the calculated fraction of ultra-basic water contributing to that particular spring during that sampling period using Equation 2.2.

Table A.3. A comparison of aqueous, inorganic geochemical parameters of waters sampled at The Cedars in 2013.

	AC	BS9	BS5	BS7	NS1	GPS1	r^2
Cl^- (mg/L)	8.68E+00	-	6.08E+01	-	3.21E+01	3.15E+02	1.00
Br^- (mg/L)	2.53E-02	-	2.02E-01	-	1.11E-01	9.54E-01	1.00
OH^- (mg/L)[a]	1.00E-01	-	2.14E+02	-	1.70E+02	6.77E+02	0.96
Mg^{2+} (mg/L)	2.57E+01	-	3.63E-01	-	4.64E-02	2.12E-01	0.20
Ca^{2+} (mg/L)	7.35E+00	-	3.46E+01	-	4.51E+01	1.92E+01	0.04
f_{UB}[b]	0.00	-	0.17	-	0.08	1.00	

- = not analyzed/not sampled; nc = indicates that there were not enough data points to confidently do the r^2 calculation or the parameter (e.g. pH) is not on a linear scale. The r^2 is a correlation co-efficient of the regression analysis of the concentration and f_{UB}, which depicts how well the parameter is described by the two component mixing model. The r^2 was calculated when there were at minimum 3 data points and no more than half of the data points were an end member.

[a] Calculated OH^- concentrations based on measured pH values

[b] The f_{UB} is the calculated fraction of ultra-basic water contributing to that particular spring during that sampling period using Equation 2.2.

Table A.4. Ion concentrations (µg/L) of ultra-basic spring water and non ultra-basic Austin Creek water at The Cedars in 2011.

	AC	BS9	BS5	BS7	NS1	GPS1	r^2
I^-	19.9	63.9	86.1	80.8	78.6	917	0.99
Li^+	2.02	10.4	9.12	8.87	7.20	39.6	0.99
Rb^+	0.240	2.74	1.33	1.07	0.566	4.70	0.83
Zn^{2+}	1.55	6.17	2.58	2.14	3.86	3.71	0.04
$Sn^{2+, 4+}$	<0.062	<0.062	0.266	0.258	0.417	0.362	0.07
Ba^{2+}	0.444	1.96	0.299	0.443	0.735	0.318	0.05
Al^{3+}	1.18	1.95	0.744	2.23	2.62	<0.728	0.01
$Mn^{2+, 3+}$	<0.095	0.200	<0.095	<0.095	0.528	0.120	0.51
Sr^{2+}	2.09	1.48	2.90	3.17	3.83	1.19	0.37
$Ti^{3+, 4+}$	<0.886	<0.886	<0.886	<0.886	<0.886	<0.886	nc
$Pb^{2+, 4+}$	0.054	0.040	0.042	0.042	0.077	0.029	0.37
S^{2-}	<2930	<2930	<2930	<2930	<2930	<2930	nc
B	1.82	<0.506	0.789	<0.506	0.645	1.89	0.28
$Cr^{2+, 3+}$	1.42	0.651	<0.415	<0.415	<0.415	<0.415	nc
Si	2460	580	<31.3	52.9	<31.3	96.6	0.28
$Fe^{2+, 3+}$	<43.9	<43.9	<43.9	<43.9	<43.9	<43.9	nc
P^{3-}	<14.6	<14.6	<14.6	<14.6	<14.6	<14.6	nc
Hg^{2+}	0.176	0.370	<0.044	0.068	0.085	0.346	0.34
$Cu^{+, 2+}$	<0.118	<0.118	<0.118	<0.118	<0.118	<0.118	nc
$Sb^{3+, 5+}$	0.025	0.042	<0.018	<0.018	<0.018	<0.018	nc
$Ni^{2+, 3+}$	0.533	0.941	<0.158	<0.158	<0.158	<0.158	nc
f_{UB}[a]	0.00	0.16	0.13	0.12	0.07	1.00	

- = not analyzed/not sampled; nc = indicates that there were not enough data points to confidently do the r^2 calculation or the parameter (e.g. pH) is not on a linear scale. The r^2 is a correlation co-efficient of the regression analysis of the concentration and f_{UB}, which depicts how well the parameter is described by the two component mixing model. The r^2 was calculated when there were at minimum 3 data points and no more than half of the data points were an end member.

[a] The f_{UB} is the calculated fraction of ultra-basic water contributing to that particular spring during that sampling period using Equation 2.2.

If an ion's concentration was below the detection limit than the detection limit was reported.

Table A.5. Ion concentrations (µg/L) of ultra-basic spring water and non ultra-basic Austin Creek water at The Cedars in 2012.

	AC	BS9	BS5	BS7	NS1	GPS1	r^2
I^-	29.4	-	110	-	85.6	1045	0.99
Li^+	0.965	-	10.6	-	6.46	41.7	0.99
Rb^+	0.263	-	0.448	-	0.360	1.46	1.00
Zn^{2+}	<35.3	-	<35.3	-	<35.3	<35.3	nc
$Sn^{2+, 4+}$	<0.379	-	<0.379	-	<0.379	0.822	nc
Ba^{2+}	0.860	-	0.444	-	0.495	0.341	0.45
Al^{3+}	<3.55	-	8.07	-	10.2	6.28	0.78
$Mn^{2+, 3+}$	0.140	-	0.501	-	0.510	0.260	0.05
Sr^{2+}	1.47	-	2.82	-	3.23	1.22	0.32
$Ti^{3+, 4+}$	<3.40	-	<3.40	-	<3.40	<3.40	nc
$Pb^{2+, 4+}$	0.109	-	0.176	-	0.144	0.429	1.00
S^{2-}	<12100	-	<12100	-	<12100	<12100	nc
B	<2.45	-	<2.45	-	<2.45	<2.45	nc
$Cr^{2+, 3+}$	1.41	-	<0.898	-	1.14	<0.898	nc
Si	907	-	<177	-	<177	<177	nc
$Fe^{2+, 3+}$	<17.7	-	<17.7	-	<17.7	<17.7	nc
P^{3-}	<14.3	-	<14.3	-	<14.3	<14.3	nc
Hg^{2+}	<0.114	-	<0.114	-	<0.114	0.254	nc
$Cu^{+, 2+}$	3.64	-	<0.979	-	2.49	1.85	nc
$Sb^{3+, 5+}$	<0.050	-	<0.050	-	<0.050	<0.050	nc
$Ni^{2+, 3+}$	<1.22	-	<1.22	-	<1.22	<1.22	nc
f_{UB}[a]	0.00	-	0.16	-	0.08	1.00	

- = not analyzed/not sampled; nc = indicates that there were not enough data points to confidently do the r^2 calculation or the parameter (e.g. pH) is not on a linear scale. The r^2 is a correlation co-efficient of the regression analysis of the concentration and f_{UB}, which depicts how well the parameter is described by the two component mixing model. The r^2 was calculated when there were at minimum 3 data points and no more than half of the data points were an end member.

[a] The f_{UB} is the calculated fraction of ultra-basic water contributing to that particular spring during that sampling period using Equation 2.2.

If an ion was below the detection limit than the detection limit was reported.

Table A.6. Hydrogen and Oxygen isotopes of fluids from The Cedars and the Tablelands from Chapter 3, Figure 3.1 and 3.4.

| | $\delta^{18}O$ | | | δ^2H | | |
	2011	2012	2013	2011	2012	2013
The Cedars						
AC	-6.5	-6.4	-6.3	-39.0	-38.4	-37.9
BS9	-1.4	-	-	-18.8	-	-
BS5	-6.6	-6.5	-6.2	-39.1	-39.1	-37.8
BS7	-6.7	-	-	-39.3	-	-
NS1	-6.7	-6.9	-5.9	-39.4	-41.6	-38.2
GPS1	-6.8	-6.8	-6.6	-39.7	-39.2	-38.5
The Tablelands						
WHB	-	-9.0	-	-	-56.2	-
WHC2A	-	-7.7	-	-	-55.0	-
WHC2B	-	-8.4	-	-	-53.8	-
WHC2C	-	-8.8	-	-	-56.0	-
WHC2A-R	-	-10.2	-	-	-62.0	-
WHC2B-R	-	-10.4	-	-	-63.5	-
WHC1	-	-10.2	-	-	-62.7	-

- = not analyzed/not sampled

Table A.7. A comparison of aqueous, inorganic geochemical parameters of waters sampled at the Tablelands in 2011.

	WHB	WHC2C	WHC2A	WHC2A-R	WHC2B	WHC2B-R	WHC1	r^2
Cl^- (mg/L)	7.17E+00	6.71E+01	4.00E+02	-	2.15E+02	-	-	1.00
Br^- (mg/L)	8.65E-03	1.56E-01	9.57E-01	-	5.00E-01	-	-	1.00
OH^- (mg/L)[a]	1.00E-02	2.69E+02	4.27E+02	-	3.39E+02	-	-	0.74
Mg^{2+} (mg/L)	5.64E+00	7.45E+00	2.37E-01	-	2.42E-01	-	-	0.72
Ca^{2+} (mg/L)	3.88E-01	9.90E+00	5.96E+01	-	5.83E+01	-	-	0.83
K^+ (mg/L)	-	-	-	-	-	-	-	nc
Na^+ (mg/L)	-	-	-	-	-	-	-	nc
NH_4^+ (mg/L)	-	-	-	-	-	-	-	nc
NO_3^- (mg/L)**	1.90E-01 (± 3.00E-03)	7.50E-01 (± 1.20E-01)	1.50E-02 (± 3.00E-04)	-	1.40E-02 (± 0.00E+00)	-	-	0.34
TON (mg/L)[b]	-	-	-	-	-	-	-	nc
PO_4^{3-} (mg/L)**	7.60E-01 (± 1.60E-01)	4.50E-01 (± 2.10E-01)	8.00E-02 (± 6.00E-02)	-	4.10E-01 (± 1.60E-01)	-	-	0.88
SO_4^{2-} (mg/L)**	2.50E-01 (± 1.30E-03)	9.20E-01 (± 1.10E-01)	8.20E-01 (± 1.00E-02)	-	3.80E-01 (± 1.00E-01)	-	-	0.14
f_{UB}[c]	0.00	0.15	1.00	-	0.53	-	-	

- = not analyzed/not sampled; nc = indicates that there were not enough data points to confidently do the r^2 calculation or the parameter is not on a linear scale. The r^2 is a correlation co-efficient of the regression analysis of the concentration and f_{UB}, which depicts how well the parameter is described by the two component mixing model. The r^2 was calculated when there were at minimum 3 data points and no more than half of the data points were an end member.

[a] Calculated OH^- concentrations based on measured pH values

[b] Calculated TON based on measured TDN and TIN (NH_4^+ and NO_3^-)

[c] The f_{UB} is the calculated fraction of ultra-basic water contributing to that particular spring during that sampling period using Equation 2.2.

**Data from Kavanagh 2012

The standard deviation associated with the concentration values are the error on replicate field samples (1σ).

Table A.8. A comparison of aqueous, inorganic geochemical parameters of waters sampled at the Tablelands in 2012.

	WHB	WHC2C	WHC2A	WHC2A-R	WHC2B	WHC2B-R	WHC1	r^2
Cl^- (mg/L)	5.94E+00	2.32E+01	1.38E+02	4.20E+02	4.15E+02	4.01E+02	4.89E+02	1.00
Br^- (mg/L)	2.68E-02	6.37E-02	3.40E-01	9.77E-01	9.79E-01	9.27E-01	1.19E+00	1.00
OH^- (mg/L)[a]	2.00E-02	8.52E+01	2.69E+02	3.39E+02	2.69E+02	2.69E+02	2.69E+02*	0.70
Mg^{2+} (mg/L)	8.65E+00	1.21E+01	6.02E+00	9.58E-02	7.27E-02	2.99E-01	2.86E-01	0.92
Ca^{2+} (mg/L)	7.71E-01	3.47E+00	1.90E+01	5.88E+01	6.01E+01	6.10E+01	4.60E+00	0.41
K^+ (mg/L)	1.58E-01	2.73E+00	3.62E+00	8.78E+00	1.25E+01	1.28E+01	-	0.90
Na^+ (mg/L)	5.82E+00	9.56E+01	1.29E+02	8.54E+02	9.33E+02	8.96E+02	-	0.97
NH_4^+ (mg/L)	2.80E-02	3.17E-01	2.91E-01	1.20E+00	1.70E+00	1.02E+00	-	0.86
NO_3^- (mg/L)	1.96E-01	1.72E-01	1.42E-01	7.70E-02	7.10E-02	8.50E-02	-	0.98
TON (mg/L)[b]	n/a	4.21E-02	8.14E-01	3.70E-02	2.93E-02	7.69E-01	-	0.01
PO_4^{3-} (mg/L)	4.50E-02	7.00E-02	3.90E-02	4.20E-02	4.90E-02	4.60E-02	-	0.15
SO_4^{2-} (mg/L)	1.11E+00	1.25E+00	1.30E+00	3.64E-01	4.38E-01	5.99E-01	-	0.86
f_{UB}[c]	0.00	0.04	0.27	0.86	0.85	0.82	1.00	

- = not analyzed/not sampled; n/a = calculation not available; nc = indicates that there were not enough data points to confidently do the r^2 calculation or the parameter is not on a linear scale. The r^2 is a correlation co-efficient of the regression analysis of the concentration and f_{UB}, which depicts how well the parameter is described by the two component mixing model. The r^2 was calculated when there were at minimum 3 data points and no more than half of the data points were an end member.

[a] Calculated OH^- concentrations based on measured pH values

[b] Calculated TON based on measured TDN and TIN (NH_4^+ and NO_3^-)

[c] The f_{UB} is the calculated fraction of ultra-basic water contributing to that particular spring during that sampling period using Equation 2.2.

* = Calculated OH^- concentration based on average pH measurements from 2009 to 2010 reported by Szponar (2012).

Table A.9. Ion concentrations (µg/L) of ultra-basic spring water and non ultra-basic Winter House Brook water at the Tablelands in 2011.

	WHB	WHC2C	WHC2A	WHC2A-R	WHC2B	WHC2B-R	WHC1	r^2
I^-	<5.51	36.5	251	-	128	-	-	1.00
Li^+	<0.129	10.4	60.0	-	34.4	-	-	1.00
Rb^+	0.222	4.85	15.4	-	9.82	-	-	0.97
Zn^{2+}	1.71	0.619	4.36	-	0.625	-	-	0.53
$Sn^{2+, 4+}$	<0.062	0.205	1.33	-	2.01	-	-	0.32
Ba^{2+}	0.314	0.484	1.76	-	0.949	-	-	0.99
Al^{3+}	2.95	3.21	2.81	-	2.12	-	-	0.15
$Mn^{2+, 3+}$	<0.095	0.144	<0.095	-	<0.095	-	-	nc
Sr^{2+}	1.91	4.98	15.2	-	7.47	-	-	0.97
$Ti^{3+, 4+}$	<0.886	1.05	<0.886	-	0.116	-	-	nc
$Pb^{2+, 4+}$	0.029	0.047	0.054	-	0.049	-	-	0.66
S^{2-}	<2920	<2920	<2920	-	<2920	-	-	nc
B	2.36	3.39	0.862	-	1.25	-	-	0.68
$Cr^{2+, 3+}$	2.09	1.76	0.491	-	0.637	-	-	0.87
Si	2626	5456	618	-	859	-	-	0.50
$Fe^{2+, 3+}$	<43.9	<43.9	<43.9	-	<43.9	-	-	nc
P^{3-}	<14.6	<14.6	<14.6	-	<14.6	-	-	nc
Hg^{2+}	<0.044	<0.044	<0.044	-	<0.044	-	-	nc
$Cu^{+, 2+}$	<0.118	0.23	<0.118	-	<0.118	-	-	nc
$Sb^{3+, 5+}$	<0.018	<0.018	<0.018	-	0.028	-	-	nc
$Ni^{2+, 3+}$	3.53	3.41	2.90	-	1.27	-	-	0.17
f_{UB}[a]	0.00	0.15	1.00	-	0.53	-	-	

- = not analyzed/not sampled; nc = indicates that there were not enough data points to confidently do the r^2 calculation or the parameter (e.g. pH) is not on a linear scale. The r^2 is a correlation co-efficient of the regression analysis of the concentration and f_{UB}, which depicts how well the parameter is described by the two component mixing model. The r^2 was calculated when there were at minimum 3 data points and no more than half of the data points were an end member.
[a] The f_{UB} is the calculated fraction of ultra-basic water contributing to that particular spring during that sampling period using Equation 2.2.
If an ion was below the detection limit than the detection limit was reported.

Table A.10. Ion concentrations (µg/L) of ultra-basic spring water and non ultra-basic Winter House Brook water at the Tablelands in 2012.

	WHB	WHC2C	WHC2A	WHC 2A-R	WHC2B	WHC 2B-R	WHC1	r^2
I^-	-	-	-	-	-	-	-	nc
Li^+	<0.802	<0.802	22.7	48.9	64.4	63.9	76.0	0.87
Rb^+	0.129	0.524	3.23	8.71	8.82	8.89	9.83	1.00
Zn^{2+}	<61.3	<61.3	<61.3	<61.3	<61.3	<61.3	<61.3	nc
$Sn^{2+, 4+}$	<5.99	<5.99	<5.99	<5.99	<5.99	<5.99	<5.99	nc
Ba^{2+}	0.812	0.576	0.825	1.70	1.89	2.04	0.862	0.47
Al^{3+}	<21.4	<21.4	<21.4	24.536	<21.4	<21.4	<21.4	nc
$Mn^{2+, 3+}$	0.100	0.354	<0.331	0.368	0.369	0.369	0.346	0.43
Sr^{2+}	2.78	4.70	7.70	16.7	16.0	16.0	4.89	0.44
$Ti^{3+, 4+}$	<3.53	<3.53	<3.53	<3.53	<3.53	<3.53	<3.53	nc
$Pb^{2+, 4+}$	<0.069	<0.069	<0.069	0.307	0.148	0.126	<0.069	0.64
S^{2-}	<6220	<6220	<6220	<6220	<6220	9925	<6220	nc
B	<8.32	<8.32	<8.32	<8.32	<8.32	<8.32	<8.32	nc
$Cr^{2+, 3+}$	3.16	1.87	1.30	<0.341	<0.341	<0.341	0.578	0.69
Si	3268	7489	4968	1663	540	1295	429	0.73
$Fe^{2+, 3+}$	<38.9	<38.9	<38.9	<38.9	<38.9	54.2	<38.9	nc
P^{3-}	<21.0	<21.0	<21.0	<21.0	<21.0	29.1	<21.0	nc
Hg^{2+}	<0.060	<0.060	<0.060	0.076	<0.060	<0.060	0.078	nc
$Cu^{+, 2+}$	<1.79	<1.79	<1.79	2.30	2.90	2.15	3.58	0.79
$Sb^{3+, 5+}$	<0.026	<0.026	0.048	<0.026	<0.026	0.052	0.490	0.49
$Ni^{2+, 3+}$	2.60	5.00	1.44	21.1	10.2	5.35	1.27	0.16
f_{UB}[a]	0.00	0.04	0.27	0.86	0.85	0.82	1.00	

- = not analyzed/not sampled; nc = indicates that there were not enough data points to confidently do the r^2 calculation or the parameter (e.g. pH) is not on a linear scale. The r^2 is a correlation co-efficient of the regression analysis of the concentration and f_{UB}, which depicts how well the parameter is described by the two component mixing model. The r^2 was calculated when there were at minimum 3 data points and no more than half of the data points were an end member.

[a] The f_{UB} is the calculated fraction of ultra-basic water contributing to that particular spring during that sampling period using Equation 2.2.

If an ion was below the detection limit than the detection limit was reported.

Appendix B: Characterizing Sedimentary Organic Matter: Preliminary Results

Methods

Sedimentary rocks were scrubbed with distilled water to remove any debris that may be adhering to the outside surface. The rocks were crushed into a fine powder using a cup and mill device which was cleaned thoroughly with ethanol and an air jet in between samples. Samples were stored in sterile plastic containers and kept cold and dark until analysis.

Semi Volatile Organic Compounds. A microwave extraction procedure adapted from the EPA method 3546 was used to extract semi-volatile organic compounds from the crushed rocks. Pre-combusted glassware was used throughout the method to mitigate any organic contamination. Approximately 50 g of powdered rock was extracted by placing 5 g of sample and 25 mL of 1:1 hexane/acetone (extraction solvent) into 10 Teflon Greehchem microwave vessels. A blank using 25 mL of extraction solvent was run with every sample set. The temperature program used to extract the organic compounds was a ramp to 115 °C for 10 min, hold at 115 °C for 10 min, and cool down for 5 minutes using a power of 1200 W program. Microwave vessels and sample was rinsed thoroughly with 1:1 hexane/acetone and filtered through a 1.5 μm glass microfibre filter. The filtrate was collected and combined into glass vials and blown down to a volume of <1 mL using an N_2 Evaporator for solid-liquid silica gel column chromatography, which was adapted from EPA methods 8092, 8100 and 3600C. Silica

gel (100-200 mesh) was activated overnight (>8 hrs) at 140 °C and stored in hexane at room temperature. The elution solvents used to separate the organic compounds were hexane (F1) for straight and branched alkanes, alkenes and alkynes, 2:1 hexane/dichloromethane (F2) for aromatic compounds, and methanol (F3) to elute what is left on the column. The first two fractions were blown down and transferred to a 2 mL gas chromatograph vial where an internal standard of 5α-cholestane (used for F1 compounds) and o-terphenyl (used for F2 compounds) at a concentration of 5 ppm was added to each gas chromatograph vial. Samples were analyzed using an Agilent 6890N GC coupled to a 5975C MSD equipped with a HP-5MS (30 m x 0.32 mm ID, 0.25 μm film thickness) column and He as the carrier gas. An autosampler was used for the injection of samples and the temperature program was 50 °C hold for 1 min, ramp 8 °C/min to 310 °C, hold for 20 min. The retention factor was calculated and used for the integrated areas of all standards and samples before any processing. Blank chromatograms were subtracted from sample chromatograms before an aliphatic hydrocarbon standard (RESTEK 31459) or polycyclic aromatic hydrocarbon calibration mix (RESTEK 31011) was used for the identification and quantification of organic compounds. Sample chromatogram peaks were compared to standard 4 point calibration curves (0.5, 1, 2, and 5 mg/L) with an r^2 of >0.99. To quantify the analytes the calibration curve generated for the standard with the most similar chemical structure was used. Compounds were identified using Wiley and NIST libraries for references and comparing sample retention times to standards. The reproducibility on replicate field samples for The Cedars ranged from 0.1 to 31.4 % RSD, with the exception of nC_{12} in FSC2 samples which had a 104 % RSD. At the Tablelands the reproducibility on replicate field samples ranged from 0.1 to 44.9 % RSD.

Elemental Analysis (EA). Powdered samples were acidified with concentrated HCl acid in a dessicator for a minimum of 24 hours for the determination of bulk elemental composition and $\delta^{13}C$ ratio of organic compounds. Samples were then stored in pre-combusted glass vials with Teflon lined caps and sent to G.G. Hatch Stable Isotope Laboratory in Ottawa, Ontario. For %N, %C, %H and %S samples were transferred into tin capsules along with Tungstic oxide, which acts as a combustion catalyst, and weighed on the microbalance before being sealed and loaded into the carousel of the autosampler and measured using a VarioEL III Elemental Analyser. Samples were flash combusted at 1800 °C with the addition of oxygen and then carried with He through the chemical column to yield N_2, CO_2, H_2O and SO_2 gas which is separated through a series of adsorption traps before being directed to the thermal conductivity detector which measures the gases as they are released. For quantification calibrated sulfanilic acid standards are prepared and measured in a range of weights. The analytical reproducibility for concentrations ranged from 0.07 to 0.11 % (1σ) and the error associated with replicate field samples was ≤ 13 % RSD, with the exception of sulphur which had an error of 43 % RSD.

Microscopy. Palynology slides of the different sedimentary organic matter samples were prepared to view their organic maturity using standard palynology processing techniques. The outside of the sedimentary organic matter samples were scrubbed thoroughly and then broken down into small pebble size chunks and weighed out. Samples were then digested in multiple acids to break down the structure and get rid of the mineral and inorganic carbon within the rock. The first digestion was in 15% hydrochloric acid (removal of carbonates) for a minimum of 24 h. Samples were washed

with distilled water a minimum of 3 times before the second digestion in concentrated

hydrofluoric acid (removal of silicates) for a minimum of 2 days. The samples were then

rinsed and sieved using a 10 μm mesh sieve to further isolate organic compounds. The

resultant organic extract was mounted on a glass microscope slide to be viewed and

photographed using a QDI 202^{TM}UV-visible-NIR Microscope Spectrophotometer, under

transmitted and ultraviolet light sources. Colour of organics was classified subjectively by

comparison with a reference colour chart from Pearson (1984).

Results

The Cedars

The composition of branched and straight chained aliphatic hydrocarbons

extracted from sedimentary organic matter samples FSC1 and FSC2 which were collected

at The Cedars can be seen in Table B.1. There was no observable consistent pattern in

odd or even high molecular weight compounds detected in spring fluids. Normal alkanes

from C_{10} to C_{32} were detected and quantified in both shale samples with the exception of

C_{11} and C_{12} which were below quantification limits in FSC1 and C_{29} whose peak co-

eluded with the chosen internal standard in both samples. Linear alkanes C_{10} to C_{19}

ranged from 0.003 to 0.024 μg/g in FSC1 and ranged from 0.005 to 0.048 μg/g in the

FSC2 sample. A general increase in concentration with increasing molecular mass was

observed with this set of linear alkanes. The range of linear alkanes C_{20}-C_{28} in FSC1 was

0.013 to 0.041 μg/g and in the FSC2 sample was 0.026 to 0.054 μg/g. Linear alkanes C_{30}-

C_{32} in FSC1 ranged from 0.035 to 0.042 μg/g and in FSC2 ranged from 0.031 to 0.039

μg/g. The highest linear alkane concentrations in FSC1 were C_{25}, C_{27}, C_{30} and C_{31}. The

highest linear alkane concentrations in FSC2 were C_{18}, C_{25}, and C_{27}. The observed branched alkanes in both samples were dimethyl undecane, trimethyl dodecane, trimethyl tetradecane, and tetramethyl pentadecane. Branched alkanes ranged in concentration from 0.004 to 0.015 μg/g in FSC1 and 0.009 to 0.038 μg/g in FSC2.

The elemental composition of sedimentary organic matter samples FSC1 and FSC2 collected from The Cedars can be seen in Table B.2. Out of the four elements sampled for (N, C, H, and S) both FSC1 and FSC2 were primarily composed of carbon and hydrogen. The percentage of nitrogen in both samples was low measuring 0.04 % in FSC1 and 0.06 % in FSC2. The percentages of carbon in these two samples were significantly different with FSC2 having much higher carbon content (0.96 %) compared to FSC1 (0.19 %). The hydrogen percentage was similar in samples measuring 0.40 % in FSC1 and 0.48 % in FSC2. Sulphur was below the detection limit in both samples. In general the percentage of all elements measured was higher in the FSC2 sample compared to the FSC1 sample.

Microscopic images of structured organics observed in FSC1 and FSC2 samples under white transmitted light can be seen in Figure B.1. Structured organics observed in palynology slides included both phytoclasts and palynomorphs. Among the phytoclasts observed were woody tissues, cuticles, and possible cortex tissue of stems or roots which are within the liptinite and huminite/vitrinite maceral groups. Palynomorphs observed were spore and pollen grains, undiagnostic cellular material and possible marine algae remains which were all within the liptinite maceral group. These organics ranged in colour from pale yellow as seen in (g), to orange as seen in (i), to dark brown and black as seen in (d) and (k). Dark brown to black organics that were unstructured and

unidentifiable were also present in slides of FSC1 and FSC2. More microscopic images of structured and unstructured organics observed in FSC1 and FSC2 samples under white transmitted light and ultraviolet light can be seen in Figure B.2. Organics range in colour from pale yellow to dark brown/black under the white transmitted light. Under ultraviolet light some organics fluoresced in colours ranging from pale yellow to orange to brown, while others did not fluoresce at all and were black under the ultraviolet light. Materials that fluoresced a bright blue colour were either mineral related or contamination associated with making the slides.

The Tablelands

High molecular weight hydrocarbon composition of HAA1, HAA2, and HAA3 extracts sampled from the Tablelands can be found in Table B.3. These samples represent the widest transect of shale collected at the Tablelands and were the best representative of sedimentary organic matter that was buried beneath the serpentinizing peridotite. There was no observable consistent pattern in odd or even high molecular weight hydrocarbons detected in these samples. Furthermore there was no consistent dominant group of alkanes identified in the samples. Straight chained alkanes C_{12-28} and C_{30-32} were detected in sedimentary organic matter samples and only one unsaturated alkane was detected (1-tetradecene). In the HAA1 sample the alkanes with the highest concentrations were C_{16}, C_{25}, C_{26}, and C_{27} (from 0.104 to 0.208 μg/g). In the HAA2 sample the alkanes with the highest concentrations were C_{15}, C_{16}, C_{17}, and C_{25} (from 0.048 to 0.104 μg/g). In the HAA3 sample the dominant alkanes with the highest concentrations were C_{17}, C_{25}, C_{26}, and C_{28} (from 0.050 to 0.062 μg/g).

The elemental composition of sedimentary organic matter samples (HAA1-6) collected from the Tablelands can be seen in Table B.2. Out of the four elements sampled for (N, C, H, and S) all samples were primarily composed of carbon and hydrogen. The percentage of nitrogen was low in all samples and ranged from 0.03 to 0.11 %. The percentage of carbon and hydrogen varied greatly between samples. Fine grained shale samples (HAA1-4) had percentages of bulk carbon ranging from 0.18 to 4.33 %. The percentage of bulk carbon in HAA5 was high at 3.76 % and in HAA6 the percentage was low at 0.08 %. The percentage of bulk hydrogen was greatest in HAA3 with a value of 1.85 % and lowest in HAA1 with a value of 0.82 % out of the fine grained shale samples. In other shale samples the hydrogen percentage was 0.87 % (HAA2) and 1.35 % (HAA4). Similar to carbon, the hydrogen percentage was high in HAA5 at 3.86 % and low in HAA6 with a percentage of 0.67%. Sulphur was below the detection limit in HAA2, HAA5, and HAA6. In all other sedimentary organic matter samples the sulphur percentage ranged from 0.22 to 0.63 %. Out of the fine grained shale samples HAA3 had the highest percentage of all four elements analyzed.

Microscopic images of organics observed in HAA1-4 under white transmitted light can be seen in Figure B.3. There were no structured organics observed in slides. All observed organics were heavily degraded and beyond the point of recognition and therefore no organics could be identified as either phytoclasts or palynomorphs. Organics ranged in colour from dark yellow to dark brown/black. The majority of organics were a dark brown to black colour. More microscopic images of unstructured organics observed in samples under white transmitted light and ultraviolet light can be seen in Figure B.4. Again organics ranged in colour from dark yellow to dark brown/black under white

transmitted light. Under ultraviolet light no organics observed in slides fluoresced and were black in colour. Materials that fluoresced a bright blue colour were either mineral related or contamination associated with making the slides.

Tables and Figures

Table B.1. High molecular weight compounds extracted and measured in F1 (hexane) of sedimentary organic matter samples from The Cedars.

Probable Structure	Concentration (µg/g)	
	FSC1	FSC2
n-decane (C_{10})	0.003 (± 0.000)	0.005
n-undecane (C_{11})	<q.l.	0.009
n-dodecane (C_{12})	<q.l.	0.009 (± 0.009)
dimethyl undecane	0.004 (± 0.000)	0.009 (± 0.003)
n-tridecane (C_{13})	0.010 (± 0.001)	0.028 (± 0.008)
trimethyl dodecane*	0.015 (± 0.000)	0.026 (± 0.005)
n-tetradecane (C_{14})	0.006	0.025 (± 0.006)
trimethyl tetradecane	0.012 (± 0.000)	0.021 (± 0.002)
n-pentadecane (C_{15})	0.015 (± 0.001)	0.036 (± 0.005)
n-hexadecane (C_{16})	0.018 (± 0.002)	0.042 (± 0.002)
n-heptadecane (C_{17})	0.022 (± 0.001)	0.045 (± 0.000)
tetramethyl pentadecane	0.015 (± 0.001)	0.038 (± 0.001)
n-octadecane (C_{18})	0.024 (± 0.001)	0.048 (± 0.000)
n-nonadecane (C_{19})	0.019 (± 0.000)	0.041 (± 0.000)
n-eicosane (C_{20})	0.013 (± 0.000)	0.035 (± 0.001)
n-henicosane (C_{21})	0.021 (± 0.000)	0.029 (± 0.000)
n-docosane (C_{22})	0.017 (± 0.000)	0.026 (± 0.000)
n-tricosane (C_{23})	0.031 (± 0.001)	0.041 (± 0.000)
n-tetracosane (C_{24})	0.028 (± 0.000)	0.037 (± 0.000)
n-pentacosane (C_{25})	0.041 (± 0.000)	0.054 (± 0.000)
n-hexacosane (C_{26})	0.035 (± 0.000)	0.045 (± 0.000)
n-heptacosane (C_{27})	0.040 (± 0.000)	0.046 (± 0.000)
n-octacosane (C_{28})	0.035 (± 0.000)	0.037 (± 0.000)
n-triacontane (C_{30})	0.042 (± 0.000)	0.039 (± 0.000)
n-hentriacontane (C_{31})	0.040 (± 0.000)	0.035(± 0.000)
n-dotriacontane (C_{32})	0.035 (± 0.001)	0.031 (± 0.000)

* = value reported is the sum of all isomers quantified; <q.l. = analyte was detected but below quantification limit

The standard deviation associated with the concentration values are the error on replicate extractions (1σ). Calibration curves for C_{24} and C_{26} only had two data points while lower alkanes (C_{10}-C_{22}) had calibration curves with 3 or more data points. All compounds above C_{26} were quantified using the C_{26} calibration curve. Odd chained hydrocarbons were quantified by rounding up and using the closest even chained hydrocarbon standard.

Table B.2. Carbon isotopic value of sedimentary organic matter samples from The Cedars and the Tablelands.

| | CEDARS | | TABLELANDS | | | | | |
	FSC1	FSC2	HAA1	HAA2	HAA3	HAA4	HAA5	HAA6
%N	0.04	0.06	0.05	0.07	0.11	0.05	0.03	0.03
%C_{org}	0.19	0.96	0.77	0.18	4.33	1.35	3.76	0.08
%H	0.40	0.48	0.82	0.87	1.85	1.35	3.86	0.67
%S	<d.l.	<d.l.	0.25	<d.l.	0.63	0.22	<d.l.	<d.l.
H/C	2.11	0.50	1.06	4.83	0.43	1.00	1.03	8.38
C/N	4.75	16.00	15.40	2.57	39.36	27.00	125.33	2.67

<d.l. = analyte was below detection limits of the analytical method used

Table B.3. High molecular weight compounds extracted and measured in F1 (hexane) of sedimentary organic matter samples from the Tablelands.

Probable Structure	Concentration (µg/g)		
	HAA1	HAA2	HAA3
n-dodecane (C_{12})	0.015	<q.l.	<d.l.
n-tridecane (C_{13})	0.036	0.046	0.023 (± 0.002)
1-tetradecene	<d.l.	<d.l.	0.018
n-tetradecane (C_{14})	0.102	0.011	<d.l.
n-pentadecane (C_{15})	0.092	0.104	0.045 (± 0.006)
n-hexadecane (C_{16})	0.208	0.063	<d.l.
n-heptadecane (C_{17})	0.063	0.073	0.056 (± 0.000)
n-octadecane (C_{18})	0.046	0.015	0.025
n-nonadecane (C_{19})	<d.l.	0.019	0.037 (± 0.004)
n-eicosane (C_{20})	0.033	0.012	0.023 (± 0.010)
n-henicosane (C_{21})	0.032	<d.l.	0.027 (± 0.002)
n-docosane (C_{22})	0.051	0.017	0.035 (± 0.002)
n-tricosane (C_{23})	0.095	0.034	0.044 (± 0.000)
n-tetracosane (C_{24})	0.096	0.028	0.049 (± 0.003)
n-pentacosane (C_{25})	0.152	0.048	0.059 (± 0.004)
n-hexacosane (C_{26})	0.104	0.030	0.062 (± 0.011)
n-heptacosane (C_{27})	0.104	0.042	0.048 (± 0.006)
n-octacosane (C_{28})	0.049	<d.l.	0.050 (± 0.016)
n-triacontane (C_{30})	<d.l.	<d.l.	0.049
n-hentriacontane (C_{31})	<d.l.	<d.l.	0.034
n-dotriacontane (C_{32})	<d.l.	<d.l.	0.042

* = value reported is the sum of all isomers quantified; <q.l. = analyte was detected but below quantification limit
The standard deviation associated with the concentration values are the error on replicate extractions (1σ). Calibration curves for C_{24} and C_{26} only had two data points while lower alkanes (C_{10}-C_{22}) had calibration curves with 3 or more data points. All compounds above C_{26} were quantified using the C_{26} calibration curve. Odd chained hydrocarbons were quantified by rounding up and using the closest even chained hydrocarbon standard.
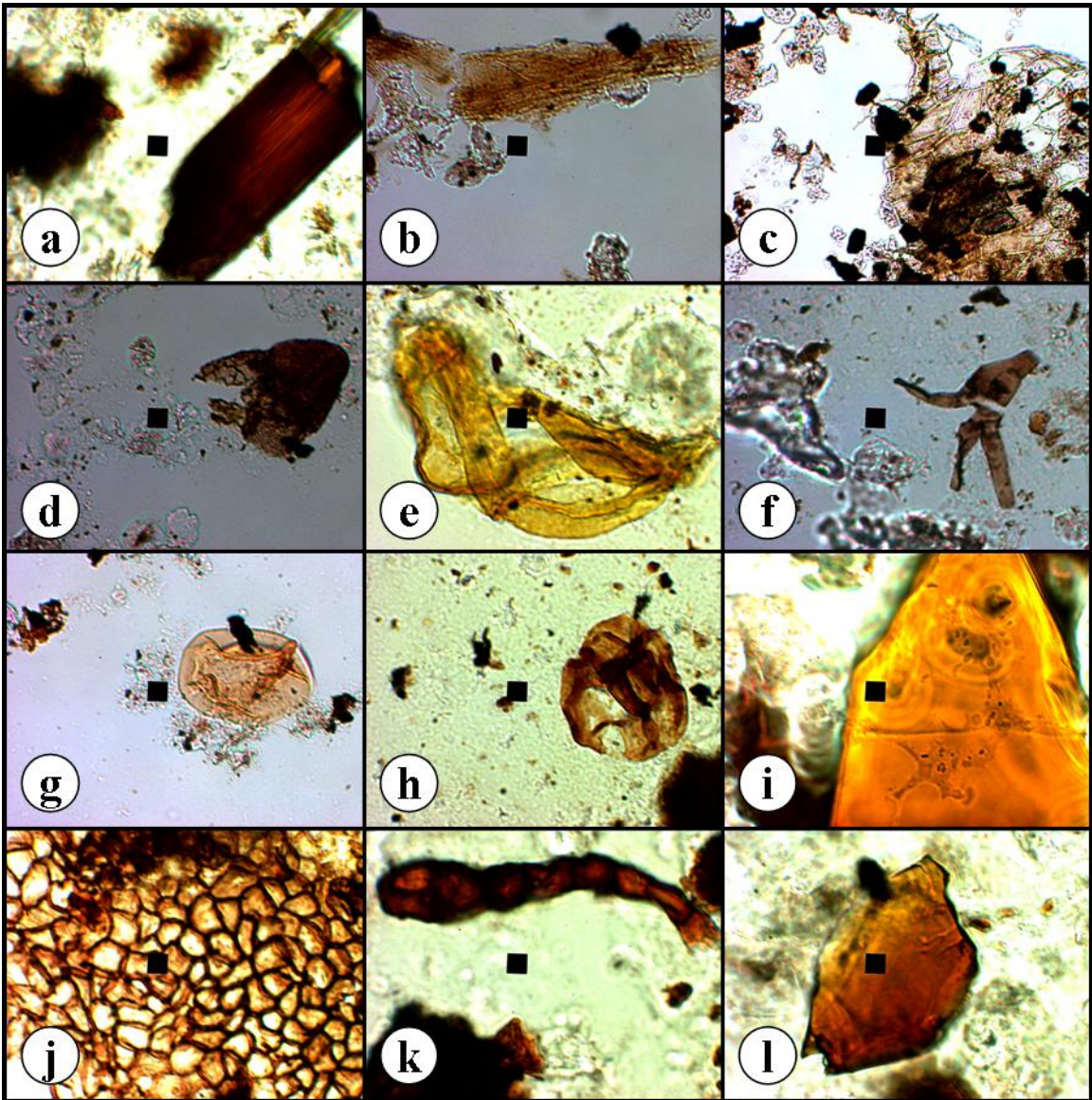
Figure B.1. Structured organics (Phytoclasts and Palynomorphs) observed in sedimentary organic matter extracted from rocks sampled from the Franciscan Subduction Complex at The Cedars. Images taken under white transmitted light and oil immersion (63x). Phytoclasts include (a) gelified woody tissue with fibrous parallel structure, (b) possible woody tissue or leaf-epidermal tissue (cuticle), (c) cuticles (leaf-epidermal tissue, elongated cells in a rectangular shape), and (d) Non woody vascular plant material (possible cortex tissue of stem or root). Palynomorphs include (e) folded cell mass likely associated with marine phytoplankton or possible pollen grain, (f) marine algae remains of uncertain botanical affinity, (g, h) spore or pollen grains, (i) palynomorph cellular mass, (j) honeycomb cell mass structure, (k, l) Unidentifiable structured cellular material.
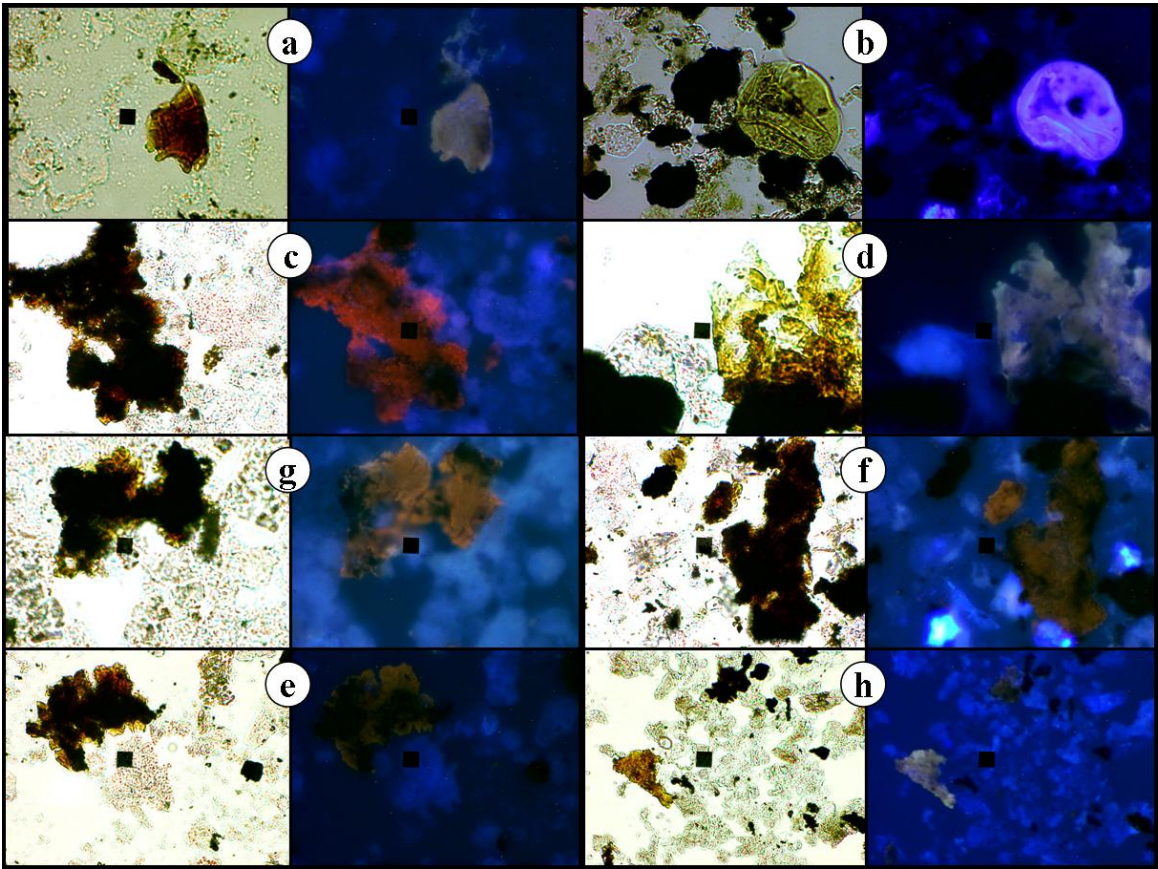
Figure B.2. Structured and unstructured organics observed in sedimentary organic matter extracted from rocks sampled from the Franciscan Subduction Complex at The Cedars. Images were taken under white transmitted light and ultraviolet light at varying magnifications: (e, h) at 10x, (b, c, f, g) at 20x, and (a, d) at 40x. Some organics fluoresced with colours ranging from pale yellow to orange to brown, while others did not fluoresce (black).
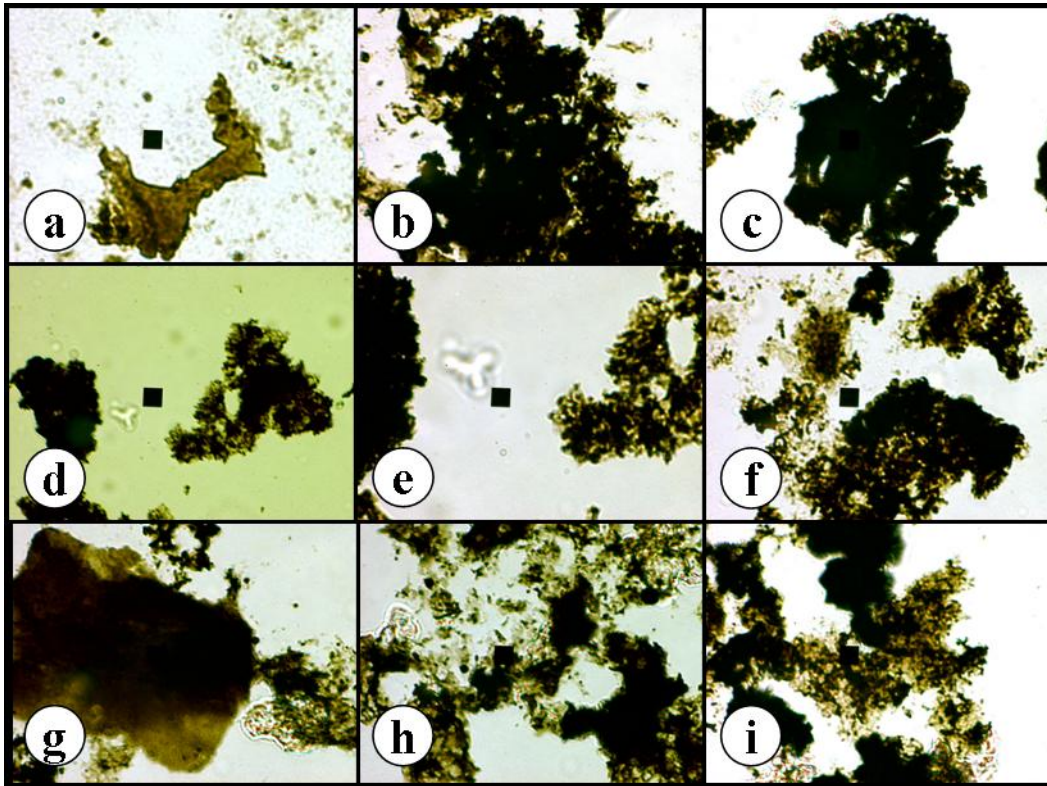
Figure B.3. Unidentifiable unstructured organics that have been heavily degraded in sedimentary organic matter extracted from rocks sampled from the Tablelands. All images taken under white transmitted light with a variety of magnifications: (a, b, c, e, f, g, h, i) 40x, and (d) 20x.
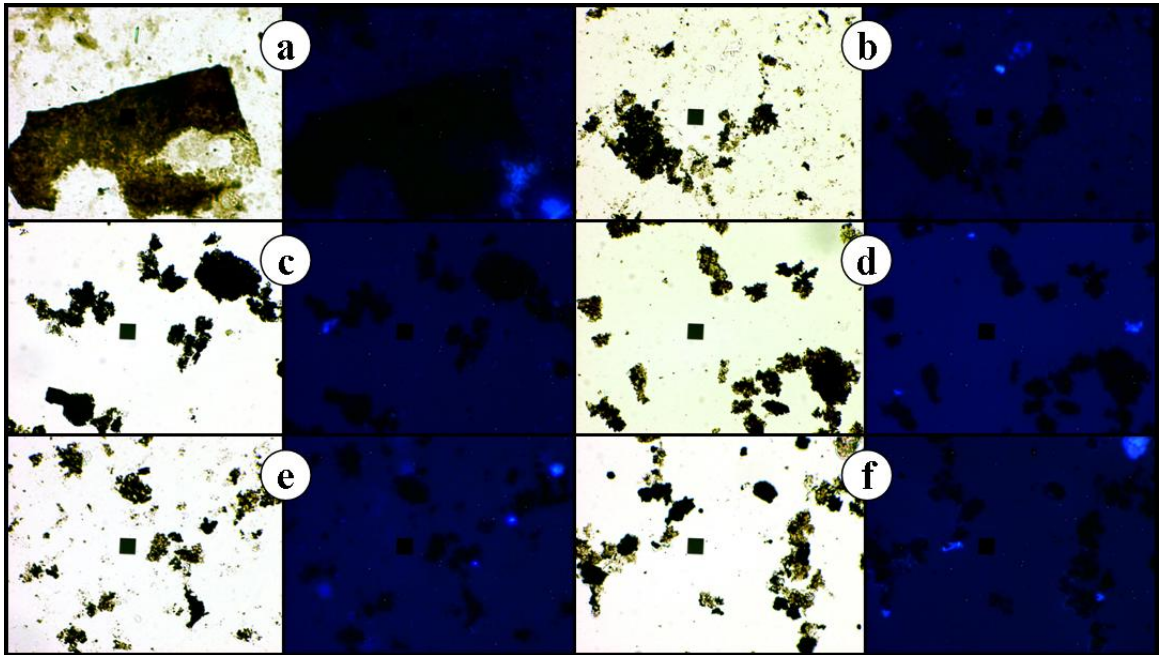
Figure B.4. Unidentifiable unstructured organics that have been heavily degraded in sedimentary organic matter extracted from rocks sampled from the Tablelands. Images were taken under white transmitted light and ultraviolet light at varying magnifications: (b, c, d, e, f) at 10x, and (a) at 40x. No organics fluoresced and were black under ultraviolet light.